Understanding microalgal self-aggregation for economic and sustainable harvesting

A thesis presented in partial fulfilment of the requirements for the degree of

Doctor of Philosophy

in

Engineering

At Massey University, Manawatū, New Zealand

Emma Muir

2026

In loving memory of my dad

Douglas Neil Muir

26 June 1969 – 16 April 2022

Abstract

The potential of microalgae biotechnology is often limited by the costs of biomass harvesting. Chemical flocculation is often used to increase particle size and improve harvesting efficiency; however, flocculants risk contamination and limit downstream applications.

Self-aggregation offers a biological alternative to flocculation: many unicellular microalgae form multicellular structures as a defence response to stress. Predator-released infochemicals are especially potent triggers that act at extremely low concentrations and could become economic alternatives to traditional flocculants. Literature showed that predator-induced aggregation can involve changes to motility, the cell wall, the extracellular matrix, and extracellular polysaccharides, but the identity of active compounds and the specific mechanisms of infochemical perception and aggregation remain poorly understood.

As a first step to this research, an assay was developed to induce a significant and reproducible self-aggregation response in microalgae. Thus, for the first time, the aggregation responses of *Chlamydomonas reinhardtii*, *Tetradesmus obliquus*, and *Chlorella vulgaris* were systematically studied under exposure to the live zooplankton *Daphnia* or concentrated *Daphnia* extracts. *C. reinhardtii* cultures treated with *Daphnia* extract formed palmelloid colonies of 4–32 cells within 24 hours, with the mean colony size exceeding four cells. This rapid and uniform response was ideal for use in experimental transcriptomic and metabolomic studies.

Subsequent transcriptomic analyses of *C. reinhardtii* revealed significant downregulation of flagella-related genes (e.g., genes encoding flagella-associated proteins or intraflagellar transport components) in palmelloid-rich cultures relative to unicellular controls. Changes were also observed in genes encoding matrix metalloproteinases (MMPs), pherophorins (PHCs), calcium signalling, the ubiquitin-proteasome system, and TRP channels. Mutant phenotypes confirmed the likely role for MMP13 as a key MMP required for cell wall degradation, and established TRP13 as a new candidate for external signal sensing linked to palmelloid formation.

These findings suggested, for the first time, that predator infochemicals induced palmelloid formation by influencing the kinases and protein turnover controlling flagella assembly, thus preventing flagella reassembly following cell division. Without flagella, cells were not able to degrade the mother cell wall and instead continued to divide within palmelloid colonies.

Untargeted metabolomic profiling using GC-MS was also carried out on *Daphnia*-extract treated *C. reinhardtii* cultures, and unicellular controls, for the first time. Hundreds of peaks were detected, from which 22 consistent compounds were identified. However, most were also present in the *Daphnia* extract, underscoring the difficulty of distinguishing between predator- and algal-derived compounds. Despite these challenges, several amino acids, including tyramine and tyrosine, and urea were identified as possible candidate *Daphnia* infochemicals, while amino acids, polyamines, and fatty acids could represent *C. reinhardtii* alarm signals during aggregation. If validated through targeted bioassays, these compounds could be used for controlled induction of palmelloids prior to harvesting or for further mechanistic studies.

The potential of using self-aggregation for harvesting was finally evaluated based on the observed aggregation dynamics in *C. reinhardtii*: the extremely low reported active concentrations of *Daphnia* infochemicals would make induction of self-aggregation more economically sustainable compared to chemical flocculation, and the natural origin may remove the barrier that exists for common flocculants to food and feed applications. However, using live zooplankton or extracts would likely require biomass at significant volumes that would be economically unviable. Instead, synthetic infochemicals could be a more affordable option. Light, temperature, cell density, the type of infochemical, and the timing of addition are key operational parameters to be controlled and their impacts on self-aggregation responses are species-specific. The aggregate phenotypes (i.e., colonies or adhered cell flocs) also determine suitability for certain harvesting processes, such as sedimentation, filtration, and centrifugation, as the size, shape, and density of aggregates, and presence of polymers can influence harvesting efficiency.

Overall, this thesis developed an aggregation assay protocol and provided the first combined transcriptomic and metabolomic investigation of *Daphnia*-induced palmelloid formation in *C. reinhardtii*. This research showed that predator-derived extracts could reproducibly trigger aggregation, and identified new candidate molecular regulators and pathways, and crucial factors to be considered when designing an aggregation-based harvesting system. While the self-aggregation response was not scaled, the variability observed across species and strains presents both challenges and opportunities for designing effective bespoke systems. Together, these findings provide new insights into the mechanisms regulating palmelloid formation and establish a foundation to design protocols and evaluate the technical and economic feasibility of a self-aggregation-based harvesting method.

Acknowledgements

I can only begin by thanking my amazing supervisor Dr Maxence Plouviez, for his scientific guidance and for being a great mentor, but more importantly for his kindness, support, and ability to sense when I need a pep talk or a coffee break on the beach. A big thank you also to my supervisor Dr Benoit Guieysse for convincing me to do a PhD in the first place – I went to him to find out more about postgrad studies and somewhat unknowingly signed the next four years of my life away. But I wouldn't change a thing, as I am so grateful for the opportunities that this journey has and continues to bring me and for all that I have learnt. Thank you Benoit and Max for your guidance and for just being genuinely lovely humans – I truly lucked out having you as my supervisors. I would also like to thank my supervisors A/Prof. Nicola Brown and Prof. Peter Lockhart for adopting me partway through, amidst the chaos, and for your guidance.

Thank you to Mrs Ann-Marie Jackson and Dr Baizura Zain for keeping the microbiology lab running smoothly and always being happy to help. Thank you to Massey University for funding my PhD scholarship and to the Royal Society of New Zealand and Cawthron Institute for providing the funding that allowed me to undertake this work. I appreciate everyone I have met at Massey along the way and the wonderful team at Cawthron Institute for hosting me for the last stretch of my PhD in beautiful Nelson.

I cannot express my gratitude enough for the people who I am lucky to call my friends: Kallpanna (my Day One, mi amor); Zoey (my ranga therapist bestie); Sarah and Marco (my favourite duo); Florencia, Federico, and Claire (their friendship got me through tough times and meant more than they knew); Carolina and Pedro (the coolest flatties who adopted me so I didn't feel alone in a new city); and Raphaëlle, Felia, and Shani (my CAP besties and adventure buddies). The last few years have truly had the lowest lows and highest highs, and I cherish our memories and couldn't have done it without their support and love.

Finally, and most importantly, I am forever thankful for my family. To Jesse and Kayla, for asking me what I'm studying three years in (in true brotherly fashion), and for having my beautiful niece Rowan, right when we most needed the joy that she brought us. To Mya, for blessing us with 16 beautiful years. And lastly to my mum and dad, Rachael and Douglas, thank you for getting me to where I am, teaching me to work hard, telling me you're proud of me, and for always being my biggest supporters. I couldn't have done it without you. 🖤

Table of contents

List of illustrations

List of tables

List of abbreviations

ANOVA	Analysis of variance
ALK	Aurora-like kinase
CaM	Calmodulin
CDPK	Calcium-dependent protein kinase
CDK	Cyclin-dependent kinase
CEP	Centrosomal protein
CPC	Cells per colony
DEG	Differentially expressed gene
ECM	Extracellular matrix
EPS	Extracellular polymeric substances/extracellular polysaccharides
FAMEs	Fatty acid methyl esters
FAP	Flagella-associated protein
FDR	False discovery rate
GC-MS	Gas chromatography-mass spectrometry
GO	Gene ontology
GPCR	G-protein-coupled receptor
IFT	Intraflagellar transport
IPS	Intracellular polysaccharides
KEGG	Kyoto Encyclopedia of Genes and Genomes
Log_2-FC	log_2-fold change
MAPK	Mitogen-activated protein kinase
MCF	Methyl chloroformate
MCS	Mean colony size (in cells per colony)
MMP	Matrix metalloproteinase
MPS	Maximum pet supplies (used to denote extract of *Daphnia* from this supplier)
NEK	NIMA-related kinase
PCA	Principal component analysis
PHC	Pherophorin
QC	Quality control
ROS	Reactive oxygen species
RSP	Radial spoke protein

RT-PCR	Reverse-transcription quantitative polymerase chain reaction
SDS	Sodium dodecyl sulphate
SNRK	Sucrose non-fermenting 1-related kinase
SOS	Sodium octyl sulphate
TAP	Tris acetate phosphate
TMS	Trimethylsilyl
TRP	Transient receptor potential
TS	Total solids

Structure of the thesis

This thesis is based on manuscripts that have been published (Chapter 1) or are in preparation for publication in international peer-reviewed journals (Chapters 3-5). Some of the results have also been presented at two international conferences (Chapter 3) and the potential and challenges of self-aggregation for harvesting have been discussed in two book chapters (Muir et al., 2025; and Plouviez et al., *in press*).

A preface is included at the beginning of Chapters 1-5 to link to the research objectives and together with the other chapters. Chapters 1-5 provide the key findings that are summarised and discussed in Chapter 6.

The relevant publications for each chapter are presented in the next section. The structure of this thesis complies with the Massey University doctoral thesis with publications guidelines, 2022.

List of papers and contributions

Chapter 1

Chapter 1 is adapted from the following previously published work, with revisions made to ensure consistency and cohesion within the context of this thesis:

Muir, E., Grossman, A. R., Chisti, Y., Fedrizzi, B., Guieysse, B., Plouviez, M. (2024). Self-aggregation for sustainable harvesting of microalgae. *Algal Research*, *83*, 103685. https:/doi.org/10.1016/j.algal.2024.103685.

Chapter 2

This chapter was developed specifically for this thesis and is not intended for publication.

Chapter 3

Muir, E., Guieysse, B., Brown, N., Plouviez, M. Transcriptomic responses of *Chlamydomonas reinhardtii* during palmelloid formation triggered by *Daphnia* infochemicals. (*Under preparation*).

Chapter 4

Muir, E., Guieysse, B., Brown, N., Plouviez, M. Characterising the metabolome of self-aggregating *Chlamydomonas reinhardtii* exposed to *Daphnia* infochemicals. (*Under preparation*).

Chapter 5

This chapter was developed specifically for this thesis and is not intended for publication.

Emma Muir was the main contributor and lead author on all the papers and also presented at the following international conferences:

- International Conference on Algal Biomass, Biofuels and Bioproducts (AlgalBBB 2024), Clearwater Beach, Florida, USA (June 2024): Muir, E., Guieysse, B., Plouviez,

M. Microalgal self-aggregation induced by predator infochemicals for sustainable harvesting.

- Aotearoa New Zealand Cellular Agriculture Symposium 2025, Nelson, New Zealand (April 2025): Muir, E., Guieysse, B., Plouviez, M. Self-aggregation for sustainable harvesting of microalgae for food applications.

Emma Muir designed and conducted all experimental work and data analysis and her supervisors offered advice and helped editing papers. The statements of contribution to doctoral thesis with publications can be found before each respective chapter.

Thesis introduction

Microalgae are widely considered promising resources for generation of renewable fuels, animal feed, bioactive compounds, and to deliver sustainable wastewater treatment services. Yet, large-scale implementation of microalgae biotechnology remains limited, and harvesting is a major bottleneck to this effort. Microalgal cultures are typically dilute (< 1 g L^{-1}), and most cells are small, have a low density, and harbour negatively charged surfaces. These conditions limit natural settling and make unassisted sedimentation, filtration, or centrifugation inefficient or energetically prohibitive. Chemical flocculants are often used to increase settling rates and efficiencies, but this practice adds costs and introduces contaminants (i.e., metal salts) that limit downstream applications, especially for food or feed purposes.

An alternative to chemically induced flocculation could lie in exploiting a natural stress response known as *self-aggregation*. Many unicellular microalgae form colonies or large aggregates, increasing their particle size, under predation or other stressors. This inducible defence could serve as a biological alternative to chemical flocculation, but its fundamental mechanisms remain poorly understood. It is known that self-aggregation can occur in multiple taxa and that cues from grazers can be powerful triggers at low concentrations. However, clear insight is lacking in how cells sense these cues, coordinate a culture-wide response, and maintain colonies under different environmental conditions. Without this understanding, the application of self-aggregation for harvesting cannot be employed effectively.

This thesis addresses these knowledge gaps using *Chlamydomonas reinhardtii* and *Daphnia* as a model system. *C. reinhardtii* is a model alga with extensive molecular resources, making it uniquely suited for linking ecological responses to cellular mechanisms. *Daphnia* is a keystone grazer in freshwater ecosystems, long known to induce algal defences. Together, they provide an ecologically relevant system for probing self-aggregation and its harvesting potential.

This research is guided by three overarching questions:

1. What morphological traits does *C. reinhardtii* employ in response to grazer cues?
2. What are the molecular pathways regulating self-aggregation?
3. Can self-aggregation be optimised and integrated into practical harvesting workflows to improve sedimentation, filtration, or centrifugation efficiency?

Chapter 1 reviews existing knowledge of microalgal self-aggregation and its potential role in harvesting. **Chapter 2** presents findings from self-aggregation bioassays, establishing *C. reinhardtii* treated with *Daphnia* extract as a robust system. **Chapters 3** and **4** investigate the transcriptomic and metabolomic responses of aggregating cultures, identifying candidate mechanisms. **Chapter 5** evaluates how self-aggregation could be deployed as a harvesting tool and the crucial parameters to be optimised. **Chapter 6** then synthesises all findings obtained during this research and discusses future research steps for understanding the mechanisms of self-aggregation and integrating aggregation into a harvesting process.

Chapter 1.

Literature review

Preface

This chapter reviews current knowledge of microalgal self-aggregation, with a focus on defensive aggregation reported in species such as *Chlamydomonas*, *Scenedesmus*, *Chlorella*, and *Microcystis*. The objective was to summarise existing knowledge of how microalgae sense environmental cues and initiate self-aggregation, and to identify knowledge gaps that must be addressed to harness self-aggregation for biomass harvesting. By doing so, this chapter establishes the foundation for the experimental work that follows, where predator-derived infochemicals are tested as triggers and the molecular mechanisms of aggregation are explored in detail.

Abstract

Microalgae can be cultivated for wastewater treatment, food and feed, fuels, and high-value metabolites. However, the low biomass concentrations typical of photoautotrophic cultures mean very large volumes must be processed during dewatering. The simplest dewatering method is sedimentation, but microalgal cells settle very slowly due to their small size, low density, and negatively charged surfaces. To overcome this, chemical flocculants are often added, but these increase costs, introduce contaminants, and reduce biomass quality. Alternative approaches such as centrifugation are more effective but require high energy input and substantial capital and operational investment. As a result, biomass recovery can be costly and carries significant environmental burdens.

Self-aggregation offers a potential biological solution: by triggering natural aggregation of algal cells, flocculants could be avoided, enabling more sustainable harvesting via sedimentation, filtration, or centrifugation. Self-aggregation has been reported in many species in response to stresses such as predation, and is influenced by shifts in light, temperature, and solute concentration. While the underlying mechanisms are not fully understood, candidate genes in *Chlamydomonas*, *Tetradesmus*, and *Microcystis* suggest roles for predator sensing, cell-to-cell signalling, extracellular polysaccharides, and cell wall modification. Predator-induced aggregation is thought to be mediated by "infochemicals" released by grazers; to date, only compounds from *Daphnia pulex* have been identified and shown to induce aggregation in *Scenedesmus gutwinskii*. If scalable, the use of such infochemicals as biological flocculants could reduce the cost of microalgae harvesting by three to five orders of magnitude, while eliminating chemical contaminations and lowering environmental impacts.

1.1 Introduction

Microalgae use sunlight and nutrients to fix carbon into biomass rich in proteins, fatty acids, polysaccharides, vitamins, minerals, and antioxidants (Mata et al., 2010). Their productivity makes microalgae promising for aquaculture and food production, wastewater treatment, and biofuel industries. Species such as *Arthrospira, Chlorella, Haematococcus, Botryococcus* and *Scenedesmus* are widely produced for health foods, aquaculture feed, cosmetics, and carotenoid pigments (Spolaore et al., 2006). Certain microalgae, including *Chlamydomonas* and *Chlorella*, can be cultivated for biodiesel production, with residual biomass converted to ethanol, methane, livestock feed, or fertilizer (Biswal et al., 2024; Mata et al., 2010; Scranton et al., 2015).

Despite this potential, commercialisation is constrained by the cost of biomass recovery. Photoautotrophic cultures in commercial facilities typically yield only 0.5–0.75 g dry biomass L^{-1} in open ponds and up to 2 g L^{-1} in photobioreactors. At such low concentrations, large volumes must be processed, and the intrinsic properties of algal cells (small size, low density, charged surfaces, and, in some species, motility) limit natural settling. As a result, costly methods such as centrifugation or chemical flocculation are usually required. Harvesting can therefore account for up to 30% of total production costs (Gudin and Thépenier, 1986), a figure that has since been cited in at least 52 papers focusing on microalgae harvesting (McGrath et al., 2024).

Table 1.1 summarises commonly used harvesting technologies. Algal suspensions are usually first thickened to a slurry of 2–7% solids through flocculation and/or gravity sedimentation or flotation. Subsequent dewatering steps, such as filtration and centrifugation, concentrate the biomass further to 15–25% solids, but these are expensive and energy-intensive (Esteves et al., 2020; Roselet et al., 2019). Recovery efficiency is also crucial: > 70% biomass retention is desirable, as higher yields reduce cost per unit biomass.

Chemical flocculants accelerate sedimentation and aid flotation by neutralising cell surface charges or bridging cells into larger aggregates (**Figure 1.1**), but these are expensive, introduce contaminants, and limit downstream applications (Barros et al., 2015).

Table 1.1. Comparison of methods commonly used for harvesting microalgae.

Technology	Purpose	Advantages	Disadvantages
Chemical flocculation	Thickening to 2–7% TS slurry	60–99% recovery efficiency Low energy demand Low capital Simple Large volume capability	Chemical costs Biomass contamination Highly variable Limited potential for water recycling
Flotation	Thickening to 2–7% TS slurry	Simple and rapid	50–90% recovery efficiency High energy demand Expensive Small volume capability Flocculants or surfactants are often required
Gravity settling	Thickening to 2–7% TS slurry	Low energy consumption Low cost Simple Chemical-free	Slow Biomass deterioration Low recovery efficiency, < 30%
Filtration	Thickening to 2–7% TS slurry Dewatering to 15–25% TS paste	70–90% recovery efficiency Low equipment cost Chemical-free Allows water recycling	Time-consuming Membrane fouling Frequent membrane replacement and/or cleaning High energy demand Best for small volumes Limited by biomass characteristics
Centrifugation	Dewatering to 15–25% TS paste	> 90% recovery efficiency Rapid and reliable Suits most microalgae Chemical-free	High capital, energy, and maintenance costs Centrifugal force limited at scale May damage cells

A more sustainable approach to flocculation would be to trigger the cells' own aggregation behaviour under defined conditions. Many microalgae naturally self-aggregate in response to stress, forming multicellular colonies or flocs. Reported triggers include temperature shifts (Li et al., 2013; Zhu et al., 2019; Zhu et al., 2017), light conditions (Suwannachuen et al., 2023), predators such as zooplankton (Berger, 2017; Fisher et al., 2016; Hou et al., 2018; Kapsetaki et al., 2016; Lurling and Beekman, 2006; Sathe and Durand, 2016), and pollutants (Cheloni and Slaveykova, 2021). If these self-aggregation responses could be deliberately triggered in large-scale cultivation systems, the resulting increase in particle size could enable gravity-based sedimentation without the need for added flocculants.

Predator-induced self-aggregation has been linked to "infochemical" transfer between grazers and microalgae. Yet the identity, structure, and versatility of such cues remain poorly understood. Equally limited is our knowledge of how microalgae sense predators and initiate aggregation at the molecular level. Unlocking these mechanisms would be essential to control and apply natural aggregation for harvesting.

In this review, current knowledge of microalgal self-aggregation is examined, with a focus on predator-induced responses and the candidate genes and mechanisms involved. How these processes might be exploited for low-cost harvesting of algal biomass is also assessed. Throughout, the term *self-aggregation* is used to describe multi-celled morphologies formed as a direct cellular response to stress. By contrast, *flocculation* is used to describe externally driven particle formation, such as that induced by chemical flocculants or electrostatic neutralisation under alkaline conditions.

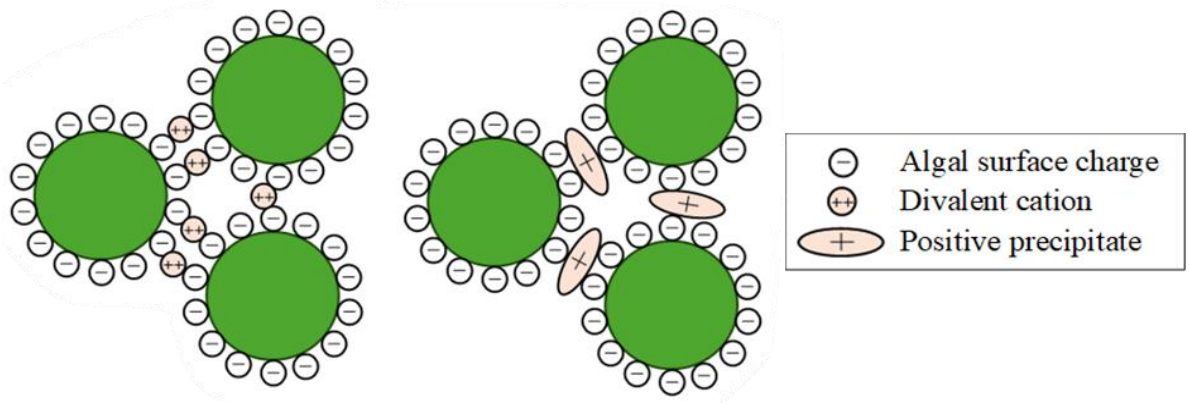

Figure 1.1. Mechanisms of microalgal aggregation via surface charge neutralisation.

1.2 Self-aggregation as a defence against predation

Live predators, or infochemicals they release, can trigger self-aggregation in unicellular microalgae as a morphological defence. This has been demonstrated in *Tetradesmus obliquus* (formerly *Scenedesmus obliquus*) (Hou et al., 2018), *Chlamydomonas reinhardtii* (Lurling and Beekman, 2006), *Chlorella vulgaris* (Fisher et al., 2016), and *Microcystis aeruginosa* (Nam et al., 2024). **Table 1.2** summarises reported predator-microalgae interactions, with the associated colony sizes and induction times. A schematic overview of these interactions and their frequency in literature is shown in **Figure 1.2**.

The strength and mechanism of predator-induced self-aggregation vary widely across predator-prey systems and depend strongly on environmental conditions. For example, in the marine alga *Phaeocystis*, exposure to infochemicals from ciliates (which feed on small cells) enhanced colony formation, whereas infochemicals from the copepod *Acartia tonsa* (which prefers medium-sized colonies) suppressed it (Long et al., 2007). Such contrasting responses reflect predator feeding preferences: some predators selectively consume small-celled microalgae, while others target larger prey. It is therefore likely that microalgae have evolved to mount a morphological defence only in response to predator-specific cues.

Importantly, the magnitude and reversibility of self-aggregation are also shaped by abiotic factors, such as light, temperature, and nutrient availability. These influences are reviewed in **Section 1.4**.

Table 1.2. Predators (live predators or their infochemicals) inducing aggregation in unicellular green microalgae and cyanobacteria (not an exhaustive list). Degree of aggregation is reported as either the mean number of cells per colony (CPC), the Cohen's d index (difference between treatment and control means expressed in standard deviation units), the largest colony size observed, or as a percentage of cells in aggregates. Time to aggregate, in hours, days, or weeks, is reported, otherwise it is the time of maximum observed aggregation as indicated.

Microalgae	Predator	Degree of aggregation	Time to aggregate	Ref.
Chlamydomonas reinhardtii	*Daphnia magna*	2–16 CPC	Max. at 1 h	a
	Daphnia pulex	Not stated	Not stated	a
	Brachionus calyciflorus	Dozens to hundreds CPC	1–2 weeks	b
		≥ 8-celled colonies	25 h	c
	Peranema trichophorum	Not stated	4–5 d	d
	Paramecium tetraurelia	8 CPC	50 weekly transfers	e
Chlamydomonas debaryana	*Peranema trichophorum*	10–100,000 CPC	4–5 d	d
Chlamydomonas moewusii	*Peranema trichophorum*	Not stated	4–5 d	d
Chlorella vulgaris	*Daphnia magna*	30%	72 h	f
	Ochromonas sp.	65%	24 h	f
	Ochromonas vallescia	8-celled colonies	10–20 generations	g
	Tetrahymena thermophila	50%	48 h	f
		36–55%	2–3 d	h
Chlorella sorokiniana	*Daphnia magna*	90%	24 h	f
	Ochromonas sp.	20%	72 h	f
	Tetrahymena thermophila	35%	72 h	f
Scenedesmus gutwinskii	*Daphnia pulex*	3.5 CPC	10 d	i
Scenedesmus subspicatus	*Daphnia magna*	Not stated	2–20 h	j
		8-celled colonies	1–5 d	k
Scenedesmus quadricauda	*Daphnia magna*	75% in 4- to 8-celled colonies	4 h	l
Scenedesmus dimorphus	*Daphnia magna*	~5.5–7 CPC	8 h to 2 d	m
	Moina macrocopa	~5.5–7 CPC	8 h to 2 d	m
Scenedesmus acutus	*Daphnia magna*	≤ 8 CPC	24–48 h	n
		~40% in 8-celled colonies	< 72 h	o
		~45% in 8-celled colonies	48 h	p

Table 1.2. (*Continued*).

Microalgae	Predator	Degree of aggregation	Time to aggregate	Ref.
Tetradesmus obliquus (*Scenedesmus obliquus*)	*Ochromonas* sp.	80%, 9 CPC	72 h	f
	Daphnia galeata	Cohen's d* = 9.9	24 h	q
	Daphnia galeata × *hyalina*	Cohen's d* = 14.1	24 h	q
	Daphnia magna	1–8 CPC	24 h	r
		8-celled colonies	48 h	s
		4- and 8-celled colonies	48 h	t
		6–7 CPC	Max. at 4–6 d	u
		80%	1 h	f
		5 CPC	3 d	v
		~3.5 CPC	3 d	w
		~4.5 CPC	3–4 d	x
		Cohen's d* 9.3	24 h	q
		4-fold increase in CPC	48 h	y
		30% in 8-celled colonies	3–5 d	z
	Tetrahymena thermophila	65%	48 h	f
	Brachionus calyciflorus	~3-fold increase in CPC	48 h	y
	Ceriodaphnia. Reticulata	Cohen's d* = 9.31	24 h	q
	Daphnia carinata	3.5 CPC	24 h	A
	Daphnia pulex	4 CPC	4–5 d	B
	Daphnia pulicaria	Cohen's d* = 31.8	24 h	q
Microcystis aeruginosa	*Ochromonas* sp.	Not stated	5–7 d	C
		1.4 CPC	3–5 d	D
	Daphnia magna	Not stated	Not stated	E
		1.5 CPC	2–3 d	m
		~7%	≤ 15 d	F
	Daphnia galeata	~10%	≤ 15 d	F
	Moina macrocopa	145 CPC	2–3 d	m

Reference letters correspond to the following sources:

a (Berger, 2017); b (Lorusso, 2018); c (Lurling and Beekman, 2006); d (Sathe and Durand, 2016); e (Herron et al., 2019); f (Kapsetaki et al., 2016); g (Boraas et al., 1998); h (Fisher et al., 2016); i (Yasumoto et al., 2005); j (Roccuzzo et al., 2020); k (Hessen and Donk, 1993); l (Pan et al., 2017); m (Ha et al., 2004); n (O'Donnell et al., 2012); o (Lürling, 1998); p (Lampert et al., 1994); q (Roccuzzo et al., 2016); r (Hou et al., 2018); s (Sun et al., 2020); t (Zhang et al., 2021); u (Zhu et al., 2017); v (Zhu et al., 2016); w (Huang et al., 2016); x (Huang et al., 2018); y (Verschoor et al., 2004); z (Wu et al., 2013); A (Yang et al., 2007); B (Jia et al., 2023); C (Wang et al., 2010); D (Yang et al., 2009); E (Becker, 2010); F (Nam et al., 2024).

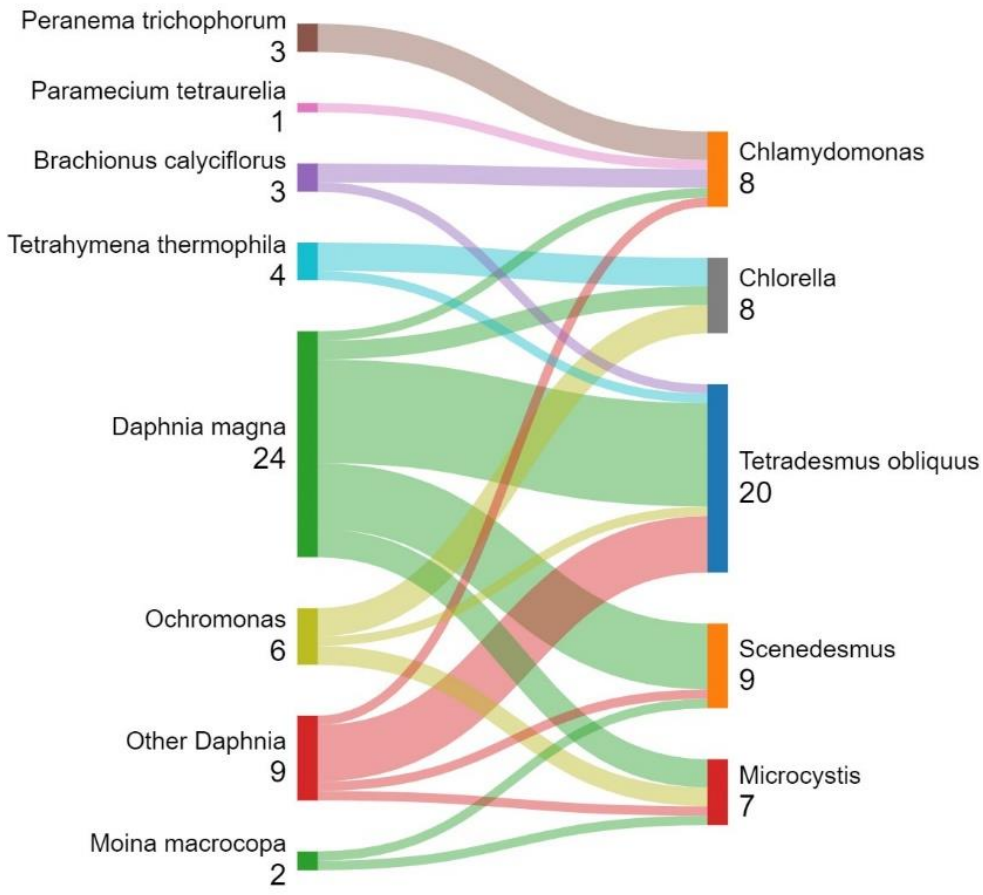

Figure 1.2. Predator (left)-microalgae (right) relationships that trigger self-aggregation and their relative frequency of reports in the literature.

1.3 Bioflocculation

Bioflocculation refers to the use of bacteria, fungi, or microalgae, or their secreted products to promote aggregation of microalgal cells. In this process, biopolymers such as exopolysaccharides (EPS) or surface proteins neutralize electrostatic repulsion and bind cells together, enabling larger flocs that settle or filter more efficiently (Salim et al., 2011; Ummalyma et al., 2017). These bioflocculants can either be produced in co-culture with microalgae or recovered from flocculating organisms and added to cultures (Ray et al., 2021).

Bioflocculants typically act through charge neutralization and bridging interactions. EPS or other polymers often contain positively charged functional groups that neutralise the negatively charged microalgal cell surface, promoting aggregation through adsorption and electrostatic attraction (**Figure 1.1**) (Nie et al., 2022). In some systems, divalent cations such as calcium further enhance bridging between algal cells and polymers. For example, Powell and Hill (2014) showed that aggregation of *Nannochloropsis oceanica* with *Bacillus* was facilitated by calcium binding to both surfaces.

Microalgae themselves can drive bioflocculation, either through co-cultivation of EPS-producing and non-flocculating species, or by extracting and reapplying EPS. For instance, co-culturing *Chlorella vulgaris* with the EPS-producer *Scotiellopsis reticulata* increased flocculation efficiency to ~60% within three hours, compared with just 8% for *C. vulgaris* alone (Spain and Funk, 2024). This approach is advantageous because it avoids the need for additional substrates or altered cultivation conditions often required by heterotrophic organisms (Salim et al., 2011).

EPS addition can also enhance conventional flocculation. Yang et al. (2020) extracted the EPS from *Scenedesmus acuminatus* and showed that supplementing cultures reduced the required dose of alum from 77.6 mg g^{-1} to 4.5 mg g^{-1} while maintaining > 90% recovery efficiency at an algal density of 1 g L^{-1}. Production costs for EPS were estimated at ~USD $2447 per metric ton (based on HCl extraction and energy inputs for blending and centrifugation), although this excluded culturing, harvesting, and labour costs. Even so, the addition of algal EPS reduced the overall chemical cost of flocculation from ~$205 to $52 per metric ton ($0.052 per m^3 of algal culture). While these results are promising, true scalability of algal EPS-based bioflocculation requires validation at industrial scale.

1.4 Flocculation and self-aggregation in response to abiotic conditions

External abiotic factors can trigger or influence flocculation and self-aggregation. Key drivers include pH, solute composition (e.g., chemical flocculants), nutrient availability, and light intensity.

1.4.1 pH and charge neutralization

Both freshwater and marine microalgae can be induced to flocculate by adjusting culture pH (Wu et al., 2012). Flocculation is typically enhanced at alkaline pH (Wu et al., 2012), though in some cases it has also been reported under acidic conditions (Liu et al., 2013). However, most species do not self-aggregate at low pH (Li et al., 2021) (See **Table 1.3**).

High pH can occur naturally when vigorous photosynthesis depletes dissolved inorganic carbon, raising alkalinity as carbonic acid is consumed faster than it is replenished by atmospheric diffusion. Practically, pH can also be increased by chemical addition. For instance, lime provides Ca^{2+} ions in addition to raising pH, making it more effective for inducing flocculation than sodium hydroxide (Liang et al., 2022). Under alkaline conditions, divalent ions such as calcium, magnesium, and phosphate form positively charged precipitates that neutralise the negatively charged algal cell surface (Li et al., 2021; Sukenik and Shelef, 1984; Vandamme et al., 2012) (**Figure 1.1**). For example, *C. vulgaris* required magnesium (0.075 mM) for flocculation at pH 11, with efficiency increasing at higher pH (Vandamme et al., 2012). Detailed mechanisms of alkaline flocculation are reviewed by Vandamme et al. (2012) and Sukenik and Shelef (1984).

At the acidic end of the spectrum, *Scenedesmus quadricauda* showed enhanced flocculation at pH 3.0, likely because protonation of negatively charged EPS groups reduced electrostatic repulsion (Aljuboori et al., 2016). Although EPS was not quantified, acid stress may also have stimulated EPS secretion, promoting aggregation. A similar phenomenon was observed in *Chlamydomonas applanata*: while growth was optimal at pH 7.4, palmelloid colonies (see **Section 1.5.3.2**) with increased EPS production formed below pH 4.4 (Visviki and Santikul, 2000). However, low pH also impaired cell division and viability, suggesting that aggregation under acidic stress is not useful for harvesting. Interestingly, *Tetradesmus obliquus* showed

reduced aggregation in response to *Daphnia magna* at low pH, possibly due to disruption of normal cellular processes (Yang et al., 2016).

Overall, pH strongly governs surface charge interactions, with high pH often promoting flocculation via divalent cation precipitation. However, extreme acidic or alkaline conditions may trigger stress-induced self-aggregation at the expense of cell viability, limiting direct application for harvesting.

Table 1.3. Influence of pH and cations on microalgae aggregation.

Effect	**Examples**
Alkalinity induced flocculation in *Chlamydomonas reinhardtii, Chlorella vulgaris*, and *Tetradesmus obliquus.*	*C. reinhardtii* flocculated at pH 11.0 with Ca^{2+} or Mg^{2+} (> 5 mM) and at pH 8.5 with Fe^{3+} (10 mM) (Fan et al., 2017). *C. vulgaris* flocculated with 95% efficiency at pH 11.5 in the presence of Mg^{2+} (20 mg L^{-1}) and PO_4^{3-} (1.9 mg L^{-1}) (Vandamme et al., 2012). Efficiency was 80% with NaOH and ~89% with $Ca(OH)_2$ at pH 12.0, with Mg^{2+} (5 mg L^{-1}) (Castrillo et al., 2013). *T. obliquus* flocculated with ~70% efficiency at pH 12.0 using $Ca(OH)_2$ (Castrillo et al., 2013).
Low pH impaired defensive aggregation in *T. obliquus.*	Defensive self-aggregation remained stable at pH 7.0–9.0 but was impaired under acidic conditions (Zhang et al., 2021).
Low pH depressed growth in *Chlamydomonas applanata*, while increasing EPS synthesis, promoting self-aggregation, and causing cell death.	Optimum growth occurred at pH 7.4. Growth was depressed at pH 4.4 and 3.4. At pH 4.4, cells showed decreased volume, reduced starch reserves, and palmelloid formation. At pH 3.4, there was excessive EPS, cell death, abnormal cell division, and loss of motility (Visviki and Santikul, 2000).
Acidity increased flocculation efficiency in EPS-producing *Scenedesmus quadricauda.*	Flocculation efficiency was 4% at pH 7.0, 28% at pH 6.5, 55% at pH 4.5, 78% at pH 3.0, and 77% at pH 2.5 (Aljuboori et al., 2016).

1.4.2 Inorganic chemicals

Abiotic chemical factors can strongly influence microalgal aggregation, particularly when present at sublethal concentrations (**Table 1.4**) (Cheloni and Slaveykova, 2021; Khona et al., 2016).

For example, *Chlamydomonas reinhardtii* formed palmelloids under elevated NaCl (100–150 mM), with aggregates appearing within 18–24 h of salt stress and reverting to unicells within 0.3–4 h after transfer to fresh medium (Khona et al., 2016). Prolonged exposure (36–48 h) prevented disaggregation and led to cell death. Similarly, *C. reinhardtii* formed palmelloids when exposed to perfluorooctanesulfonic acid (PFOS) and paraquat at sublethal concentrations. In these cases, aggregated cells remained intact while unicells showed chlorophyll bleaching, membrane damage, and oxidative stress (Cheloni and Slaveykova, 2021). Reversibility was again observed, with palmelloids reverting to single cells within 24–48 h once toxicants were removed (Cheloni and Slaveykova, 2021). Exposure to naphthenic acids also induced self-aggregation and altered cell wall surface proteins in *C. reinhardtii*, resulting in macroscopic aggregates composed of unicells, palmelloids, and an EPS matrix (Goff et al., 2013).

Other green algae also respond to surfactants. *T. obliquus* aggregated in response to sodium dodecyl sulphate (SDS) and surfactant FFD-6, at 5 mg L^{-1} and 0.01 mg L^{-1}, respectively (Lürling and Beekman, 2002). SDS also induced aggregation in *Desmodesmus subspicatus*, *Scenedesmus acutus*, *Tetradesmus dimorphus* (0.1–10 mg L^{-1}) (Oda et al., 2022), and *S. gutwinskii* (10 µg L^{-1}) (Yasumoto et al., 2005).

Nutrient availability also modulates aggregation. For instance, Zn^{2+} ions mediated flocculation in *S. quadricauda* by neutralising surface charges (Aljuboori et al., 2016), while increased Ca^{2+} enhances EPS production and self-aggregation in *Microcystis aeruginosa* (0.1 g L^{-1} compared to 0.015 g L^{-1} Ca^{2+}) (Wang et al., 2011). Conversely, nutrient deprivation itself can induce aggregation: *Staurosira* and *Desmodesmus* self-aggregated under nutrient depletion, raising settling velocity to ~1 m h^{-1} (Huntley et al., 2015). This effect enabled complete pond-scale settling: a 60 m^3 raceway pond depleted of nutrients self-aggregated and settled 1 h of paddlewheel stoppage, achieving a 20-fold increase in biomass concentration without chemical or energy inputs. Consistent results were reported by Moorthy et al. (2017), who measured a

Scenedesmus settling velocity of 1.03 m h^{-1} under optimised flocculant, temperature, and pH conditions, compared with just 0.03 m h^{-1} under standard growth conditions.

Nutrient and trace elements availability also interact with predator-induced aggregation. *T. obliquus* exposed to *D. magna* infochemicals formed smaller or fewer aggregates when magnesium or calcium were low, or when zinc or nitrogen levels were high (Hou et al., 2018; Zhu et al., 2019; Zhu et al., 2015). Aggregated cells also showed increased tolerance to zinc toxicity (Zhu et al., 2019). By contrast, free copper ions (Huang et al., 2016), cadmium (Jia et al., 2023), herbicides (Zhu et al., 2016), and the antibiotic Norfloxacin (Pan et al., 2017), impaired aggregation responses to *Daphnia* filtrate in *T. obliquus* and *S. quadricauda*.

Carbon availability can also play a role. When atmospheric CO_2 was increased from 390 ppm to 750 ppm at 25 °C, *T. obliquus* formed larger unicells and more eight-celled colonies in response to *D. magna*. Elevated CO_2 increased dissolved organic carbon by 7.4–12.5% on day two, supporting growth and photosynthesis and enhancing aggregation (Huang et al., 2018; Zhang et al., 2021).

Table 1.4. Influence of nutrients, trace elements, environmental pollutants, and CO_2 on microalgae aggregation.

Effect	Examples
NaCl stress induced palmelloid formation in *Chlamydomonas reinhardtii.*	*C. reinhardtii* formed palmelloids under 100–150 mM NaCl, which dispersed after resuspension in normal medium (Khona et al., 2016).
Micropollutants induced palmelloid formation in *C. reinhardtii* even below toxicity thresholds.	Copper, cadmium, perfluorooctanesulfonic acid (PFOS), and paraquat triggered palmelloid formation and damaged single cells. Cells reverted to single form after resuspension in normal medium (Cheloni and Slaveykova, 2021).
Free Cu^{2+} impaired growth, photosynthesis, and aggregation of *Tetradesmus obliquus* in response to *Daphnia* filtrate.	In the presence of *Daphnia* filtrate, copper ions > 2.91×10^{-3} μmol L^{-1} reduced *T. obliquus* growth by > 17% and decreased mean colony size by 43%. Growth, colony size, and photosynthetic efficiency all declined with increasing copper concentration (Huang et al., 2016).
Cd^{2+} impaired self-aggregation of *Tetradesmus obliquus* in response to *Daphnia* filtrate.	*T. obliquus* growth rate and colony size declined with increasing cadmium concentration in the presence of *Daphnia* filtrate (Jia et al., 2023).
Antibiotic exposure impaired self-aggregation in *Scenedesmus quadricauda* in response to *Daphnia.*	In the presence of live *Daphnia*, colony size of *S. quadricauda* decreased with increasing concentrations of the antibiotic norfloxacin (Pan et al., 2017).
Herbicides impaired self-aggregation of *T. obliquus* in response to *Daphnia* filtrate.	In the presence of *Daphnia* filtrate, glyphosate and 2,4-D (0.20–2.0 mg L^{-1}) reduced colony abundance without affecting algal growth or photosynthesis; atrazine at the same concentration decreased all three (Zhu et al., 2016).

Table 1.4 (*Continued*).

Effect	Examples
Anionic surfactants induce colony formation in Scenedesmaceae.	SDS induced colony formation in *T. obliquus*, *Desmodesmus subspicatus*, *S. acutus*, *T. dimorphus*, and *S. gutwinskii*. FFD-6 also induced colony formation in *T. obliquus* (Lürling and Beekman, 2002; Oda et al., 2022).
Naphthenic acids induced aggregation and palmelloid formation in *C. reinhardtii*.	Naphthenic acids (100 mg L^{-1}) induced palmelloids and large EPS-matrix-containing aggregates in wild-type *C. reinhardtii*, but not in two cell wall-deficient mutants (Goff et al., 2013).
Mg^{2+} depletion reduced defensive aggregation in *T. obliquus.*	Under *Daphnia* infochemical exposure, Mg^{2+} at 0.73 mg L^{-1} decreased the proportion of multi-celled colonies compared to at 7.3 mg L^{-1}. Absence of Mg^{2+} suppressed large-colony formation. Time to reach max. colony size was unaffected (Hou et al., 2018).
Elevated Zn^{2+} reduced defensive aggregation in *T. obliquus.*	Under *Daphnia* infochemical exposure, Zn^{2+} at 0.887 μmol L^{-1} reduced aggregate size by 46.9% compared to 0.024 μmol L^{-1}. Aggregation decreased at concentration as low as 0.131 μmol L^{-1}, but growth and photosynthesis were unaffected (Zhu et al., 2019).
Aggregate formation improved Zn^{2+} tolerance in *T. obliquus.*	At 25–30 °C, inhibition increased more slowly with rising Zn^{2+} concentration when *Daphnia* infochemicals induced aggregation, compared with the control (Zhu et al., 2019).
Zn^{2+} enhanced aggregation in EPS-producing *S. quadricauda*.	Addition of $ZnCl_2$ (9.54 g L^{-1}) increased flocculation efficiency (pH 7) to 82.7%, compared to 11–15% when $CaCl_2$, $MnCl_2$, $MgCl_2$, or $CoCl_2$ at similar concentrations. Washed cells (with reduced EPS) showed only 26.5% efficiency under $ZnCl_2$ (Aljuboori et al., 2016).

Table 1.4 (*Continued*).

Effect	Examples
Low Ca^{2+} reduced aggregation in *T. obliquus* under *Daphnia* infochemicals.	Data not reported (Hou et al., 2018).
High Ca^{2+} induced aggregation in *Microcystis aeruginosa.*	Ca^{2+} at 0.1 g L^{-1} promoted larger colonies and increased EPS production compared to 0.015 g L^{-1} (Wang et al., 2011).
Elevated CO_2 increased growth and defensive aggregation in *T. obliquus.*	Growth rate increased by 18% when CO_2 rose from 390 ppm to 750 ppm. Colony abundance increased in response to *Daphnia* filtrate under elevated CO_2 (Huang et al., 2018; Zhang et al., 2021).
Low N enhanced defensive aggregation in *T. obliquus* and *M. aeruginosa.*	In *T. obliquus* exposed to *Daphnia* infochemicals, colony abundance was higher at low N (2 mg L^{-1}) after three days compared to 32 mg L^{-1}; growth rate decreased by 6% at 2 mg L^{-1} (Zhu et al., 2015). In *M. aeruginosa*, aggregation in response to *Ochromonas* grazing increased when N was reduced to 10–25% of the typical BG-11 medium levels (255 mg L^{-1} N) (Wang et al., 2010).
Low N and P induced aggregation, while high N and P reduced colony size in *M. aeruginosa.*	Lowering N (1.98 mg L^{-1}) and P (0.65 mg L^{-1}) induced aggregation in *M. aeruginosa*. Reducing N and P while increasing C further enhanced EPS production. High N alone did not affect colony size, but high P alone significantly reduced it (Yang and Kong, 2013).
High P and combined high N and P reduced colony size in existing *M. aeruginosa* colonies.	In lake-water colonies, adding P alone (≥ 0.164 mg L^{-1}) or high P and N (≥ 0.328 mg L^{-1} P and ≥ 6.2 mg L^{-1} N) reduced colony size relative to the control. N addition alone (≥ 3.1 mg L^{-1}) had no effect (control: total P = 0.082 mg L^{-1}; total N = 1.55 mg L^{-1}) (Ma et al., 2014).

1.4.3 Temperature

Temperature influences self-aggregation primarily by altering metabolic processes such as photosynthesis, growth, and EPS production or consumption (**Table 1.5**). For example, elevated temperatures increased the growth rate of *M. aeruginosa*, but cells exhibited lower polysaccharide content and reduced colony size, likely because polysaccharides were mobilised for protein and nucleic acid synthesis to support rapid growth and division (Li et al., 2013).

Temperature can also modulate self-aggregation responses to other triggers. In *T. obliquus*, elevated temperatures inhibited self-aggregation induced by *D. magna* infochemicals. This inhibition may be linked to reduced CO_2 solubility at higher temperatures, which increases the energy required for CO_2-concentrating mechanisms and diverts resources away from carbohydrate synthesis needed for aggregation (Zhang et al., 2021; Zhu et al., 2019). High temperature further counteracted the positive effects of elevated CO_2 on both growth and aggregation, again due to decreased CO_2 solubility (Zhang et al., 2021).

Temperature exerts a dual effect: while moderate conditions support EPS production and colony stability, extreme heat or cold can either drive stress-induced aggregation or suppress it by diverting energy away from polysaccharide synthesis.

Table 1.5. Influence of temperature on microalgae aggregation.

Effect	Examples
Increased temperature enhanced growth in *Tetradesmus obliquus.*	Raising temperature from 25 °C to 31 °C increased growth rate (Zhang et al., 2021).
Elevated temperature inhibited aggregation in *T. obliquus* in response to *Daphnia* infochemicals.	Elevated temperature reduced abundance of eight-celled colonies in response to *Daphnia* infochemicals (Zhang et al., 2021). At 30 °C, colony size increase was only 55.4% of that at 25 °C (Zhu et al., 2019). Higher temperature also decreased colony abundance in controls after 96 h (Zhu et al., 2019).
Elevated temperature counteracted the enhancement effect of high CO_2 on defensive aggregation in *T. obliquus.*	High CO_2 enhanced aggregation in response to *Daphnia* infochemicals but high temperatures (31 °C) reduced this effect (Zhang et al., 2021).
Elevated temperature promoted the inhibition effect of Zn^{2+} on defensive aggregation in *T. obliquus*.	Warming enhanced the inhibition effect of Zn^{2+} on colony formation in response to *Daphnia* infochemicals (Zhu et al., 2019).
Elevated temperature increased growth rate in *Microcystis aeruginosa*, but reduced IPS, EPS, and colony size.	Between 15–30 °C, specific growth rate rose from 0.30 to 0.80 d^{-1}. EPS decreased from 0.82 to 0.18 pg $cell^{-1}$, with small colonies (< 100 μm) at low growth and single or paired cells at high growth (Li et al., 2013).
Temperature did not affect EPS concentration in *M. aeruginosa.*	Across 15–30 °C, EPS concentration remained unchanged (Yang and Kong, 2013).

1.4.4 Light

Light intensity and quality strongly influence self-aggregation (**Table 1.6**). For instance, *C. reinhardtii* co-cultured with the predator *Brachionus calyciflorus* under continuous illumination (one-stage system) lost their flagella, secreted EPS, and formed colonies. By contrast, in a two-stage system where *C. reinhardtii* was transferred into a predator-containing vessel kept in the dark, predation rates were higher and mean aggregate size was lower. In the two-stage system, 76 ± 20% of the population remained unicellular compared with 46 ± 14% in the one-stage illuminated system (Lurling and Beekman, 2006). These findings indicate that light is a prerequisite for colony formation, consistent with Boraas et al. (1998), who showed that *Chlorella* colonies induced by *Ochromonas* were stable under continuous light but disassembled rapidly in the dark.

Light can influence self-aggregation both through its role in supported metabolism and by causing photo-oxidative stress. At elevated intensities, aggregation has been interpreted as a protective response to shield cells from excess light (Suwannachuen et al., 2023). For example, a *C. reinhardtii* strain isolated from ~4,000 m elevation (and thus pre-adapted to oxidative stress) formed palmelloids in response to high light: after two days of exposure to 1000 μmol photons m^{-2} s^{-1}, 80–90% of cells were in palmelloids compared to only 5–10% at 50 μmol photons m^{-2} s^{-1}. By contrast, a light-sensitive strain of the same species exhibited < 5% of cells in palmelloids under high light and showed clear signs of photodamage.

Light quality also plays a role. UVB exposure reduced growth and self-aggregation in *T. obliquus* exposed to *D. magna* infochemicals (Sun et al., 2020). Mechanistically, UVB inhibited RuBisCo (carbon assimilation), phosphoglucomutase (carbon flux toward polysaccharide synthesis), and ADP-glucose pyrophosphorylase (starch synthesis), ultimately lowering polysaccharide availability and aggregation capacity (Sun et al., 2020).

Together, these studies show that light acts as both an enabler and a stressor, driving aggregation through metabolic support or as a defence against photodamage, but also constraining aggregation when photosynthetic processes are inhibited.

Table 1.6. Influence of light intensity and UVB on microalgae aggregation.

Effect	Example
High light intensity increased growth rate in *Microcystis aeruginosa*, but reduced IPS, EPS, and colony size (see also **Table 1.5**).	At 25 °C, max. growth rate (~0.70 d^{-1}) occurred at 60 μmol m^{-2} s^{-1}; min. (0.29 d^{-1}) occurred at 10 μmol m^{-2} s^{-1} (25 °C) and 30 μmol m^{-2} s^{-1} (15 °C) (Li et al., 2013).
Medium light intensity maximised growth rate in *M. aeruginosa.*	At 25 °C, the highest growth rate (0.13 d^{-1}) occurred at 40 μmol m^{-2} s^{-1}, compared to lower rates at 5 and 100 μmol m^{-2} s^{-1} (Yang and Kong, 2013).
High light intensity increased EPS in *M aeruginosa.*	EPS peaked at 2.43 ± 34 pg $cell^{-1}$ at 100 μmol m^{-2} s^{-1}, compared to ~1.5 pg $cell^{-1}$ at 5 and 40 μmol m^{-2} s^{-1} (Yang and Kong, 2013).
High light intensity induced aggregation in *M aeruginosa* in response to *Daphnia* infochemicals.	In toxic wild-type strain PCC 7806, aggregation occurred at 120 μmol m^{-2} s^{-1} but not at 40 μmol m^{-2} s^{-1} (Becker, 2010).
Light was essential for *Chlamydomonas reinhardtii* aggregation in response to *Brachionus calyciflorus.*	Under continuous illumination, *C. reinhardtii* lost flagella, secreted EPS, and formed colonies in response to the predator. Fewer cells aggregated in darkness (Lurling and Beekman, 2006).
UVB inhibited colony formation in *T. obliquus* in response to *Daphnia.*	UVB reduced colony formation, daughter cell production, and growth rate. Effects were more severe with *Daphnia* infochemicals. Photosynthetic machinery was significantly impaired (Sun et al., 2020).

1.5 Physical mechanisms of self-aggregation

1.5.1 Predator infochemicals

Microalgae can detect chemical cues secreted by predators, known as *infochemicals*, and respond by self-aggregating (**Figure 1.3**). These cues are typically tested by exposing algal cultures to filtered medium that previously contained grazers. For example, *Daphnia* filtrate has been shown to induce aggregation in *Chlamydomonas reinhardtii* (Berger, 2017)*, Chlorella sorokiniana* (Kapsetaki et al., 2017)*, Chlorella vulgaris* (Fisher et al., 2016), *Scenedesmus acutus* (O'Donnell et al., 2012), and *Tetradesmus obliquus*. Because this is an inducible defence, the response is reversible: cells typically disaggregate when transferred into predator-free medium (Albini et al., 2019; Fisher et al., 2016; Sathe and Durand, 2016; Wu et al., 2013). In some cases, however, cue activity diminishes over time: Wu et al. (2013) reported that the proportion of eight-celled *T. obliquus* colonies decreased between days 5–7 of exposure, likely because the infochemicals degraded. Other studies that examined the reversibility of predator-induced self-aggregation are summarised in **Table 1.7.**

Beyond *Daphnia*, infochemicals from a range of predators have been showed to trigger algal aggregation, including the rotifer *Brachionus* (Lorusso, 2018), the flagellate *Ochromonas* (Yang et al., 2009), the euglenoid *Peranema* (Sathe and Durand, 2016), and the ciliate *Tetrahymena* (Kapsetaki et al., 2016).

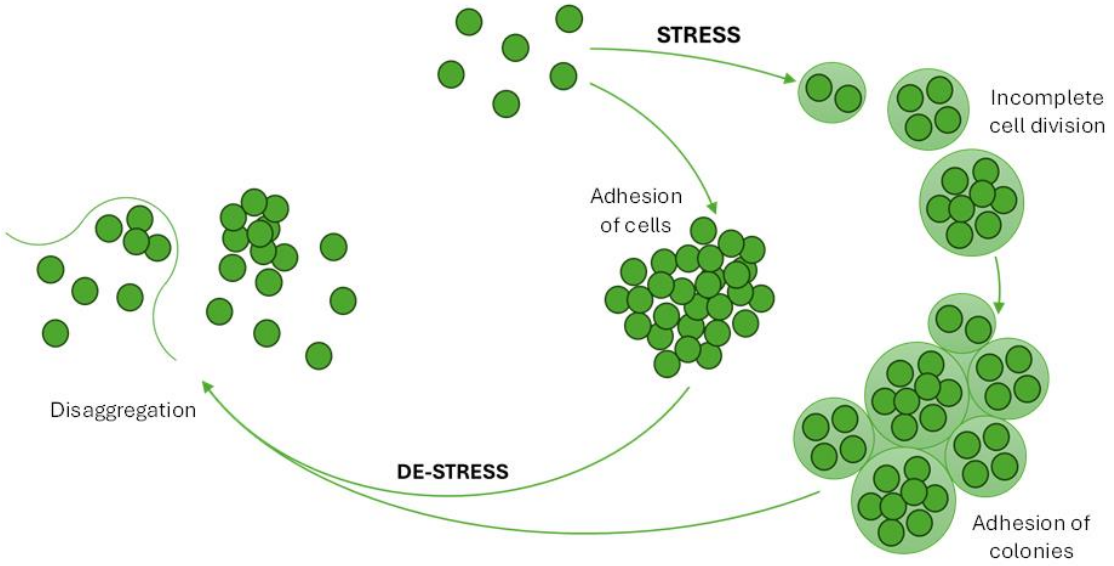

Figure 1.3. Mechanisms of self-aggregation: colony formation via incomplete cell division, and aggregate formation via EPS-mediated adhesion.

Although bioassays with predator filtrates are widely reported, the chemical identity of active infochemicals has only been characterised in a few cases. A series of studies isolated and identified compounds from *Daphnia pulex* that trigger colony formation in *Scenedesmus gutwinskii* (Yasumoto et al., 2008a, 2008b; Yasumoto et al., 2006; Yasumoto et al., 2005). Most of the 23 compounds were aliphatic sulphates and sulfamates (**Table 1.8**), a rare class of molecules in nature. Nearly 50 aliphatic sulphates and sulfamates have been isolated from marine invertebrates (Kellner Filho et al., 2019), and 22 of these were reported to induce defensive morphologies in microalgae, *Daphnia*, and marine invertebrates. These molecules combine a sulphate group with a long hydrophobic chain, giving them surfactant-like properties (Kellner Filho et al., 2019). The counter-ions were not identified but are presumed to be Na^+.

More recently, Nam et al. (2024) reported chemical cues from *Daphnia magna* and *Daphnia galeata* that affected the cyanobacterium *Microcystis aeruginosa*. Chemicals identified by LC-MS from both *D. magna* and *D. galeata* were: methyl ferulate, cyclohexanone, 3, 5-dimethyl, hexanedioic acid, bis(2-ethylhexyl) ester, erythritol, hydroxybutanoic acid, ergosterol, 9, 10 anthracenedione, 2-ethyl, and hydrocortisone acetate. Additionally, the chemicals identified from *D. galeata* were: 2-propanol, 1, 3-dichloro-, p-tolyl acetate, linoleic acid, and 1, 4-benzenedicarboxylic acid, methyl ester. Chemicals identified by GC-MS from both *D. magna* and *D. galeata* were, diethyl phthalate, proxyphylline, isobutyl acetate, 1, 2-benzenedicarboxylic acid, bis, 1-tridecene, oleic acid, methyl ester, and n-hexadecanoic acid.

These chemicals elicited an increase in the level of reactive oxygen species and the concentration of microcystin-LR, an increased colony formation, and inhibition of *M. aeruginosa* growth (Nam et al., 2024). However, this study primarily investigated the correlation between these infochemicals and the concentration of *M. aeruginosa* cells rather than colony formation. Both growth and colony formation were influenced by these chemicals, but the presence of these chemicals was not directly correlated with self-aggregation. Therefore, further investigation is needed to define the mechanisms of colony formation in *M. aeruginosa* following exposure of the cultures to infochemicals. Interestingly, some of these infochemicals were only detected in groups in which the *Daphnia* had been pre-exposed to *M. aeruginosa*, suggesting that the production of such chemicals was a direct consequence of the interaction between *M. aeruginosa* and *Daphnia*.

Table 1.7. Reports on growth rate and reversibility of self-aggregation.

Microalgae	Aggregation trigger	Growth rate	Aggregation reversibility	Reference
Tetradesmus obliquus	*Daphnia* filtrate	Decreased	Reversible	a
		No change	Not stated	b,c,d,e,f,g
		No change	Reversible	h
		Increased	Not stated	i
	+UVB	Decreased	Not stated	i
	Anionic surfactants	No change	Not stated	j
Scenedesmus acutus	*Daphnia* filtrate	No change	Not stated	k, l
Scenedesmus subspicatus	*Daphnia* filtrate	No change	Not stated	m
Microcystis aeruginosa	*Daphnia* filtrate			
	(high light)	No change	Not stated	n
	(low light)	Decreased	Not stated	n
	Microcystins	No change	Not stated	o
	Low light	Decreased	Not stated	p
	Daphnia filtrate	Decreased	Not stated	q
	Ochromonas filtrate	No change	Not stated	r
Chlorella vulgaris	*T. thermophila*	No change	Reversible	s
Chlorella sorokiniana	*Daphnia* filtrate			
	(darkness)	Decreased	Not reversible	t
	(illuminated)	No change	Reversible	t
Chlamydomonas reinhardtii	PFOS	Decreased	Reversible	u
	Cadmium	Decreased	Reversible	u
	NaCl salt stress	Not stated	Reversible	v
	Brachionus	No change	Not stated	w
	High light stress	Decreased	Not stated	x
	Naphthenic acid	Decrease	Not stated	y
Mutant CC-3395	Naphthenic acid	No change	Not stated	y

Reference letters correspond to the following sources:

a (Albini et al., 2019); b (Hou et al., 2018); c (Huang et al., 2018); d (Huang et al., 2016); e (Jia et al., 2023); f (Zhu et al., 2016); g (Zhu et al., 2017); h (Wu et al., 2013); i (Sun et al., 2020); j (Lürling and Beekman, 2002); k (Lampert et al., 1994); l (O'Donnell et al., 2012); m (Roccuzzo et al., 2020); n (Becker, 2010); o (Gan et al., 2012); p (Li et al., 2013); q (Nam et al., 2024); r (Yang et al., 2009); s (Fisher et al., 2016); t (Kapsetaki and West, 2019); u (Cheloni and Slaveykova, 2021); v (Khona et al., 2016); w (Lurling and Beekman, 2006); x (Suwannachuen et al., 2023); y (Goff et al., 2013).

Table 1.8. Infochemicals produced by *Daphnia pulex* which induce self-aggregation in *Scenedesmus gutwinskii* (Yasumoto et al., 2008a, 2008b; Yasumoto et al., 2006; Yasumoto et al., 2005). The active concentrations are shown where reported.

Structure	Molecular formula	Concentration in *Daphnia* (µg g^{-1})	Active concentration (ng mL^{-1})	Ref.
dec-3-en-1-yl sulphate	$C_{10}H_{19}O_4S^-$	0.64	1–1000	a
dodeca-3,6-dien-1-yl sulphate	$C_{12}H_{21}O_4S^-$	0.04	10–1000	a
dodeca-3,6,9-trien-1-yl sulphate	$C_{12}H_{19}O_4S^-$	0.07	100–1000	a
8-methylnon-1-yl sulphate (isodecyl sodium sulphate)	$C_{10}H_{21}O_4S^-$	0.02	0.1–1000	a
octyl sulphate	$C_8H_{17}O_4S^-$	0.02	1–1000	a
decyl sulphate	$C_{10}H_{21}O_4S^-$	0.32	1–1000	a
2,6-dimethylheptyl sulphate	$C_9H_{19}O_4S^-$	0.90		b
6-methyloctyl sulphate	$C_9H_{19}O_4S^-$	0.5		b
7-methyloctyl sulphate	$C_9H_{19}O_4S^-$	0.8		c
3-decenyl sulphate	$C_{10}H_{19}O_4S^-$	0.05		c
9-methyldec-3-en-1-yl sulphate	$C_{11}H_{21}O_4S^-$	0.03		c
4,7-decadienyl sulphate	$C_{10}H_{17}O_4S^-$	0.38		c
3-dodecenyl sulphate	$C_{12}H_{23}O_4S^-$	0.05		c
3-decenyl sulfamate	$C_{10}H_{20}O_3NS^-$	0.8		c
3,6-dodecadienyl sulfamate	$C_{12}H_{22}O_3NS^-$	0.04		c
decyl sulfamate	$C_{10}H_{22}O_3NS^-$	0.08		c
nonyl sulfamate	$C_9H_{20}O_3NS^-$	0.06		c
octyl sulfamate	$C_8H_{18}O_3NS^-$	0.15		c
9-methyldecyl sulfamate	$C_{11}H_{24}O_3NS^-$	0.01		c
8-methylnonyl sulfamate	$C_{10}H_{22}O_3NS^-$	0.02		c
7-methyloctyl sulfamate	$C_9H_{20}O_3NS^-$	0.15		c
4,8-dimethylnonyl sulphate	$C_{11}H_{23}O_4S^-$	0.2		d
3-methyl-4-decenyl sulphate	$C_{11}H_{21}O_4S^-$	0.08		d

Reference letters correspond to the following sources:

a (Yasumoto et al., 2005); b (Yasumoto et al., 2006); c (Yasumoto et al., 2008b); d (Yasumoto et al., 2008a).

1.5.2 Cell-cell communication

Intraspecific cell-to-cell communication via chemical cues is well documented in bacteria, fungi, and algae. Microalgae not only respond to chemical cues from other species but may also secrete chemicals to signal to neighbouring conspecifics (Marianna et al., 2017; Van Donk et al., 2011). Although microalgae are thought to release molecules that trigger self-aggregation or alert populations to predators or stress, these compounds have not yet been identified. Evidence for such signalling comes from *C. reinhardtii*, where filtered medium from heat-shocked, aggregated cultures was able to induce aggregation in non-stressed cells, suggesting the presence of a transferable "aggregation signal" (de Carpentier et al., 2022). Identifying such molecules could enable novel, low-cost methods to deliberately trigger self-aggregation for harvesting purposes.

Volatile organic compounds (VOCs) released by microalgae are hypothesized to play roles in intercellular communication, including predator signalling (Havaux, 2014; Zuo, 2019). VOCs mediate a wide range of ecological interactions (Saha and Fink, 2022). For example, the marine microalga *Microchloropsis salina* released VOCs when grazed by the rotifer *Brachionus plicatilis*, including β-cyclocitral, a carotenoid-derived signal also known to form in plants under photooxidative stress (Havaux, 2014; Reese et al., 2019). Oxidized carotenoids such as β-cyclocitral can alter expression of stress-resistance genes (Havaux, 2014). In cyanobacteria, *Microcystis* releases β-cyclocitral as a defence against *D. magna*, inducing predator swimming velocity and potentially altering grazing behaviour (Jüttner et al., 2010). Other algae, including diatoms, defend against predation by releasing chemical toxins (Zuo, 2019).

Microchloropsis release of VOCs was also observed under predator exposure, although it remains unclear whether this is a targeted defence response (Reese et al., 2019). In *C. reinhardtii*, VOC emissions increased under oxidative stress, light, and temperature stress, as well as during nutrient deficiency and changes in salinity or acidity (Zuo, 2019). Acetic acid and salt stresses, for instance, induced the population-wide production of antioxidant enzymes, suggesting that stressed cells may release a diffusible warning signal (Zuo et al., 2012a; Zuo et al., 2012b). Similarly, in *T. obliquus*, stress-associated metabolites such as astaxanthin esters were reported in cultures that formed colonies in response to *Daphnia* (Albini et al., 2019).

Understanding how microalgae release chemical cues, whether to communicate with conspecifics or to influence predator behaviour, remains an open field of research (Saha and

Fink, 2022). Whether cell–cell communication underlies stress-induced self-aggregation is still uncertain. However, current evidence suggests that microalgae can produce aggregation-related chemical signals, both to coordinate population-level responses and to alter predator interactions.

1.5.3 Aggregate formation

Self-aggregation has been reported as a stress response, resulting either in small, uniform colonies in which cells may share a wall or membrane, or in large, irregular aggregates (Goff et al., 2013; Herron et al., 2019; Kapsetaki et al., 2017; Sun et al., 2020) (See **Figure 1.3**). Two primary mechanisms are thought to underlie aggregation: incomplete cell division and cell adhesion, both of which may involve the increased synthesis of extracellular polysaccharides (EPS) (Harke et al., 2017; Sun et al., 2020; Yang et al., 2007).

1.5.3.1 Role of extracellular polysaccharides (EPS)

EPS facilitates colony formation by enveloping daughter cells after division and promoting adhesion between neighbouring cells, leading to the development of large, sinking colonies (Khona et al., 2016; Xiao et al., 2018; Yang et al., 2007). EPS can also protect cells from digestion by grazers (Lurling and Beekman, 2006).

1.5.3.2 Palmelloids as a protective strategy

Palmelloid formation in *Chlamydomonas* represents a distinct morphological defence, where daughter cells remain enclosed within a shared mother cell wall. This structural barrier shields cells from hostile environments. For instance, Cheloni and Slaveykova (2021) showed that palmelloids resisted micropollutant damage, while single cells were harmed. Similarly, *C. reinhardtii* palmelloids withstood exposure to rose Bengal (singlet oxygen), heat shock, and nitrosative stress, while single cells were killed (de Carpentier et al., 2022).

1.5.3.3 Influence of the cell wall

Cell wall modifications may also influence aggregation. The cell-wall deficient mutants of *C. reinhardtii*, CC-400 and CC-3395, did not aggregate in response to the surfactant that triggered self-aggregation in wildtype cells (Goff et al., 2013). These results suggest that self-aggregation is strongly influenced by cell wall properties.

1.5.3.4 Species-specific mechanisms

The mechanisms driving aggregation and the resulting colony sizes differ across species. In some algae, colony formation is primarily due to incomplete cell division. For example, *T. obliquus* and *S. gutwinskii* exposed to predator infochemicals formed mostly two-, four-, and eight-celled colonies (binary fission multiples), rather than colonies with three, five, or six cells (Sun et al., 2020; Yasumoto et al., 2005). Similarly, *Chlamydomonas* palmelloids also contain 4, 8, or 16-cells, sometimes encased by multiple cell walls (Cheloni and Slaveykova, 2021; Khona et al., 2016).

Other species show dual mechanisms. *C. sorokiniana*, *C. vulgaris*, and *T. obliquus* exposed to *D. magna* formed colonies through both adhesion of existing cells and incomplete division (Kapsetaki et al., 2017).

1.5.3.5 Mixed-species aggregation

Microalgae can also form mixed-species aggregates. *C. sorokiniana*, *C. vulgaris*, and *T. obliquus* have been observed to co-aggregate in response to *D. magna* (Kapsetaki et al., 2017). Within these aggregates, adhesion was the dominant process: 94% of *C. sorokiniana*, 62% of *C. vulgaris*, and 44% of *T. obliquus* cells were present in adhesion-based colonies, while the rest resulted from incomplete division.

Although mixed-species aggregates do occur, cells preferentially aggregate with conspecifics. The tendency toward mixed aggregates appears to depend more on cell size and motility than on genetic relatedness (Sathe and Durand, 2016).

1.5.4 Growth rate

While cell division itself can contribute to colony formation, the overall growth rate varies among self-aggregating microalgae (see **Table 1.7**). In *M. aeruginosa*, light intensity strongly influenced growth, which in turn affected colony size. Cells grew faster under moderate light (40–60 μmol m^{-2} s^{-1}) than under higher light (100–120 μmol m^{-2} s^{-1}). Faster growth was associated with decreased EPS concentrations and the formation of smaller, less abundant colonies (Li et al., 2013; Yang and Kong, 2013)

This pattern has been interpreted as a trade-off between growth and aggregation. In photosynthetically growing microalgae, the production of photosynthate and the degradation of polysaccharides supply carbon for protein and nucleic acid synthesis during rapid growth. These metabolic pathways may compete with EPS production, reducing the resources available for aggregation (Li et al., 2013).

By contrast, in *T. obliquus*, which formed coenobia through cell division, growth rate appears more strongly influenced by environmental factors such as Mg^{2+} concentration (Hou et al., 2018), Cu^{2+} (Huang et al., 2016), elevated CO_2 (Huang et al., 2018), Cd^{2+}, and salinity (Jia et al., 2023). Notably, exposure to *Daphnia* filtrate, while inducing aggregation, did not significantly affect the growth rate itself.

1.6 Genetic basis of self-aggregation

1.6.1 Transcriptomic studies

Several studies have examined the molecular basis of self-aggregation in stressed microalgae. In *Chlamydomonas reinhardtii*, transcriptomic analyses found 151 differentially expressed genes (DEGs) in cells exposed to live *Daphnia magna* compared to unaggregated controls, and identified five potential candidates for facilitating self-aggregation (Berger, 2017). Another study of *C. reinhardtii* aggregates triggered by *Brachionus calyciflorus* found that upregulated genes were associated with stress responses, nutrient assimilation, nucleic acid binding and modification, cell-cycle regulation, and the extracellular matrix (Lorusso, 2018). Genomic and proteomic analyses of *C. reinhardtii* also revealed aggregation responses to abiotic stressors (de Carpentier et al., 2022; Khona et al., 2016).

In *Tetradesmus obliquus*, self-aggregation in response to *D. magna* exposure involved changes in polysaccharide synthesis and cell signalling (Sun et al., 2020; Zhu, Sun, et al., 2021).

In *Microcystis aeruginosa,* exposure to live *Daphnia* induced more DEGs with stronger expression than exposure to *Daphnia* infochemicals alone (Harke et al., 2017). While *Microcystis* was previously thought to deter grazing with secondary metabolites such as microcystin, aeruginosin, cyanopeptolin, and microviridin, the genes encoding these pathways were not differentially expressed in response to predator cues (Harke et al., 2017). Instead, transcriptomic analyses identified stress- and growth-related responses, including upregulation of 11 heat shock protein genes (Harke et al., 2017). Another study, linked microcystin production in three *Microcystis* species to enhanced colony size and increased expression of polysaccharide synthesis genes (Gan et al., 2012).

1.6.2 Self-aggregation and the evolution of multicellularity

Facultative self-aggregation in microalgae has been proposed as an evolutionary stepping stone towards multicellularity. The emergence of multicellular morphotypes in unicellular algae under environmental pressure provides a possible model for this transition (Hanschen et al., 2016; Kapsetaki and West, 2019). For example, *Chlorella vulgaris* retained an eight-celled morphology indefinitely after continuous culture with the predator *Ochromonas*, suggesting

that persistent external pressure can lock in new morphologies (Boraas et al., 1998). Similarly, *C. reinhardtii* evolved stable multicellular structures after long-term exposure to predation by *Paramecium tetraurelia* (Herron et al., 2019).

Comparative genomic studies support this link. DEGs identified in *C. reinhardtii* during predation (Berger, 2017; Lorusso, 2018) were compared with the genomes of the Volvocine algae such as *Volvox carteri* and *Gonium pectorale*, which diverged from a *Chlamydomonas*-like ancestor. In *V. carteri*, 82% of the DEGs upregulated during aggregation were expanded, while 73% of downregulated DEGs were constricted (Lorusso, 2018). These patterns suggest that genes associated with stress-induced aggregation in *Chlamydomonas* may have been co-opted during the evolution of multicellularity in Volvocales.

1.6.3 Cell cycle regulation

Changes in cell cycle regulation are thought to represent one of the earliest steps in the evolution of multicellularity (Hanschen et al., 2016). Undifferentiated colonies often arise from failures in daughter cell separation–a process linked to modification in cyclin-dependent kinases genes. Comparative genomics indicates that *V. carteri* and *G. pectorale* possess cell cycle regulatory genes derived from *C. reinhardtii* (Hanschen et al., 2016; Lorusso, 2018). For instance, *Gonium* colonies form through incomplete separation of daughter cells following multiple fission, the same mechanism seen in unicellular *Chlamydomonas* (Hanschen et al., 2016).

Transcriptomic studies have reinforced this link. Lorusso (2018) reported that five cell cycle regulatory genes in *C. reinhardtii* were differentially expressed during aggregation induced by *B. calyciflorus*. Beyond green algae, similar patterns have been found in other phytoplankton: in the chain-forming diatom *Skeletonema marinoi*, copepod grazing reduced chain length, accompanied by regulation of nine cyclin genes (Amato et al., 2018). Together, these findings support the hypothesis that modifications to cell cycle regulation played a central role in both facultative self-aggregation and the evolution of multicellularity.

1.6.4 Changes to cell structure and metabolic pathways

1.6.4.1 Extracellular matrix

Genes encoding pherophorins, matrix metalloproteinases (MMPs), and hydroxyproline-rich glycoproteins are likely involved in *C. reinhardtii* self-aggregation (Berger, 2017; de Carpentier et al., 2022; Khona et al., 2016; Lorusso, 2018). Pherophorins are glycoproteins found in the extracellular matrix (ECM) of *Volvocales* (Berger, 2017; Godl et al., 1995). Together with MMPs, they contribute to ECM structure and also participate in degrading cell wall components (Hanschen et al., 2016). The ECM is important for connecting cells in temporary and permanent colonies (Lorusso, 2018).

During *C. reinhardtii* self-aggregation in response to predation, six pherophorin genes were differentially expressed (Berger, 2017; Lorusso, 2018). Pherophorins, MMPs, and hydroxyproline-rich glycoproteins have also been linked to palmelloid formation and disaggregation under light and NaCl stress (Khona et al., 2016; Suwannachuen et al., 2023). Some glycoproteins and MMPs were upregulated during stress-induced palmelloid formation, while others were upregulated during recovery and disaggregation, suggesting that these proteins play a role in both palmelloid formation and disaggregation (Khona et al., 2016).

Proteomic and transcriptomic analyses of *C. reinhardtii* aggregates exposed to abiotic stress identified 131 deregulated proteins in wildtype cultures compared to aggregated mutants, including 16 pherophorins and several MMPs (de Carpentier et al., 2022). Importantly, three mutants deficient in pherophorin genes lost their ability to self-aggregate, demonstrating that pherophorins are essential for aggregation (de Carpentier et al., 2022). Other ECM-associated proteins identified in these studies included VSPs and lysyl oxidases (de Carpentier et al., 2022).

The evolution of a more complex ECM has been proposed as a key step in the transition to multicellularity. The second evolutionary phase–organismal side increase–has been associated with expansion of pherophorin and MMP gene families (Hanschen et al., 2016). Co-option of ECM-related genes for new functions was likely critical for establishing multicellular organisation (Hallmann, 2006; Olson and Nedelcu, 2016). At least 15 pherophorins have been identified as structural building blocks of the ECM in *C. reinhardtii*, *G. pectorale* and *V. carteri* (Hallmann, 2006). Several pherophorin genes identified as DEGs in *C. reinhardtii* are also

present, albeit modified, in the *V. carteri* genome (Berger, 2017; Lorusso, 2018). The specific structure of pherophorins determines ECM mesh size, which in turn defines colony architecture (Hallmann, 2006). The dominance of ECM in *Volvox* morphology highlights why pherophorin and MMP gene families are expanded in *Volvox* relative to *Chlamydomonas* (Hanschen et al., 2016).

1.6.4.2 Polysaccharides

There is evidence that genes involved in polysaccharide production are involved in self-aggregation in *T. obliquus* and *Microcystis*, and Khona et al. (2016) reported increased EPS content during palmelloid formation in *C. reinhardtii*. However, expression of polysaccharide-related genes/proteins in self-aggregating *C. reinhardtii* was not reported in studies previously discussed (Berger, 2017; de Carpentier et al., 2022; Khona et al., 2016; Lorusso, 2018) or in other studies of *C. reinhardtii* palmelloid-formation (Cheloni and Slaveykova, 2021; Lurling and Beekman, 2006; Suwannachuen et al., 2023). As noted earlier, the EPS content is generally observed to increase in microalgae undergoing self-aggregation, and analyses of the *T. obliquus* and *Microcystis* genomes report upregulation of polysaccharide-related genes during self-aggregation in response to predation. Other proteins potentially related to EPS formation reported to increase during *C. reinhardtii* aggregation are related to catabolism, glycosylation, and sugar binding (de Carpentier et al., 2022). The same study identified four ephrin A/B receptor-like proteins that may mediate cell-cell adhesion (de Carpentier et al., 2022).

In *T. obliquus*, self-aggregation in response to *D. magna* infochemicals has been linked with regulation of three key polysaccharide biosynthesis genes: *RuBisCO* (encodes ribulose-1,5-biphosphate carboxylase/oxygenase), *PGM* (encodes phosphoglucomutase) and *ADPase* (encodes ADP-glucose pyrophosphorylase) (Sun et al., 2020). Exposure to *D. magna* infochemicals elicited increased expression of all three genes, while exposure to UVB (in the presence of infochemicals) diminished their expression and also reduced the extent of aggregation. Regardless of the UVB levels, *PGM* was always expressed more when *D. magna* infochemicals were present and is likely key to polysaccharide production and the aggregation response. This is consistent with *PGM's* importance as a regulatory gene for polysaccharide biosynthesis in both prokaryotes and eukaryotes (Sun et al., 2020).

Further work supports this link: *T. obliquus* exposed to *D. magna* infochemicals showed increased EPS and altered 54 metabolites, alongside upregulation of polysaccharide production

and signal transduction genes (Zhu, Sun, et al., 2021). Aggregated cells exhibited elevated lipid content and downregulation of ribosome-related pathways, suggesting a metabolic trade-off favouring lipid synthesis and EPS production over growth and protein synthesis (Zhu, Sun, et al., 2021). These results are consistent with the reported downregulation of lipase genes during *C. reinhardtii* aggregation (de Carpentier et al. (2022).

In *Microcystis*, 22 DEGs potentially linked to EPS synthesis were identified during exposure to *Daphnia* (Harke et al., 2017). In addition, cultures treated with microcystin-RR showed enhanced EPS production and upregulation for genes for capsular and exopolysaccharide synthesis, including *capD*, *tagH*, *csaB*, and *epsL* (Gan et al., 2012; Xiao et al., 2018). Together, these findings suggest that although *C. reinhardtii* shows inconsistent transcriptional signatures, polysaccharide biosynthesis is a conserved feature of aggregation in *T. obliquus* and *Microcystis.*

1.6.4.3 Flagella and motility

Genes related to flagella and motility are differentially expressed during self-aggregation, with genes associated with the flagellum potentially involved in the evolution of multicellularity in some algae. In *C. reinhardtii*, two flagella proteins were upregulated during recovery from salinity stress (Khona et al., 2016), whereas 18 of the 20 most downregulated DEGs in during *B. calyciflorus*-induced aggregation were linked to flagella and motility (Lorusso, 2018). Among these were *tubA1*, *tubB1*, and *dyhA*, which encode tubulins and dynein–structural components of the flagellum–and are thought to have had roles in the development of multicellularity (Klein et al., 2017; Lorusso, 2018). The flagella-associated protein gene *FAP139* was also differentially expressed in response to predation (Berger, 2017).

The flagella in *C. reinhardtii* are known to mediate adhesion during mating, suggesting that motility structures may also facilitate cell-to-cell adhesion during aggregation (Berger, 2017). In cyanobacteria, predator cues may regulate analogous structural adaptations: two genes related to gas vesicle proteins were significantly upregulated in *Microcystis* exposed to *D. magna* and *D. pulex* infochemicals (Harke et al., 2017). Gas vesicles can alter buoyancy, allowing cells to adjust vertical position in the water column as a predator-avoidance strategy (Harke et al., 2017).

These findings highlight that in addition to EPS and ECM pathways, motility and buoyancy genes contribute to the aggregation response, either by regulating adhesion directly (*Chlamydomonas*) or by enabling spatial escape from predators (*Microcystis*).

1.6.5 Cell signalling cascades

Expression of calcium-calmodulin signalling genes were enriched in *C. reinhardtii* exposed to *D. magna,* suggesting that signal cascades may be involved in predator detection and initiation of self-aggregation (Berger, 2017). However, beyond this observation, few studies have reported signalling cascades involved in *C. reinhardtii* aggregation, and further research is needed.

In *T. obliquus*, several signalling-related DEGs were identified following exposure to *D. magna* (Zhu, Sun, et al., 2021). These included *SnRK2*, which encodes a protein involved in stress resistance and environmental stress signalling (including sulfur deprivation) in plants and *C. reinhardtii* (González-Ballester et al., 2010; Kulik et al., 2011). Another upregulated transcript, *c72720_g1*, encodes a G-protein-coupled receptor (GPCR), suggesting a role in infochemical detection (Zhu, Sun, et al., 2021). GPCR responses are thought to activate the phosphatidylinositol C family (PLC) signalling pathway, consistent with increased expression of PLC-related genes (*c29068_g1* and *c31227_g1*) (Zhu, Sun, et al., 2021). GPCRs are transmembrane receptors that sense extracellular molecules and trigger intracellular signalling, while GTPases (G-proteins) serve as central regulators of GPCR-mediated cascades (Goldsmith and Dhanasekaran, 2007).

Evidence from other taxa supports a role for GPCR- and MAPK (mitogen-activated protein kinase)-mediated pathways in algal stress and aggregation responses. In the diatom *S. marinoi*, GPCR signalling was implicated in responses to copepod grazing (Amato et al., 2018). MAPK cascades, which often act downstream of GPCRs (Naor et al., 2000), regulate growth, development, and cell division in plants, and mediate signalling under biotic and abiotic stress (Livanos et al., 2012; Pitzschke et al., 2009). MAPK involvement in algal aggregation has been directly shown in *Scenedesmus subspicatus*: proteomic analysis linked predator-induced aggregation to MAPK signal transduction (Roccuzzo et al., 2020).

MAPK signalling also contributes to cell wall regulation, ECM production, adhesion, and biofilm formation in fungi, such as *Aspergillus fumigatus* (Manfiolli et al., 2018). In *C.*

reinhardtii, a G-protein α-subunit has been reported to mediate heat and osmotic stress responses via a MAPK pathway (Lee et al., 2017). In *Microcystis*, the gene encoding a histidine kinase – a sensor involved in stress signalling – was upregulated following exposure to *Daphnia* infochemicals (Harke et al., 2017).

These observations suggest that predator cues may activate self-aggregation in microalgae through GPCR- and MAPK-mediated signalling cascades, although further research is needed to determine the full signalling pathways mediating predator sensing and self-aggregation.

1.6.6 Other genes

In addition to the gene categories discussed above, other genes have been reported as differentially expressed during predation-triggered self-aggregation.

Membrane and light response

Of the 20 most downregulated DEGs detected in *C. reinhardtii* exposed to *B. calyciflorus*, two were associated with membrane coat proteins and light response (Lorusso, 2018).

Septins

The gene *LCI23*, an ortholog of septin, was upregulated in *C. reinhardtii* (Berger, 2017). Septins are cytoskeletal proteins involved in cytokinesis and in processes such as sporulation and conjugation, suggesting a role in cell division-linked aggregation responses.

Cellulases

An ortholog of a cellulase gene (Cre06.g270500) was upregulated in *C. reinhardtii* (Berger, 2017). Since cellulases are involved in plant cell wall remodelling, they may also function in microalgal aggregation through modification of the cell wall. Interestingly, this cellulase was upregulated when aggregation had already slowed, leading Berger (2017) to propose a role in aggregate dispersal rather than formation.

Transmembrane protein

A gene encoding a putative transmembrane protein (*g18292*) was upregulated in *C. reinhardtii* exposed to live *D. magna* (Berger, 2017). This gene is also present in the colonial alga *G. pectorale*. Transformation of *C. reinhardtii* with the *Gonium* ortholog of *g18292* resulted in a

multicellular phenotype, with 72% of cells occurring in colonies compared to 5% in wildtype and 90% in *Gonium*. Because these colonies persisted over multiple sub-culturings, *g18292* appears to promote both temporary and permanent aggregation. Its dual role in predator-induced self-aggregation and stable multicellularity suggests that co-option of aggregation-related genes contributed to multicellularity in the *Volvocales*.

RLS1 and the *regA* gene cluster

The *RLS1* gene was differentially expressed in *C. reinhardtii* during self-aggregation, consistent with earlier reports linking *RLS1* to stress responses (Nedelcu, 2009). *RLS1* is present in both *C. reinhardtii* and *Gonium* and is the closest homolog to the *regA* gene cluster of *Volvox.* The *regA* cluster regulates somatic differentiation by repressing growth and reproduction in soma cells, a key innovation in the evolution of multicellularity (Hanschen et al., 2016; König and Nedelcu, 2020; Lorusso, 2018). Although absent in *Gonium*, *regA* is present in *Volvox*, suggesting that the gene cluster was co-opted after divergence of the *Gonium* and *Volvox* lineages. Importantly, *regA* appears to have retained a role in stress response even after neofunctionalisation for soma differentiation (König and Nedelcu, 2020).

Stress and metabolism in *T. obliquus*

In *T. obliquus*, predator exposure upregulated three calcium-dependent protein kinases genes (plant-pathogen interaction pathways), three genes involved in intracellular redox processes (glutathione S-transferase, cytochrome P450, and ubiquinol-cytochrome C reductase), and one gene encoding magnesium chelatase, an enzyme critical for chlorophyll biosynthesis (Zhu, Sun, et al., 2021).

Photosynthesis and stress in *Microcystis*

In *Microcystis*, 15 of the top 20 DEGs under high grazing pressure (*D. magna* 120 L^{-1} and *D. pulex* 200 L^{-1}) were associated with photosynthesis, and one with carbohydrate uptake (Harke et al., 2017). Most DEGs showed positive log-fold changes in these treatments. Notable responses included genes for sulphate transport, transposases, heat shock proteins, and *clpB*, a key gene in a stress-induced multichaperone system.

Together, these findings highlight the diversity of genetic pathways that can be co-opted into the aggregation response. Beyond EPS- and ECM-related mechanisms, predator-induced aggregation engages genes linked to stress responses, metabolism, and structural remodelling.

Some of these genes, such as *g18292*, *RLS1*, and the *regA* cluster, bridge immediate ecological defence with longer-term evolutionary transitions, underscoring the role of self-aggregation as both a survival strategy and a precursor to multicellularity.

1.7 Could infochemicals be the new flocculants?

In principle, microalgal self-aggregation could be triggered by simulating the presence of predators. Predator-derived infochemicals are active at concentrations orders of magnitude lower than commercial chemical flocculants; for example, ~0.1 μg L^{-1} compared to ≥ 0.5 g L^{-1} for metal salts such as alum (Esteves et al., 2020; Yasumoto et al., 2005). This low-dose effectiveness raises the possibility of using infochemicals as a cost-efficient harvesting strategy without reducing biomass productivity or quality.

As an example, filtrate from *Peranema trichophorum* was used to self-aggregate and settle *Chlamydomonas reinhardtii* at a ratio of 1 L filtrate to 100 L algal culture (2×10^6 cells mL^{-1}). At a reported preparation cost of USD $1 per litre of filtrate (Sathe and Durand, 2015), this treatment would cost ~$10 per cubic metre of algal culture. By comparison, harvesting with commercial flocculants costs only $0.01–0.26 per m^3 (**Table 1.9**), while EPS-derived bioflocculants have been estimated at $0.052 per m^3 (see **Section 1.3**). Thus, predator filtrate is currently uneconomical, and both the cost of production and the required dosage would need to be substantially reduced.

However, identifying infochemicals and developing inexpensive production methods could make this approach viable. For example, two *Daphnia pulex* infochemicals, sodium n-decyl sulphate and sodium n-octyl sulphate, are already commercially available and can trigger *Scenedesmus gutwinskii* self-aggregation at an estimated cost of just $\$2 \times 10^{-6}$–$2 \times 10^{-4}$ per m^3 (Yasumoto et al., 2005) (**Table 1.9**). Similarly, sodium dodecyl sulphate (SDS), while not an infochemical, has been shown to induce self-aggregation in *T. obliquus* and *S. gutwinskii* at very low doses, at an estimated cost of $\$2 \times 10^{-5}$ per m^3. These figures illustrate that the extremely low concentrations required make infochemicals a potentially economical alternative to traditional flocculants.

The choice of grazer species also matters. While *Daphnia magna* is the most studied grazer (24 of 52 reports; **Figure 1.2**), other species have been reported to induce stronger aggregation. For example, *D. pulex* induced more pronounce aggregation in *C. reinhardtii* than *D. magna* (Berger, 2017); *Daphnia galeata* triggered greater aggregation in *Microcystis aeruginosa* (Nam et al., 2024); *Ochromonas sp.* and *Tetrahymena thermophila* induced stronger responses in *C. vulgaris* (Kapsetaki et al., 2016); and *Daphnia pulicaria* was more effective than *D. pulex* in *T. obliquus* (Roccuzzo et al., 2016). These findings emphasize the variation among microalgal

species and their predators and suggest that screening infochemicals from a broader range of grazers may identify compounds with superior commercial potential.

Table 1.9. Costs of commercial flocculants, surfactants and infochemicals.

Flocculant	**Price (USD ton^{-1})**	**Active dose (per L)**	**Cost (USD m^{-3})**	**Ref.**
Commercial flocculants				
Aluminium sulphate	120–180*	100–750 mg	0.01–0.15	a, b
CPAM	1200*	≤ 30 mg	≤ 0.04	c
Ferric chloride	600–900*	400 mg	0.26–0.4	c
Surfactant				
Sodium dodecyl sulphate	1500*	10 µg	1.65×10^{-5}	d, e
***Daphnia pulex* infochemicals**				
Sodium n-decyl sulphate	1500*	1–10 µg	1.65×10^{-6}–1.65×10^{-5}	d
Sodium n-octyl sulphate	18,140*	1–10 µg	2×10^{-5}–2×10^{-4}	d
Predator filtrate				
Peranema trichophorum filtrate	~907	0.01 L	10	f

* https://www.made-in-china.com. Reference letters correspond to the following sources: a (Esteves et al., 2020); b (Gani et al., 2017); c (Zhang et al., 2024); d (Yasumoto et al., 2005); e (Zhu et al., 2020); f (Sathe and Durand, 2015).

1.8 Conclusions

Self-aggregation has been widely reported across diverse microalgal species. Although inconsistencies remain in the proposed mechanisms and the specific genes, receptors, and signalling pathways involved are still not fully resolved, the current evidence indicates that predator-induced aggregation engages pathways linked to mobility, cell-to-cell adhesion, cell wall synthesis, and the production of EPS and the extracellular matrix (Berger, 2017; Harke et al., 2017; Lorusso, 2018; Sun et al., 2020). While it is not yet clear whether these mechanisms are conserved across all microalgae, similarities observed among different microalgal taxa and other microorganisms point to shared strategies in cue sensing, signal cascades, and cell-to-cell communication.

Bioflocculation, mediated by fungi, bacteria or other algae, has emerged as a promising alternative to chemical flocculation, offering sustainable harvesting options through co-culturing or the use of microalgal biopolymers. However, substantial research is required to develop systems that are cost-effective at full scale.

An alternative strategy to flocculation is to trigger self-aggregation directly by mimicking predator signals. Because predator infochemicals act at extremely low concentrations, this approach could be both sustainable and economical compared with traditional flocculants. For example, *Daphnia pulex* infochemicals can induce *Scenedesmus gutwinskii* aggregation at costs four orders of magnitude lower than conventional flocculants (**Table 1.9**). Nevertheless, responses may vary by species, and some predators are more effective than others. To evaluate the commercial potential of infochemicals, future research should focus on identifying cues from a broader range of predators, testing their efficiency under field conditions, and assessing their applicability across diverse microalgal species.

It is also important to investigate the reversibility of infochemical-induced aggregation. Aggregation triggered by predation, chemical pollutants, or salt stress has been reported to reverse once cells are returned to normal growth media, raising questions about the stability of such systems in large-scale operations.

Overall, predator-derived infochemicals represent an exciting opportunity: not only as a potential commercial harvesting tool, but also as a model for understanding aggregation dynamics in natural ecosystems. Confirming the identity of the key genes mediating these responses could enable the engineering of mutants that readily self-aggregate, or the

identification of pheromone-like molecules that reliably induce aggregation. Such advances could significantly expand both the applied and fundamental understanding of microalgal self-aggregation.

References

Albini, D., Fowler, M. S., Llewellyn, C., & Tang, K. W. (2019). Reversible colony formation and the associated costs in *Scenedesmus obliquus*. *Journal of Plankton Research*, *41*, 419-429. https://doi.org/10.1093/plankt/fbz032

Aljuboori, A. H. R., Uemura, Y., & Thanh, N. T. (2016). Flocculation and mechanism of self-flocculating lipid producer microalga *Scenedesmus quadricauda* for biomass harvesting. *Biomass and Bioenergy*, *93*, 38-42. https://doi.org/10.1016/j.biombioe.2016.06.013

Amato, A., Sabatino, V., Nylund, G. M., Bergkvist, J., Basu, S., Andersson, M. X., Sanges, R., Godhe, A., Kiørboe, T., Selander, E., & Ferrante, M. I. (2018). Grazer-induced transcriptomic and metabolomic response of the chain-forming diatom *Skeletonema marinoi*. *The ISME Journal*, *12*, 1594-1604. https://doi.org/10.1038/s41396-018-0094-0

Barros, A. I., Gonçalves, A. L., Simões, M., & Pires, J. C. M. (2015). Harvesting techniques applied to microalgae: A review. *Renewable and Sustainable Energy Reviews*, *41*, 1489-1500. https://doi.org/10.1016/j.rser.2014.09.037

Becker, S. (2010). Biotic factors in induced defence revisited: Cell aggregate formation in the toxic cyanobacterium *Microcystis aeruginosa* PCC 7806 is triggered by spent *Daphnia* medium and disrupted cells. *Hydrobiologia*, *644*, 159-168. https://doi.org/10.1007/s10750-010-0109-y

Berger, C. M. (2017). *The genetic basis of cooperative aggregation in the green alga Chlamydomonas reinhardtii (Master's thesis). Kansas State University.*

Biswal, T., Shadangi, K. P., & Sarangi, P. K. (2024). Technologies of microalgae biomass cultivation for bio-fuel production: Challenges and benefits. In *Biorefineries: Production of Fuels and Platform Chemicals* (pp. 147-178). https://doi.org/10.1002/9781119724872.ch7

Boraas, M. E., Seale, D. B., & Boxhorn, J. E. (1998). Phagotrophy by a flagellate selects for colonial prey: A possible origin of multicellularity. *Evolutionary Ecology*, *12*, 153-164. https://doi.org/10.1023/A:1006527528063

Castrillo, M., Lucas-Salas, L. M., Rodríguez-Gil, C., & Martínez, D. (2013). High pH-induced flocculation–sedimentation and effect of supernatant reuse on growth rate and lipid productivity of *Scenedesmus obliquus* and *Chlorella vulgaris*. *Bioresource Technology*, *128*, 324-329. https://doi.org/10.1016/j.biortech.2012.10.114

Cheloni, G., & Slaveykova, V. I. (2021). Morphological plasticity in *Chlamydomonas reinhardtii* and acclimation to micropollutant stress. *Aquatic Toxicology*, *231*, 105711. https://doi.org/10.1016/j.aquatox.2020.105711

de Carpentier, F., Maes, A., Marchand, C. H., Chung, C., Durand, C., Crozet, P., Lemaire, S. D., & Danon, A. (2022). How abiotic stress-induced socialization leads to the formation of massive aggregates in *Chlamydomonas*. *Plant Physiology*, *190*, 1927-1940. https://doi.org/10.1093/plphys/kiac321

Esteves, A. F., Almeida, C. J., Gonçalves, A. L., & Pires, J. C. (2020). Microalgae harvesting techniques. In E. Jacob-Lopes, M. M. Maroneze, M. I. Queiroz, & L. Q. Zepka (Eds.), *Handbook of Microalgae-Based Processes and Products* (pp. 225-281). Academic Press. https://doi.org/10.1016/B978-0-12-818536-0.00010-5

Fan, J., Zheng, L., Bai, Y., Saroussi, S., & Grossman, A. R. (2017). Flocculation of *Chlamydomonas reinhardtii* with different phenotypic traits by metal cations and high pH. *Frontiers in Plant Science*, *8*, 1997. https://doi.org/10.3389/fpls.2017.01997

Fisher, R. M., Bell, T., & West, S. A. (2016). Multicellular group formation in response to predators in the alga *Chlorella vulgaris*. *Journal of Evolutionary Biology*, *29*, 551-559. https://doi.org/10.1111/jeb.12804

Gan, N., Xiao, Y., Zhu, L., Wu, Z., Liu, J., Hu, C., & Song, L. (2012). The role of microcystins in maintaining colonies of bloom-forming *Microcystis* spp. *Environmental Microbiology*, *14*, 730-742. https://doi.org/10.1111/j.1462-2920.2011.02624.x

Gani, P., Mohamed sunar, N., Peralta, H. M., & Abdul Latiff, A. A. (2017). Effect of pH and alum dosage on the efficiency of microalgae harvesting via flocculation technique. *International Journal of Green Energy*, *14*, 395-399. https://doi.org/10.1080/15435075.2016.1261707

Godl, K., Hallmann, A., Rappel, A., & Sumper, M. (1995). Pherophorins: A family of extracellular matrix glycoproteins from *Volvox* structurally related to the sex-inducing pheromone. *Planta*, *196*, 781-787. https://doi.org/10.1007/BF01106774

Goff, K. L., Headley, J. V., Lawrence, J. R., & Wilson, K. E. (2013). Assessment of the effects of oil sands naphthenic acids on the growth and morphology of *Chlamydomonas reinhardtii* using microscopic and spectromicroscopic techniques. *Science of The Total Environment*, *442*, 116-122. https://doi.org/10.1016/j.scitotenv.2012.10.034

Goldsmith, Z. G., & Dhanasekaran, D. N. (2007). G Protein regulation of MAPK networks. *Oncogene*, *26*, 3122-3142. https://doi.org/10.1038/sj.onc.1210407

González-Ballester, D., Casero, D., Cokus, S., Pellegrini, M., Merchant, S. S., & Grossman, A. R. (2010). RNA-seq analysis of sulfur-deprived *Chlamydomonas* cells reveals aspects of acclimation critical for cell survival. *The Plant Cell*, *22*, 2058-2084. https://doi.org/10.1105/tpc.109.071167

Gudin, C., & Thépenier, C. (1986). Bioconversion of solar energy into organic chemicals by microalgae. *Adv Biotechnol Process*, *6*, 73-110.

Ha, K., Jang, M. H., & Takamura, N. (2004). Colony formation in planktonic algae induced by zooplankton culture media filtrate. *Journal of Freshwater Ecology*, *19*, 9-16. https://doi.org/10.1080/02705060.2004.9664506

Hallmann, A. (2006). The pherophorins: Common, versatile building blocks in the evolution of extracellular matrix architecture in *Volvocales*. *The Plant Journal*, *45*, 292-307. https://doi.org/10.1111/j.1365-313X.2005.02627.x

Hanschen, E. R., Marriage, T. N., Ferris, P. J., Hamaji, T., Toyoda, A., Fujiyama, A., Neme, R., Noguchi, H., Minakuchi, Y., Suzuki, M., Kawai-Toyooka, H., Smith, D. R., Sparks, H., Anderson, J., Bakarić, R., Luria, V., Karger, A., Kirschner, M. W., Durand, P. M., Michod, R. E., Nozaki, H., & Olson, B. J. S. C. (2016). The *Gonium pectorale* genome demonstrates co-option of cell cycle regulation during the evolution of multicellularity. *Nature Communications*, *7*, 11370. https://doi.org/10.1038/ncomms11370

Harke, M. J., Jankowiak, J. G., Morrell, B. K., & Gobler, C. J. (2017). Transcriptomic responses in the bloom-forming cyanobacterium *Microcystis* induced during exposure to zooplankton. *Applied and Environmental Microbiology*, *83*, e02832-02816. https://doi.org/10.1128/AEM.02832-16

Havaux, M. (2014). Carotenoid oxidation products as stress signals in plants. *The Plant Journal*, *79*, 597-606. https://doi.org/10.1111/tpj.12386

Herron, M. D., Borin, J. M., Boswell, J. C., Walker, J., Chen, I. C. K., Knox, C. A., Boyd, M., Rosenzweig, F., & Ratcliff, W. C. (2019). De novo origins of multicellularity in response to predation. *Scientific Reports*, *9*, 2328. https://doi.org/10.1038/s41598-019-39558-8

Hessen, D., & Donk, E. (1993). Morphological changes in *Scenedesmus* induced by substances released from *Daphnia*. *Archive for Hydrobiology*, *127*, 129-140. https://doi.org/10.1127/archiv-hydrobiol/127/1993/129

Hou, X., Zhou, Q., Wang, Z., Kong, Q., Sun, Y., Zhang, L., Zhu, X., Huang, Y., & Yang, Z. (2018). Magnesium depletion suppresses the anti-grazer colony formation in *Scenedesmus obliquus*. *Environmental Science and Pollution Research*, *25*, 34228-34235. https://doi.org/10.1007/s11356-018-3191-8

Huang, Y., Cui, G., Li, B., Zhu, X., & Yang, Z. (2018). Elevated atmospheric CO2 enhances grazer-induced morphological defense in the freshwater green alga *Scenedesmus obliquus*. *Limnology and Oceanography*, *63*, 1004-1014. https://doi.org/10.1002/lno.10715

Huang, Y., Nan, H., Zhu, X., Li, B., Zhang, Z., & Yang, Z. (2016). Waterborne copper impairs grazer-induced colony formation and photosynthetic efficiency in *Scenedesmus obliquus*. *Limnology and Oceanography*, *61*, 625-634. https://doi.org/10.1002/lno.10236

Huntley, M. E., Johnson, Z. I., Brown, S. L., Sills, D. L., Gerber, L., Archibald, I., Machesky, S. C., Granados, J., Beal, C., & Greene, C. H. (2015). Demonstrated large-scale production of marine microalgae for fuels and feed. *Algal Research*, *10*, 249-265. https://doi.org/10.1016/j.algal.2015.04.016

Jia, X., Pan, Y., & Zhu, X. (2023). Salinization and heavy metal cadmium impair growth but have contrasting effects on defensive colony formation of *Scenedesmus obliquus*. *Science of The Total Environment*, *862*, 160693. https://doi.org/10.1016/j.scitotenv.2022.160693

Jüttner, F., Watson, S. B., von Elert, E., & Köster, O. (2010). β-cyclocitral, a grazer defence signal unique to the cyanobacterium *Microcystis*. *Journal of Chemical Ecology*, *36*, 1387-1397. https://doi.org/10.1007/s10886-010-9877-0

Kapsetaki, S., Fisher, R., & West, S. (2016). Predation and the formation of multicellular groups in algae. *Evolutionary Ecology Research*, *17*, 651-669.

Kapsetaki, S., Tep, A., & West, S. (2017). How do algae form multicellular groups? *Evolutionary Ecology Research*, *18*, 663–675.

Kapsetaki, S. E., & West, S. A. (2019). The costs and benefits of multicellular group formation in algae. *Evolution*, *73*, 1296-1308. https://doi.org/10.1111/evo.13712

Kellner Filho, L. C., Picão, B. W., Silva, M. L. A., Cunha, W. R., Pauletti, P. M., Dias, G. M., Copp, B. R., Bertanha, C. S., & Januario, A. H. (2019). Bioactive aliphatic sulfates

from marine invertebrates. *Marine Drugs*, *17*, 527. https://doi.org/10.3390/md17090527

Khona, D. K., Shirolikar, S. M., Gawde, K. K., Hom, E., Deodhar, M. A., & D'Souza, J. S. (2016). Characterization of salt stress-induced palmelloids in the green alga, *Chlamydomonas reinhardtii*. *Algal Research*, *16*, 434-448. https://doi.org/10.1016/j.algal.2016.03.035

Klein, B., Wibberg, D., & Hallmann, A. (2017). Whole transcriptome RNA-Seq analysis reveals extensive cell type-specific compartmentalization in *Volvox carteri*. *BMC Biology*, *15*, 111. https://doi.org/10.1186/s12915-017-0450-y

König, S. G., & Nedelcu, A. M. (2020). The genetic basis for the evolution of soma: Mechanistic evidence for the co-option of a stress-induced gene into a developmental master regulator. *Proceedings of the Royal Society B: Biological Sciences*, *287*, 20201414. https://doi.org/10.1098/rspb.2020.1414

Kulik, A., Wawer, I., Krzywińska, E., Bucholc, M., & Dobrowolska, G. (2011). SnRK2 protein kinases—key regulators of plant response to abiotic stresses. *OMICS: A Journal of Integrative Biology*, *15*, 859-872. https://doi.org/10.1089/omi.2011.0091

Lampert, W., Rothhaupt, K. O., & von Elert, E. (1994). Chemical induction of colony formation in a green alga (*Scenedesmus acutus*) by grazers (*Daphnia*). *Limnology and Oceanography*, *39*, 1543-1550. https://doi.org/10.4319/lo.1994.39.7.1543

Lee, C. S., Ahn, W., & Choi, Y. E. (2017). The G-protein alpha-subunit gene CGA1 is involved in regulation of resistance to heat and osmotic stress in *Chlamydomonas reinhardtii*. *Cellular and Molecular Biology*, *63*, 29-39. https://doi.org/10.14715/cmb/2017.63.2.5

Li, M., Zhu, W., Gao, L., & Lu, L. (2013). Changes in extracellular polysaccharide content and morphology of *Microcystis aeruginosa* at different specific growth rates. *Journal of Applied Phycology*, *25*, 1023-1030. https://doi.org/10.1007/s10811-012-9937-7

Li, T., Hu, J., & Zhu, L. (2021). Self-flocculation as an efficient method to harvest microalgae: A mini-review. *Water*, *13*, 2585. https://doi.org/10.3390/w13182585

Liang, C., Yang, Y., Xia, Y., Yuan, W., Chen, J., Zheng, Z., & Zheng, X. (2022). The optimization of *Chlorella vulgaris* flocculation harvesting by chitosan and calcium hydroxide. *Indian Journal of Microbiology*, *62*, 266-272. https://doi.org/10.1007/s12088-022-01004-1

Liu, J., Zhu, Y., Tao, Y., Zhang, Y., Li, A., Li, T., Sang, M., & Zhang, C. (2013). Freshwater microalgae harvested via flocculation induced by pH decrease. *Biotechnology for Biofuels*, *6*, 98. https://doi.org/10.1186/1754-6834-6-98

Livanos, P., Apostolakos, P., & Galatis, B. (2012). Plant cell division. *Plant Signaling & Behavior*, *7*, 771-778. https://doi.org/10.4161/psb.20530

Long, J. D., Smalley, G. W., Barsby, T., Anderson, J. T., & Hay, M. E. (2007). Chemical cues induce consumer-specific defenses in a bloom-forming marine phytoplankton. *Proceedings of the National Academy of Sciences*, *104*, 10512-10517.

Lorusso, N. (2018). *Consequences of an inducible defence: The ecological and evolutionary repercussions of temporary colony formation in Clamydomonas reinhardtii.* (Dissertation). Rutgers, The State University of New Jersey.

Lürling, M. (1998). Effect of grazing-associated infochemicals on growth and morphological development in *Scenedesmus acutus* (Chlorophyceae). *Journal of Phycology*, *34*, 578-586. https://doi.org/10.1046/j.1529-8817.1998.340578.x

Lurling, M., & Beekman, W. (2006). Palmelloids formation in *Chlamydomonas reinhardtii*: Defence against rotifer predators? *International Journal of Limnology*, *42*, 65-72. https://doi.org/10.1051/limn/2006010

Lürling, M., & Beekman, W. (2002). Extractable substances (anionic surfactants) from membrane filters induce morphological changes in the green alga *Scenedesmus obliquus* (*Chlorophyceae*). *Environmental Toxicology and Chemistry*, *21*, 1213-1218. https://doi.org/10.1002/etc.5620210614

Ma, J., Brookes, J. D., Qin, B., Paerl, H. W., Gao, G., Wu, P., Zhang, W., Deng, J., Zhu, G., Zhang, Y., Xu, H., & Niu, H. (2014). Environmental factors controlling colony formation in blooms of the cyanobacteria *Microcystis* spp. in Lake Taihu, China. *Harmful Algae*, *31*, 136-142. https://doi.org/10.1016/j.hal.2013.10.016

Manfiolli, A. O., Dos Reis, T. F., de Assis, L. J., de Castro, P. A., Silva, L. P., Hori, J. I., Walker, L. A., Munro, C. A., Rajendran, R., Ramage, G., & Goldman, G. H. (2018). Mitogen activated protein kinases (MAPK) and protein phosphatases are involved in *Aspergillus fumigatus* adhesion and biofilm formation. *The Cell Surface*, *1*, 43-56. https://doi.org/10.1016/j.tcsw.2018.03.002

Marianna, V., John, A. R., & Mario, G. (2017). Intraspecific chemical communication in microalgae. *The New Phytologist*, *215*, 516-530. https://doi.org/10.1111/nph.14524

Mata, T. M., Martins, A. A., & Caetano, N. S. (2010). Microalgae for biodiesel production and other applications: A review. *Renewable and Sustainable Energy Reviews*, *14*, 217-232. https://doi.org/10.1016/j.rser.2009.07.020

McGrath, S. J., Laamanen, C. A., Senhorinho, G. N. A., & Scott, J. A. (2024). Microalgal harvesting for biofuels – Options and associated operational costs. *Algal Research*, *77*, 103343. https://doi.org/10.1016/j.algal.2023.103343

Moorthy, R. K., Premalatha, M., & Arumugam, M. (2017). Batch sedimentation studies for freshwater green alga *Scenedesmus abundans* using combination of flocculants. *Frontiers in Chemistry*, *5*, 37. https://doi.org/10.3389/fchem.2017.00037

Nam, G., An, G., Na, J., & Jung, J. (2024). Control of *Microcystis aeruginosa* by *Daphnia*: Experimental evidence and identification of involved infochemicals. *Environmental Pollution*, *352*, 124144. https://doi.org/10.1016/j.envpol.2024.124144

Naor, Z., Benard, O., & Seger, R. (2000). Activation of MAPK cascades by G-protein-coupled receptors: The case of gonadotropin-releasing hormone receptor. *Trends in Endocrinology & Metabolism*, *11*, 91-99. https://doi.org/10.1016/s1043-2760(99)00232-5

Nedelcu, A. M. (2009). Environmentally induced responses co-opted for reproductive altruism. *Biology Letters*, *5*, 805-808. https://doi.org/10.1098/rsbl.2009.0334

Nie, Y., Wang, Z., Wang, W., Zhou, Z., Kong, Y., & Ma, J. (2022). Bio-flocculation of *Microcystis aeruginosa* by using fungal pellets of *Aspergillus oryzae*: Performance and mechanism. *Journal of Hazardous Materials*, *439*. https://doi.org/10.1016/j.jhazmat.2022.129606

O'Donnell, D. R., Fey, S. B., & Cottingham, K. L. (2012). Nutrient availability influences kairomone-induced defenses in *Scenedesmus acutus* (Chlorophyceae). *Journal of Plankton Research*, *35*, 191-200. https://doi.org/10.1093/plankt/fbs083

Oda, Y., Sakamoto, M., & Miyabara, Y. (2022). Colony formation in three species of the family Scenedesmaceae (*Desmodesmus subspicatus, Scenedesmus Acutus, Tetradesmus Dimorphus*) exposed to sodium dodecyl sulfate and its interference with grazing of *Daphnia galeata*. *Archives of Environmental Contamination and Toxicology*, *82*, 37-47. https://doi.org/10.1007/s00244-021-00890-8

Olson, B. J., & Nedelcu, A. M. (2016). Co-option during the evolution of multicellular and developmental complexity in the volvocine green algae. *Current Opinion in Genetics & Development*, *39*, 107-115. https://doi.org/10.1016/j.gde.2016.06.003

Pan, Y., Liu, C., Li, F., Zhou, C., Yan, S., Dong, J., Li, T., & Duan, C. (2017). Norfloxacin disrupts *Daphnia magna*-induced colony formation in *Scenedesmus quadricauda* and facilitates grazing. *Ecological Engineering*, *102*, 255-261. https://doi.org/10.1016/j.ecoleng.2017.02.037

Pitzschke, A., Schikora, A., & Hirt, H. (2009). MAPK cascade signalling networks in plant defence. *Current Opinion in Plant Biology*, *12*, 421-426. https://doi.org/10.1016/j.pbi.2009.06.008

Powell, R. J., & Hill, R. T. (2014). Mechanism of algal aggregation by *Bacillus* sp. strain RP1137. *Appl Environ Microbiol*, *80*, 4042-4050. https://doi.org/10.1128/aem.00887-14

Ray, A., Banerjee, S., & Das, D. (2021). Microalgal bio-flocculation: Present scenario and prospects for commercialization. *Environmental Science and Pollution Research*, *28*. https://doi.org/10.1007/s11356-021-13437-0

Reese, K. L., Fisher, C. L., Lane, P. D., Jaryenneh, J. D., Moorman, M. W., Jones, A. D., Frank, M., & Lane, T. W. (2019). Chemical profiling of volatile organic compounds in the headspace of algal cultures as early biomarkers of algal pond crashes. *Scientific Reports*, *9*, 13866. https://doi.org/10.1038/s41598-019-50125-z

Roccuzzo, S., Beckerman, A. P., & Pandhal, J. (2016). The use of natural infochemicals for sustainable and efficient harvesting of the microalgae *Scenedesmus* spp. for biotechnology: insights from a meta-analysis. *Biotechnology Letters*, *38*, 1983-1990. https://doi.org/10.1007/s10529-016-2192-2

Roccuzzo, S., Couto, N., Karunakaran, E., Kapoore, R. V., Butler, T. O., Mukherjee, J., Hansson, E. M., Beckerman, A. P., & Pandhal, J. (2020). Metabolic insights into infochemicals induced colony formation and flocculation in *Scenedesmus subspicatus* unraveled by quantitative proteomics. *Frontiers in Microbiology*, *11*, 792. https://doi.org/10.3389/fmicb.2020.00792

Roselet, F., Vandamme, D., Muylaert, K., & Abreu, P. C. (2019). Harvesting of microalgae for biomass production. In *Microalgae Biotechnology for Development of Biofuel and Wastewater Treatment* (pp. 211-243). https://doi.org/10.1007/978-981-13-2264-8_10

Saha, M., & Fink, P. (2022). Algal volatiles – the overlooked chemical language of aquatic primary producers. *Biological Reviews*, *97*, 2162-2173. https://doi.org/10.1111/brv.12887

Salim, S., Bosma, R., Vermuë, M. H., & Wijffels, R. H. (2011). Harvesting of microalgae by bio-flocculation. *Journal of Applied Phycology*, *23*, 849-855. https://doi.org/10.1007/s10811-010-9591-x

Sathe, S., & Durand, P. M. (2015). A low cost, non-toxic biological method for harvesting algal biomass. *Algal Research*, *11*, 169-172. https://doi.org/10.1016/j.algal.2015.06.021

Sathe, S., & Durand, P. M. (2016). Cellular aggregation in *Chlamydomonas* (Chlorophyceae) is chimaeric and depends on traits like cell size and motility. *European Journal of Phycology*, *51*, 129-138. https://doi.org/10.1080/09670262.2015.1107759

Scranton, M. A., Ostrand, J. T., Fields, F. J., & Mayfield, S. P. (2015). *Chlamydomonas* as a model for biofuels and bio-products production. *The Plant Journal*, *82*, 523-531. https://doi.org/10.1111/tpj.12780

Spain, O., & Funk, C. (2024). A step towards more eco-friendly and efficient microalgal harvesting: Inducing flocculation in the non-naturally flocculating strain *Chlorella vulgaris* (13-1) without chemical additives. *Algal Research*, *79*, 103450. https://doi.org/10.1016/j.algal.2024.103450

Spolaore, P., Joannis-Cassan, C., Duran, E., & Isambert, A. (2006). Commercial applications of microalgae. *Journal of Bioscience and Bioengineering*, *101*, 87-96. https://doi.org/10.1263/jbb.101.87

Sukenik, A., & Shelef, G. (1984). Algal autoflocculation-verification and proposed mechanism. *Biotechnology and Bioengineering*, *26*, 142-147. https://doi.org/10.1002/bit.260260206

Sun, Y., Zhang, X., Zhang, L., Huang, Y., Yang, Z., & Montagnes, D. (2020). UVB radiation suppresses antigrazer morphological defense in *Scenedesmus obliquus* by inhibiting algal growth and carbohydrate-regulated gene expression. *Environmental Science and Technology*, *54*, 4495-4503. https://doi.org/10.1021/acs.est.0c00104

Suwannachuen, N., Leetanasaksakul, K., Roytrakul, S., Phaonakrop, N., Thaisakun, S., Roongsattham, P., Jantasuriyarat, C., Sanevas, N., & Sirikhachornkit, A. (2023). Palmelloid formation and cell aggregation are essential mechanisms for high light tolerance in a natural strain of *Chlamydomonas reinhardtii*. *International Journal of Molecular Sciences*, *24*, Article 8374. https://doi.org/10.3390/ijms24098374

Ummalyma, S. B., Gnansounou, E., Sukumaran, R. K., Sindhu, R., Pandey, A., & Sahoo, D. (2017). Bioflocculation: An alternative strategy for harvesting of microalgae - An overview. *Bioresource Technology*, *242*, 227-235. https://doi.org/10.1016/j.biortech.2017.02.097

Van Donk, E., Ianora, A., & Vos, M. (2011). Induced defences in marine and freshwater phytoplankton: A review. *Hydrobiologia*, *668*, 3-19. https://doi.org/10.1007/s10750-010-0395-4

Vandamme, D., Foubert, I., Fraeye, I., Meesschaert, B., & Muylaert, K. (2012). Flocculation of *Chlorella vulgaris* induced by high pH: Role of magnesium and calcium and practical implications. *Bioresource Technology*, *105*, 114-119. https://doi.org/10.1016/j.biortech.2011.11.105

Verschoor, A. M., Van Der Stap, I., Helmsing, N. R., Lürling, M., & Van Donk, E. (2004). Inducible colony formation within the Scenedesmaceae: Adaptive responses to

infochemicals from two different herbivore taxa. *Journal of Phycology*, *40*, 808-814. https://doi.org/10.1111/j.1529-8817.2004.04007.x

Visviki, I., & Santikul, D. (2000). The pH tolerance of *Chlamydomonas applanata* (Volvocales, Chlorophyta). *Archives of Environmental Contamination and Toxicology*, *38*, 147-151. https://doi.org/10.1007/s002449910018

Wang, W., Liu, Y., & Yang, Z. (2010). Combined effects of nitrogen content in media and *Ochromonas* sp. grazing on colony formation of cultured *Microcystis aeruginosa*. *Journal of Limnology*, *69*, 193. https://doi.org/10.4081/jlimnol.2010.193

Wang, Y.-W., Zhao, J., Li, J.-H., Li, S.-S., Zhang, L.-H., & Wu, M. (2011). Effects of calcium levels on colonial aggregation and buoyancy of *Microcystis aeruginosa*. *Current Microbiology*, *62*, 679-683. https://doi.org/10.1007/s00284-010-9762-7

Wu, X., Zhang, J., Qin, B., Cui, G., & Yang, Z. (2013). Grazer density-dependent response of induced colony formation of *Scenedesmus obliquus* to grazing-associated infochemicals. *Biochemical Systematics and Ecology*, *50*, 286-292. https://doi.org/10.1016/j.bse.2013.05.001

Wu, Z., Zhu, Y., Huang, W., Zhang, C., Li, T., Zhang, Y., & Li, A. (2012). Evaluation of flocculation induced by pH increase for harvesting microalgae and reuse of flocculated medium. *Bioresource Technology*, *110*, 496-502. https://doi.org/10.1016/j.biortech.2012.01.101

Xiao, M., Li, M., & Reynolds, C. S. (2018). Colony formation in the cyanobacterium *Microcystis*. *Biological Reviews*, *93*, 1399-1420. https://doi.org/10.1111/brv.12401

Yang, J., Li, B., Zhang, C., & Luo, H. (2016). PH-associated changes in induced colony formation and growth of *Scenedesmus obliquus*. *Fundamental and Applied Limnology*, *187*, 241-246. https://doi.org/10.1127/fal/2016/0846

Yang, L., Zhang, H., Cheng, S., Zhang, W., & Zhang, X. (2020). Enhanced microalgal harvesting using microalgae-derived extracellular polymeric substance as flocculation aid. *ACS Sustainable Chemistry & Engineering*, *8*, 4069-4075. https://doi.org/10.1021/acssuschemeng.9b06156

Yang, Z., & Kong, F. (2013). Abiotic factors in colony formation: Effects of nutrition and light on extracellular polysaccharide production and cell aggregates of *Microcystis aeruginosa*. *Chinese Journal of Oceanology and Limnology*, *31*, 796-802. https://doi.org/10.1007/s00343-013-2264-2

Yang, Z., Kong, F., Shi, X., Xing, P., & Zhang, M. (2007). Effects of *Daphnia*-associated infochemicals on the morphology, polysaccharides content and PSII-efficiency in *Scenedesmus obliquus*. *International Review of Hydrobiology*, *92*, 618-625. https://doi.org/10.1002/iroh.200710963

Yang, Z., Kong, F., Zhang, M., Yang, Z., Yu, Y., & Qian, S. (2009). Effect of filtered cultures of flagellate *Ochromonas* sp. on colony formation in *Microcystis aeruginosa*. *International Review of Hydrobiology*, *94*, 143-152. https://doi.org/10.1002/iroh.200811103

Yasumoto, K., Nishigami, A., Aoi, H., Tsuchihashi, C., Kasai, F., Kusumi, T., & Ooi, T. (2008a). Isolation and absolute configuration determination of aliphatic sulfates as the *Daphnia* kairomones inducing morphological defense of a phytoplankton - Part 2.

Chemical and Pharmaceutical Bulletin, *56*, 129-132. https://doi.org/10.1248/cpb.56.129

Yasumoto, K., Nishigami, A., Aoi, H., Tsuchihashi, C., Kasai, F., Kusumi, T., & Ooi, T. (2008b). Isolation of new aliphatic sulfates and sulfamate as the *Daphnia* kairomones inducing morphological change of a phytoplankton *Scenedesmus gutwinskii*. *Chemical and Pharmaceutical Bulletin*, *56*, 133-136. https://doi.org/10.1248/cpb.56.133

Yasumoto, K., Nishigami, A., Kasai, F., Kusumi, T., & Ooi, T. (2006). Isolation and absolute configuration determination of aliphatic sulfates as the *Daphnia* kairomones inducing morphological defense of a phytoplankton. *Chemical and Pharmaceutical Bulletin*, *54*, 271-274. https://doi.org/10.1248/cpb.54.271

Yasumoto, K., Nishigami, A., Yasumoto-Hirose, M., Kasai, F., Okada, Y., Kusumi, T., & Ooi, T. (2005). Aliphatic sulfates released from *Daphnia* induce morphological defense of phytoplankton: Isolation and synthesis of kairomones. *Tetrahedron Letters*, *46*, 4765-4767. https://doi.org/10.1016/j.tetlet.2005.05.027

Zhang, B., Wei, Z., & Mao, B. (2024). Flocculation with intermittent dosing for enhanced microalgae harvesting. *Separation and Purification Technology*, *330*, 125445. https://doi.org/10.1016/j.seppur.2023.125445

Zhang, L., Sun, Y., Cheng, J., Cui, G., Huang, Y., & Yang, Z. (2021). Warming mitigates the enhancement effect of elevated air CO_2 on anti-grazer morphological defense in *Scenedesmus obliquus*. *Science of The Total Environment*, *770*, 145341. https://doi.org/10.1016/j.scitotenv.2021.145341

Zhu, X., Sun, Y., Zhang, L., Wang, J., Gu, L., Huang, Y., & Yang, Z. (2021). Multi-omics reveal the pathways involved in induced defensive colony formation of *Tetradesmus obliquus* in response to *Daphnia* grazing cues. *Limnology and Oceanography*, *66*, 1819-1831. https://doi.org/10.1002/lno.11726

Zhu, X., Sun, Y., Zhang, X., Heng, H., Nan, H., Zhang, L., Huang, Y., & Yang, Z. (2016). Herbicides interfere with antigrazer defenses in *Scenedesmus obliquus*. *Chemosphere*, *162*, 243-251. https://doi.org/10.1016/j.chemosphere.2016.07.087

Zhu, X., Wang, Y., Hou, X., Kong, Q., Sun, Y., Wang, J., Huang, Y., & Yang, Z. (2019). High temperature promotes the inhibition effect of Zn^{2+} on inducible defense of *Scenedesmus obliquus*. *Chemosphere*, *216*, 203-212. https://doi.org/10.1016/j.chemosphere.2018.10.116

Zhu, X., Wang, Z., Sun, Y., Gu, L., Zhang, L., Wang, J., Huang, Y., & Yang, Z. (2020). Surfactants at environmentally relevant concentrations interfere the inducible defense of *Scenedesmus obliquus* and the implications for ecological risk assessment. *Environmental Pollution*, *261*, 114131. https://doi.org/10.1016/j.envpol.2020.114131

Zhu, X., Yang, J., Xu, N., Chen, G., & Yang, Z. (2015). Combined effects of nitrogen levels and *Daphnia* culture filtrate on colony size of *Scenedesmus obliquus*. *Algal Research*, *9*, 94-98. https://doi.org/10.1016/j.algal.2015.03.002

Zhu, X., Yang, J., Zhang, X., Zhang, L., Wang, X., & Huang, Y. (2017). Low temperature and *Daphnia*-associated infochemicals promote colony formation of *Scenedesmus obliquus* and its harvesting. *Biotechnology Letters*, *39*, 85-90. https://doi.org/10.1007/s10529-016-2223-z

Zuo, Z.-J. (2019). Why algae release volatile organic compounds - The emission and roles. *Frontiers in Microbiology*, *10*. https://doi.org/10.3389/fmicb.2019.00491

Zuo, Z.-J., Zhu, Y.-R., Bai, Y.-L., & Wang, Y. (2012a). Volatile communication between *Chlamydomonas reinhardtii* cells under salt stress. *Biochemical Systematics and Ecology*, *40*, 19-24. https://doi.org/10.1016/j.bse.2011.09.007

Zuo, Z.-J., Zhu, Y., Bai, Y., & Wang, Y. (2012b). Acetic acid-induced programmed cell death and release of volatile organic compounds in *Chlamydomonas reinhardtii*. *Plant Physiology and Biochemistry*, *51*, 175-184. https://doi.org/10.1016/j.plaphy.2011.11.003

Chapter 2.

Safety in numbers: Self-aggregation as a defence against *Daphnia*

Preface

From the literature review presented in **Chapter 1**, the zooplankton *Daphnia* was selected as the model grazer for a series of bioassays with the microalgae *Chlamydomonas reinhardtii*, *Chlorella vulgaris*, and *Tetradesmus obliquus*. This chapter presents the development, testing, and results of bioassay protocols used to evaluate how effectively *Daphnia* and their infochemicals could induce microalgal self-aggregation. These bioassays were used to identify the most practical and reproducible protocol (i.e., the trigger and microalgae) for subsequent transcriptomic (**Chapter 3**) and metabolomic analyses of aggregating cultures (**Chapter 4**).

Abstract

Microalgal self-aggregation has potential biotechnological applications, as dense aggregates improve settleability and could provide an alternative to chemical flocculation for biomass harvesting. However, the mechanisms that initiate and regulate self-aggregation remain poorly understood. To investigate this, *Daphnia* was chosen as a model grazer, and microalgae were incubated with live *Daphnia*, their culture filtrate, or their extracted infochemicals. Live *Daphnia* induced self-aggregation in *Chlamydomonas reinhardtii* and *Tetradesmus obliquus*, with ~60% of cells forming colonies within 24 h, whereas *Chlorella vulgaris* did not aggregate. Live *Daphnia* also introduced contaminants. *Daphnia* culture filtrate and concentrated extracts prepared from freeze-dried *Daphnia* also triggered aggregation. To our knowledge this is the first report of aggregation in microalgae treated with concentrated zooplankton extracts. The most consistent response was observed in *C. reinhardtii* exposed to a solvent extract, which was subsequently dried, and the extracted compounds resuspended in distilled water. Within 24 hours, *C. reinhardtii* had formed palmelloid colonies of 4–32 cells, with the mean colony size exceeding four cells per colony; these colonies further adhered into aggregates of hundreds of cells. Because this response was consistent and robust, the *C. reinhardtii*-*Daphnia* extract system was selected for deeper investigation through transcriptomics and metabolomics analyses (**Chapters 3** and **4**).

2.1 Introduction

Microalgae can form protective colonies that reduce the risk of ingestion and digestion by zooplankton predators (Fisher et al., 2016; Hou et al., 2018; Kapsetaki et al., 2016; Lurling and Beekman, 2006). This defence, termed *self-aggregation*, is a reversible morphological response used by many species under diverse stress conditions. The zooplankton grazers *Daphnia* are particularly well known to induce self-aggregation in microalgae (Berger, 2017; Ha et al., 2004; Kapsetaki et al., 2016; Pan et al., 2017; Roccuzzo et al., 2020). In response to *Daphnia* or their chemicals cues, microalgae form colonies after cell division or adhere together into large aggregates (**Chapter 1**).

Although this phenomenon is well documented, the mechanisms by which microalgae detect grazers and initiate colony formation remain unclear. In most cases, the chemical cues released by *Daphnia* (broadly termed *infochemicals*) have not been identified and their modes of action are unknown. While one series of studies characterised *Daphnia* compounds active in triggering aggregation in *Scenedesmus gutwinskii* (Yasumoto et al., 2008a, 2008b; Yasumoto et al., 2006; Yasumoto et al., 2005) (see **Chapter 1**), these have not been tested in any other algae. Understanding these interactions is important not only to improve our ecological knowledge, but also for biotechnology, as controlled self-aggregation could improve microalgal harvesting by enhanced settleability.

The purpose of this chapter was to investigate self-aggregation responses in several model algal species exposed to *Daphnia* and their infochemicals. The ease and reproducibility of producing each trigger (e.g., maintaining live *Daphnia* vs. producing extracts) and the consistency of the algal response (i.e., the size of aggregates and proportion of total cells involved) from these bioassays were used to select a single *Daphnia*-alga pairing for further study: the selected system was carried forward into transcriptomic and metabolomic analyses (**Chapters 3** and **4**) to provide mechanistic insight into the self-aggregation response, where a clear difference between treated and control cultures was essential.

2.2 Materials and methods

2.2.1 Organism culture maintenance

2.2.1.1 Microalgae

Chlamydomonas reinhardtii CC-1690 was cultured and maintained in sterile tris-acetate-phosphate (TAP) liquid media and *Chlorella vulgaris* UTEX 259 and *Tetradesmus obliquus* UTEX 3155 in sterile BG-11 liquid media. The microalgae were cultured in conical flasks, closed with cotton stoppers, and incubated at 22 °C on an orbital shaker (115 rpm) under continuous light (24 ± 1 μmol m^{-2} s^{-1}). To avoid nutrient limitation and significant pH decline, cultures were refreshed weekly by adding up to 5 mL of culture to 100 mL of sterile fresh media. Actively growing, recently refreshed microalgae cultures were used in bioassays to ensure that nutrient availability and increasing pH were not a contributing factor to any response.

2.2.1.2 *Daphnia*

Daphnia magna eggs were purchased from GreenWaterFarm (Thailand); the eggs were added to distilled water and hatching took between five days to two weeks. Additionally, live *Daphnia* (either *Daphnia carinata* or *Daphnia thomsoni*; reported here as *D. thomsoni*) were purchased from Maximum Pet Supplies (Lower Hutt, New Zealand) and Science Resource Box (Canterbury, New Zealand) (**Figure 2.1**).

Daphnia were cultured in 1 L glass Duran bottles, with the openings covered with thin cloth secured by a rubber band. An aquarium (21 L Aqua One EcoStyle 37) was also set-up with standard built-in lighting and an Aqua One precision air pump (**Figure 2.1**). Both were kept at room temperature (20 ± 2°C) on a bench under a window, with indirect natural light and laboratory lighting. The *Daphnia* were fed with several millilitres of *C. reinhardtii* culture, approximately three times per week, or whenever the water became colourless. Water changes of 20% were carried out weekly, to remove accumulated *Daphnia* waste products.

Figure 2.1. Photographs of live *Daphnia magna* culture in an aquarium (left), *Daphnia thomsoni* in a bioassay plate (middle), and pond organisms imaged in brightfield at 4× magnification (right; *Daphnia*, *Volvox* algae, and copepods).

2.2.2 Bioassay set-up

To investigate self-aggregation in different microalgal species, and ultimately to examine its underlying mechanisms, a series of bioassays were conducted in axenic cultures of *C. reinhardtii*, *C. vulgaris*, and *T. obliquus*. These took place in sterile 6-well Falcon tissue culture plates, where each well contained 5 mL of culture and the various treatments (**Figure 2.2**). The plates were covered with Parafilm to allow for gas transfer while keeping the cultures sterile and incubated under the same conditions as the stock cultures (see **Section 2.2.1.1**).

2.2.3 Aggregation triggers

Four types of self-aggregation "triggers" were tested:

1. **Live *Daphnia*** – *D. magna* and *D. thomsoni* were used to confirm reports that live grazers induced self-aggregation in these microalgal species (**Chapter 1**).
2. **Mixed pond zooplankton extract** – Infochemicals were extracted from a mixed community of pond zooplankton to assess whether algae respond to cues from multiple grazer species present in natural environments.
3. ***Daphnia* filtrate** – Filtered culture medium from a *D. magna* culture was tested to capture the full suite of compounds released by live *Daphnia*.
4. ***Daphnia* extracts** – Concentrated extracts were prepared from dried or frozen *Daphnia* using either water or organic solvents to recover infochemicals.

The preparation of these triggers is described in the following sections.

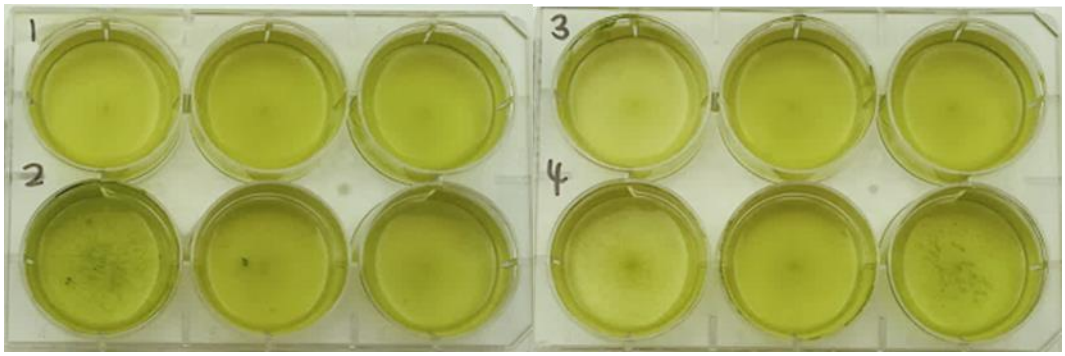

Figure 2.2. Example of bioassay plates containing microalgae cultures.

2.2.3.1 Live *Daphnia*

When required for bioassay, *Daphnia* were collected using a pipette or a Brine shrimp collector sieve, placed into distilled water to rinse, then transferred again to fresh water. Individual *Daphnia* were then pipetted into the bioassay plates, based on a previously reported active density of 1 daphnid per mL (Berger, 2017; Kapsetaki et al., 2016):

- In *C. reinhardtii*, *D. magna* were added to a final concentration of 3 and 6 daphnids per mL, and *D. thomsoni* to 1 and 2 per mL.
- In *C. vulgaris*, *D. magna* were added to 1.25 and 3 $mL^{-1.}$
- In *T. obliquus*, *D. magna* were added to 1.25 mL^{-1}.

2.2.3.2 Pond zooplankton extract

To test the effects of zooplankton from a natural environment, organisms were harvesting from the freshwater pond on Massey University's Manawatu campus (New Zealand) in spring. The suspended organisms were collected by straining the pond water through a mesh cloth and were then stored frozen. These included copepods, *Daphnia*, and algae such as *Volvox* (**Figure 2.1**).

The biomass was defrosted and centrifuged, and the cell pellet was freeze-dried. The dried biomass was vortexed with distilled water at a 1:2 ratio (volume of wet biomass pre-drying to volume of water), left to stand for 20 minutes, then centrifuged. The supernatant was filtered through 0.22 µm sterile Minisart filter units and stored frozen until use.

This pond extract was added to bioassay cultures to a final volume of 0.2% v/v (plus 0.8% distilled water), and 1% v/v. Control cultures contained 1% v/v sterile distilled water.

2.2.3.3 *Daphnia* filtrate

The water in which *D. magna* were cultured (see **Section 2.2.1.2**) was filtered through 0.22 µm sterile Minisart filter units and added to microalgae bioassay cultures at 37% v/v. Control cultures contained 37% v/v sterile distilled water.

2.2.3.4 *Daphnia* extracts

Considering the varied effectiveness of the *Daphnia* filtrate (see **Section 2.3.3**), extracts were prepared from commercially frozen or freeze-dried *Daphnia*, to test concentrated infochemicals. These extracts were also more reproducible, making potential future work to isolate and/or identify active infochemicals more practical (see **Chapter 4**).

Frozen *Daphnia* (Nutris brand) were purchased from Hollywood Fish Farm (New Zealand) (**Figure 2.3**). Freeze-dried *Daphnia* were obtained in bulk from Maximum Pet Supplies (Lower Hutt, New Zealand) and from Fishly (Sera brand; New Zealand) (**Figure 2.3**). Based on size and appearance, the freeze-dried daphnids most closely resembled *D. thomsoni* or *Daphnia carinata* and were larger than *D. magna*.

The preparation of these extracts is described below. All extracts were filtered through Whatman GF/F glass microfibre filters and sterile 0.22 µm Minisart filter units and stored frozen until use.

Water Extract

Frozen Nutris *Daphnia* were freeze-dried (three cubes, 0.55 g dry weight), crushed, and suspended in distilled water (36 mL). The suspension was vortexed with glass beads for one minute, allowed to stand for 40 minutes, and then centrifuged (3300 x *g*, 5 min) to recover the supernatant. The extract was stored frozen. Treated bioassay cultures contained water extract at 1% v/v and controls contained sterile distilled water at 1% v/v.

Solvent Extract

Solvent was used to extract a wider range of chemicals from *Daphnia* compared to water, to potentially illicit a stronger aggregation response. Frozen Nutris *Daphnia* were freeze-dried (three cubes, 0.55 g dry weight), crushed, and extracted with methanol, chloroform, and water (36 mL; 5:2:2, v/v/v) following the protocol of Lee and Fiehn (2008). The suspension was

mixed on an orbital shaker (150 rpm, 1 h), refrigerated overnight (4 °C), and centrifuged (3300 x *g*, 5 min) to recover the supernatant. Treated bioassay cultures contained solvent extract at 1% and 2% v/v, control cultures contained sterile distilled water at 2% v/v, and the 1% extract treatment also contained 1% v/v distilled water. As a solvent control, cultures were also treated with the same volume of fresh solvent.

Resuspended solvent extracts

To test the bioactivity of infochemicals without direct solvent effects on microalgae, solvent extracts were first prepared as above, before the solvent and most of the water were then removed from the supernatant using rotary evaporation (Heidolph VV2000). The concentrate was freeze-dried to ensure complete solvent removal, then resuspended in distilled water. These extracts were prepared from frozen *Daphnia*, which was tested in all three algae, from Sera *Daphnia*, which was tested in *C. reinhardtii* and *C. vulgaris*, and from Maximum Pet Supplies (MPS) *Daphnia*, which was tested in *C. reinhardtii*. The initial biomass amounts, solvent volumes, and final resuspended volumes are provided in **Table 2.1**.

Figure 2.3. Freeze-dried Sera *Daphnia* (A), frozen Nutris *Daphnia* (B), and freeze-dried Maximum Pet Supplies *Daphnia* (C).

2.2.4 Morphological analysis

C. reinhardtii cell concentration and colony formation were monitored using light microscopy. 100 µL of each sample was fixed with Lugol's iodine at 2% v/v and 10 µL was placed on a haemocytometer and imaged in brightfield at 10× magnification (Olympus U-LH100HG BX53). Images of all four haemocytometer grid corners were later manually analysed for each sample, by counting the number of unicellular, paired, and aggregated cells, from which the total cell concentration and the colony size distribution were calculated. Large aggregates of hundreds or thousands of cells could not be quantified using this method and instead were imaged and described as macroscopic aggregates.

Table 2.1. Types of *Daphnia* extracts prepared, with biomass source, starting weight, solvent system, and final extract volume.

Extract name	**Daphnia source**	***Daphnia* dry weight (g)**	**Solvent volume (mL)**	**Final volume (mL)**
Resuspended frozen extract	Nutris frozen *Daphnia*	40 cubes/ 7.32 g	200	100
Resuspended sera extract	Sera freeze-dried *Daphnia*	4.4	120	60
Resuspended MPS extract	Maximum Pet Supplies freeze-dried *Daphnia*	125	2450	520

2.3 Results and Discussion

The following sections describe the results of a series of bioassays in which live *Daphnia* and various forms of infochemicals were added to microalgal cultures to trigger and quantify the self-aggregation response. Figures associated with *C. vulgaris* and *T. obliquus* are provided in **Appendix C**.

2.3.1 Live *Daphnia*

The addition of live *Daphnia* induced varying degrees of aggregation. However, upon addition to bioassay cultures, *D. thomsoni* died within four hours, *D. magna* typically died within a day, and both species introduced ciliate, rotifer, and bacterial contaminants into the cultures (**Figure 2.4**).

Chlamydomonas reinhardtii

Within 24 h, *C. reinhardtii* formed four-celled colonies in cultures treated with *D. thomsoni* (1-2 mL^{-1}) or *D. magna* at 6 mL^{-1}, but fewer cells aggregated in cultures treated with 3 *D. magna* mL^{-1} (**Figure 2.5**). The proportion of cells aggregating and the morphology of aggregates was inconsistent in cultures treated with live *Daphnia*, possibly due to *Daphnia* mortality or the influence of bacteria. Aggregates with various morphologies were observed, including dense masses of cells, thin sheets of cells, and small matrices with few cells attached (**Figure 2.4** and **Figure 2.6**). However, bacteria were visible during microscopic examination of cultures treated with *D. magna* and *D. thomsoni* (**Figure 2.4**), often reaching significant concentrations within 24 hours.

Notably, *C. reinhardtii* growth rate was considerably enhanced in cultures treated with live *Daphnia* compared to controls (**Figure 2.5**). This may have been part of a stress response to the *Daphnia* or contaminants.

Chlorella vulgaris

C. vulgaris did not aggregate in cultures treated with *D. magna* (1.25–3 mL^{-1}; **Appendix C**, **Figure C.1**-**Figure C.3**). There were no visible signs of bacterial contamination in treated cultures, which may have been due to BG-11 media having no carbon source unlike TAP media (acetic acid), and therefore bacteria never grew noticeably.

Tetradesmus obliquus

Within 24 h, *T. obliquus* cultures treated with *D. magna* (1.25 mL^{-1}) formed small colonies which adhered into slightly larger aggregates (**Figure C.7** and **Figure C.8**), and the growth rate was enhanced compared to control cultures (**Figure C.9**). As with *C. vulgaris*, there was no obvious bacterial contamination, likely because *T. obliquus* was also cultured in BG-11.

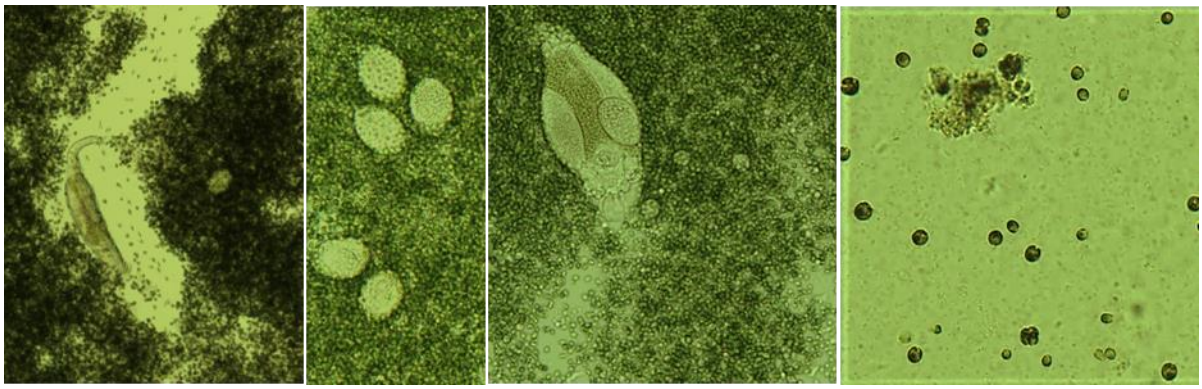

Figure 2.4. *C. reinhardtii* aggregates, rotifers, and bacteria, eight days after cultures were treated with *D. magna* (1.25 mL^{-1}). Images were taken in brightfield at 4–10× magnification.

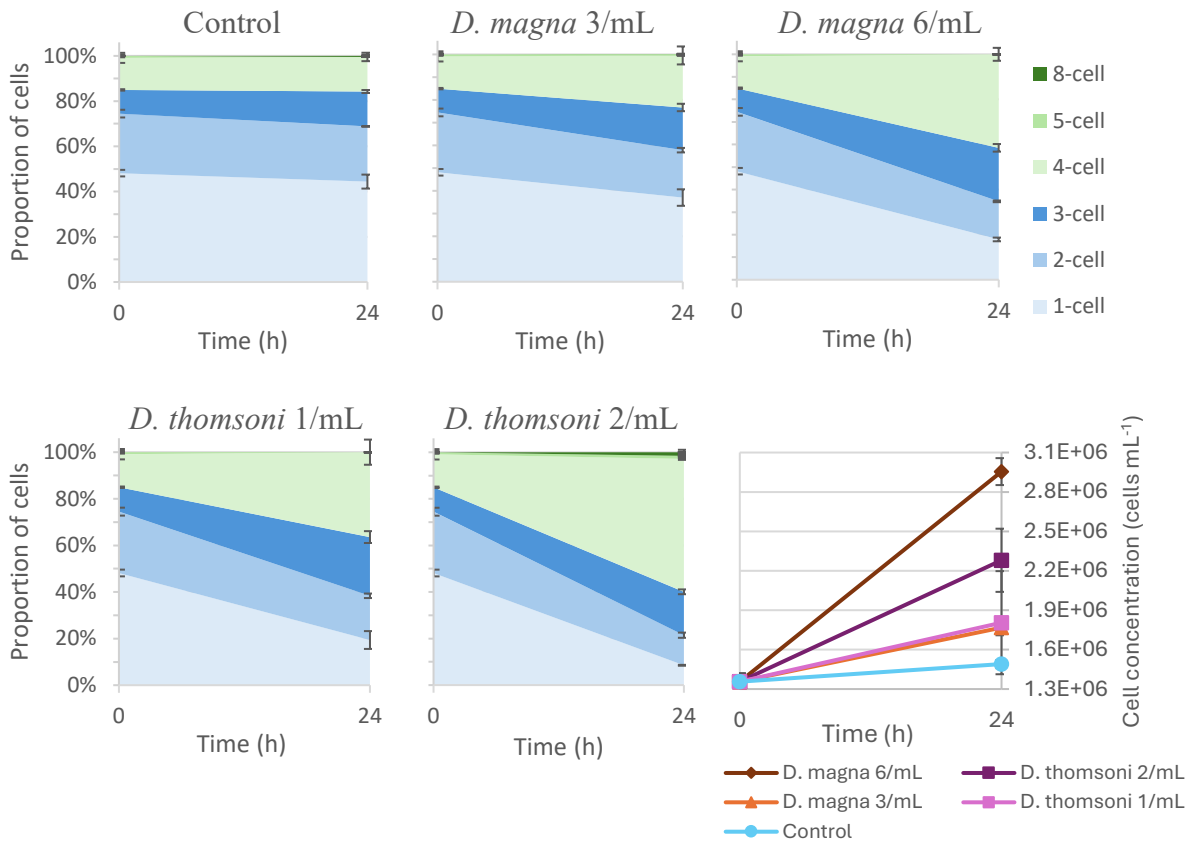

Figure 2.5. Proportion of *C. reinhardtii* cells, unicellular and in colonies, and cell concentration, over 24 hours, in controls and cultures treated with *D. magna* (3–6 mL^{-1}) and *D. thomsoni* (1–2 mL^{-1}). Error bars represent the standard errors ($N = 2$ technical replicates).

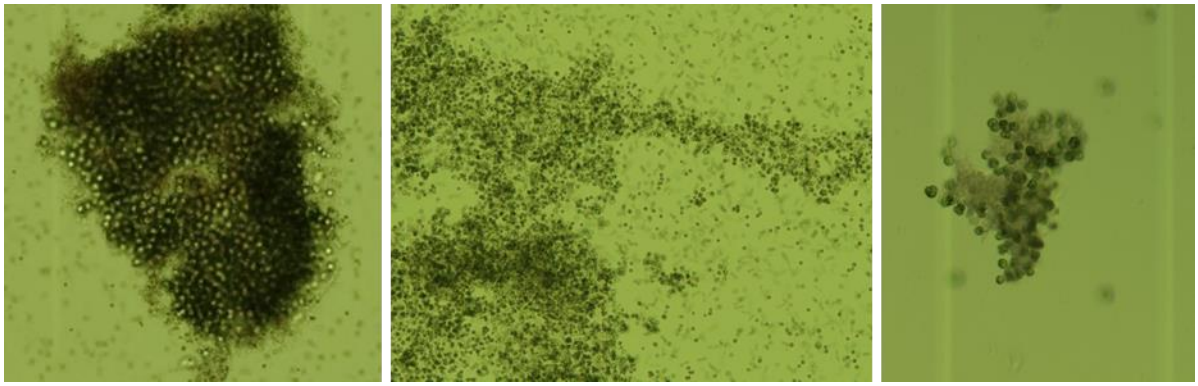

Figure 2.6. Aggregates in *C. reinhardtii* cultures treated with *D. magna* (left and middle; 4× magnification) and *D. thomsoni* (right; 10× magnification). Images were taken using brightfield microscopy (4–10× magnification).

2.3.2 Pond organism extract

T. obliquus was the only species to aggregate in cultures treated with pond extract (0.2–1% v/v), forming small colonies which were more abundant in cultures treated with the higher dose (**Figure C.10**) In contrast, most cells in *C. reinhardtii* (**Figure 2.7**) and *C. vulgaris* (**Figure C.4**) cultures remained unicellular or paired.

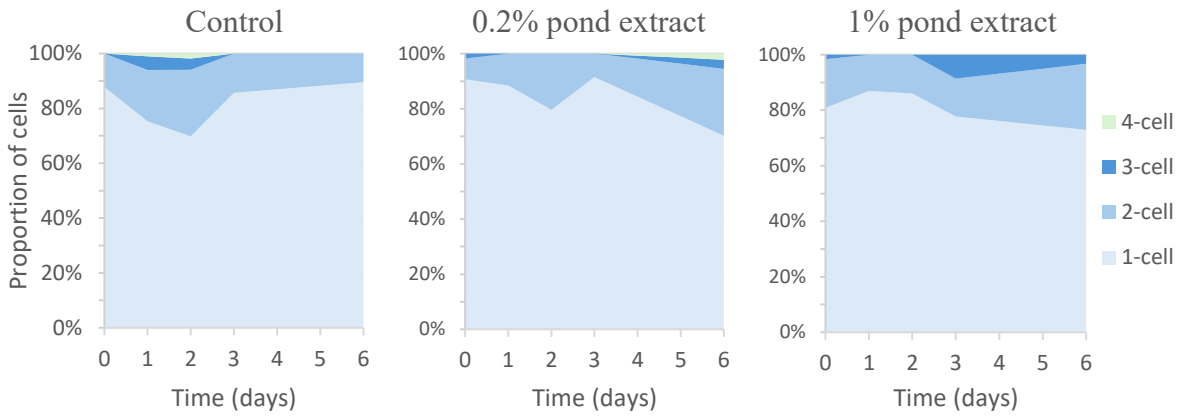

Figure 2.7. Proportion of *C. reinhardtii* cells, unicellular and in colonies, over six days, in the control and cultures treated with pond extract at 0.2–1% v/v.

2.3.3 *Daphnia* filtrate

In contrast to pond extract treatments, *C. reinhardtii* and *C. vulgaris* cultures treated with *Daphnia* filtrate (37% v/v) exhibited self-aggregation at 24 h, whereas *T. obliquus* did not. *C. reinhardtii* contained a large proportion of four- and eight-celled colonies, with just 13% of cells unicellular compared to 33% in the control (**Figure 2.8**). Treated *C. vulgaris* cultures contained small and large aggregates but were otherwise unicellular (**Figure C.1** and **Figure C.2**). *T. obliquus* exhibited only a slight increase in the abundance of colonies at 24 h in treated cultures compared to the control, but this was not significant or consistent over 96 h (**Figure C.7** and **Figure C.8**).

The infochemicals may have been present at concentrations too low to induce aggregation in *T. obliquus*, but it would be difficult to test this filtrate at a higher dose, as replacing a significant fraction of the culture medium would undoubtably effect the microalgae (the 37% v/v dose tested here may have already done so). Therefore, predator filtrate may be too dilute to be used as a robust aggregation trigger. Further, producing filtrate relies on a healthy culture without

crashes and the culture age, frequency of water changes, *Daphnia* population density, and feeding rate must be kept consistent, making this filtrate difficult to reproduce.

2.3.4 *Daphnia* water extract

C. reinhardtii treated with water extract (1% v/v) did not aggregate relative to the control within 24 h, however the cell concentration was significantly higher at 24–48 h (**Figure 2.9** and **Figure 2.10**). After four hours, treated *C. vulgaris* cultures contained numerous small macroscopic aggregates, and these adhered into very large flocs (~1 floc per mL, in all replicates) that were present from 1–4 days, while the suspended cells remained unicellular (**Figure C.1** and **Figure C.2**). From 24–72 h, treated *T. obliquus* cultures contained a significant proportion of 16- to 64-celled colonies (**Figure C.7** and **Figure C.8**). For example, at 24 h, 61% of cells in the water extract treatment were in colonies (of ≥ 4 cells), compared to just 7% in the control.

These results showed that the three species had very different responses to the water extract, with *T. obliquus* forming colonies, *C. vulgaris* forming large aggregates, and *C. reinhardtii* not aggregating. Therefore, a solvent extract was used next with the aim of extracting more infochemicals from the *Daphnia* biomass.

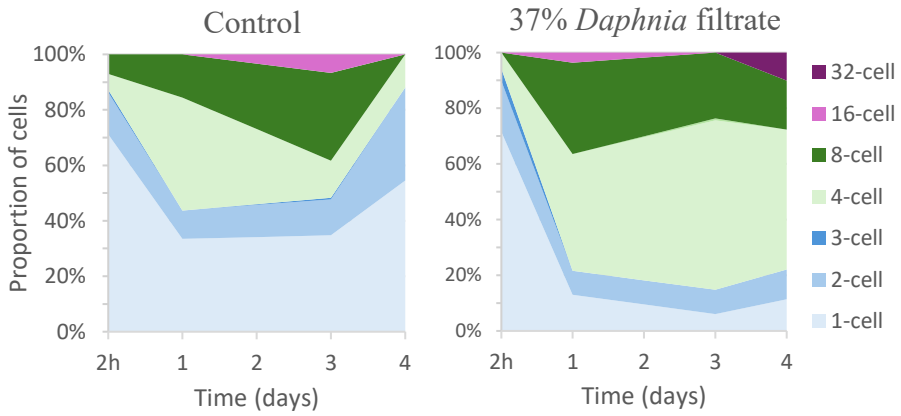

Figure 2.8. Proportion of *C. reinhardtii* cells, unicellular and in colonies, over four days, in the control and cultures treated with *Daphnia* filtrate (37% v/v).

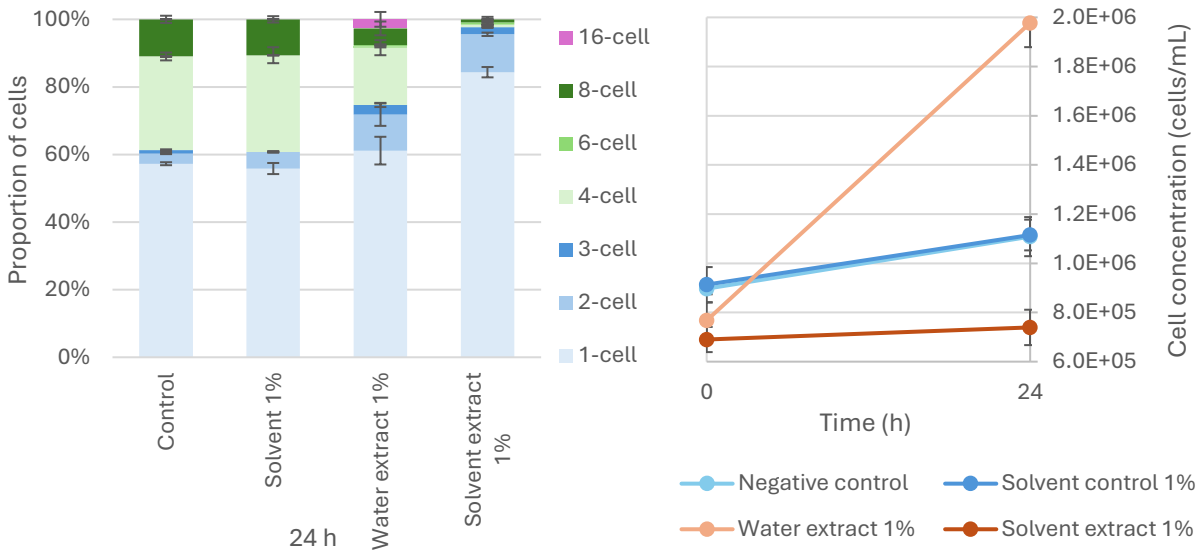

Figure 2.9. Proportion of *C. reinhardtii* cells, unicellular and in colonies, at 24 hours (left), and cell concentration over 24 h (right), in controls and cultures treated with solvent (1% v/v), water extract (1% v/v) and solvent extract (1% v/v). Error bars represent the standard errors (*N* = 3 biological replicates).

2.3.5 *Daphnia* solvent extract

C. reinhardtii

At 24 h, the controls and cultures treated with solvent (1% v/v) both contained four- and eight-celled colonies, with no difference in colony size distribution or cell concentration between the two treatments (**Figure 2.9**). After 96 h, the cultures treated with solvent had a slightly lower cell concentration compared to the controls (**Figure 2.10**).

In contrast, at 24 h, cultures treated with solvent extract (1% v/v) contained predominantly unicellular and paired cells and had exhibited no increase in cell concentration (**Figure 2.9**); after 48 h the cultures were colourless (**Figure 2.10**).

While the solvent had only a minor growth limiting effect compared to the controls after four days, the bleaching of cultures treated with solvent extract suggests that the extracted infochemicals (which likely differed from those in the water extract) or the combination of solvent and infochemicals had inhibited growth and caused the bleaching.

C. vulgaris

C. vulgaris cultures treated with solvent at 1% formed large aggregates within four hours and even more so within 24 h. Within the same timeframes, cultures treated with solvent extract at 1% exhibited the strongest aggregation response, with the entire culture aggregating (**Figure C.1** and **Figure C.2**). This showed that solvent alone, and the combined exposure to solvent and extracted infochemicals, could induce aggregation in *C. vulgaris*. However, when cultures were treated with doses of 2% v/v, exposure to both solvent and solvent extract appeared to bleach the culture, indicating that a solvent dose of 2% v/v was too strong (**Figure C.1**).

T. obliquus

T. obliquus cultures treated with solvent extract at 1% v/v formed small colonies (4–8 cells), though these were slightly smaller than colonies formed in cultures treated with water extract (4–64 cells) (**Figure C.7**). Macroscopic aggregates were observed in cultures treated with solvent extract but not in those treated with solvent (1% v/v) (**Figure C.8**). Since these colonies were smaller than in cultures treated with water extract, this suggests that the solvent itself may have had an inhibitory effect on colony formation in *T. obliquus*, in complete contrast to *C. vulgaris*.

Summary

The solvent extract bleached *C. reinhardtii*, but induced aggregation in *C. vulgaris* and *T. obliquus*. Meanwhile the solvent alone had minimal effect on *C. reinhardtii*, induced aggregation in *C. vulgaris* and had no apparent effect on *T. obliquus*. These results show varied species-specific responses, and an interaction effect of solvent and infochemicals on self-aggregation. To investigate the effects of solvent-extracted infochemicals alone, the solvent extract was dried and resuspended in water and tested next in the bioassays.

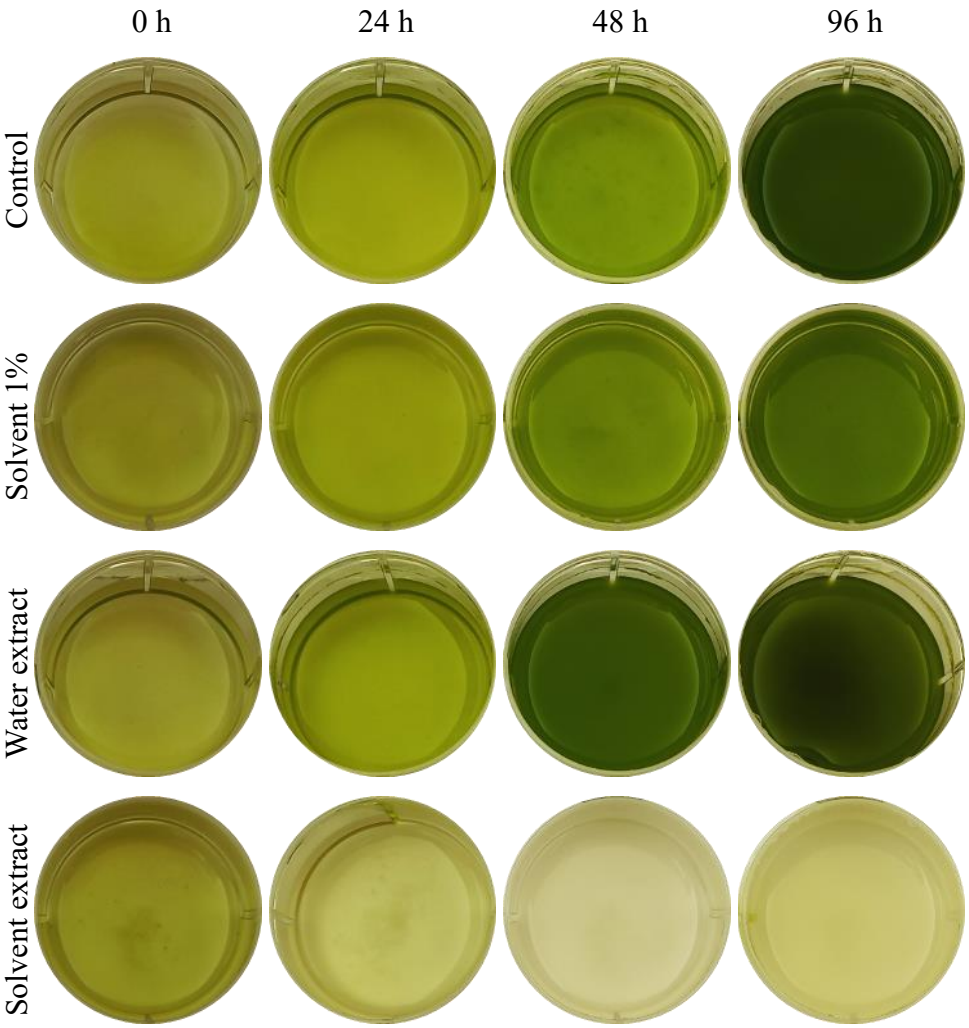

Figure 2.10. Photographs of *C. reinhardtii* bioassay wells taken at 0, 24, 48, and 96 h (left to right, respectively), in the control, and cultures treated with solvent (1% v/v), water extract (1% v/v) and solvent extract (1% v/v). Controls and treatments were carried out in triplicate.

2.3.6 Resuspended *Daphnia* solvent extracts

Resuspended solvent extracts had surfactant-like properties, including increased surface tension and notable foaming during rotary evaporation. *Daphnia pulex* infochemicals have previously been identified as surfactants (see **Chapter 5**) (Yasumoto et al., 2005).

These resuspended solvent extracts reproducibly induced self-aggregation. The mean colony size of *C. reinhardtii* cultures treated with resuspended Sera or MPS extract increased significantly within 16–24 h after extract addition, while controls remained unicellular (**Figure 2.11**).

The Sera resuspended extract also induced colony formation in *C. vulgaris* and the resuspended extract from frozen *Daphnia* induced self-aggregation in all three species, with aggregation increasing with dose (**Appendix C**, **Figure C.5**, **Figure C.11** and **Figure C.12**).

C. reinhardtii cultures treated with resuspended Sera extract formed four- and eight-celled colonies which adhered together into large aggregates (**Figure 2.12**). These colonies of 2^n cells, formed following cell division, are referred to as *palmelloids* and share a mother cell wall (**Chapter 1**). In contrast, the *C. vulgaris* aggregates had cells adhered to a visible matrix, rather than in colonies surrounded by a cell wall (**Appendix C**, **Figure C.6**).

C. reinhardtii cultures treated with the resuspended MPS extract formed even larger macroscopic aggregates, than the Sera extract. The 10% dose of MPS extract induced larger aggregates than 5%, but the size did not increase further with the 20% dose (**Figure 2.13**).

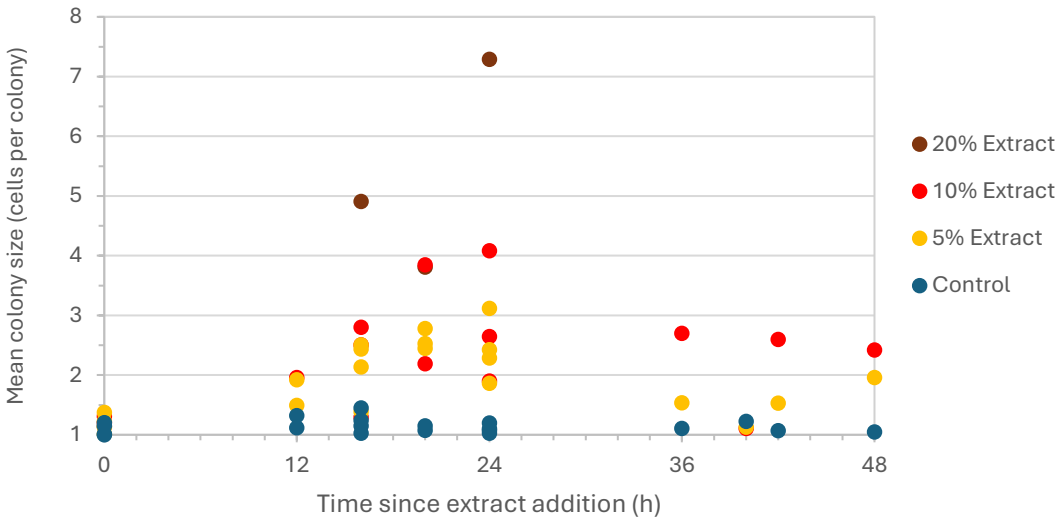

Figure 2.11. The mean colony size in *C. reinhardtii* controls and cultures treated with extract. This includes data from five experiments testing resuspended Sera and resuspended MPS extract at 5–20% v/v.

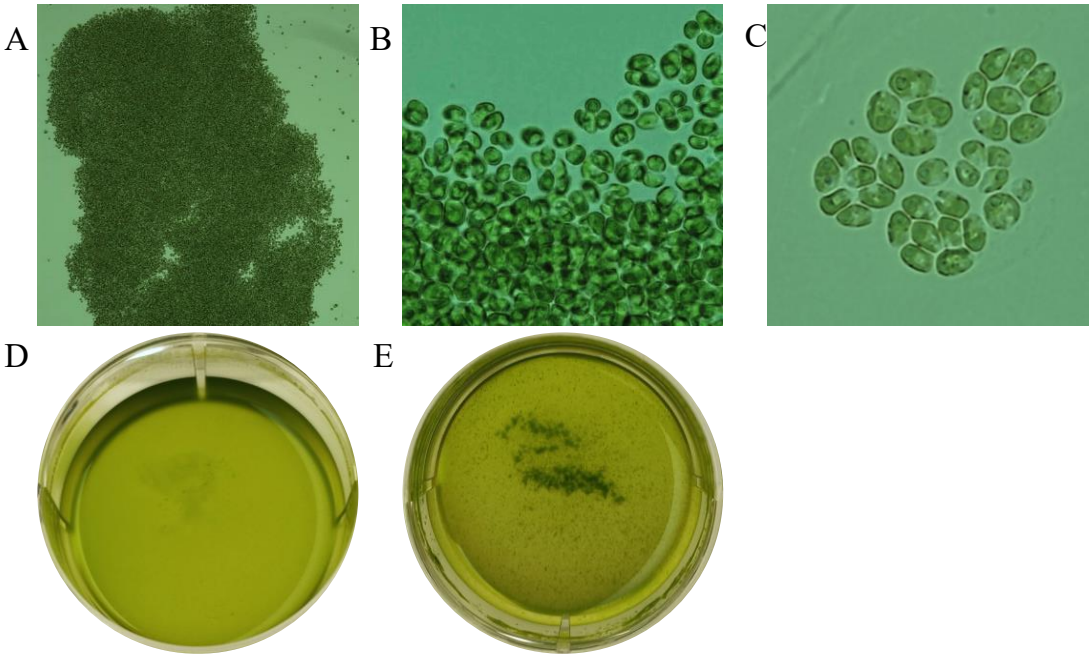

Figure 2.12. Brightfield microscopy images of *C. reinhardtii* cells treated with resuspended Sera extract, imaged at 10x (A), 40x (B), and 100x (C) magnification, and photographs of bioassay wells containing the control (D) and treated culture (E) after five days.

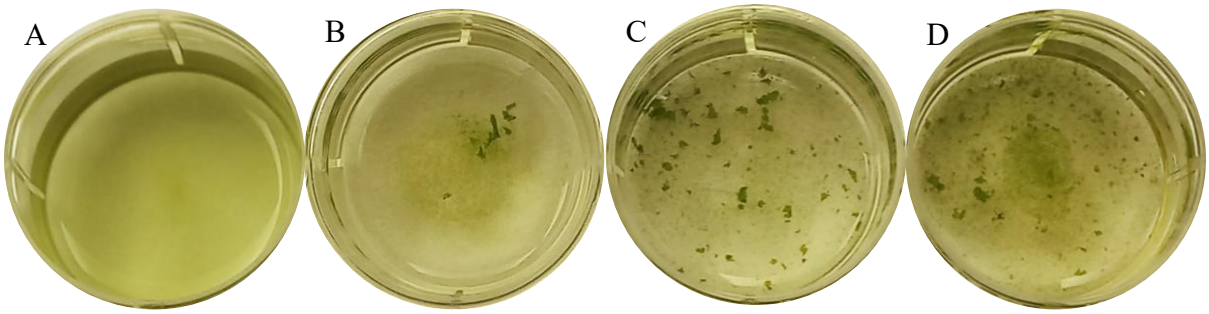

Figure 2.13. Photographs of *C. reinhardtii* bioassay wells at 48 h, in control (A), and resuspended MPS extract treatments at 5% v/v (B), 10% v/v (C), and 20% v/v (D).

To investigate if prolonged exposure through repeated extract addition induced larger aggregates, the MPS extract was added to *C. reinhardtii* cultures every 24 h for four days. However, across days 2–7, these cultures contained predominantly four-celled colonies, whereas cultures treated with extract only once (at 0 h) contained 16- and 32-celled colonies across days 3–7 (**Figure 2.14**).

The cultures treated with extract each day also had a lower cell concentration at day three compared to the one-off treatments and controls, which suggests that the extract had an inhibitory effect on growth when present at higher concentrations or for a prolonged period, and the smaller colony size was likely a direct consequence of the lower growth rate.

Another bioassay was conducted to investigate the influence of initial cell concentration in *C. reinhardtii* on the aggregation response, which indeed had an effect on the rate of colony formation: cultures with ~5 × 10^5 cells mL^{-1} when treated with resuspended MPS extract aggregated within 12 h (**Figure 2.15**), whereas cultures with ~5 × 10^4 cells mL^{-1} had only begun to aggregate between 24–48 h (**Figure 2.14**). Interestingly, when aggregation was delayed, the colonies that eventually formed were larger: ≤ 32 cells in the delayed culture (**Figure 2.14**) compared with 4–8 cells in the faster culture (**Figure 2.15**).

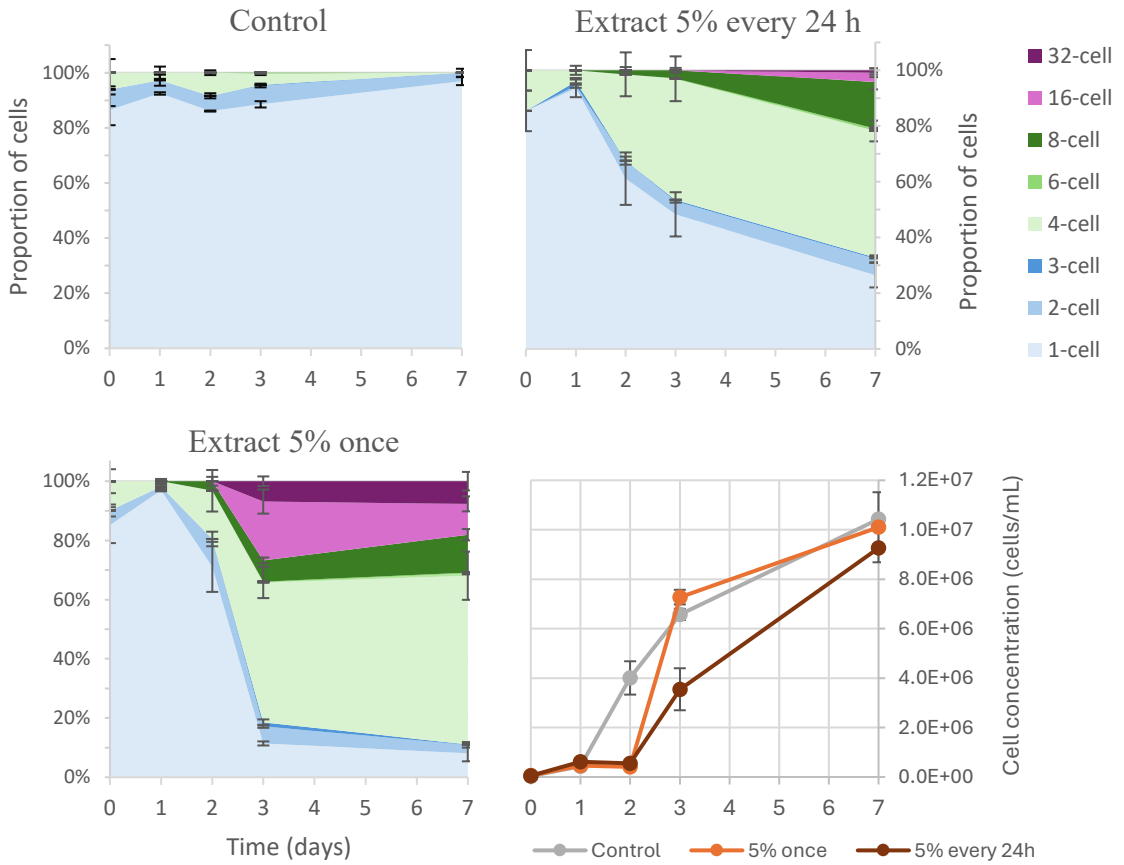

Figure 2.14. Cell concentration and proportion of *C. reinhardtii* cells in colonies in controls and cultures treated with resuspended MPS extract at 5% v/v added every 24 h up to four days (top right) and 5% v/v added only once at 0 h (bottom left). Error bars represent the standard errors (N = 3 biological replicates).

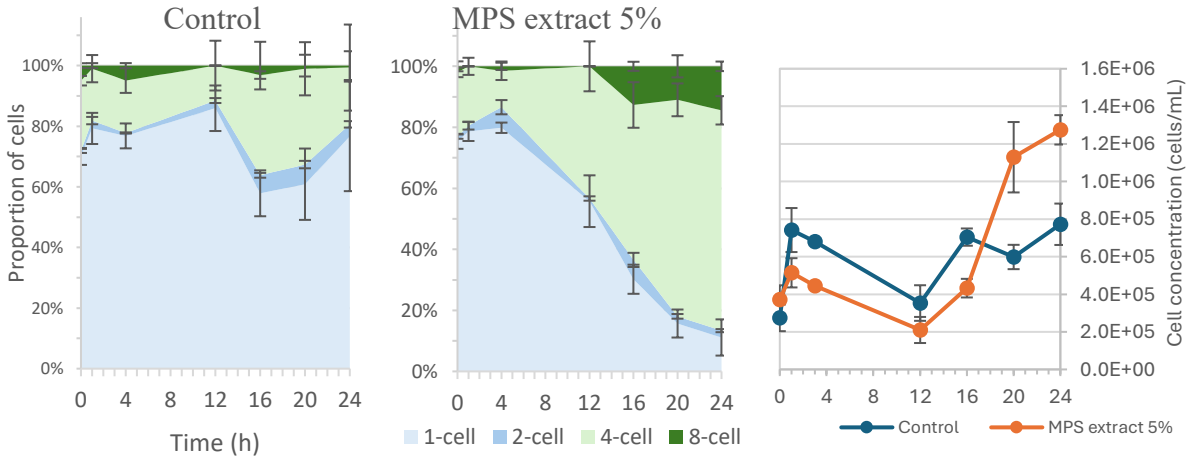

Figure 2.15. *C. reinhardtii* cell concentration and proportion of cells, unicellular and in colonies, over 24 hours, in controls and cultures treated with resuspended MPS extract (5% v/v). Error bars represent the standard errors (N = 3 biological replicates).

2.4 Conclusions

This study provides the first systematic comparison of different forms of *Daphnia* chemical cues on self-aggregation across multiple microalgal species. *C. reinhardtii*, *C. vulgaris* and *T. obliquus* all exhibited some level of aggregation in response to live *Daphnia* or their infochemicals, although the degree and morphology of the aggregation varied between species and triggers. These findings demonstrate that microalgae can employ a common defensive strategy (i.e., self-aggregation) in distinctive ways (i.e., colony formation or EPS-mediated adhesion of cells), depending on both the species and the nature of the cue.

Live *Daphnia* induced self-aggregation in *C. reinhardtii* and *T. obliquus* but not in *C. vulgaris*. In *C. reinhardtii*, palmelloids and macroscopic aggregates were observed, although microscopic examination suggested the presence of a matrix likely contributed by bacteria. Contamination by bacteria and other zooplankton, as well as the rapid mortality of *Daphnia* in algal cultures, limited the usefulness of live grazers for controlled assays.

To address these challenges, *Daphnia* infochemicals were extracted using several approaches. These extracts could be sterilised, reproduced, and potentially subjected to chemical characterisation, as demonstrated in previous studies (e.g., Yasumoto et al., 2005). Notably, the extracts exhibited surfactant-like properties, raising the possibility that the active compounds were similar to those reported by Yasumoto et al. (2005).

Of the methods tested, the solvent extract prepared from freeze-dried *Daphnia*, dried, and resuspended in water consistently and reproducibly induced rapid palmelloid formation in *C. reinhardtii*. This response was culture-wide, with the majority of cells forming colonies. By contrast, *C. vulgaris* remained largely unicellular even when some aggregates were present. The uniform population-level response reported with *C. reinhardtii* is particularly valuable for biotechnological applications, such as biomass harvesting, and for experimental studies comparing transcriptomic and metabolomic profiles of aggregated vs non-aggregated cultures.

In conclusion, this work established a reproducible bioassay system using *C reinhardtii* and *Daphnia* extracts, providing a robust foundation for future mechanistic studies. Subsequent research employed this system to investigate the molecular basis of *Daphnia*-induced self-aggregation in *C. reinhardtii* through transcriptomic (**Chapter 3**) and metabolomic analyses (**Chapter 4**).

References

Berger, C. M. (2017). *The genetic basis of cooperative aggregation in the green alga Chlamydomonas reinhardtii (Master's thesis). Kansas State University.*

Fisher, R. M., Bell, T., & West, S. A. (2016). Multicellular group formation in response to predators in the alga *Chlorella vulgaris*. *Journal of Evolutionary Biology*, *29*, 551-559. https://doi.org/10.1111/jeb.12804

Ha, K., Jang, M. H., & Takamura, N. (2004). Colony formation in planktonic algae induced by zooplankton culture media filtrate. *Journal of Freshwater Ecology*, *19*, 9-16. https://doi.org/10.1080/02705060.2004.9664506

Hou, X., Zhou, Q., Wang, Z., Kong, Q., Sun, Y., Zhang, L., Zhu, X., Huang, Y., & Yang, Z. (2018). Magnesium depletion suppresses the anti-grazer colony formation in *Scenedesmus obliquus*. *Environmental Science and Pollution Research*, *25*, 34228-34235. https://doi.org/10.1007/s11356-018-3191-8

Kapsetaki, S., Fisher, R., & West, S. (2016). Predation and the formation of multicellular groups in algae. *Evolutionary Ecology Research*, *17*, 651-669.

Lee, D. Y., & Fiehn, O. (2008). High quality metabolomic data for *Chlamydomonas reinhardtii*. *Plant Methods*, *4*, 7. https://doi.org/10.1186/1746-4811-4-7

Lurling, M., & Beekman, W. (2006). Palmelloids formation in *Chlamydomonas reinhardtii*: Defence against rotifer predators? *International Journal of Limnology*, *42*, 65-72. https://doi.org/10.1051/limn/2006010

Pan, Y., Liu, C., Li, F., Zhou, C., Yan, S., Dong, J., Li, T., & Duan, C. (2017). Norfloxacin disrupts *Daphnia magna*-induced colony formation in *Scenedesmus quadricauda* and facilitates grazing. *Ecological Engineering*, *102*, 255-261. https://doi.org/10.1016/j.ecoleng.2017.02.037

Roccuzzo, S., Couto, N., Karunakaran, E., Kapoore, R. V., Butler, T. O., Mukherjee, J., Hansson, E. M., Beckerman, A. P., & Pandhal, J. (2020). Metabolic insights into infochemicals induced colony formation and flocculation in *Scenedesmus subspicatus* unraveled by quantitative proteomics. *Frontiers in Microbiology*, *11*, 792. https://doi.org/10.3389/fmicb.2020.00792

Yasumoto, K., Nishigami, A., Aoi, H., Tsuchihashi, C., Kasai, F., Kusumi, T., & Ooi, T. (2008a). Isolation and absolute configuration determination of aliphatic sulfates as the *Daphnia* kairomones inducing morphological defense of a phytoplankton - Part 2. *Chemical and Pharmaceutical Bulletin*, *56*, 129-132. https://doi.org/10.1248/cpb.56.129

Yasumoto, K., Nishigami, A., Aoi, H., Tsuchihashi, C., Kasai, F., Kusumi, T., & Ooi, T. (2008b). Isolation of new aliphatic sulfates and sulfamate as the *Daphnia* kairomones inducing morphological change of a phytoplankton *Scenedesmus gutwinskii*. *Chemical and Pharmaceutical Bulletin*, *56*, 133-136. https://doi.org/10.1248/cpb.56.133

Yasumoto, K., Nishigami, A., Kasai, F., Kusumi, T., & Ooi, T. (2006). Isolation and absolute configuration determination of aliphatic sulfates as the *Daphnia* kairomones inducing morphological defense of a phytoplankton. *Chemical and Pharmaceutical Bulletin*, *54*, 271-274. https://doi.org/10.1248/cpb.54.271

Yasumoto, K., Nishigami, A., Yasumoto-Hirose, M., Kasai, F., Okada, Y., Kusumi, T., & Ooi, T. (2005). Aliphatic sulfates released from *Daphnia* induce morphological defense of phytoplankton: Isolation and synthesis of kairomones. *Tetrahedron Letters*, *46*, 4765-4767. https://doi.org/10.1016/j.tetlet.2005.05.027

Chapter 3.

Mechanisms of palmelloid defence revealed through transcriptomics

---

Preface

The bioassays in **Chapter 2** revealed that *Daphnia* infochemicals reliably induced self-aggregation as palmelloids in the majority of *C. reinhardtii* cells, making this an effective model system for transcriptomic analysis. In addition, *C. reinhardtii* was chosen as the study organism because its genome is fully sequenced and CLiP mutant strains are readily available from the Chlamydomonas resource center (chlamycollection.org).

This study investigated the transcriptomic responses of *Chlamydomonas reinhardtii* cultures aggregated by exposure to *Daphnia* extract to generate hypotheses about the physical mechanisms and chemical signalling pathways mediating self-aggregation.

The findings presented in this chapter provided new insight into how microalgae form protective colonies in response to grazers. These results are also critical for understanding how self-aggregation might be exploited as a sustainable tool for harvesting microalgal biomass, as explored further in **Chapter 5**.

Abstract

This chapter presents the first transcriptomic analysis of palmelloid formation in *Chlamydomonas reinhardtii* exposed to *Daphnia* infochemicals. Palmelloid formation is a stress-induced self-aggregation response that occurs when daughter cells are not released after cell division and instead remain encapsulated within the mother cell wall. Within 12 hours of exposure to *Daphnia* extract, *C. reinhardtii* cultures developed palmelloids containing 4–16 cells. In the context of this thesis, palmelloid formation would be beneficial to increase the recovery efficiency of harvesting methods, by increasing the average algal particle size without requiring contaminating flocculants.

RNA sequencing revealed downregulation of genes encoding structural flagellar proteins, including tubulin, centrosomal proteins, intraflagellar transport proteins, pherophorins, and cell wall-degrading enzymes such as matrix metalloproteinases (MMPs). These results evidence, for the first time, that *C. reinhardtii* delays flagella reassembly, thereby preventing the degradation of the mother cell wall via degradative enzymes, which traps daughter cells in palmelloids. Supporting this, a mutant lacking the gene *MMP13* spontaneously formed palmelloids, consistent with impaired cell wall degradation.

Significant changes were also observed in signalling-related genes, particularly kinases linked to calcium signalling, cyclin-dependent kinases, ubiquitin-proteasome pathway components, and transient receptor potential (TRP) channels. A mutant deficient in *TRP13* showed little to no aggregation under low light or *Daphnia* extract, highlighting a potential role as a sensor of external cues. While some TRP channels are known sensors, this is the first evidence of a sensing role in TRP13. By contrast, mutants disrupted for *FAP199* (encoding a flagella-associated protein) and *PHC18* (encoding a pherophorin) still formed palmelloids under stress, suggesting overlapping functions within these gene families or an indirect role.

Together, these findings presented strong evidence of delayed flagellar regeneration which likely directly impaired normal cell wall degradation and release of cells. *MMP13* and *TRP13* were identified as strong candidate regulators of palmelloid formation, involved in cell wall degradation and infochemical sensing, respectively. This work provides new insight into the molecular regulation of predator-induced self-aggregation in *C. reinhardtii* and establishes a foundation for further studies into the mechanisms and applications of palmelloid formation.

3.1 Introduction

Triggering self-aggregation on demand could offer a sustainable and cost-effective alternative to chemical flocculants for biomass harvesting; however, this application requires understanding of the underlying processes of infochemical detection and colony formation and maintenance. Although predator-induced aggregation is well documented, the molecular processes that initiate and sustain this response remain poorly understood (**Chapter 1**).

Preliminary bioassays (**Chapter 2**) confirmed that *Daphnia* infochemicals induced *C. reinhardtii* palmelloid formation. This is a known stress response, where cells remain encapsulated, continuing to divide within a mother cell wall; cells can be later released if conditions normalise or otherwise undergo programmed cell death (de Carpentier et al., 2019). Mother cell wall degradation has been suggested to occur through the action of degradative enzymes, which are released by daughter cells via extracellular vesicles, or ectosomes, through the flagella (Wood et al., 2013). However, the full picture – the identity of these enzymes, and the mechanisms regulating their production, transport, possible activation, and activity – is unknown.

This study used transcriptomics to generate hypotheses about the infochemical sensors, signalling cascades, enzymatic processes, and structural changes underlying palmelloid formation in *C. reinhardtii*. Cultures were treated with *Daphnia* extract, and the transcriptomes were compared with untreated unicellular control cultures using RNA sequencing to identify differentially expressed genes. The genome of *C. reinhardtii* had been sequenced, allowing the potential roles of individual genes or gene families with strong differential expression to be discussed, and mutant strains were used for investigating candidate genes.

3.2 Materials and methods

3.2.1 Microalgae strains and culture maintenance

Table 3.1 lists all *C. reinhardtii* strains used in this study. *C. reinhardtii* wildtype CC-1690 was used for the transcriptomics study. Mutant *C. reinhardtii* strains (i.e., deficient in a specific gene) were selected based on significantly differentially expressed genes in CC-1690 which were hypothesised to be involved in palmelloid formation (see **Section 3.2.6**). These were purchased from the Chlamydomonas resource center (chlamycollection.org), along with their background strain CC-5325.

All strains were maintained on sterile tris-acetate-phosphate (TAP) agar and used to create axenic liquid TAP cultures under aseptic conditions. All reagents and equipment were autoclaved (121 °C, 15 min) before use.

Cultures for transcriptomics

To prepare stock CC-1690 cultures, 250 mL conical flasks containing 100 mL liquid TAP media and closed with cotton bungs were autoclaved, before inoculation with a single cell colony from agar. Fresh cultures were prepared weekly by transferring 1 mL from an existing culture into 100 mL sterile TAP medium. Cultures were incubated (INFORS HT Multitron) at 22 °C on an orbital shaker (115 rpm) under constant fluorescent light from above (24 ± 1 µmol m^{-2} s^{-1}; Hg 15 Watt, F15T8/CW).

Mutant cultures

Mutants strains, CC-1690, and CC-5325 were cultured in TAP media in conical flasks closed with cotton stoppers, incubated at 22 °C, with no shaking. The incubator had LED lighting around the top, bottom, and sides, and cultures were on a wire shelf (this setup exposed the cultures to light from all directions). The light intensity ranged from 8.2 ± 0.5 to 188.6 ± 10.6 µmol m^{-2} s^{-1} (see **Section 3.2.6**). Cultures were refreshed regularly by emptying the flasks under a laminar flow cabinet and refilling with sterile TAP medium.

3.2.2 Inducing self-aggregation for transcriptomics

3.2.2.1 *Daphnia* extract

Previous work demonstrated that exposure to extracts from freeze-dried *Daphnia* effectively triggered the formation of palmelloid colonies in *C. reinhardtii* (**Chapter 2**). The "resuspended MPS extract" described in **Chapter 2** was used in this study to characterise the transcriptome of *C. reinhardtii* during palmelloid formation through RNA sequencing and later untargeted metabolomics (**Chapter 4**). The extract is referred to here as "*Daphnia* extract."

Table 3.1. *Chlamydomonas reinhardtii* strains from the Chlamydomonas resource center (chlamycollection.org).

Strain	Description
CC-1690 wild type mt+	Wild type strain used for bioassays and RNA-seq experiment
LMJ.RY0402.064808	*TRP13* deficient
LMJ.RY0402.206125	*MMP13* deficient
LMJ.RY0402.117932	*PHC18* deficient
LMJ.RY0402.182125	*FAP199* deficient
CC-5325 cw15 mt-	Background strain of mutants (same as CC-4533 cw15 mt-)

3.2.2.2 Self-aggregation experiment

To prepare unicellular (control) and aggregated (treatment) *C. reinhardtii* cultures for transcriptomics and metabolomics (**Chapter 4**), *C. reinhardtii* cultures were prepared and treated as described below:

A single *C. reinhardtii* colony was inoculated into sterile liquid TAP medium. After four days, this stock culture contained predominantly unicellular and paired cells, confirming that the microalgae were not under any stress. Nine 1 L conical flasks containing 545 mL sterile TAP medium were adjusted to pH 7.55 with 1.25 mL sterile 1M NaOH and inoculated with 5 mL stock culture to give an initial optical density of 0.006 (at 683 nm; Shimadzu UV-1800 spectrophotometer). The cell density was ~3×10^4 cells mL^{-1}. These flasks were incubated at 22 °C, on an orbital shaker (115 rpm), under constant fluorescent light (24 ± 1 μmol m^{-2} s^{-1}). The position of the flasks were randomly changed each day to minimise any variation in growth

between flasks caused by potential positional light variation. Following a three-day acclimation and growth period, the cell density reached ~1.7×10^6 cells mL^{-1} in all flasks. Treatments were then applied in triplicate:

- **Controls** received 10% v/v sterile distilled water.
- **5% treatments** received 5% v/v *Daphnia* extract, and 5% v/v distilled water.
- **10% treatments** received 10% v/v *Daphnia* extract.

Samples were collected 0.5 h before extract addition, immediately after (0 h), and at 1, 2, 12, 14, 16, 20, 24, 36, and 42 h (under sterile conditions). At all timepoints, 3 mL was pipetted from each flask into Falcon tubes for immediate morphological analysis and cell pellets were harvested for transcriptomic and metabolomic analyses: 10–60 mL (~8×10^7 cells) were removed from each flask and divided equally into two Falcon tubes which were centrifuged immediately (3300 × *g*, 5 min) and the supernatant was discarded. Cell pellets were immediately frozen and stored at -80 °C until RNA extraction, following the PureLink® RNA Mini Kit user guide.

3.2.2.3 Morphological analysis

Colony formation, cell concentration, optical density, and pH were monitored at each sampling point from -0.5 h to 42 h. Optical density and pH were measured immediately after sampling. Total cell concentration, colony size distribution, and the proportion of cells occurring as unicells or in colonies, were manually counted in ImageJ from microscope images taken at 10× magnification, as described in **Chapter 2** and following the methods of Sun et al. (2020) and Zhu, Wang, et al. (2021).

To observe aggregates in finer detail, samples were provided to the Massey Microscopy Centre, where they were prepared (fixation, cutting, and staining) and observed under a FEI Tecnai G2 Biotwin transmission electron microscope (results in **Appendix D**).

3.2.2.4 Statistical analysis

Two-way ANOVA tests were run using R-studio, on pH, total cell concentration, concentration of single cells or colonies, proportion of cells single or in colonies, and the mean colony size, to test effects of treatment and time. All parameters were measured in triplicate at each

timepoint, and results are reported as mean ± standard error. The ANOVA *p*-values were adjusted for multiple testing using the Benjamini-Hochberg method to control the false discovery rate; for each parameter, the Levene's and Shapiro-Wilk tests were used to check that residuals were normally distributed, and that the variances were equal across treatment-time groups, as commonly applied in aggregation studies (Albini et al., 2019; Xiao et al., 2017). Where the residuals were not normally distributed, log, square root, and cube root transformations were used to improve it, or a Box-Cox transformation was applied (Zuur et al., 2010). The best transformation per parameter was selected based on the Shapiro-Wilk p-value. For parameters with significant ANOVA effects, post-hoc pairwise comparisons were carried out using Tukey's HSD test, on treatment, time, and their interactions, which adjusts *p*-values for multiple comparisons (Albini et al., 2019; Oda et al., 2022). R packages used in statistical analyses included **car**, **broom**, **emmeans**, and **ggplot2**.

3.2.3 RNA extraction and sequencing

The control and *Daphnia* treatments, at the timepoints 1, 12, 20, and 36 h, were selected for transcriptomics, based on the following rationale:

Timepoints:

- 1 h – to identify changes in gene expression occurring soon after extract addition.
- 12 h – the first timepoint where significant aggregation was observed.
- 20 h – cultures had been aggregated for several hours, and it was from this point that the abundance of colonies had started to reduce in the 5% treatment.
- 36 h – the abundance of colonies had significantly reduced in the 5% treatment while the 10% had maintained its aggregated state.

Treatments:

- The control and the 5% and 10% treatments were selected to identify differences in gene expression between the treatments and control, and between the two treatments when the 5% treatment started to return to its unicellular state and the 10% treatment maintained its colonies.

From one of the two frozen cell pellets sampled from each flask (> 1×10^7 cells), RNA was extracted using the Invitrogen™ PureLink® RNA Mini Kit (cat. no. 12183018A), following the

user guide with slight modification from the standard protocol, in combination with Invitrogen™ bead tubes (cat. no. A29790) to lyse the cells:

1. 1 mL Lysis buffer and 10 µL 2-mercaptoethanol were quickly pipetted into the Falcon tubes containing frozen cell pellets.
2. Tubes were closed and vortexed briefly to suspend cells.
3. The solutions were pipetted into cold bead tubes and shaken (30 s, MP Fastprep-24 tissue and cell homogeniser).
4. Tubes were incubated (-18 °C, 4 min).
5. Tubes were centrifuged (14,000 × *g*, RT, 2 min).
6. Supernatants were carefully pipetted into 1.5 mL microcentrifuge tubes.
7. The subsequent binding, washing, and elution of RNA was performed according to the PureLink™ RNA Mini Kit protocol. The RNA was eluted from the spin cartridge using 10 µL RNase-free water, which was added back through the column for a second elution.
8. The RNA were stored at -80 °C, prior to and following treatment to remove extracted DNA using the Invitrogen™ TURBO DNA-*free*™ Kit (cat. no. AM1907), according to standard protocol.

To avoid contamination and RNA degradation, all surfaces, pipettes, and gloves were cleaned throughout with Invitrogen™ RNase *AWAY*™ Decontamination Reagent (Cat. No. 10328011), and only sterile, RNase-free pipette tips and microcentrifuge tubes were used.

RNA quality was checked by electrophoresis on a 1% (w/v) agarose gel (**Appendix E**, **Figure E.1**). The concentration and purity of extracted RNA was checked by measuring the absorbance at 230, 260 and 280 nm using a NanoDrop™ UV-Vis spectrophotometer to (**Appendix E**, **Table E.1**).

For all samples, 5–10 µL aliquots of RNA were made up to 30 µL with RNase-free distilled water (to achieve 100–150 ng μL^{-1} concentration) in GenTegra-RNA 0.5 mL screwcap microtubes (GTR5100-S), gently mixed with a pipette, and dried (24 h, room temperature) in a laminar flow cabinet. Once dry, tubes were capped and shipped to Custom Science Ltd (New Zealand) where the RNA was resuspended, and the concentration was measured using a Qubit fluorometer (**Table E.1**). Stranded mRNA library preparation, library QC, and sequencing were provided by Custom Science on an Illumina Novaseq system, delivering 6 GB data (> 20M high quality pairs of reads) per sample. All samples passed QC checks.

3.2.4 Gene expression data analysis

Reads were mapped to *C. reinhardtii* genome CC-4532 v6.1 (Phytozome genome ID: 707). Differential expression analysis of read counts between control and *Daphnia* extract treatments was performed using the statistical R-package **DESeq2.v1**, following other transcriptomic studies: (Klein et al., 2017; Plouviez et al., 2021; Thiriet-Rupert et al., 2021; Zhang et al., 2023). This performed Wald tests for each gene to test the significance of the log_2-fold change (log_2-FC) between two treatments. FDR adjusted *p*-values were calculated using the Benjamini-Hochberg method, with a significance threshold of $p < 0.05$ (Thiriet-Rupert et al., 2021). Genes were retained as differentially expressed when the adjusted $p < 0.05$. Log_2 fold-change thresholds of > 1.25 or < -1.25 were applied prior to analysis of the DEGs, however where multiple genes in a gene family were differentially expressed, those under this threshold were also described and presented in gene tables.

Phytozome (https://phytozome-next.jgi.doe.gov/) (Goodstein et al., 2011), UniProt (https://www.uniprot.org/), and the DAVID Bioinformatics gene ID conversion tool (https://davidbioinformatics.nih.gov/conversion.jsp) (Huang da et al., 2009; Sherman et al., 2022) were used to convert gene symbols and/or JGI gene model identifiers to UniProt accessions. The DAVID Bioinformatics functional annotation clustering tool and PANTHER gene list analysis tool (https://pantherdb.org/geneListAnalysis.do) {Mi, 2013 #630} were used to group the differentially expressed genes (DEGs) by their function and identify enriched pathways (Mi et al., 2013; Sherman et al., 2022).

3.2.5 Validation of RNA sequencing by RT-qPCR

Reverse-transcription quantitative polymerase chain reaction (RT-qPCR) was conducted to estimate gene expression and validate RNA sequencing results. Strongly differentially expressed genes, *MMP13* and *FAP199*, were selected, along with *CBLP* (*RACK1*) which is constitutively expressed in *C. reinhardtii* and therefore used as the endogenous reference or 'housekeeping' gene (Tokutsu et al., 2021). These genes were tested using RNA extracted from the control and 5% *Daphnia* treatments, sampled at 0 h and 36 h. The full method and results are provided in **Appendix F**.

3.2.6 Mutant bioassays

Mutant strains and CC-5325 (**Table 3.1**) were used in bioassays with *Daphnia* extract, to investigate if the absence of each gene disrupted the self-aggregation response. CC-1690 was also used for comparison. As light intensity can influence self-aggregation (**Chapter 1**), bioassays were carried out under low light intensity (8.2 ± 0.5 μmol m^{-2} s^{-1}) and high light intensity (188.6 ± 10.6 μmol m^{-2} s^{-1}) to investigate this effect and find conditions in which CC-5325 would aggregate in response to *Daphnia* extract. Cultures were incubated for at least one week after light intensity was adjusted, prior to any testing.

All strains were cultured in 250 mL flasks over eight days following a refresh with new medium, to observe their typical phenotypes and growth kinetics under regular incubation conditions (22 °C and constant light intensity) without *Daphnia* extract.

To test their self-aggregation response, *Daphnia* extract was added in triplicate at 10% v/v to cultures in sterile 6-well Falcon plates, and cell morphology was compared against controls each day.

3.3 Results and Discussion

3.3.1 Cell concentration and pH

C. reinhardtii cell concentration increased in all treatments over the duration of the experiment, from a mean of 6.48×10^5 at 0 h to 6.87×10^6 cells mL^{-1} at 42 h (**Figure 3.1**). Similarly, the pH increased in all treatments with time, from a mean of 7.64 at 0 h to 8.31 at 42 h (**Figure 3.1**). While the cell concentration appeared slightly higher in treatments relative to the control, there was no significant effect of treatment on cell concentration or pH at any time up to 42 h (Tukey HSD, $p > 0.05$); therefore, the increased colony formation in *Daphnia* treatments (see **Section 3.3.2.1**) was not an artefact of increased cell division or a response to pH changes and was indeed in response to the *Daphnia* infochemicals. Raw data is provided in **Appendix G** and full two-way ANOVA and Tukey HSD test results for pH and cell concentration are provided in **Appendix H**. The optical density showed very similar trends as the cell concentration (**Appendix G**, **Table G.4**).

3.3.2 Palmelloid formation

C. reinhardtii formed four-, eight- and 16-celled palmelloid colonies within 12 h in *Daphnia* extract-treated cultures but not in the control (**Figure 3.2**), as shown by the mean colony size (MCS; **Figure 3.3**) and the colony size distribution (**Figure 3.4**). Significant changes are discussed based on the Tukey HSD *p*-values; full results from the two-way ANOVA and Tukey HSD tests for all parameters are provided in **Appendix H** and **Supplementary Data File S1**, respectively.

3.3.2.1 Aggregation

In the first two hours, the mean colony size (MCS; **Figure 3.3**) and proportion of cells in colonies (**Figure 3.4**) did not differ between treatments. Across this period, the 5% and 10% treatments averaged ~1.2 cells per colony with < 25% of cells in colonies, similar to the control. Control cultures showed little change throughout, averaging ~1.2 cells per colony and ~13% of cells in colonies across all timepoints (**Figure 3.3** and **Figure 3.4**).

By 12 h, both *Daphnia* treatments were dominated by four-celled colonies (~45–48% of all cells) with additional eight-celled colonies (~10–15%) while controls remained largely unicellular (**Figure 3.4**). The abundance of single cells dropped significantly in the *Daphnia* treatments relative to the control.

From 14–24 h, colony formation strengthened further. At 24 h, the 5% treatment reached 2.3 cells per colony, and the 10% treatment reached 2.6 cells per colony, compared with just 1.1 cells per colony in the control (**Figure 3.3**). Meanwhile, two-thirds to three-quarters of cells in the *Daphnia* treatments were in colonies, whereas only 5% of control cells were aggregated (**Figure 3.4**).

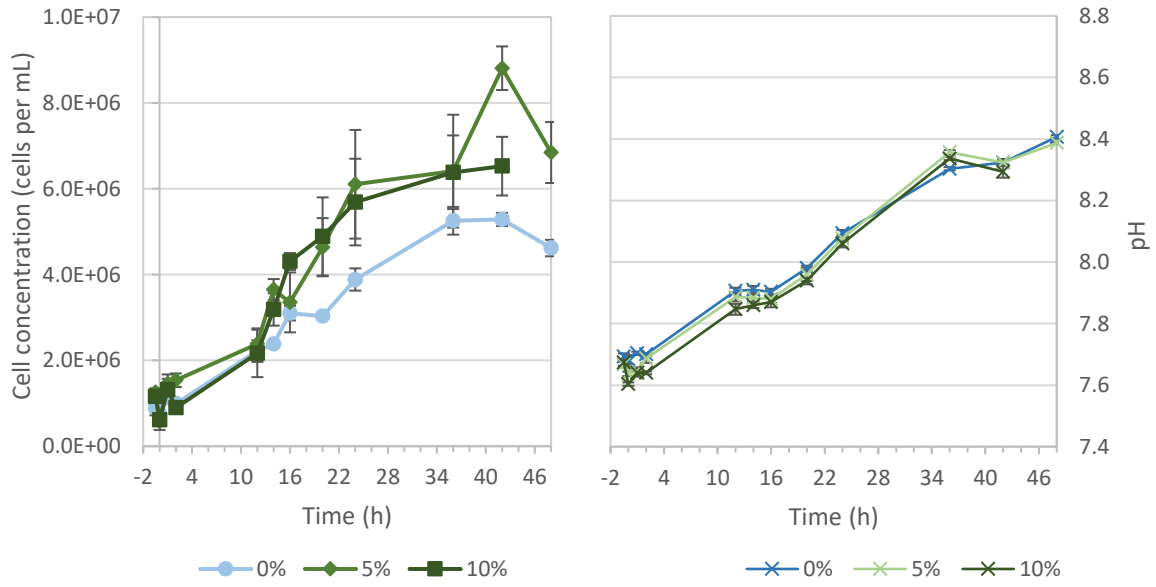

Figure 3.1. Cell concentration (left) and pH (right) of *C. reinhardtii* in control cultures (0%) and cultures treated with 5% and 10% *Daphnia* extract. Error bars represent the standard error (N = 3).

3.3.2.2 Disaggregation?

By 36–42 h, differences between treatments became clearer. The MCS of the 5% treatment dropped to ~1.5 cells per colony, not significantly different from the control, and < 45% of cells were in colonies. In contrast, the 10% treatment maintained an MCS of ~2.6 and ~76% of cells in colonies, significantly higher than both the 5% treatment and control.

The concentration of single cells and colonies (**Figure 3.5**) indicated whether cultures were actively forming palmelloids, at steady state, or if colonies were releasing their cells. In the 10% treatment, most divisions produced colonies rather than single cells: the single cell concentration was ~9.3 × 10^5 cells mL^{-1}, while the colony concentration increased significantly from ~2.7 × 10^5 at 12 h to ~1.1 × 10^6 cells mL^{-1} at 24 h.

In the 5% treatment, colony concentration also rose initially (~8.0 × 10^4 at 2 h to ~1.0 × 10^6 at 24 h) but then plateaued, with no significant changes after 12 h and no difference from the 10% treatment. However, single cell numbers increased markedly from 24–42 h, reaching ~4.6 × 10^6 cells mL^{-1}, comparable to the control (~4.7 × 10^6) and significantly higher than the 10% treatment (~1.3 × 10^6).

These results show that 10% v/v *Daphnia* extract sustained colony formation for the full 42 h, whereas 5% induced colonies that remained stable but allowed resumption of normal cell division after 24 h. Because colony numbers did not decline in the 5% treatment, the rise in single cells likely reflected division of already unicellular cells rather than 'hatching' of palmelloids. This suggests that infochemicals could have degraded over time in the lower-dose treatment, reducing the aggregation response. Consistent with this, cue activity has previously been reported to diminish with time (Wu et al., 2013).

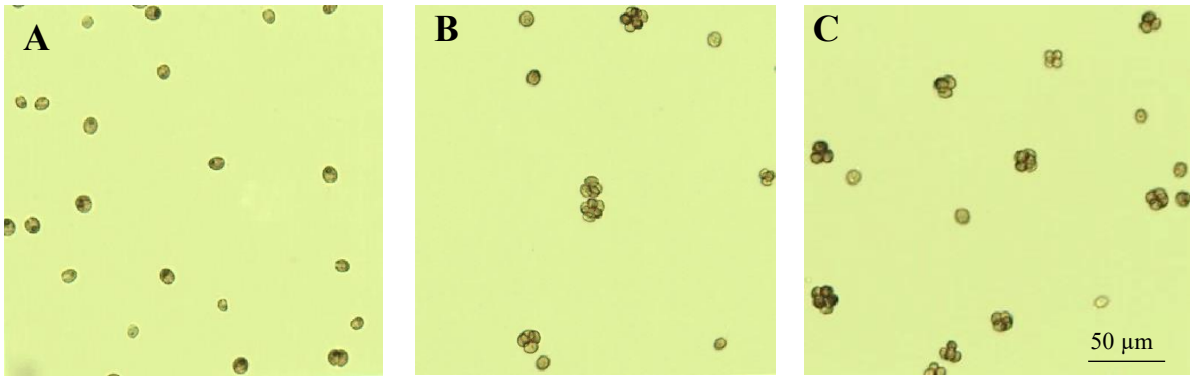

Figure 3.2. Colonies and single cells of *C. reinhardtii* at 16 h in control culture (A), 5% *Daphnia* extract treatment (B), and 10% *Daphnia* extract treatment (C). Images were taken in brightfield at 10× magnification.

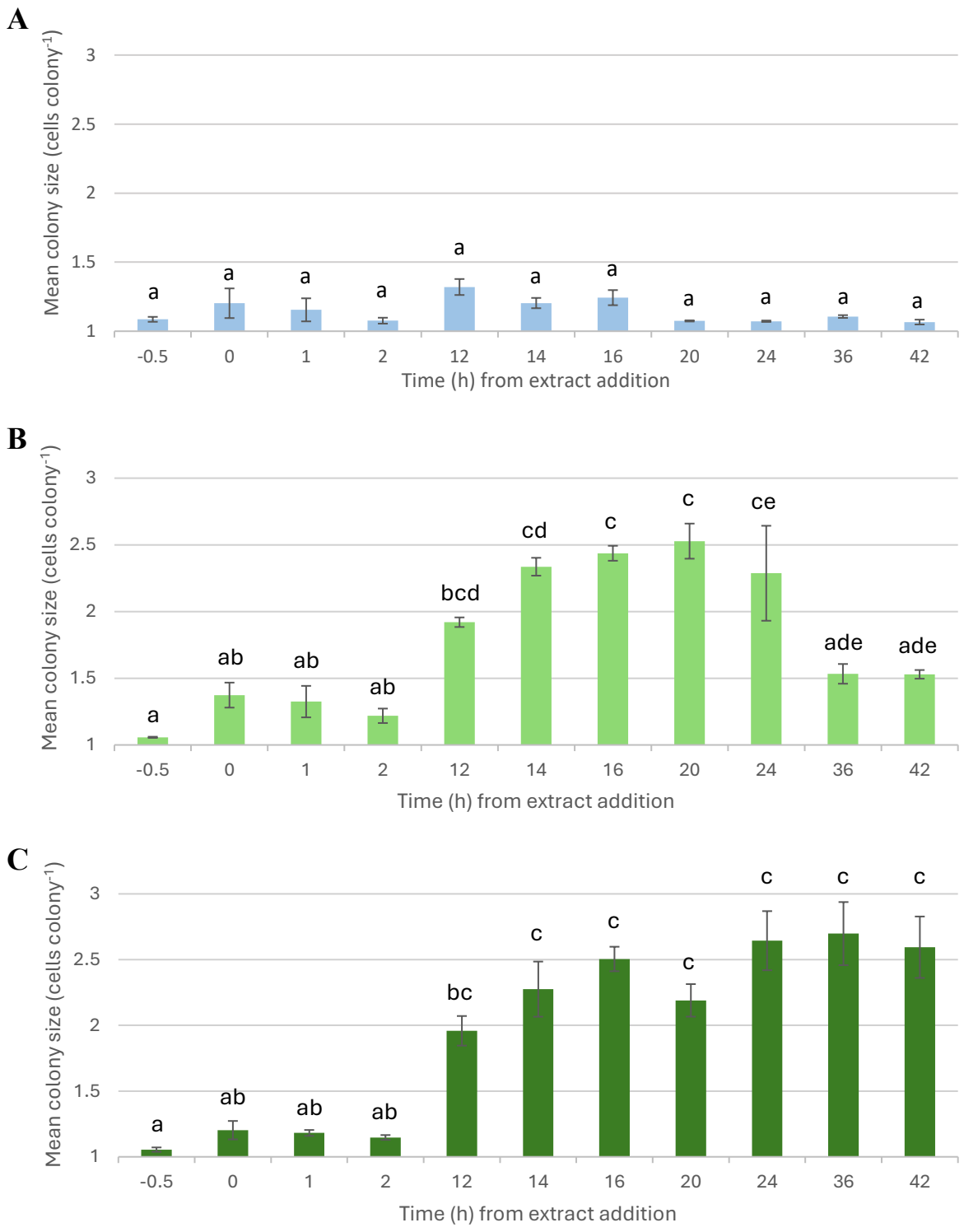

Figure 3.3. Mean colony size (MCS) of *C. reinhardtii* in control cultures (A), 5% *Daphnia* extract treatment (B), and 10% *Daphnia* extract treatment (C). Error bars represent standard errors ($N = 3$). Bars sharing the same letter within each graph are not significantly different (Tukey HSD, $p < 0.05$).

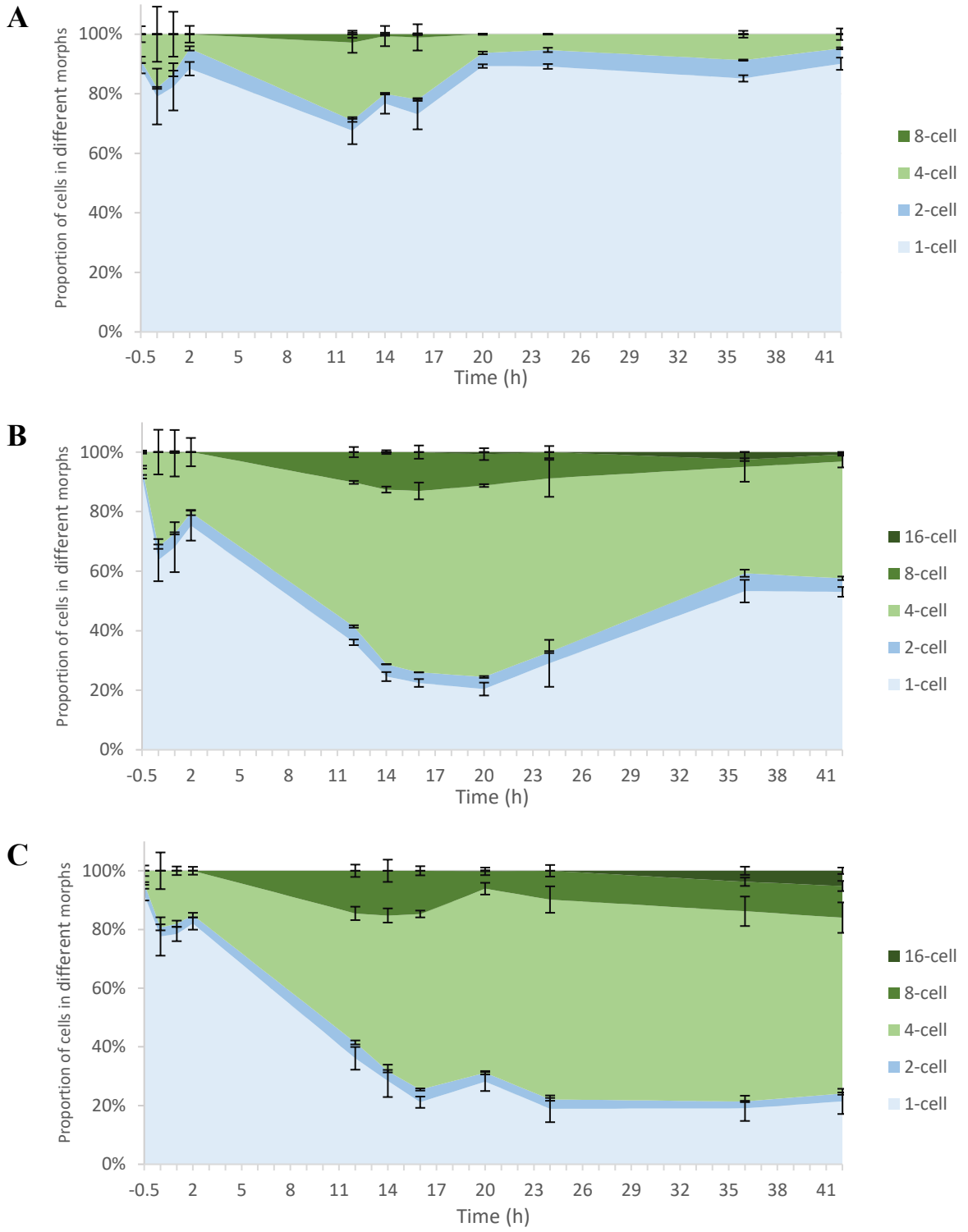

Figure 3.4. Proportion of total cells that are single or in colonies, of *C. reinhardtii* in control cultures (A), 5% *Daphnia* extract treatment (B), and 10% *Daphnia* extract treatment (C). Error bars represent standard errors ($N = 3$).

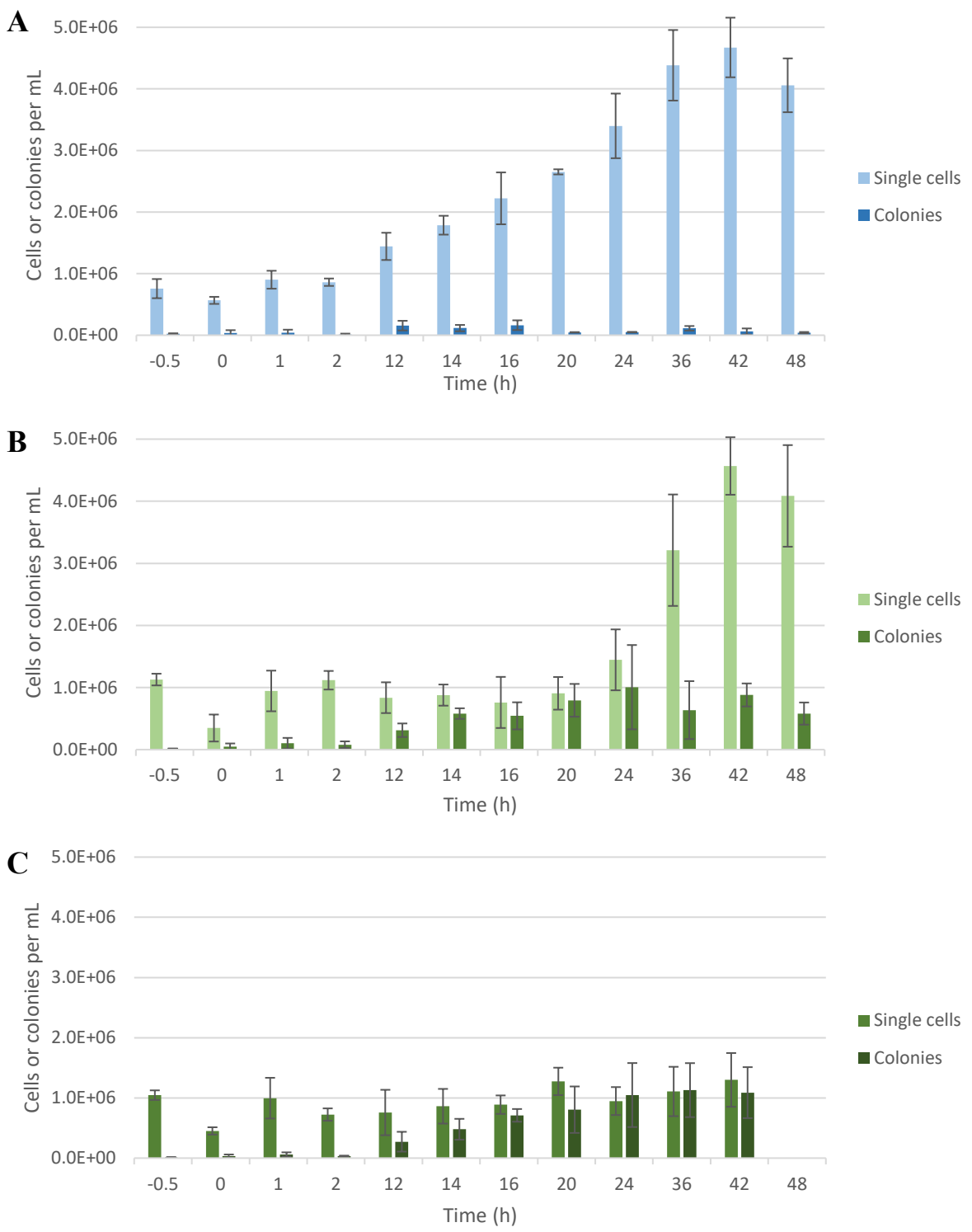

Figure 3.5. Concentration of *C. reinhardtii* single cells and colonies in control cultures (A), 5% *Daphnia* extract treatment (B), and 10% *Daphnia* extract treatment (C). Error bars represent standard errors ($N = 3$). Note: the colony concentration is the number of colonies not the number of cells in those colonies.

3.3.3 Transcriptomics

3.3.3.1 RNA sequencing

RNA sequencing output

RNA sequencing was conducted on aggregated cultures treated with 5% and 10% v/v *Daphnia* extract, alongside untreated controls, to investigate transcriptomic responses during aggregation characterised as palmelloid formation. Illumina sequencing generated 779,920,913 filtered reads, of which an average of 74.27% per sample were mapped to the published genome (*C. reinhardtii* CC-4532 v.6.1, Phytozome genome ID: 707, **Appendix J**, **Table J.1**).

Principal component analysis (PCA)

The PCA plots (**Appendix J**, **Figure J.1** and **Figure J.2**) show clear clustering of similar gene expression profiles within each sample. The first two principal components (PCs) explained 66% of the total variance, showing that most biological variation was captured in the PCA. PC1 primarily captured variance between the 36 h samples and the earlier timepoints, which were more closely related to each other. PC2 distinguished between control and *Daphnia* treated cultures, with the 5% and 10% treatments clustering together. Tight clustering of biological replicates within each group further confirmed the quality and reproducibility of the data.

Differentially expressed genes (DEGs)

Comparisons between aggregated (*Daphnia* extract-treated) and unicellular (control) cultures identified differentially expressed genes (DEGs) associated with palmelloid formation and infochemical exposure. In total, reads were mapped to 4406 genes, and 3161 of these were differentially expressed in *Daphnia* treatments relative to the control. To focus on the strongest signals, a fold change threshold of $|\log_2\text{-FC}| > 1.25$ and $p_{adj} < 0.05$ was applied. Unless otherwise specified, all reported DEGs are within this threshold. The overall distribution of the DEGs is shown in **Figure 3.6**.

Across treatments, 306 genes were upregulated and 432 downregulated in the 5% treatment, while 334 were upregulated and 395 downregulated in the 10% treatment. The largest number of DEGS occurred at 1 h and 36 h post-treatment (**Figure 3.6**). Of these, 216 (50.9 %)

upregulated and 237 (40.2 %) downregulated DEGs were shared between the 5% and 10% treatments (**Figure J.3**). The distribution of DEGs across all four timepoints is shown in **Figure J.4**.

The top 200 DEGs, ranked by log_2-FC relative to the control, are listed in **Table J.2**. A full list of DEGs, including gene symbols, JGI gene model identifiers, UniProt accessions, and expression values, is provided in **Supplementary Data File S2**.

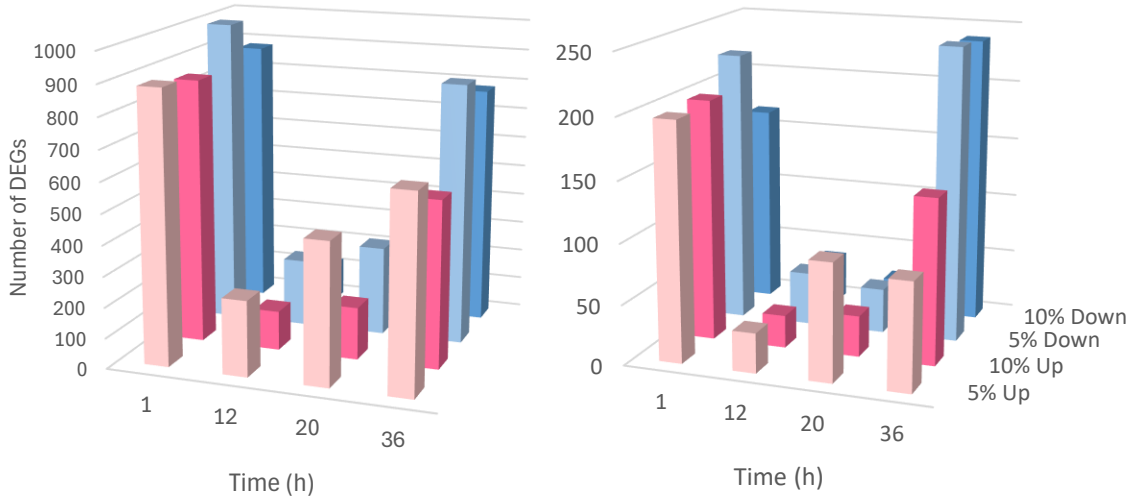

Figure 3.6. Number of differentially expressed genes (DEGs) in *C. reinhardtii* under 5% and 10% *Daphnia* extract treatments relative to the control. The left graph shows total DEGs, while the right graph shows only DEGs with $|log_2\text{-FC}| > 1.25$, at 1, 12, 20, and 36 h.

3.3.3.2 RT-qPCR

RT-qPCR of *MMP13* and *FAP199* supported the RNA-seq trends, with *MMP13* downregulated and *FAP199* upregulated in the 5% (**Figure 3.7**). Although qPCR data were more variable, reflecting noise from both target and the housekeeping genes across replicates, the overall direction of change was consistent with the RNA-seq results.

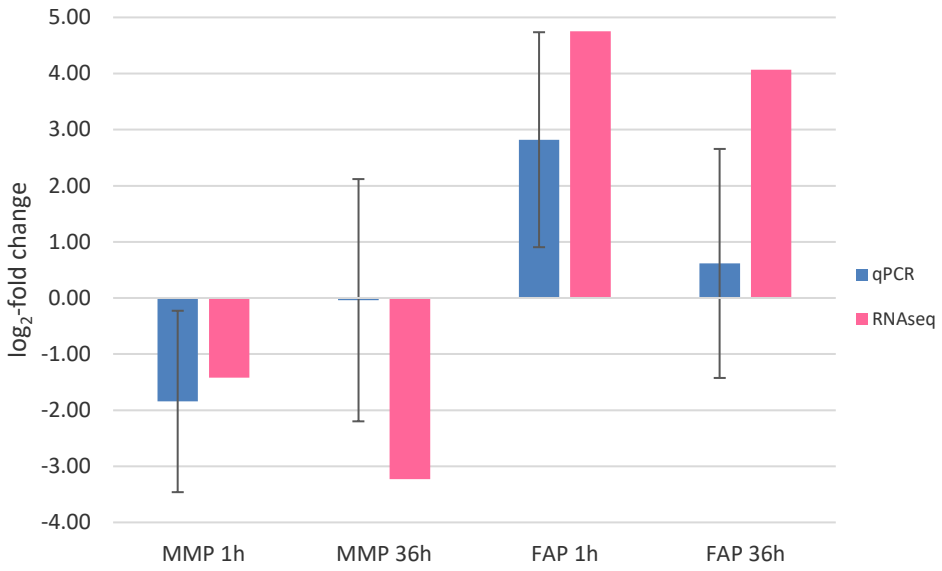

Figure 3.7. Log_2-fold change of *MMP13* and *FAP199* between the 5% treatment and control, from qPCR and RNA-seq. Error bars represent the standard deviation.

3.3.3.3 Live *Daphnia*

A study by Berger (2017) investigated the transcriptome of *C. reinhardtii* exposed to live *D. magna*, reporting 131 differentially expressed genes (DEGs); of these, 43 were also differentially expressed in *Daphnia* extract treatments in this study (**Table 3.2**). Most of these genes showed consistent trends: they were upregulated shortly after exposure to *Daphnia* (1–2 h) and later downregulated or returned to baseline expression (i.e., similar level to the control).

The overlapping gene set included genes involved in core metabolism (e.g., *MAS1* – glyoxylate cycle; *IDH2* and *OGD1/2* – TCA cycle; *PCK1* – gluconeogenesis), nutrient uptake and transport (*PHO1* – phosphate metabolism; *FEA2* – iron uptake; *HLA3* – CO_2 fixation), and stress protection (*HSP22F*, *HSP90A*, *HSP70A/E* – heat shock proteins; *TEF18* – detox/stress tolerance). Several genes also mapped to lipid and fatty acid metabolism (*CIS2*, *FAD2*) and protein folding or peroxisome function (*CPN60C*, *CGL108*). This overlap suggests that *C. reinhardtii* employs a conserved metabolic and stress-related response to *Daphnia*, whether the cue is direct predation or infochemicals.

Table 3.2. Overlapping differentially expressed genes (DEGs) between Berger (2017), who treated *C. reinhardtii* cultures with live *D. magna*, and this study's *Daphnia* extract treatments. Gene symbols, functional categories, and log_2-FC in each treatment are shown.

Gene		**Log2-FC**									
		5%				**10%**				***D. magna***	
		1h	**12h**	**20h**	**36h**	**1h**	**12h**	**20h**	**36h**	**1-2h**	**8h+**
PHO1	Starch phosphorylase	4.2				4.1				up	down
PHT3A	Phosphate transporter	1.8	0.7	1.3		1.8	0.8	0.9		up	down
HSP22F	Heat shock protein		-1.1		1.7		-1.7		2.5	down	down
PDC3	Anaerobic metabolism	1.8		1.0	0.8	1.8			1.4	up	down
MAS1	Glyoxylate cycle	1.7			-2.2	1.7			-0.9	up	down
FEA2	Iron uptake	1.5	2.4			1.5				up	up
HSP90A	Heat shock protein	2.0			-1.4	1.9				up	down
HSP70A	Heat shock protein	1.9			-1.4	1.8				up	down
HSP70E	Heat shock protein	1.2				1.5				up	down
CPN60C	Protein folding	1.7			-1.2	2.3				up	down
SDHAF2	Kreb's cycle and ETC	1.7			-0.7	2.0				up	down
OGD2	TCA cycle	1.7		0.5	-0.5	1.6				up	down
FAD2	Fatty acid metabolism	2.2				2.0					down
OGD1	TCA cycle	1.7			-0.6	1.8				up	down
CGL108	Peroxisome biogenesis	1.3			-1.1	1.5				up	down
CIS2	Lipid metabolism	1.7			-0.7	1.5				up	down
UCP2C	Uncoupling protein	1.2			-1.2	1.2				up	down
ACH1	TCA cycle	1.8				1.7				up	down
TEF18	Detox/stress tolerance	1.4		0.9		1.2				up	down
AST1	Amino acid metabolism	1.2			-0.8	1.3				up	down
IDH2	Carbon metabolism	1.5				1.8				up	down
PCK1	Gluconeogenesis	0.9			-1.3	1.0				up	down
SHY1	Cellular respiration	1.0				1.1			1.1	up	down
HLA3	Membrane protein				1.4					up	up
CAH5	CO_2 fixation				1.2					down	up
AKC3	ABC1 kinase protein		0.9							down	up
PLS1	Phospholipid scramblase	0.8								up	
FBP2	Carbon metabolism	0.4				0.4				up	down

3.3.3.4 Functional enrichment

Enriched gene ontology (GO) terms and KEGG pathways (-log FDR < 0.05, $p < 0.05$) were identified using the DAVID functional annotation tool. GO terms were classified into *cellular components*, *biological processes*, and *molecular functions*. The cellular component terms and KEGG pathways are presented in **Table 3.3** and **Table 3.4**, while full lists of enriched biological process and molecular function terms are provided in **Table J.3** and **Table J.4** (**Appendix J**).

Upregulated DEGs

Daphnia infochemicals rapidly activated core metabolic and stress pathways: At one hour, upregulated DEGs were enriched for biological processes linked to energy, RNA, and protein metabolism, along with stress responses (**Table J.3**). Stress response terms were also enriched at 20 hours, and photosynthesis at 36 hours in the 10% treatment. Enriched cellular components included gene expression machinery, photosynthetic complexes, and respiration pathways (**Table 3.3**). Molecular functions involved protein processing, heme/iron binding, and oxidoreductase activity across 1, 20, and 36 hours (**Table J.4**). *Plasma membrane* enrichment was also reported in *C. reinhardtii* exposed to *Brachionus calyciflorus* (Lorusso, 2018). Because plasma membrane proteins mediate environmental sensing and signal transduction, predator detection and aggregation responses may rely on shared receptor-mediated pathways across different predator cues.

Downregulated DEGs

Nearly all enriched cellular component terms were related to the flagella (**Table 3.3**). Indeed, 14 of these flagella/motility-related terms were also enriched in downregulated DEGs during *C. reinhardtii* self-aggregation triggered by *B. calyciflorus* (Lorusso, 2018), indicating that suppression of flagellar genes is a consistent hallmark of aggregation, regardless of the predator involved. In this study, at one hour and/or 36 hours, downregulated DEGs were strongly associated with flagella and motility-related biological processes, including microtubule-based movement, intraflagellar transport, DNA replication, and oxidative stress responses (**Table J.3**). Molecular functions included losses in microtubule and dynein activity and transmembrane transport (**Table J.4**).

Table 3.3. Enriched *cellular component* GO terms of upregulated and downregulated *C. reinhardtii* DEGs in 5% and 10% *Daphnia* extract treatments. Numbers indicate the count of DEGs per GO term; colour intensity reflects enrichment level (-log FDR < 0.05, $p < 0.05$).

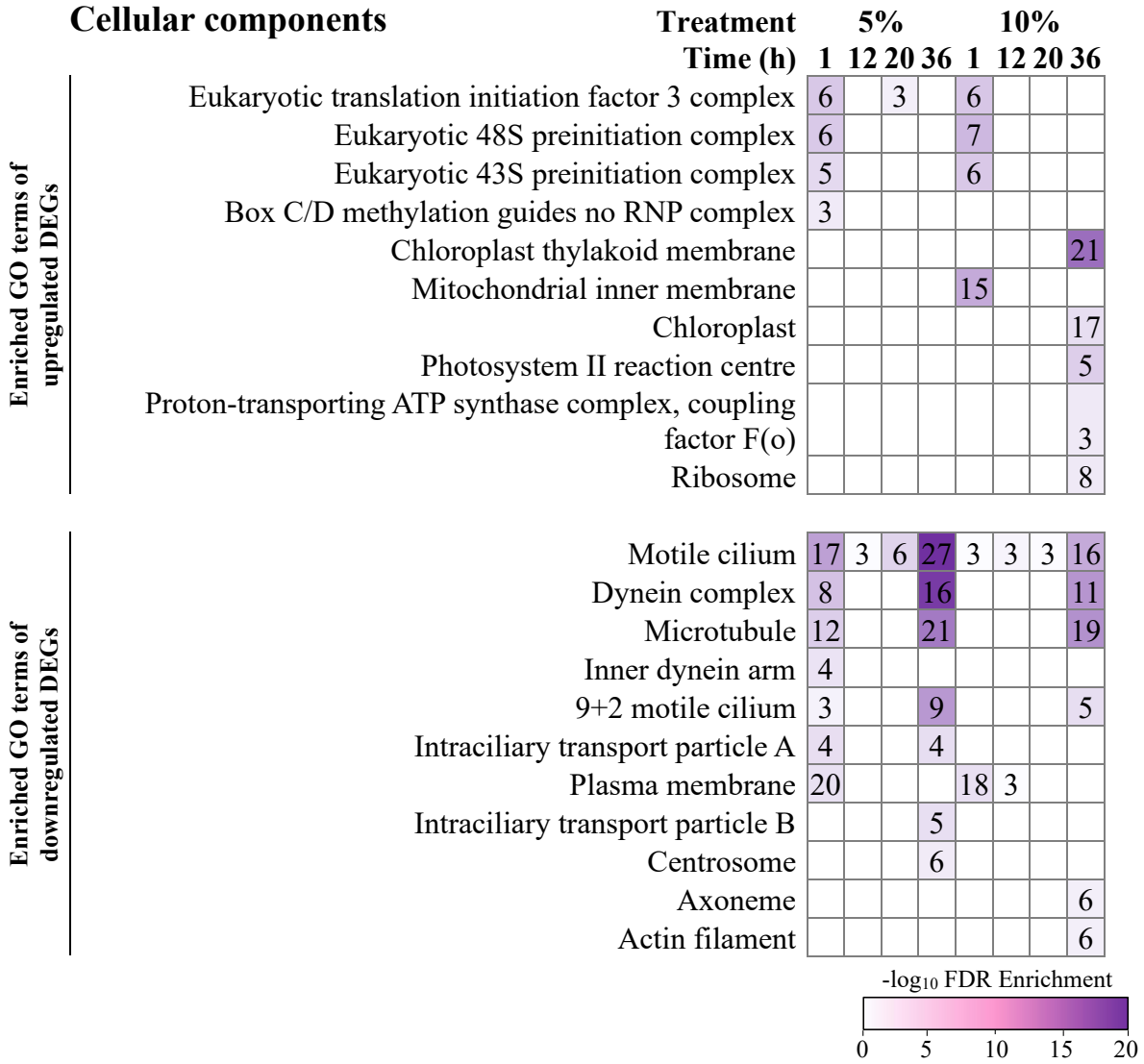

KEGG pathways

At one hour, upregulated DEGs were enriched in energy/carbon metabolism and protein synthesis/processing (**Table 3.4**). At 36 h, photosynthesis pathways were strongly enriched in the 10% treatments, alongside broader metabolic pathways. Downregulated DEGs were linked to motor proteins, autophagy, and DNA replication at one and/or 36 hours. These suggest a trade-off, with energy and biosynthesis enhanced while motility and cell cycle progression are dialled down, supporting palmelloid formation.

Table 3.4. Enriched KEGG pathways of upregulated and downregulated *C. reinhardtii* DEGs in 5% and 10% *Daphnia* extract treatments. Numbers indicated the count of DEGs per GO term; colour intensity reflects enrichment level (-log FDR < 0.05, $p < 0.05$).

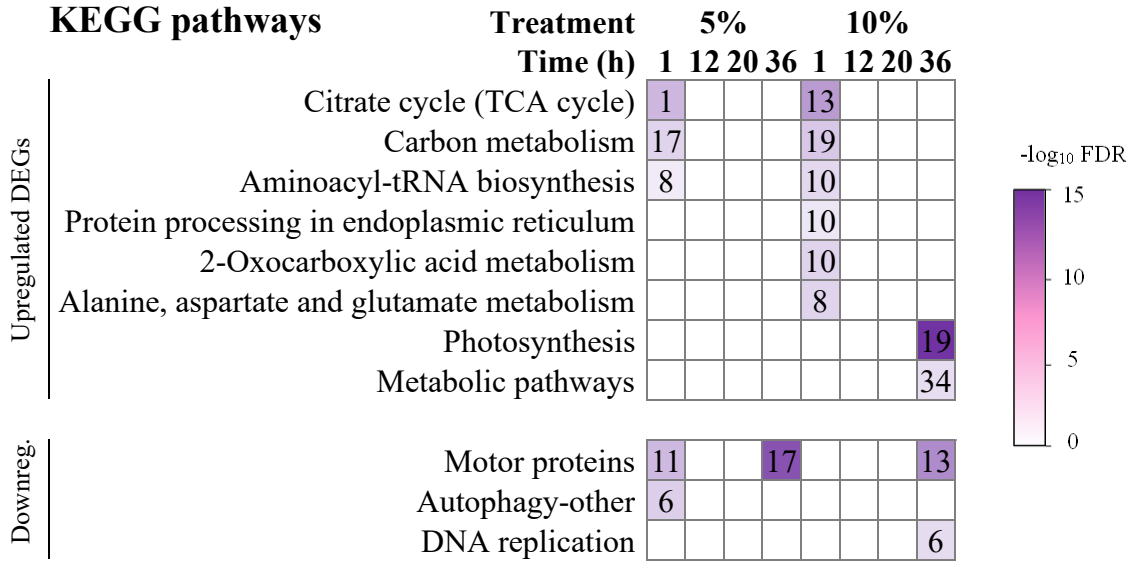

3.3.3.5 Dose-dependent DEGs

At 36 hours, the 5% *Daphnia* treatment had a lower proportion of cells in colonies compared with earlier timepoints and the 10% treatment. To investigate if the transcriptome could explain this difference, gene sets from the 5% and 10% *Daphnia* treatments were compared ($|\log_2\text{-FC}| > 1.25$, $p < 0.05$). In total, 40 genes had significantly higher expression and 17 had significantly lower expression in the 10% treatment relative to the 5% treatment (**Figure 3.8**). Most of these differences occurred at 36 hours, with 39 genes upregulated and 13 downregulated. The relative gene expressions in the 10% vs. 5% treatment, and of each treatment relative to the control, are shown in **Table 3.5** and **Table 3.6**.

Upregulated DEGs in the 10% treatment were associated with five significantly enriched GO terms (**Table 3.7**), relating to transmembrane transport, the plasma membrane, and protein folding. Notably, these same genes were downregulated in the 5% treatment relative to the control at 36 hours, when the 5% treatment had resumed producing single cells (**Table 3.6**). This pattern suggests that higher expression of these genes coincided with active palmelloid formation, while their downregulation correlated with the resumption of normal cell division (i.e., the formation of single cells).

These results suggest that sustained palmelloid formation at higher *Daphnia* extract concentrations is underpinned by shifts in genes linked to transmembrane transport, protein folding, and membrane-associated functions. Such processes are likely connected to upstream signalling cascades that sense and translate infochemical cues into palmelloid formation.

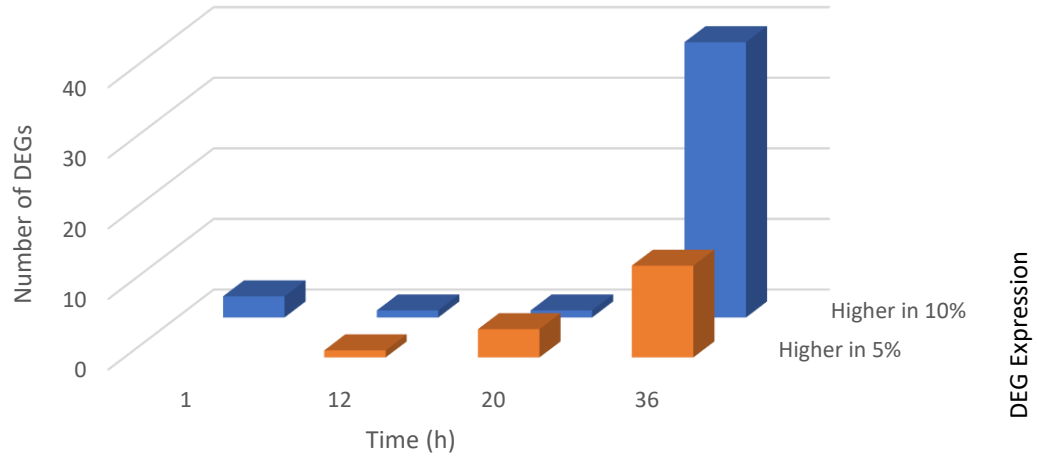

Figure 3.8. Number of *C. reinhardtii* differentially expressed genes (with $|\log_2\text{-FC}| > 1.25$) between 5% and 10% *Daphnia* extract treatments at 1, 12, 20, and 36 h.

Table 3.5. All DEGs that were downregulated in 10% treatments relative to 5% treatments, and their $\log_2$-FC between all treatments.

Gene		**Log₂-FC**											
		5% relative to 0%				**10% relative to 0%**				**10% relative to 5%**			
		1h	**12h**	**20h**	**36h**	**1h**	**12h**	**20h**	**36h**	**1h**	**12h**	**20h**	**36h**
METE1	Cre03.g180750		-3.1				-6.9	-4.2			-3.8	-4.3	
LCI1	Cre03.g162800				2.7		-6.4						-2.8
CEP131	Cre09.g394732	-1.0				-1.8			-2.3				-1.9
FBB6L1	Cre13.g589450		-1.7			-1.0	-1.6	-1.5				-1.8	
CGL127	Cre01.g032550								-2.0				-1.7
FAP233	Cre09.g393450								-1.4				-1.6
GPX3	Cre03.g197750	-1.2				-1.0			-1.5				-1.6
FOR1	Cre03.g166700	-0.8				-1.2			-1.7				-1.5
SHMT2	Cre06.g293950	0.6		1.4	0.7	0.6			0.7			-1.4	
FAP24	Cre02.g081050		-0.8				-1.0	-1.2				-1.4	
CAH2	Cre04.g223050								-1.3				-1.4
POB11	Cre06.g273450	-0.8			-1.3	-1.2			-2.7				-1.4
CDKB1	Cre08.g372550					-1.0			-1.7				-1.4
OPR115													-1.3
CGL46	Cre06.g278212				-0.9				-2.1				-1.3
THIC1	Cre05.g240850	-0.7	-1.2	-1.5		-0.7	-1.5	-2.3	-0.9				-1.3
MIND1	Cre12.g522950								-1.8				-1.2

Table 3.6. All DEGs that were upregulated in 10% treatments relative to 5% treatments, and their log_2-FC between all treatments.

Gene		Log2-FC											
		5% relative to 0%				10% relative to 0%				10% relative to 5%			
		1h	12h	20h	36h	1h	12h	20h	36h	1h	12h	20h	36h
GFY4	Cre17.g702900				-7.6				-2.0				5.6
CAD1	Cre03.g207800	3.4	2.5	1.2		4.6	4.2	2.6			1.7	1.4	1.1
PFR1	Cre02.g095137	1.1			-3.5	1.0							2.9
VLE1	Cre01.g049950	1.6		1.0	-1.3	1.5		1.0	1.1				2.5
HYDEF1	Cre06.g296750	0.9			-1.6								2.3
psbM	CreCp.g802290								3.5				2.1
GSTS1	Cre16.g688550	1.2			1.3	2.4	1.1	0.9	2.2	1.2			0.9
HYDG1	Cre06.g296700	1.0			-1.6	0.9							2.0
GFY5	Cre17.g702950				-2.4								2.0
ACS3	Cre07.g353450				-2.4								2.0
GFY3	Cre17.g700750				-1.7								1.8
GFY1	Cre17.g700450	1.4	1.1			1.6			1.4				1.8
CPN60C	Cre06.g309100	1.7			-1.2	2.3							1.7
HCP4	Cre09.g391650	1.6		2.4	-2.6	1.4		2.3					1.7
ADH1	Cre17.g746997	1.2				0.8			1.3				1.7
HSP70A	Cre08.g372100	1.9			-1.4	1.8							1.7
PFH10	Cre02.g084450				-1.6								1.7
VAMP4	Cre04.g224800								1.5				1.7
AOX1	Cre09.g395950	0.9			-1.3	1.1							1.6
CLPB1	Cre11.g467644				-1.6	1.9							1.6
NAR1C	Cre04.g217915	1.3			-1.0	1.1							1.5
EZY17	Cre13.g583450	-1.2			-1.2								1.5
CDK1	Cre01.g008650				-0.8								1.5
HSP90A	Cre09.g386750	2.0			-1.4	1.9							1.5
CDI1	Cre12.g557900					0.8			0.7	0.8			0.7
MMP29	Cre13.g605200		1.3	1.1	-2.3	1.1		1.3					1.5
FKB62	Cre09.g398067				-2.0	1.1							1.5
MRPS106	Cre03.g211409	1.2	1.1	1.1	-0.9	1.4		1.0					1.4
NAR1E	Cre12.g541250	1.1			-2.1	0.9							1.4
PFL1	Cre01.g044800				-1.3								1.4
FAP195	Cre15.g639100				-1.2								1.4
PFH3	Cre10.g443050												1.4
GPX1	Cre02.g078300	1.5				2.8				1.4			
GDH2	Cre05.g232150		1.1		-1.2								1.3
PSRP1	Cre05.g237450				-0.7				0.7				1.3
HSP70E	Cre16.g677000	1.2				1.5							1.3
SULTR3	Cre09.g401293	1.5	0.8	0.8	-1.2	1.2		0.9					1.3
STM6	Cre12.g542500	-1.6			-1.4								1.3
LCI34	Cre03.g191250				-0.9								1.3
MAS1	Cre03.g144807	1.7			-2.2	1.7			-0.9				1.2

Table 3.7. Gene ontology terms associated with upregulated *C. reinhardtii* DEGs in 10% *Daphnia* extract treatment relative to 5% treatment. Numbers indicated the count of DEGs per GO term; colour intensity reflects enrichment level (-log FDR < 0.05, $p < 0.05$).

Category	GO Term	
Molecular Function	Acetate: proton symporter activity	4
Molecular Function	ATP-dependent protein folding chaperone	4
Biological Process	Acetate transmembrane transport	4
Biological Process	Succinate transmembrane transport	4
Cellular Function	Plasma membrane	8

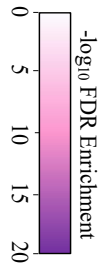

3.3.3.6 Signalling cascades

To explore this further, DEGs related to signalling pathways were examined. The transcriptomic data revealed that *Daphnia* infochemicals triggered extensive changes in genes associated with signalling pathways, including calcium signalling, protein kinases, ubiquitin-mediated regulation, transient receptor potential (TRP) channels, and voltage-gated Ca^{2+} channels. Together, these results provide insight into how external cues are converted into the cellular changes that drive palmelloid formation.

Ca^{2+} signalling

Calcium signalling is central in cellular responses, but microalgae show diverse Ca^{2+} "toolkits," differing from plants and animals and also between microalgal lineages (Pivato and Ballottari, 2021). In *C. reinhardtii*, Ca^{2+} regulates flagella beating, photo- and chemotaxis, deflagelation, and stress responses. In response to external cues (such as predator infochemicals), Ca^{2+} enters the cytoplasm through membrane-bound channels. This Ca^{2+} signal is then "translated" by calmodulin (CaM), which binds Ca^{2+} and activates downstream effectors, such as kinases, phosphatases, transcription factors, and feeds back to modulate ion channels. Calcium-dependent protein kinases (CDPKs) also bind Ca^{2+} and phosphorylate downstream proteins.

TRP and VDCC channels, CaM, and CDPKs

TRP channels act as frontline sensors, mediating Ca^{2+} influx in response to chemical and light stimuli (Pivato and Ballottari, 2021; Wheeler, 2017). In *Daphnia* treatments, *TRP2*, *TRP11*, and *TRP13* were upregulated, while *TRP1*, *TRP6*, and *TRP22* were downregulated (**Table J.5**).

TRP13 and *TRP11* are thought to be related to members of the TRPM or TRPV subfamilies, which are involved in sensing temperature and chemicals, and ion homeostasis and signalling cascades, respectively (Arias-Darraz et al., 2015; Hou et al., 2023). TRP channels, to our knowledge, have not previously been directly linked to palmelloid formation in *Chlamydomonas*, however, *TRP2* has previously been shown to be involved in acclimation to low CO_2 in *C. reinhardtii* (Christensen et al., 2020), while a mutant of *TRP11* showed impaired deflagelation in response to the algicidal surfactant orfamide A, which triggers deflagelation driven by Ca^{2+} signalling (Hou et al., 2023). The gene *TRP13*, which has not been characterised, was the third most upregulated DEG in *Daphnia* treatments, therefore a *TRP13* knockout mutant was studied to test whether its absence impaired palmelloid formation (see **Section 3.3.3.9**).

C. reinhardtii also contains **voltage-gated Ca^{2+} channels**, homologous to animal VDCCs (Pivato and Ballottari, 2021). These channels, similar to TRP channels, mediate influx of Ca^{2+} into the cell. In this study, seven genes (*CAV1-7*) were downregulated (**Table J.5**).

Five calmodulin-related genes and eight CDPK genes were downregulated in *Daphnia* treatments (**Table J.5**), while one calmodulin-related gene was upregulated and two CDPKs were both up- and downregulated across timepoints. This differs from *T. obliquus*, which upregulates CDPK transcripts during aggregation (Zhu, Sun, et al., 2021), suggesting divergence in molecular mechanisms despite similar ecological responses; *C. reinhardtii* may rely more on post-translational control rather than upregulation of gene transcription, whereas *T. obliquus* may rely more on transcriptional induction of signalling components.

The combined downregulation of several TRP and VDCC genes suggests that *C. reinhardtii* may intentionally dampen Ca^{2+}-mediated signalling while in palmelloids. This muted signalling would prevent flagella reassembly and hatching, thereby delaying daughter cell release and promoting palmelloid persistence. Downregulation of calmodulin and CDPK genes may reflect the same dampening or alternatively indicate a shift towards post-translational regulation rather than transcriptional regulation.

In contrast, the strong upregulation of three TRP channels, including *TRP13*, and the transient upregulation of the Ca^{2+}-binding protein gene *CRT2* at 1 hour (**Table J.5**), points to an early infochemical-induced Ca^{2+} spike before subsequent suppression.

Aurora-like kinases (ALKs)

Aurora-like kinases regulate flagellar assembly and disassembly through phosphorylation events (Cao et al., 2009); in this study, several were differentially expressed in *Daphnia* treatments, including *ALK1*, *ALK2*, and *ALK3*, along with *FLS1* and *FLS2* (**Table J.5**). ALK1 (formerly CALK) is phosphorylated during flagella loss or shortening and dephosphorylated during flagellar assembly (Cao et al., 2009; Luo et al., 2011; Pan and Snell, 2005). FLS1 regulates ALK1 to promote flagella disassembly, while FLS2 directly interacts with IFT70 (Pan, 2023). These findings suggest that predator infochemicals influence palmelloid formation at least partly by modulating the kinases than govern flagella turnover.

ROS and MAPK signalling

Reactive oxygen species (ROS) mediate mitogen-activated protein kinase (MAPK) activity, which in plants is connected to the regulation of cell division and stress responses (Jalmi and Sinha, 2015; Roccuzzo et al., 2020). MAPK cascades are evolutionarily conserved signalling pathways essential for transducing environmental cues (Mathien et al., 2021).

In this study, *MAPKKKK1* (*SIK1*) and *MAPK3* were downregulated (Table J.5). Since MAPK activity is primarily regulated by phosphorylation rather than transcript abundance (Mathien et al., 2021), these transcriptomic data alone cannot confirm whether the pathway was active during aggregation. Downregulation may reflect suppression of MAPK signalling as part of pathway fine-tuning or may simply represent transcriptional adjustments that do not correspond to protein activity.

Nevertheless, MAPK signalling genes have been reported to be upregulated in *C. reinhardtii* during perchlorate-induced aggregation (Zhang et al., 2023) and differential expression of MAPK proteins has been observed in *Scenedesmus subspicatus* during *Daphnia* infochemical-induced aggregation. These findings suggest that MAPK involvement in/or as a result of cue sensing may be a conserved feature of green algae.

Finally, MAPK signalling is also regulated by the ubiquitin-proteasome system, which controls the stability and abundance of MAPK components (Mathien et al., 2021). In this study, ubiquitin-proteasome pathway components were strongly upregulated (see below), further supporting the idea that MAPK signalling is regulated during aggregation.

Other kinases families

Sucrose non-fermenting 1-related kinases (SNRKs), typically involved in stress responses, were also strongly affected. Ten SNRK genes were downregulated and three upregulated (no $\log_2$-FC threshold; **Table J.5**), of which, 10 were SnRK2 gene family members, which are involved in *Chlamydomonas* acclimation to sulfur deprivation (González-Ballester et al., 2010); in previous reports, *SNRK2*, was upregulated in *T. obliquus* exposed to *Daphnia magna* infochemicals (Zhu, Sun, et al., 2021).

NIMA-related kinases (NEKs), which regulate flagella assembly and disassembly, flagella length, intraflagellar transport, and the cell cycle, were downregulated in this study (**Table J.5**) (Bradley and Quarmby, 2005; Mahjoub et al., 2002). NEKs localise to the centrosome, basal bodies, flagella, and cytoplasm, where they are thought to phosphorylate IFT components, microtubule-associated proteins (MAPs), and motor proteins such as dynein and kinesin.

Cyclin-dependent kinases (CDKs), central to cell cycle control and flagella disassembly prior to mitosis (Cao et al., 2009), were also differentially expressed.

Ubiquitination

Forty-six DEGs were annotated to the ubiquitin proteasome pathway (P00060), including genes encoding proteasome subunits, ubiquitin-activating enzyme E1, conjugating enzyme E2, and ligase E3 (**Table J.6**). Ubiquitination is critical for tagging proteins for degradation, conformational changes, or transport, and has been implicated in ciliary disassembly. In *Chlamydomonas*, polyubiquitylation of α-tubulin is required for disassembly, suggesting that the ubiquitin-proteasome system contributes to the turnover of flagellar and cell wall-associated proteins during palmelloid formation.

Signalling cascade summary

These results reveal candidate signalling processes underlying the response of *C. reinhardtii* to *Daphnia* infochemicals. TRP channels, particularly the consistently and strongly upregulated *TRP13*, emerge as key front-line sensors of predator cues, initiating Ca^{2+} influx and downstream responses. Voltage-gated Ca^{2+} channels, calmodulin, and CDPK genes were largely downregulated, consistent with a shift toward muted Ca^{2+} signalling and reliance on post-translational regulation. The transient upregulation of *CRT2* at one hour suggests an initial Ca^{2+} surge before suppression.

Downstream, calcium-calmodulin signalling, kinases such as ALKs, NEKs, and CDKs, and MAPK cascades appear to regulate structural changes in the flagella and the cell cycle that maintain palmelloid colonies. Divergence from *T. obliquus*, where many of these transcripts are induced, indicates that *Chlamydomonas* employs distinct molecular strategies despite convergent ecological outcomes.

ROS likely integrate with MAPK cascades to fine-tune stress responses, while the strong upregulation of ubiquitin-proteasome pathway genes suggests targeted protein turnover and controlled flagella disassembly are critical for palmelloid persistence.

Overall, this provides novel evidence pointing to a regulatory model where external predator cues are detected at the plasma/flagella membrane, relayed via Ca^{2+}-dependent cascades and protein kinases, and consolidated through ubiquitin-mediated degradation of flagellar components. Together, these pathways delay flagella reassembly and cell wall degradation, trapping daughter cells inside palmelloid colonies.

3.3.3.7 Cell wall degradative enzymes and glycoproteins

The mechanisms regulating daughter cell release during *C. reinhardtii* cell division are not fully understood. Beyond motility and sensing, flagella also function in communication and extracellular secretion. Evidence indicates that degradative enzymes required for mother cell wall breakdown are secreted from daughter cell flagella via extracellular vesicles (ectosomes) (Luxmi and King, 2024; Wang et al., 2021).

Sporangin (VLE1)

A key enzyme in this process is sporangin (VLE1, vegetative lytic enzyme 1), a subtilisin-like protease that degrades the mother cell wall to release daughter cells (Kubo et al., 2009). In this study, *VLE1* was consistently upregulated across time-points (**Table 3.6**). On its own, this seems paradoxical given that palmelloid formation is defined by delayed daughter cell release. However, VLE1 may not act alone: it could be involved in activation of complementary enzymes (e.g., MMPs) or itself require post-translational activation (Kim et al., 2024; Luxmi et al., 2018). Thus, transcript upregulation may represent readiness rather than immediate enzymatic activity, allowing encapsulated colonies to persist.

Matrix metalloproteinases (MMPs)

MMPs are secreted proteases implicated in mother cell wall degradation and extracellular signalling. Here, five MMP genes were upregulated and 17 downregulated (four with $\log_2$-FC > 1.25; 13 with $\log_2$-FC < -1.25; **Table J.7**). This aligns with earlier transcriptomic and proteomic studies showing MMPs to be differentially expressed during *C. reinhardtii* aggregation under abiotic stress; these were *MMP32* (de Carpentier et al., 2022) and *MMP3* and *MMP13* (Khona et al., 2016), all of which were downregulated in the corresponding studies and in this study.

The most strongly downregulated MMP in this study was *MMP13*, which has previously been detected in ectosomes and enriched relative to flagella membranes (Long et al., 2016). Its suppression here and its presence in ectosomes supports the hypothesis that MMPs are released by daughter cells to degrade the mother cell wall, and their suppression would trap daughter cells inside the mother cell wall, forming colonies. This hypothesis is further investigated in **Section 3.3.3.9.**

Pherophorins (PHCs)

Pherophorins are extracellular matrix (ECM) glycoproteins implicated in maintaining and degrading the cell wall (**Chapter 1**), after being secreted through ectosomes. In *Daphnia* extract treatments, six PHC genes were upregulated and 25 downregulated pherophorins (three with $\log_2$-FC > 1.25; 17 with $\log_2$-FC < -1.25; **Table J.8**). This mixed pattern suggests complex and possibly redundant roles: some PHCs may stabilise the ECM while others promote its loosening. The knockout mutant of PHC18, the most strongly upregulated PHC, was tested to evaluate whether its absence impaired palmelloid formation (see **Section 3.3.3.9**).

Regulatory cascades

Previous studies proposed that *MMP1*, *MMP3* and *MMP13* are induced by the dual-specificity kinase DYRKP1, then activated by proteases such as VLE1 (Kim et al., 2024). However, in this study, *DYRKP1* showed only weak downregulation ($\log_2$-FC of -0.43 at one timepoint). This weak signal suggests that other kinases or regulators may coordinate the timing of enzyme activation during predator-induced palmelloid formation.

Summary

Overall, these results suggest that palmelloid formation relies on a finely tuned imbalance of degradative activity: *VLE1* transcripts increase, but the full degradation of the mother cell wall does not occur without sufficient MMP activity, especially *MMP13*. PHC regulation adds a second layer of control, stabilising ECM structure while maintaining capacity for release. Together, VLE1 priming, MMP suppression, and PHC modulation points to a mechanism in which *Daphnia* infochemicals shift the balance toward cell wall retention, delaying daughter cell release and promoting colony persistence.

3.3.3.8 Are flagella essential for cell wall degradation?

C. reinhardtii may persist in a palmelloid state because the absence of flagella prevents the activation and delivery of degradative enzymes required for daughter cell release. Without flagella, there is no ectosomal delivery of degradative enzymes and the mother cell wall cannot be broken down. Under normal conditions, flagella are disassembled prior to mitosis and reassembled before newly divided cells 'hatch' from the mother cell wall, providing both motility and a mechanism for enzyme secretion (Pan, 2023). Consistent with this, mutants lacking flagella or flagellar motility frequently remain trapped in palmelloids (Brown et al., 2015; Hou et al., 2007; Wingfield and Lechtreck, 2018). This contrast between normal and palmelloid division cycles is illustrated in **Figure 3.9**.

In this study, transcriptomics revealed widespread suppression of flagellar genes: 163 downregulated DEGs (with $\log_2$-FC < -1.25) were associated with flagella and motility GO terms. This indicates that cells did not regrow their flagella at any stage following division. The absence of flagella would in turn prevent secretion of degradative enzymes via ectosomes, blocking normal hatching and causing daughter cells to remain enclosed within palmelloids.

The following sections examine in detail the flagella-associated genes that were differentially expressed in *Daphnia* extract treatments, supporting the hypothesis that suppressed flagellar reassembly is a central mechanism underlying palmelloid persistence.

Structural flagella-associated genes were downregulated

Each *C. reinhardtii* cell has two centrioles (basal bodies) that serve as the nucleation site for the axoneme, the central structure of the flagella, which is made up of microtubules and inner

and outer dynein arms (motor proteins which are responsible for flagella movement). During cell division, flagella are normally disassembled (starting at the tip, the flagella are shortened and resorbed within the cell) (Pan, 2023), and the basal bodies shift internally to act as centrosomes, organising spindle microtubules for mitosis (Joukov and De Nicolo, 2019). This alternating role explains why flagella are disassembled prior to cell division (Rasi et al., 2009). Severing the basal body microtubules is also required to detach them from the axoneme (Parker et al., 2010).

In *Daphnia* treatments, many gene ontology terms linked to the flagella and motility (e.g., dynein complex, axoneme, radial spokes, microtubule, actin filaments, centrosome) were significantly enriched among downregulated DEGs (**Table 3.3**), supporting the absence of flagellum assembly.

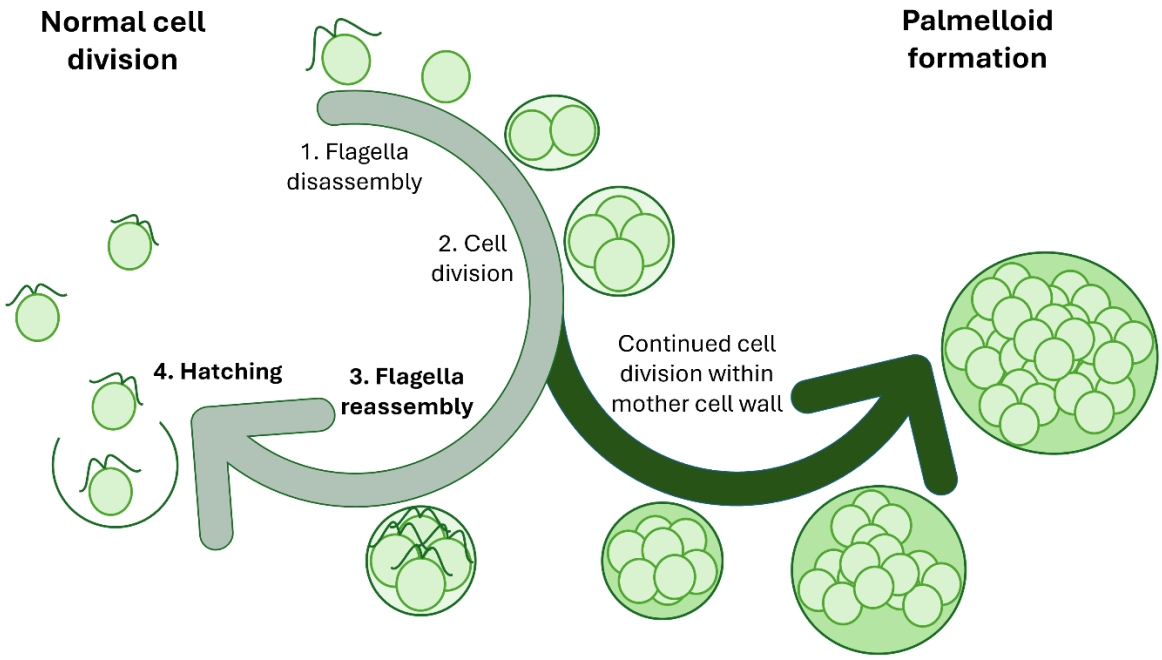

Figure 3.9. Normal versus palmelloid cell division in *Chlamydomonas reinhardtii*. Under standard conditions (left), flagella are disassembled before mitosis and are reassembled following cytokinesis, daughter cells secrete degradative enzymes via flagellar ectosomes, hatch from the mother cell wall, and resume motility. In the presence of predator-derived infochemicals (right), flagella are not reassembled, ectosomal secretion is impaired, and daughter cells continue dividing inside the mother cell wall resulting in palmelloid colony formation.

Flagella-associated proteins (FAPs)

FAPs stabilise the axoneme and regulate dynein function, modulating the structure of the flagella. Of ~378 FAP genes in the *C. reinhardtii* genome, 293 were downregulated and 27 upregulated in *Daphnia* treatments (91 with $\log_2$-FC < -1.25 and 10 with $\log_2$-FC > 1.25) (**Appendix J**, **Table J.9** and **Table J.10**). Downregulated genes included *FAP85* (encoding for an inner microtubule stabiliser), *FAP20*, *FAP276*, and *FAP106* (encoding for inner junction proteins), *FAP57* and *FAP120* (encoding for inner dynein arms stabilisers), and *FAP46*, *FAP54*, *FAP74*, and *FAP221* (encoding for central pair projections) (Bangera et al., 2023; Brown et al., 2012; Ikeda et al., 2009; Khalifa et al., 2020; Kirima and Oiwa, 2018; Lin et al., 2019). Normally, FAP gene expression rises during flagella assembly and falls during disassembly (Chamberlain et al., 2008; Tammana and Tammana, 2017; Tammana et al., 2013). *FAP199*, the most upregulated DEG, was studied further using a knockout mutant (see **Section 3.3.3.9**).

Tubulin

Four tubulin genes (*TUA1*, *TUA2*, *TUB1*, *TUB2*), encoding α- and β-tubulin, were downregulated (**Appendix J**, **Table J.11**). As tubulin is the building block of microtubules, tubulin abundance normally increases during flagella assembly; stress can disrupt tubulin stability and drive disassembly of microtubules (Chamberlain et al., 2008).

Centrosomal proteins (CEPs)

CEPs contribute to the structure and function of the centrosome (i.e., microtubule organisation and cell division). Four CEP genes (*CEP95, CEP131, CEP83*, *CEP19* were downregulated (**Table J.11**). *CEP131*, involved in centriolar satellites and flagella maintenance, shifted from downregulated in both *Daphnia* treatments at one hour to upregulation in the 5% treatment at 36 hours, coinciding with partial disaggregation.

Radial spoke proteins (RSPs)

Fifteen RSP genes were downregulated, and one was upregulated (**Table J.11**). RSPs are found in the axoneme and regulate dynein motor activity and flagellar movement (Pigino and Ishikawa, 2012).

Intraflagellar transport (IFT) genes were downregulated

IFT is essential for flagellar assembly and disassembly. In *Daphnia* treatments, 22 IFT genes were downregulated (12 with log_2-FC < -1.25; **Appendix J**, **Table J.12**), and intraciliary transport particle A/B GO terms were enriched among downregulated DEGs.

IFT motors and particle proteins normally assemble into trains that traffic tubulin and other proteins via kinesin to the tip for assembly and return cargo via dynein (Chamberlain et al., 2008; Kobayashi and Dynlacht, 2011; Wingfield and Lechtreck, 2018). This cycle maintains steady state flagellar length, with continuous disassembly balanced by IFT-mediated reassembly (Chamberlain et al., 2008). Disassembly occurs when IFT entry ceases, causing gradual shortening of the flagella (Pan and Snell, 2005). Downregulated IFT genes included *IFT22* (controls particle supply to the flagella) and *IFT52* (normally upregulated during assembly).

Summary

The downregulation of FAPs, tubulin, CEPs, RSPs, and IFT components suggests that predator infochemicals suppress the genetic program required to rebuild flagella. Without reassembly, basal bodies remain locked in their centrosomal role after mitosis and cannot nucleate new flagella. This loss of flagella not only prevents motility but also blocks ectosomal secretion of degradative enzymes, trapping daughter cells within the mother cell wall.

3.3.3.9 Knock-out mutants to confirm the role of key genes

To validate hypotheses generated from the transcriptomic data, functional assays using knock-out mutants were performed. Transcriptomics identified several candidate genes potentially involved in palmelloid formation, but differential expression alone cannot confirm their role. Mutant analysis therefore provided an opportunity to test whether loss of specific genes altered the ability of *C. reinhardtii* to form palmelloids in response to *Daphnia* infochemicals.

Mutant selection

Based on the transcriptomic data, four genes were selected for functional investigation using knock-out mutants obtained from the Chlamydomonas resource center: *FAP199, TRP13,*

PHC18, and *MMP13.* The aim was to test whether the loss of these genes altered palmelloid formation in *Daphnia* extract-treated cultures.

- ***FAP199*** was strongly upregulated in *Daphnia*-treated cultures (**Table 3.8**) and previously identified to be enriched in *Chlamydomonas* ectosomes (Long and Huang, 2013). This suggests a possible role related to degradative enzyme or signalling molecule transport during palmelloid formation.
- ***TRP13*** was the third most upregulated gene in *Daphnia* treatments (**Table 3.8**). While there have been no published studies characterising the gene or linking it to aggregation, Arias-Darraz et al. (2015) reported from reciprocal BLAST analysis that *TRP13* is a TRP channel related to members of the TRPM or TRPV subfamilies, which are involved in sensing temperature and chemicals, and ion homeostasis and signalling cascades, respectively. The TRP13 mutant was studied to show whether loss of this signalling channel impaired palmelloid formation.
- ***PHC18***: The most upregulated pherophorin gene under *Daphnia* treatment (**Table 3.8**). Pherophorins are involved in cell wall maintenance and degradation, and previous studies reported their upregulation during palmelloid formation (**Chapter 1**). Mutants affected in pherophorin genes have also previously been reported to lose their ability to aggregate (de Carpentier et al., 2022).
- ***MMP13***: In contrast to *FAP199*, *TRP13*, and *PHC18*, this matrix metalloproteinase gene was downregulated in *Daphnia* treatments (**Table 3.8**). MMPs can degrade the mother cell wall (**Chapter 1**). It was therefore hypothesised that loss of MMP13 might prevent daughter cell release, leading to spontaneous palmelloid formation or increased sensitivity to stress.

Table 3.8. Log_2-FC of genes selected for further investigation using knock-out *C. reinhardtii* mutants.

Gene		**Log₂-FC**							
		5%				**10%**			
		1h	**12h**	**20h**	**36h**	**1h**	**12h**	**20h**	**36h**
FAP199	Cre09.g399400	4.7	3.0	3.2	4.1	4.4	3.3	3.6	3.9
TRP13	Cre03.g175050	3.9	3.5	3.4	3.6	3.7	3.6	3.8	3.8
PHC18	Cre24.g755997	3.3	2.3	3.0	2.9	2.8	2.4	2.9	2.4
MMP13	Cre03.g144564	-1.4		-2.0	-3.2	-0.8		-1.2	-3.0

Bioassays under varying light intensity

Daphnia extract was added to cultures at 10% v/v, under both low (8 μmol m^{-2} s^{-1}) and high light (188 μmol m^{-2} s^{-1}). All cultures grew actively (**Figure 3.10** and **Figure 3.11**).

Mutant background (CC-5325) and wildtype (CC-1690)

CC-5325 cultures treated with *Daphnia* extract did not aggregate significantly more than controls under low (**Figure 3.12**) or high light (**Figure 3.13**). Both treatments contained more palmelloids under high light compared to under low light.

In CC-1690, both *Daphnia* treatments and controls under high light were significantly aggregated (**Figure 3.13**). As CC-1690 is unicellular at lower light levels, this aggregation was likely driven by high-light stress.

To identify genes involved in aggregation, the background strain must itself aggregate in response to *Daphnia* extract, providing a baseline for comparison with mutant strains. Therefore, different light levels were tested to determine the conditions under which CC-5325 would aggregate in *Daphnia* extract bioassays. Because CC-5325 did not aggregate under low or high light, further tests were run in CC-1690 and CC-5325 at intermediate light intensities. CC-5325 did not aggregate in response to *Daphnia* extract under any light intensity (8–188 μmol m^{-2} s^{-1}); CC-1690 did not aggregate in any treatment at 8–19 μmol m^{-2} s^{-1} but formed colonies at 38 μmol m^{-2} s^{-1} in *Daphnia* treatments, and in both controls and *Daphnia* treatments at 56–188 μmol m^{-2} s^{-1}. These results are disclosed and discussed in full in **Chapter 5**.

FAP199 and PHC18 mutants

Under *Daphnia* extract treatment, FAP199 and PHC18 mutants showed significantly higher palmelloid abundance compared to controls, under both low and high light (**Figure 3.12** and **Figure 3.13**). For example, at day three: the FAP199 mutant had ~50–70% (low and high light, respectively) of cells in four-celled palmelloids in *Daphnia* treatments vs. < 5% in the controls; the PHC18 mutant had ~30–50% (low and high light, respectively) in four–celled palmelloids in *Daphnia* treatments vs. ≤ 10% in the controls.

TRP13 mutant

The TRP13 mutant strain behaved very similarly to CC-5325. Under *Daphnia* extract treatment (10% v/v), the TRP13 mutant was slightly more aggregated than the control at both light levels,

but the difference was minimal. Under low light, there was only a pronounced difference at days three to four, with the control containing < 5% of cells in colonies and the *Daphnia* treatment containing 20–30%. Under high light, both treatments contained ~40% colonies, which decreased to 20–30% in the *Daphnia* treatment and ~10% in the control.

MMP13 mutant

Under both low and high light, the MMP13 cultures treated with *Daphnia* extract formed larger palmelloids relative to controls (**Figure 3.12** and **Figure 3.13**). Under both light conditions the proportions of single cells were similar between treatments, but the colonies were larger in *Daphnia* treatments, especially under low light. The growth and aggregation dynamics at low and high light are provided in **Appendix K**.

Low-light stress

After three months of liquid culturing under low light, cultures were exhibiting signs of low light stress: FAP199, MMP13, and PHC18 mutants contained palmelloids at days two and three after a culture refresh; these grew very large in FAP199 (≤ 32-celled) and MMP13 (≤ 64-celled), which were replaced by irregular aggregates containing cell lysate before day six (**Figure 3.14**). This cell rupture and death, consistent with a declining cell concentration (**Figure K.1**), was likely due to low-light stress. In contrast, at high light, MMP13 remained in stable palmelloids while FAP199 and PHC18 were unicellular (**Figure 3.15**), which further suggests that palmelloid formation followed by cell death in the three mutants under low light was indeed stress-induced.

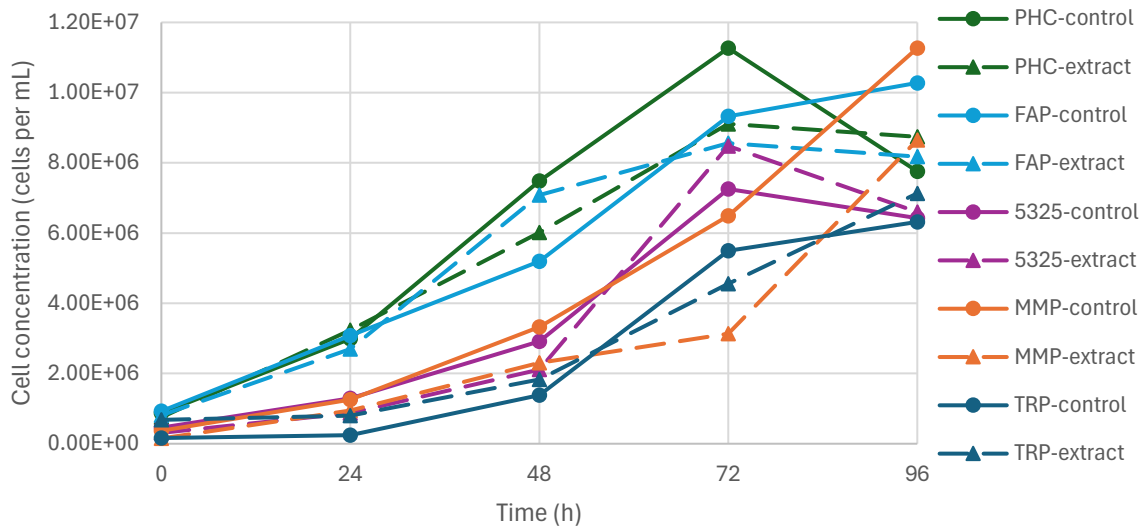

Figure 3.10. Cell concentration in *Daphnia* extract-treated cultures and controls of *C. reinhardtii* CC-5325 and mutants FAP199, MMP13, PHC18, and TRP13, over four days under constant low light (8.2 ± 0.5 µmol m^{-2} s^{-1}).

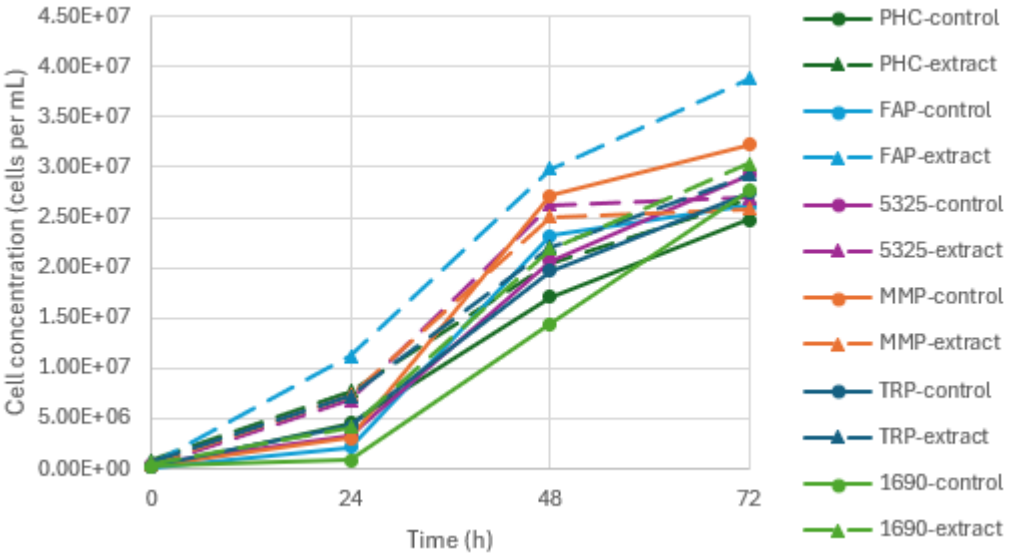

Figure 3.11. Cell concentration in *Daphnia* extract-treated cultures and controls of *C. reinhardtii* CC-5325 and CC-1690, and mutants FAP199, MMP13, PHC18, and TRP13, over three days under constant high light (188.6 ± 10.6 µmol m^{-2} s^{-1}).

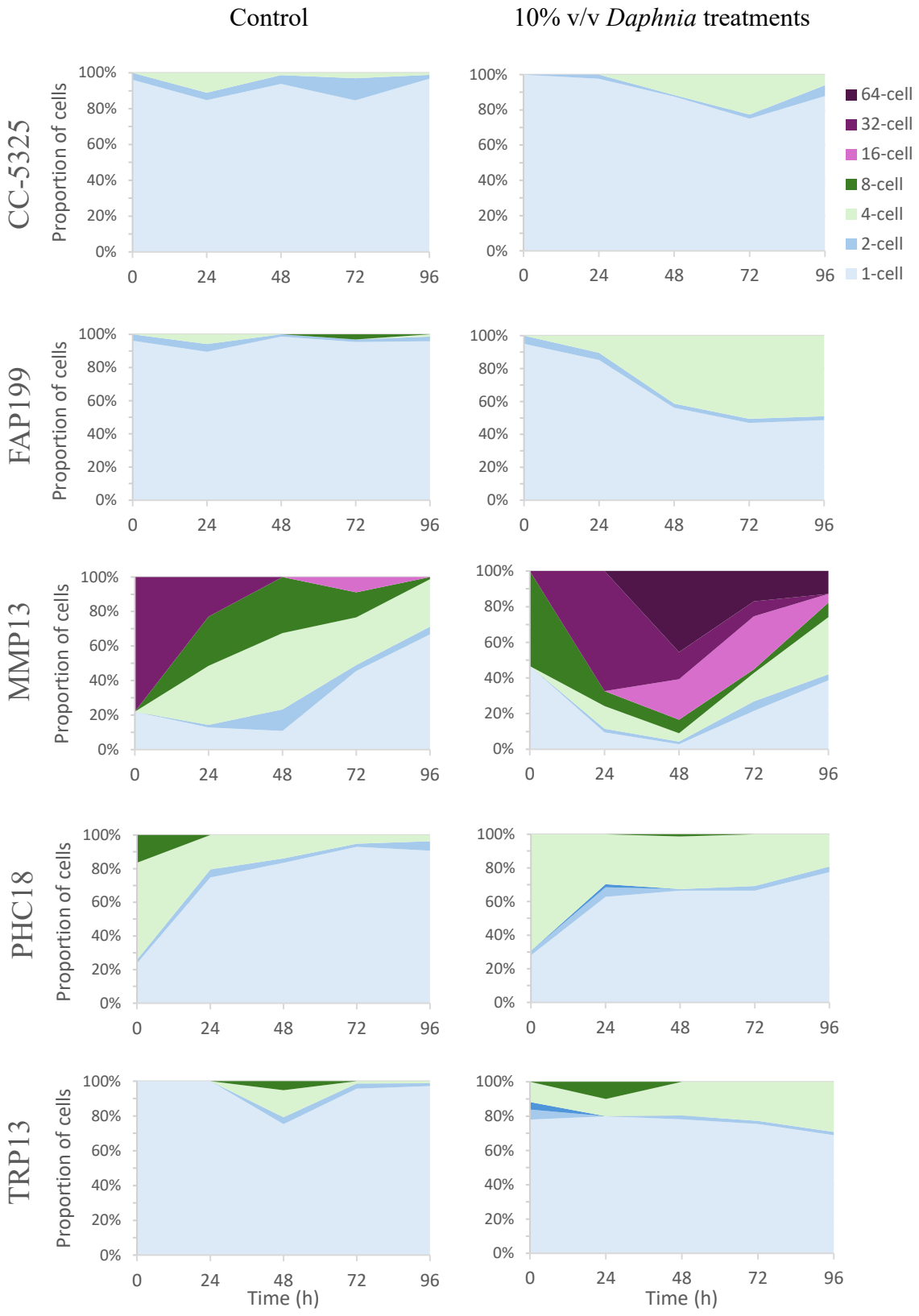

Figure 3.12. Proportion of cells, single and in colonies, in *Daphnia* extract-treated cultures (10% v/v) and controls of *C. reinhardtii* CC-5325 and mutants FAP199, MMP13, PHC18, and TRP13, over four days under constant low light (8.2 ± 0.5 µmol m^{-2} s^{-1}).

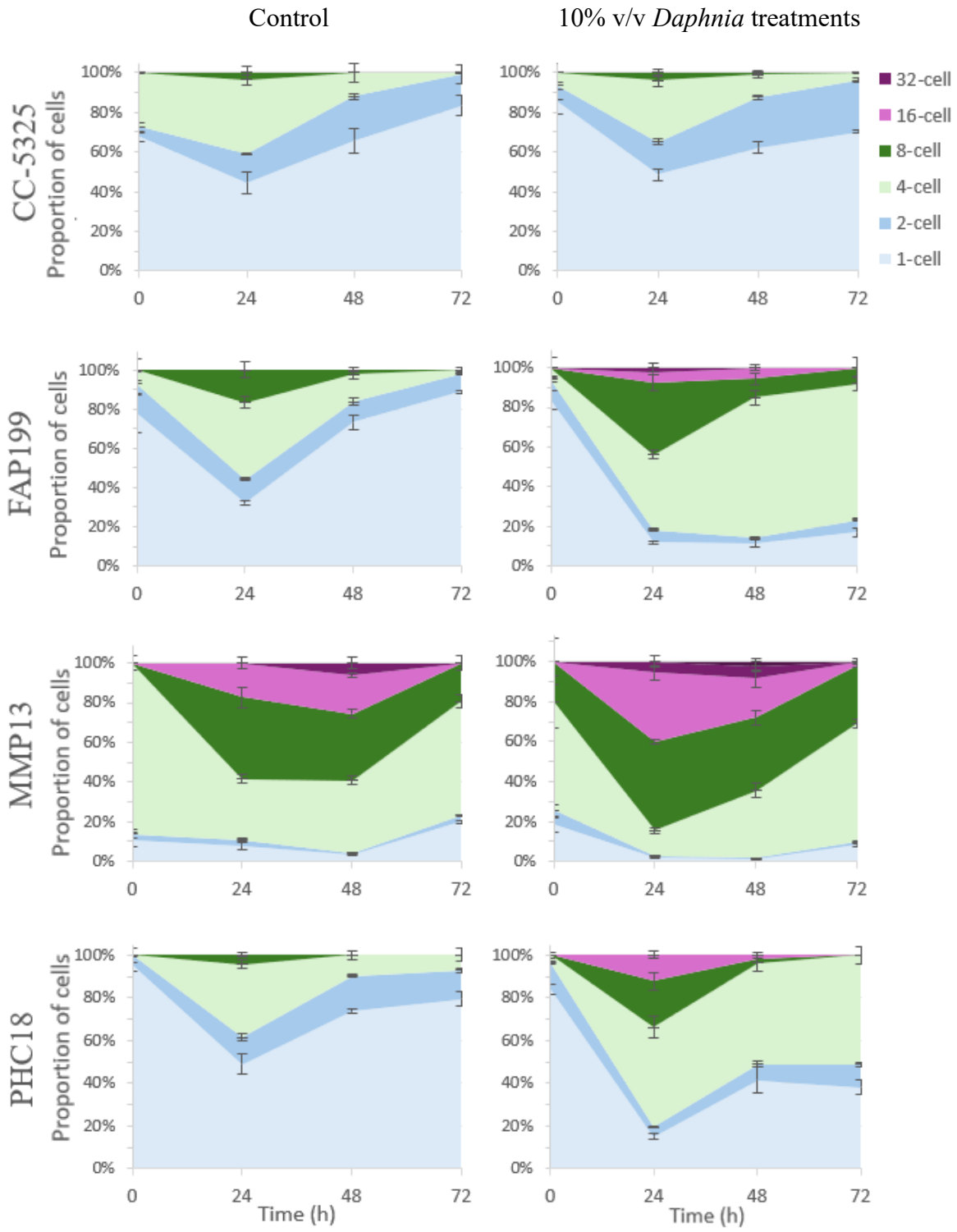

Figure 3.13. Proportion of cells, single and in colonies, in *Daphnia* extract-treated cultures (10% v/v) and controls of *C. reinhardtii* CC-5325 and mutants FAP199, MMP13, and PHC18 over three days under constant high light (188.6 ± 10.6 µmol m^{-2} s^{-1}).

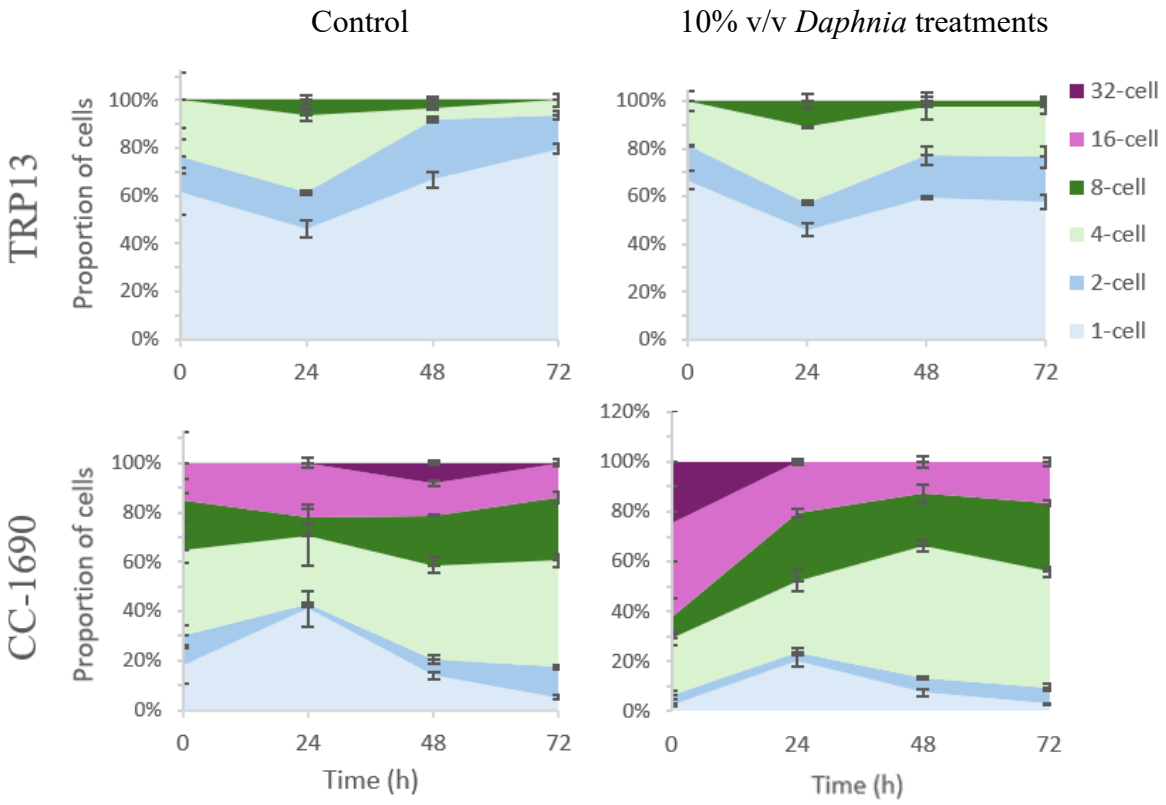

Figure 3.13. (*Continued*).

Low light

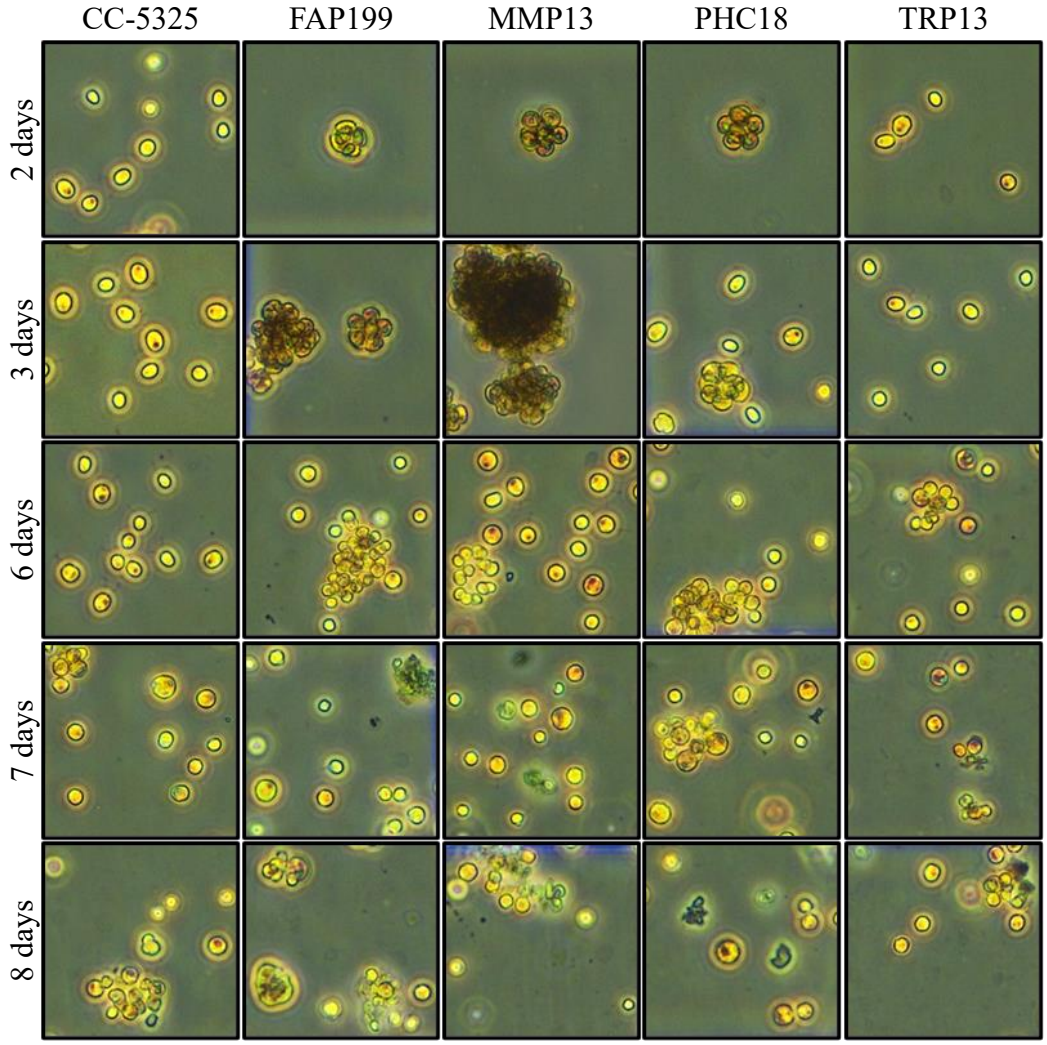

Figure 3.14. Cells and colonies in *C. reinhardtii* CC-5325 and FAP199, MMP13, PHC18, and TRP13 mutants, over eight days, under constant low light (8.2 ± 0.5 µmol m^{-2} s^{-1}). Images were taken in Brightfield at 10× magnification. Scale: each image is 100 × 100 µm.

High light

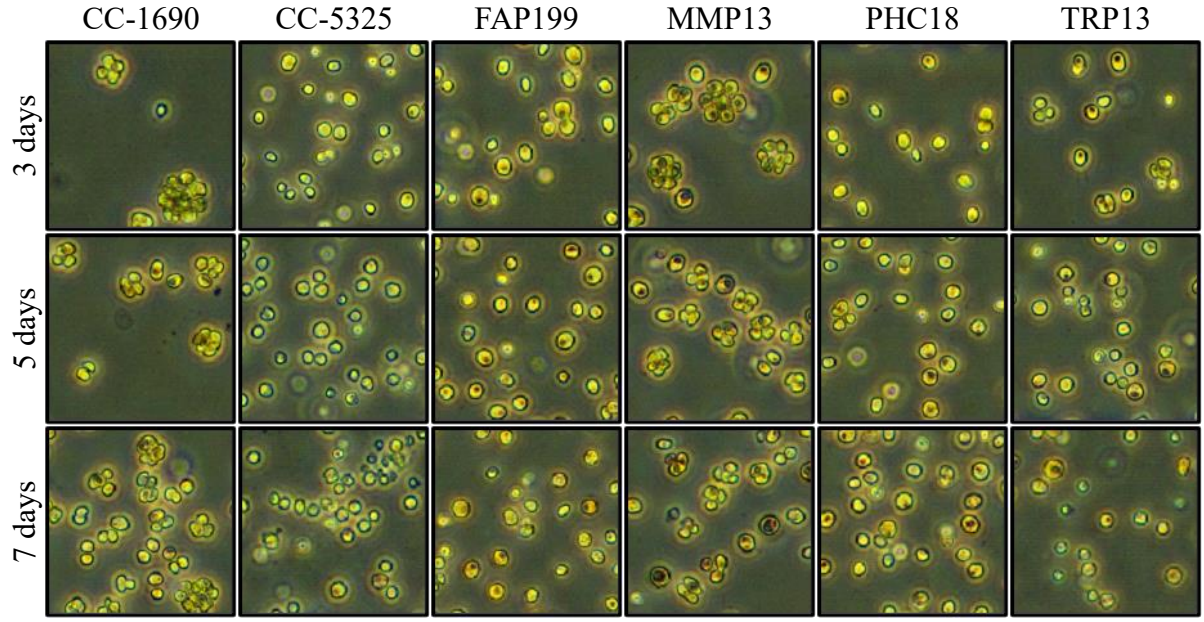

Figure 3.15. Cells and colonies in *C. reinhardtii* CC-1690, CC-5325, and in FAP199, MMP13, PHC18, and TRP13 mutants, at days three, five, and seven under constant high light (188.6 ± 10.6 µmol m^{-2} s^{-1}). Images were taken in Brightfield at 10× magnification. Scale: each image is 100 × 100 µm.

Implications

The mutant analyses provided important tests of the hypotheses generated from the transcriptomic data:

- ***PHC18* and *FAP199***: Both genes were strongly upregulated in CC-1690 cultures treated with *Daphnia* extract, yet knockout mutants formed palmelloids in response to *Daphnia* extract and light stress. This suggests that upregulation of *PHC18* and *FAP199* may be correlative with aggregation rather than causative. However, there were five other PHC genes and 26 other FAP genes that were upregulated in *Daphnia* treatments, and functional overlap within these protein families may have compensated for the loss of these single genes, allowing palmelloid formation to proceed.
- ***TRP13***: This transient receptor potential channel gene was highly upregulated in aggregating CC-1690 and was expected to be involved in infochemical sensing: The TRP13 mutant remained largely unicellular, showing only weak palmelloid formation under *Daphnia* treatment compared to other mutants, and was the only mutant to not

exhibit aggregation and cell death after prolonged low light exposure. This points to a plausible role in sensing chemical cues and light and initiating signal cascades for self-aggregation. While the absence of aggregation in the CC-5325 background complicates interpretation, and future work in an aggregating background strain such as CC-1690 would allow for stronger confirmation of the role of these mutants, the strong aggregation responses of *PHC18* and *FAP199* mutants show that these strains are indeed capable of strong aggregation under these conditions, and therefore the reduced aggregation seen in the TRP13 mutant makes the gene a plausible candidate for involvement with sensing infochemicals and initiating aggregation.

- ***MMP13***: As hypothesised, loss of *MMP13* led to a strong palmelloid phenotype, with cultures remaining aggregated even under control conditions. This was consistent with previous reports (Kim et al., 2024), and strongly supports the role of *MMP13* as a key matrix metalloproteinase required for mother cell wall degradation and daughter cell release. Larger colonies under *Daphnia* extract or light stress suggest that additional regulators also contribute to the increase in colony size.
- **Strain effects**: A striking outcome of these experiments was the clear divergence between CC-5325 and CC-1690. While CC-1690 consistently formed palmelloids under *Daphnia* and light stress, CC-5325 did not. This underscores how strain-specific differences can strongly shape phenotypes and highlights the importance of strain choice in functional studies. For future transcriptomics experiments aimed at linking genes to aggregation, using mutants with a responsive background strain would allow for more conclusive evidence toward the role of mutants.

In summary, the mutant analyses confirmed *MMP13* as a strong candidate for involvement in mother cell wall degradation and palmelloid release, supporting a previous report of downregulation during NaCl stress (Khona et al., 2016). *TRP13* also emerged as a plausible candidate sensor of external chemical or light cues. By contrast, *PHC18* and *FAP199* did not appear essential to aggregation as their mutants showed strong aggregation; this likely reflects functional overlap within gene families or indirect association with aggregation. Knock-out of multiple genes may be required to see an impact of PHC's or FAP's on the aggregation response. Together, these results refine the candidate gene list and demonstrate the importance of strain context in interpreting genetic and transcriptomic data.

3.3.3.10 Conceptual model of predator-induced palmelloid formation

Together, these results support a strong mechanistic model in which suppressed flagellar reassembly is a central driver of palmelloids persistence in *C. reinhardtii* (**Figure 3.16**). In this model, predator-derived infochemicals diffuse through the mother cell wall and activate TRP channels in the daughter cell plasma membrane, triggering Ca^{2+} influx. Signalling cascades lead to turnover of flagellar proteins driven by ubiquitination, and basal bodies remain in a centrosome role, driving mitosis but not flagella regeneration. Without flagella, ectosomal secretion of degradative enzymes and ECM glycoproteins cannot occur; downregulation of MMPs and PHCs further prevents mother cell wall breakdown. Together, these processes suppress daughter cell release and maintain palmelloid colonies.

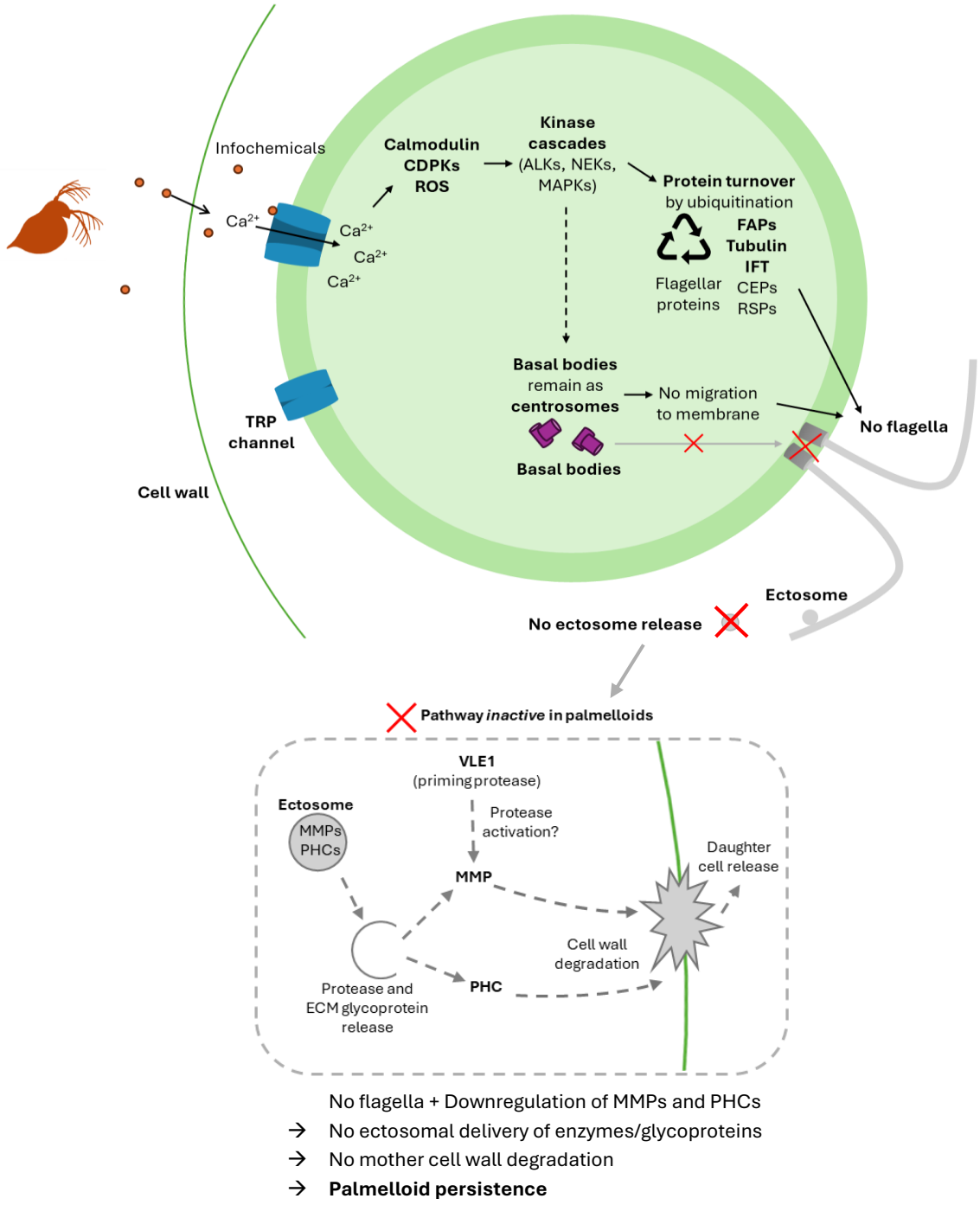

Figure 3.16. Mechanistic model of predator-infochemical signalling leading to palmelloid formation in *Chlamydomonas reinhardtii*. Predator-derived infochemicals activate TRP channels, triggering Ca^{2+} signalling cascades, turnover of flagellar proteins, and basal bodies remain in a centrosome role, driving mitosis but not flagella regeneration. Without flagella, and through downregulation of MMPs and PHCs, cell wall degradation cannot occur. The grey panel denoted the ectosomal pathway which is inactive in palmelloids.

3.4 Conclusions

This study provides the first evidence of transcriptomic changes in *Chlamydomonas reinhardtii* cultures forming palmelloid colonies in response to *Daphnia*-derived infochemicals. RNA sequencing revealed significant shifts in signalling-related gene expression, particularly in transient receptor potential (TRP) channels, calcium-dependent kinases, cyclin-dependent kinases, and components of the ubiquitin-proteasome pathway. Notably, a *TRP13* knockout failed to show strong aggregation under low light stress or in the presence of *Daphnia* extract, implicating *TRP13* as a key candidate mediator of external signal sensing.

Downstream, transcriptomic analysis showed strong suppression of genes required for flagella reassembly, including flagella-associated proteins (FAPs), tubulin, centrosomal proteins, radial spoke proteins, and intraflagellar transport (IFT) components. Basal bodies remained locked in their centrosomal role after mitosis, continuing cell division without forming new flagella, blocking ectosomal secretion of matrix metalloproteinases and pherophorin glycoproteins. Consistent with this, an *MMP13* knockout mutant spontaneously formed palmelloids, supporting the model that mother cell wall degradation requires both VLE1 and MMPs. The upregulation of *VLE1* and simultaneous suppression of *MMP13*, demonstrates that these proteases require activation. Pherophorin (PHC18) and FAP199 mutants still formed palmelloids under *Daphnia* extract treatment, likely reflecting functional overlap within these large gene families.

These findings support a regulatory model in which *Daphnia* infochemicals are sensed by TRP channels, activating Ca^{2+}-dependent signalling and kinase cascades, which in turn converge on the ubiquitin-proteasome system to destabilise flagellar proteins. These signalling cascades may be subsequently dampened, preventing flagella regeneration. The failure to reassemble flagella prevents ectosomal secretion of VLE1, MMPs, and PHCs, while selective suppression of MMPs and PHCs further stabilises the mother cell wall. The loss of flagella function and control of enzymatic activity explains how daughter cells remain encapsulated within palmelloid colonies.

Looking forward, linking these mechanistic insights to applied contexts, such as engineering palmelloid-prone strains, identifying precise infochemicals, or manipulating signalling nodes, could pave the way for practical use of self-aggregation in sustainable microalgae harvesting systems.

References

Albini, D., Fowler, M. S., Llewellyn, C., & Tang, K. W. (2019). Reversible colony formation and the associated costs in *Scenedesmus obliquus*. *Journal of Plankton Research*, *41*, 419-429. https://doi.org/10.1093/plankt/fbz032

Arias-Darraz, L., Colenso, C. K., Veliz, L. A., Vivar, J. P., Cardenas, S., & Brauchi, S. (2015). A TRP conductance modulates repolarization after sensory-dependent depolarization in *Chlamydomonas reinhardtii*. *Plant Signal Behav*, *10*, e1052924. https://doi.org/10.1080/15592324.2015.1052924

Bangera, M., Dungdung, A., Prabhu, S., & Sirajuddin, M. (2023). Doublet microtubule inner junction protein FAP20 recruits tubulin to the microtubule lattice. *Structure*, *31*, 1535-1544.e1534. https://doi.org/10.1016/j.str.2023.09.010

Berger, C. M. (2017). *The genetic basis of cooperative aggregation in the green alga Chlamydomonas reinhardtii (Master's thesis). Kansas State University.*

Bradley, B., & Quarmby, L. (2005). A NIMA-related kinase, Cnk2p, regulates both flagellar length and cell size in *Chlamydomonas*. *Journal of cell science*, *118*, 3317-3326. https://doi.org/10.1242/jcs.02455

Brown, J. M., Cochran, D. A., Craige, B., Kubo, T., & Witman, G. B. (2015). Assembly of IFT trains at the ciliary base depends on IFT74. *Curr Biol*, *25*, 1583-1593. https://doi.org/10.1016/j.cub.2015.04.060

Brown, J. M., DiPetrillo, C. G., Smith, E. F., & Witman, G. B. (2012). A FAP46 mutant provides new insights into the function and assembly of the C1d complex of the ciliary central apparatus. *Journal of Cell Science*, *125*, 3904-3913. https://doi.org/10.1242/jcs.107151

Cao, M., Li, G., & Pan, J. (2009). Regulation of cilia assembly, disassembly, and length by protein phosphorylation. *Methods Cell Biol*, *94*, 333-346. https://doi.org/10.1016/s0091-679x(08)94017-6

Chamberlain, K. L., Miller, S. H., & Keller, L. R. (2008). Gene expression profiling of flagellar disassembly in *Chlamydomonas reinhardtii*. *Genetics*, *179*, 7-19. https://doi.org/10.1534/genetics.107.082149

Christensen, R., Dave, R., Mukherjee, A., Moroney, J., & Machingura, M. (2020). Identification and characterization of a transient receptor potential ion channel (TRP2) involved in acclimation to low CO2 conditions in *Chlamydomonas reinhardtii*. *Plant Molecular Biology Reporter*, *38*. https://doi.org/10.1007/s11105-020-01218-x

de Carpentier, F., Lemaire, S. D., & Danon, A. (2019). When unity is strength: The strategies used by *Chlamydomonas* to survive environmental stresses. *Cells*, *8*. https://doi.org/10.3390/cells8111307

de Carpentier, F., Maes, A., Marchand, C. H., Chung, C., Durand, C., Crozet, P., Lemaire, S. D., & Danon, A. (2022). How abiotic stress-induced socialization leads to the formation of massive aggregates in *Chlamydomonas*. *Plant Physiology*, *190*, 1927-1940. https://doi.org/10.1093/plphys/kiac321

González-Ballester, D., Casero, D., Cokus, S., Pellegrini, M., Merchant, S. S., & Grossman, A. R. (2010). RNA-seq analysis of sulfur-deprived *Chlamydomonas* cells reveals aspects of acclimation critical for cell survival. *The Plant Cell*, *22*, 2058-2084. https://doi.org/10.1105/tpc.109.071167

Goodstein, D. M., Shu, S., Howson, R., Neupane, R., Hayes, R. D., Fazo, J., Mitros, T., Dirks, W., Hellsten, U., Putnam, N., & Rokhsar, D. S. (2011). Phytozome: a comparative platform for green plant genomics. *Nucleic Acids Research*, *40*, D1178-D1186. https://doi.org/10.1093/nar/gkr944

Hou, Y., Bando, Y., Carrasco Flores, D., Hotter, V., Das, R., Schiweck, B., Melzer, T., Arndt, H.-D., & Mittag, M. (2023). A cyclic lipopeptide produced by an antagonistic bacterium relies on its tail and transient receptor potential-type Ca2+ channels to immobilize a green alga. *New Phytologist*, *237*, 1620-1635. https://doi.org/10.1111/nph.18658

Hou, Y., Qin, H., Follit, J. A., Pazour, G. J., Rosenbaum, J. L., & Witman, G. B. (2007). Functional analysis of an individual IFT protein: IFT46 is required for transport of outer dynein arms into flagella. *J Cell Biol*, *176*, 653-665. https://doi.org/10.1083/jcb.200608041

Huang da, W., Sherman, B. T., & Lempicki, R. A. (2009). Systematic and integrative analysis of large gene lists using DAVID bioinformatics resources. *Nat Protoc*, *4*, 44-57. https://doi.org/10.1038/nprot.2008.211

Ikeda, K., Yamamoto, R., Wirschell, M., Yagi, T., Bower, R., Porter, M. E., Sale, W. S., & Kamiya, R. (2009). A novel ankyrin-repeat protein interacts with the regulatory proteins of inner arm dynein f (I1) of *Chlamydomonas reinhardtii*. *Cell Motil Cytoskeleton*, *66*, 448-456. https://doi.org/10.1002/cm.20324

Jalmi, S. K., & Sinha, A. K. (2015). ROS mediated MAPK signaling in abiotic and biotic stress-striking similarities and differences. *Frontiers in Plant Science*, *Volume 6 - 2015*. https://doi.org/10.3389/fpls.2015.00769

Joukov, V., & De Nicolo, A. (2019). The centrosome and the primary cilium: the yin and yang of a hybrid organelle. *Cells*, *8*, 701. https://www.mdpi.com/2073-4409/8/7/701

Khalifa, A. A. Z., Ichikawa, M., Dai, D., Kubo, S., Black, C. S., Peri, K., McAlear, T. S., Veyron, S., Yang, S. K., Vargas, J., Bechstedt, S., Trempe, J. F., & Bui, K. H. (2020). The inner junction complex of the cilia is an interaction hub that involves tubulin post-translational modifications. *Elife*, *9*. https://doi.org/10.7554/eLife.52760

Khona, D. K., Shirolikar, S. M., Gawde, K. K., Hom, E., Deodhar, M. A., & D'Souza, J. S. (2016). Characterization of salt stress-induced palmelloids in the green alga, *Chlamydomonas reinhardtii*. *Algal Research*, *16*, 434-448. https://doi.org/10.1016/j.algal.2016.03.035

Kim, M., Jorge, G. L., Aschern, M., Cuiné, S., Bertrand, M., Mekhalfi, M., Putaux, J.-L., Yang, J.-S., Thelen, J. J., Beisson, F., Peltier, G., & Li-Beisson, Y. (2024). The DYRKP1 kinase regulates cell wall degradation in *Chlamydomonas* by inducing matrix metalloproteinase expression. *The Plant Cell*, *36*, 4988-5003. https://doi.org/10.1093/plcell/koae271

Kirima, J., & Oiwa, K. (2018). Flagellar-associated protein FAP85 is a microtubule inner protein that stabilizes microtubules. *Cell Struct Funct*, *43*, 1-14. https://doi.org/10.1247/csf.17023

Klein, B., Wibberg, D., & Hallmann, A. (2017). Whole transcriptome RNA-Seq analysis reveals extensive cell type-specific compartmentalization in *Volvox carteri*. *BMC Biology*, *15*, 111. https://doi.org/10.1186/s12915-017-0450-y

Kobayashi, T., & Dynlacht, B. D. (2011). Regulating the transition from centriole to basal body. *Journal of Cell Biology*, *193*, 435-444. https://doi.org/10.1083/jcb.201101005

Kubo, T., Kaida, S., Abe, J., Saito, T., Fukuzawa, H., & Matsuda, Y. (2009). The *Chlamydomonas* hatching enzyme, sporangin, is expressed in specific phases of the cell cycle and is localized to the flagella of daughter cells within the sporangial cell wall. *Plant and Cell Physiology*, *50*, 572-583, Article pcp016. https://doi.org/10.1093/pcp/pcp016

Lin, J., Le, T. V., Augspurger, K., Tritschler, D., Bower, R., Fu, G., Perrone, C., O'Toole, E. T., Mills, K. V., Dymek, E., Smith, E., Nicastro, D., & Porter, M. E. (2019). FAP57/WDR65 targets assembly of a subset of inner arm dyneins and connects to regulatory hubs in cilia. *Mol Biol Cell*, *30*, 2659-2680. https://doi.org/10.1091/mbc.E19-07-0367

Long, H., & Huang, K. (2013). Analysis of flagellar protein ubiquitination. In W. F. Marshall (Ed.), *Methods in Enzymology* (Vol. 524, pp. 59-73). Academic Press. https://doi.org/10.1016/B978-0-12-397945-2.00004-4

Long, H., Zhang, F., Xu, N., Liu, G., Diener, D. R., Rosenbaum, J. L., & Huang, K. (2016). Comparative analysis of ciliary membranes and ectosomes. *Curr Biol*, *26*, 3327-3335. https://doi.org/10.1016/j.cub.2016.09.055

Lorusso, N. (2018). *Consequences of an inducible defence: The ecological and evolutionary repercussions of temporary colony formation in Clamydomonas reinhardtii.* (Dissertation). Rutgers, The State University of New Jersey.

Luo, M., Cao, M., Kan, Y., Li, G., Snell, W., & Pan, J. (2011). The phosphorylation state of an aurora-like kinase marks the length of growing flagella in *Chlamydomonas*. *Current Biology*, *21*, 586-591. https://doi.org/10.1016/j.cub.2011.02.046

Luxmi, R., Blaby-Haas, C., Kumar, D., Rauniyar, N., King, S. M., Mains, R. E., & Eipper, B. A. (2018). Proteases shape the *Chlamydomonas* secretome: comparison to classical neuropeptide processing machinery. *Proteomes*, *6*. https://doi.org/10.3390/proteomes6040036

Luxmi, R., & King, S. M. (2024). Cilia provide a platform for the generation, regulated secretion, and reception of peptidergic signals. *Cells*, *13*, 303. https://doi.org/10.3390/cells13040303

Mahjoub, M. R., Montpetit, B., Zhao, L., Finst, R. J., Goh, B., Kim, A. C., & Quarmby, L. M. (2002). The FA2 gene of *Chlamydomonas* encodes a NIMA family kinase with roles in cell cycle progression and microtubule severing during deflagellation. *J Cell Sci*, *115*, 1759-1768. https://doi.org/10.1242/jcs.115.8.1759

Mathien, S., Tesnière, C., & Meloche, S. (2021). Regulation of mitogen-activated protein kinase signaling pathways by the ubiquitin-proteasome system and its pharmacological

potential. *Pharmacological Reviews*, *73*, 1434-1467. https://doi.org/10.1124/pharmrev.120.000170

Mi, H., Muruganujan, A., Casagrande, J. T., & Thomas, P. D. (2013). Large-scale gene function analysis with the PANTHER classification system. *Nat Protoc*, *8*, 1551-1566. https://doi.org/10.1038/nprot.2013.092

Oda, Y., Sakamoto, M., & Miyabara, Y. (2022). Colony formation in three species of the family Scenedesmaceae (*Desmodesmus subspicatus, Scenedesmus Acutus, Tetradesmus Dimorphus*) exposed to sodium dodecyl sulfate and its interference with grazing of *Daphnia galeata*. *Archives of Environmental Contamination and Toxicology*, *82*, 37-47. https://doi.org/10.1007/s00244-021-00890-8

Pan, J. (2023). Ciliary disassembly. In S. K. Dutcher (Ed.), *The Chlamydomonas Sourcebook (Third Edition)* (pp. 357-371). Academic Press. https://doi.org/10.1016/B978-0-12-822508-0.00003-4

Pan, J., & Snell, W. J. (2005). *Chlamydomonas* shortens its flagella by activating axonemal disassembly, stimulating IFT particle trafficking, and blocking anterograde cargo loading. *Developmental Cell*, *9*, 431-438. https://doi.org/10.1016/j.devcel.2005.07.010

Parker, J. D., Hilton, L. K., Diener, D. R., Rasi, M. Q., Mahjoub, M. R., Rosenbaum, J. L., & Quarmby, L. M. (2010). Centrioles are freed from cilia by severing prior to mitosis. *Cytoskeleton (Hoboken)*, *67*, 425-430. https://doi.org/10.1002/cm.20454

Pigino, G., & Ishikawa, T. (2012). Axonemal radial spokes: 3D structure, function and assembly. *Bioarchitecture*, *2*, 50-58. https://doi.org/10.4161/bioa.20394

Pivato, M., & Ballottari, M. (2021). *Chlamydomonas reinhardtii* cellular compartments and their contribution to intracellular calcium signalling. *J Exp Bot*, *72*, 5312-5335. https://doi.org/10.1093/jxb/erab212

Plouviez, M., Fernández, E., Grossman, A. R., Sanz-Luque, E., Sells, M., Wheeler, D., & Guieysse, B. (2021). Responses of *Chlamydomonas reinhardtii* during the transition from P-deficient to P-sufficient growth (the P-overplus response): The roles of the vacuolar transport chaperones and polyphosphate synthesis. *Journal of Phycology*, *57*, 988-1003. https://doi.org/10.1111/jpy.13145

Rasi, M. Q., Parker, J. D., Feldman, J. L., Marshall, W. F., & Quarmby, L. M. (2009). Katanin knockdown supports a role for microtubule severing in release of basal bodies before mitosis in *Chlamydomonas*. *Mol Biol Cell*, *20*, 379-388. https://doi.org/10.1091/mbc.e07-10-1007

Roccuzzo, S., Couto, N., Karunakaran, E., Kapoore, R. V., Butler, T. O., Mukherjee, J., Hansson, E. M., Beckerman, A. P., & Pandhal, J. (2020). Metabolic insights into infochemicals induced colony formation and flocculation in *Scenedesmus subspicatus* unraveled by quantitative proteomics. *Frontiers in Microbiology*, *11*, 792. https://doi.org/10.3389/fmicb.2020.00792

Sherman, B. T., Hao, M., Qiu, J., Jiao, X., Baseler, M. W., Lane, H. C., Imamichi, T., & Chang, W. (2022). DAVID: a web server for functional enrichment analysis and functional annotation of gene lists (2021 update). *Nucleic Acids Research*, *50*, W216-W221. https://doi.org/10.1093/nar/gkac194

Sun, Y., Zhang, X., Zhang, L., Huang, Y., Yang, Z., & Montagnes, D. (2020). UVB radiation suppresses antigrazer morphological defense in *Scenedesmus obliquus* by inhibiting

algal growth and carbohydrate-regulated gene expression. *Environmental Science and Technology*, *54*, 4495-4503. https://doi.org/10.1021/acs.est.0c00104

Tammana, D., & Tammana, T. V. S. (2017). *Chlamydomonas* FAP265 is a tubulin polymerization promoting protein, essential for flagellar reassembly and hatching of daughter cells from the sporangium. *PLOS ONE*, *12*, e0185108. https://doi.org/10.1371/journal.pone.0185108

Tammana, T. V. S., Tammana, D., Diener, D. R., & Rosenbaum, J. (2013). Centrosomal protein CEP104 (*Chlamydomonas* FAP256) moves to the ciliary tip during ciliary assembly. *J Cell Sci*, *126*, 5018-5029. https://doi.org/10.1242/jcs.133439

Thiriet-Rupert, S., Gain, G., Jadoul, A., Vigneron, A., Bosman, B., Carnol, M., Motte, P., Cardol, P., Nouet, C., & Hanikenne, M. (2021). Long-term acclimation to cadmium exposure reveals extensive phenotypic plasticity in *Chlamydomonas*. *Plant Physiol*, *187*, 1653-1678. https://doi.org/10.1093/plphys/kiab375

Tokutsu, R., Fujimura-Kamada, K., Yamasaki, T., Okajima, K., & Minagawa, J. (2021). UV-A/B radiation rapidly activates photoprotective mechanisms in *Chlamydomonas reinhardtii*. *Plant Physiol*, *185*, 1894-1902. https://doi.org/10.1093/plphys/kiab004

Wang, J., Nikonorova, I. A., Silva, M., Walsh, J. D., Tilton, P. E., Gu, A., Akella, J. S., & Barr, M. M. (2021). Sensory cilia act as a specialized venue for regulated extracellular vesicle biogenesis and signaling. *Current Biology*, *31*, 3943-3951.e3943. https://doi.org/10.1016/j.cub.2021.06.040

Wheeler, G. (2017). Calcium-dependent signalling processes in *Chlamydomonas*. In (pp. 233-255). https://doi.org/10.1007/978-3-319-66365-4_8

Wingfield, J. L., & Lechtreck, K.-F. (2018). *Chlamydomonas* basal bodies as flagella organizing centers. *Cells*, *7*, 79. https://doi.org/10.3390/cells7070079

Wood, Christopher R., Huang, K., Diener, Dennis R., & Rosenbaum, Joel L. (2013). The cilium secretes bioactive ectosomes. *Current Biology*, *23*, 906-911. https://doi.org/10.1016/j.cub.2013.04.019

Wu, X., Zhang, J., Qin, B., Cui, G., & Yang, Z. (2013). Grazer density-dependent response of induced colony formation of *Scenedesmus obliquus* to grazing-associated infochemicals. *Biochemical Systematics and Ecology*, *50*, 286-292. https://doi.org/10.1016/j.bse.2013.05.001

Xiao, M., Willis, A., Burford, M. A., & Li, M. (2017). Review: a meta-analysis comparing cell-division and cell-adhesion in *Microcystis* colony formation. *Harmful Algae*, *67*, 85-91. https://doi.org/10.1016/j.hal.2017.06.00

Zhang, X., Zhang, Y., Chen, Z., Gu, P., Li, X., & Wang, G. (2023). Exploring cell aggregation as a defense strategy against perchlorate stress in *Chlamydomonas reinhardtii* through multi-omics analysis. *Science of The Total Environment*, *905*, 167045. https://doi.org/10.1016/j.scitotenv.2023.167045

Zhu, X., Sun, Y., Zhang, L., Wang, J., Gu, L., Huang, Y., & Yang, Z. (2021). Multi-omics reveal the pathways involved in induced defensive colony formation of *Tetradesmus obliquus* in response to *Daphnia* grazing cues. *Limnology and Oceanography*, *66*, 1819-1831. https://doi.org/10.1002/lno.11726

Zhu, X., Wang, Z., Zhou, Q., Sun, Y., Zhang, L., Wang, J., Yang, Z., & Huang, Y. (2021). Species-specific effects of macrophytes on the anti-grazer morphological defense in

Scenedesmus obliquus. *Ecological Indicators*, *120*, 106942. https://doi.org/10.1016/j.ecolind.2020.106942

Zuur, A. F., Ieno, E. N., & Elphick, C. S. (2010). A protocol for data exploration to avoid common statistical problems. *Methods in Ecology and Evolution*, *1*, 3-14. https://doi.org/10.1111/j.2041-210X.2009.00001.x

Chapter 4.

The chemistry of defence: Metabolomic characterisation of palmelloid formation

---

Preface

Building on the transcriptomic analysis presented in **Chapter 3**, this chapter investigated the metabolomic responses of *Chlamydomonas reinhardtii* cultures treated with *Daphnia* extract. The aim was to identify *C. reinhardtii* metabolites produced during palmelloid formation in response to *Daphnia* infochemicals and, from these, infer pathways involved in palmelloid formation.

Daphnia infochemicals reliably induced palmelloid formation in the majority of *C. reinhardtii* cells, as shown in **Chapters 2** and **3**, making this an effective model system for metabolomic analysis. This chapter was designed to corroborate hypotheses generated from transcriptomics

(**Chapter 3**) and to provide a complementary perspective on the molecular processes underlying self-aggregation.

This chapter provides the first metabolomic characterisation of *C. reinhardtii* following exposure to *Daphnia* infochemicals. The results highlight candidate compounds that may act as predator cues and underscore the importance of carefully designed metabolic approaches. By identifying the chemical signals driving palmelloid formation, future work can develop reliable, cost-effective strategies to induce aggregation at scale for harvesting. Together, the metabolomic and transcriptomic insights establish a foundation for advancing fundamental understanding of algal-grazer interactions and refining practical approaches to harvesting (discussed further in **Chapter 5**).

Abstract

This chapter investigated metabolomic changes in *Chlamydomonas reinhardtii* undergoing self-aggregation in response to *Daphnia* infochemicals, using untargeted gas chromatography-mass spectrometry (GC-MS). Combined with transcriptomic analyses (**Chapter 3**), this metabolic approach aimed to generate hypotheses on the mechanisms underlying predator-induced palmelloid formation. To our knowledge, this is the first metabolomics analysis of *C. reinhardtii* under *Daphnia* infochemical exposure.

Within 12 hours of exposure to *Daphnia* extract, *C. reinhardtii* formed palmelloids of 4–16 cells, while controls remained unicellular. GC-MS profiling detected 22 consistent metabolites, 15 of which differed significantly in abundance between *Daphnia* treatments and the controls. However, 21 of these were more abundant in the *Daphnia* extract itself, suggesting that apparent treatment effects may reflect direct metabolite transfer rather than microalgal metabolic responses. This finding underscores the need for refined experimental designs and expanded metabolite libraries to distinguish predator-derived compounds from genuine microalgal responses. These refinements will be essential for understanding algal metabolomic responses to grazing cues and to identify candidate infochemicals for advancing the use of self-aggregation as a sustainable harvesting method.

Among the metabolites detected, several, including tyramine, tyrosine, other amino acids, and urea, are plausible candidates for *Daphnia*-derived infochemicals capable of triggering self-aggregation. At the same time, compounds such as putrescine, fatty acids, and amino acids are known stress signals in plants and microorganisms and were detected in *C. reinhardtii*; they therefore may reflect *C. reinhardtii* releasing metabolites that act as intraspecific cues to reinforce aggregation. Confirmation of these roles through targeted bioassays could enable chemical induction of self-aggregation as a harvesting strategy.

4.1 Introduction

Microalgae can alter their morphology in response to predators, including forming colonies that reduce ingestion by filter-feeding zooplankton such as *Daphnia* (**Chapter 1**). While predator-induced self-aggregation is well documented, the molecular mechanisms that allow microalgae to detect predator cues and initiate aggregation remain poorly understood. Triggering aggregation on demand could significantly enhance the efficiency of biomass harvesting, but doing so requires a detailed understanding of the cellular processes, particularly metabolite-level responses, that underpin the response.

In **Chapter 3**, transcriptomic analysis of *C. reinhardtii* revealed broad downregulation of flagella-related genes in palmelloid cultures, suggesting that palmelloid cells failed to regenerate flagella, thereby preventing degradation of the mother cell wall and retaining daughter cells within colonies.

This chapter builds on those findings by examining the metabolic responses of *C. reinhardtii* during exposure to *Daphnia* infochemicals. Untargeted gas chromatography-mass spectrometry (GC-MS) was selected for its ability to profile a wide range of low molecular weight, volatile, and derivatisable metabolites, providing complementary information to the transcriptomic data. Because no studies have previously characterised the *C. reinhardtii* metabolome under *Daphnia* extract exposure, this work was exploratory and therefore used untargeted GC-MS to detect differentially accumulated metabolites between treated and untreated cultures. The *Daphnia* extract itself was also analysed to help distinguish predator-derived compounds from those produced by the algae.

The objectives of this chapter were to determine whether exposure to *Daphnia* infochemicals and the subsequent self-aggregation results in measurable metabolic responses in *C. reinhardtii* and to identify metabolites that differ significantly between treated cultures and controls.

By addressing these aims, the suitability of untargeted GC-MS for detecting chemically mediated microalgal defence responses was evaluated and methodological considerations were identified for distinguishing predator-derived compounds from genuine microalgal metabolites. This provides a foundation for future work to develop a harvesting approach using self-aggregation as a flocculant alternative.

4.2 Materials and methods

4.2.1 Triggering *C. reinhardtii* self-aggregation

4.2.1.1 Microalgae culture maintenance

C. reinhardtii CC-1690 was maintained on sterile tris-acetate-phosphate (TAP) agar and in axenic liquid TAP cultures, incubated at 22 °C under constant fluorescent light (24 ± 1 µmol m^{-2} s^{-1}) and orbital agitation (115 rpm) (see **Chapter 3** for full method).

4.2.1.2 *Daphnia* infochemical extracts

Previous work demonstrated that exposure to extracts prepared from freeze-dried *Daphnia* effectively triggered the formation of palmelloid colonies in *C. reinhardtii* (**Chapter 2**). Frozen *Daphnia* and two types of freeze-dried *Daphnia* were extracted using methanol, chloroform and water (5:2:2 v/v/v) following the protocol of Lee and Fiehn (2008); the solvent was evaporated, and the extract resuspended in water. These *Daphnia* and extraction methods are described in **Chapter 2**; the "resuspended MPS extract" was used to trigger self-aggregation for transcriptomics (**Chapter 3**) and untargeted metabolomics (this chapter). This extract, along with the "resuspended sera extract" and "resuspended frozen extract" (**Chapter 2**) and *Daphnia* tissue and filtrate from a laboratory culture of *Daphnia thomsoni*, were analysed for chemical characterisation by GC-MS.

4.2.1.3 Experimental procedure

C. reinhardtii cultures were prepared in 1 L conical flasks containing 545 mL sterilised TAP medium and acclimated for three days under continuous light and orbital agitation, as described in **Chapter 3**. Treatments were applied in triplicate:

- **Controls** received 10% v/v distilled water.
- **5% treatments** received 5% v/v *Daphnia* extract and 5% v/v distilled water.
- **10% treatments** received 10% v/v *Daphnia* extract.

Samples were collected 0.5 h before extract addition, immediately after (0 h), and at 1, 2, 12, 14, 16, 20, 24, 36, and 42 h. At each timepoint, cell pellets were harvested for transcriptomic and metabolomic analyses: 10–60 mL (~8×10^7 cells) were removed from each experimental flask and divided equally into two Falcon tubes for transcriptomics and metabolomic analyses. The tubes were centrifuged immediately (3300 × *g*, 5 min), the supernatant was discarded, and the cell pellets frozen at -80 °C.

4.2.1.4 Self-aggregation quantification

C. reinhardtii colony formation, cell concentration, optical density, and pH were monitored at each sampling point from -0.5 h to 42 h. Optical density and pH were measured immediately after sampling. Total cell concentration, colony size distribution, and the proportion of cells occurring as singles or in colonies, were manually counted in ImageJ from microscope images taken at 10× magnification, as described in **Chapter 2**.

4.2.2 Metabolite extraction

4.2.2.1 *C. reinhardtii*

C. reinhardtii metabolites were extracted as follows:

1. Frozen *C. reinhardtii* cell pellets were freeze-dried and weighed into microcentrifuge tubes.
2. 500 µL of cold MeOH (50% aq.) was added to each tube (samples, blanks and QCs).
3. Tubes were vortexed vigorously until cells were suspended.
4. Tubes were placed in dry ice until frozen.
5. Tubes were centrifuged (-9 °C, 2465 × *g*, 5 min).
6. The supernatants were transferred to microcentrifuge tubes.
7. Steps 2–6 were repeated with cold MeOH (80%, aq.), pooling the supernatants in the same microcentrifuge tubes as step 6.
8. For TMS derivatisation: 50–200 µL of each supernatant was transferred to GC vials with silanized inserts. For MCF derivatisation: the entire supernatant was transferred (see **Section 4.2.3.1**).
9. 20 µL of standard mix was added to a GC vial.

10. For TMS derivatisation only: 20 µL of d_{27}-Myristic acid 0.75 mg mL^{-1} was added as an internal standard to each vial.
11. Vials were capped and incubated (-80 °C, 30 min).
12. Vials were dried in a SpeedVac (0.8 hPa, ramp rate: 3–5, no heating) for ~4 h until completely dry. Note: blanks took 24 h to dry.
13. Dried vials were kept in a desiccator overnight before derivatisation.

For the full *C. reinhardtii* GC-MS analysis, quality controls (QCs) were prepared by combining equal weights of every sample and weighing out 1 mg of this mix into two microcentrifuge tubes. These were prepared as above, and after step seven, both were combined, before 200 µL was transferred to each of eight GC vials.

4.2.2.2 *Daphnia* extract

The *Daphnia* extract, described in **Section 4.2.1.2** and used to trigger *C. reinhardtii* self-aggregation, was prepared for derivatisation as follows:

1. 1 mL of MPS *Daphnia* extract was freeze-dried and frozen at -80 °C.
2. The extract was fully resuspended in 1.5 mL of cold MeOH (50%, aq.).
3. 200, 110, and 20 µL, in triplicate, were added to GC vials with silanized inserts (equivalent to 133, 73, and 13 µL of the original extract, respectively).
4. For TMS derivatisation only: 20 µL of d_{27}-Myristic acid 0.75 mg mL^{-1} was added to each vial as the internal standard.
5. Vials were capped and incubated (-80 °C, 30 min).
6. Vials were dried in a SpeedVac (0.8 hPa, ramp rate: 3-5, no heating) for ~4 h until completely dry.
7. Dried vials were kept in a desiccator overnight before derivatisation.

4.2.3 Metabolite derivatisation

Preliminary trials were conducted to evaluate different methods and their metabolite detection outputs. These trials tested two derivatisation methods as well as the biomass requirements and extracted volumes needed for reliable metabolite profiling. The derivatisation methods were carried out as described in the following sections.

4.2.3.1 Methyl chloroformate (MCF) derivatisation

MCF derivatisation, needed for the quantification of amino and organic acids, was carried out as described by Smart et al. (2010):

1. 20 µL of d_4-alanine was added as an internal standard to each vial, to a standard amino acid mix, and to empty microcentrifuge tubes to make derivatisation blanks.
2. Tubes were frozen at -80 °C and then freeze-dried.
3. 400 µL of 1 M NaOH was added to the samples, standard mix, blanks, and QCs, and vortexed.
4. 334 µL of MeOH and 68 µL of pyridine were added to each sample.
5. The samples were transferred to silanized glass tubes.
6. 40 µL of methyl chloroformate was added to each tube, followed by vortexing for 30 s.
7. Step 6 was repeated once.
8. 400 µL $CHCl_3$ was added using a positive displacement pipettor to each tube, followed by a gentle vortex for 10 s.
9. 800 µL of 50 mM $NaHCO_3$ was added to each tube, followed by vortexing for 10 s.
10. Tubes were centrifuged (1258 × *g*, 5 min).
11. The upper aqueous phase of each tube was removed.
12. ~100 mg anhydrous Na_2SO_4 was added to remove residual water.
13. The chloroform solutions were transferred into GC-MS vials with glass inserts.
14. 200 µL of alkane mix was added into a GC vial with insert.

Compounds were derivatised with MCF and identified using the Fiehn library. Results are reported as the corresponding parent compounds.

4.2.3.2 Trimethylsilyl (TMS) derivatisation

TMS derivatisation, needed for detecting sugars, amino acids, and organic acids, was carried out as described by Zarate et al. (2016):

1. To each dried metabolite sample, 80 µL methoxyamine hydrochloride in pyridine (0.02 g mL^{-1}) was added.
2. The vials were vortexed.
3. Solutions were incubated (28 °C, 90 min).

4. 80 µL MSTFA (N-methyl-N-(trimethylsilyl)trifluoroacetamide) was added to each vial.
5. Solutions were incubated (37 °C, 30 min).

Compounds were derivatised with MSTFA and identified as their TMS derivatives using the Fiehn library. Fatty acid methyl esters (FAMEs C8-C30) were run as retention index standards. In some cases, the closest library match corresponded to a methyl ester (e.g., methyl caprate, methyl myristate, methyl palmitate), reflecting the abundance of methyl ester spectra in reference databases. In all such cases, metabolites were reported here as the corresponding free acids, detected as their TMS derivatives. d_{27}-Myristic acid was used as an internal standard; in some runs the library also returned a separate identification as 'methyl myristate', which was subsequently treated as a misassignment of the internal standard peak rather than an additional metabolite.

4.2.4 Data acquisition by GC-MS

4.2.4.1 Rationale for GC-MS

GC-MS was selected for this study because it provides robust, reproducible detection of small, volatile, and derivatisable metabolites central to algal stress responses (Beale et al., 2018). The extensive spectral libraries available for GC-MS allow for confident compound identification, essential for distinguishing *C. reinhardtii* metabolites from *Daphnia*-derived compounds. Compared to LC-MS, which is better suited for large, polar, and thermally unstable molecules but often requires more biomass, GC-MS offered the best balance of sensitivity, coverage, and practicality for this exploratory metabolomics study.

4.2.4.2 Data acquisition

GC-MS analysis was performed on an Agilent 7890A Gas-Chromatograph coupled to a 5975MSD quadrupole mass selective detector with an electron ionisation source (Agilent Technologies, Santa Clara, CA, USA). Separation of metabolites was achieved on an Agilent ZORBAX DB5-MS column (30 m × 250 µm × 0.25 µm) and 10 m Duragard Capillary Column (122-5532G). The method followed the Agilent G1676AA Fiehn GC/MS Metabolomics RTL Library User Guide (Agilent Technologies, 2013). The inlet was set to 250 °C (9.02 psi) and operated in split mode (1:10), with a split flow of 11.1 mL min^{-1}, total flow of 15.2 mL min^{-1},

and helium carrier gas at 1.1 mL min^{-1}. Gas saver mode was activated 3 minutes post-injection, increasing split vent flow to 20.0 mL min^{-1}. Oven temperature was held at 60 °C for 1 min, ramped at 10 °C min^{-1} to 325 °C, held for 10 min, then returned to 60 °C for 1 min (total run time 37.5 min). The transfer line, MS source, and quadrupole were set to 290 °C, 250 °C, and 150 °C, respectively. A solvent delay of 5.90 min was applied. The MS scanned m/z 50 to 600 with a detection threshold of 150 ion counts. Daily quality controls included a method blank, a mixed sample QC, a standard mix, and a FAMEs standard. Sample order was randomised, with 20 samples run per day.

4.2.5 GC-MS data pre-processing

Raw gas chromatography-mass spectrometry files were converted to an AIA Common Data Format (CDF) for processing with the MassOmics R package (batch processing of untargeted metabolomics; Smart, 2010). Data were deconvoluted, and compounds were identified using the Automated Mass Spectral Deconvolution and Identification System (AMDIS - http://www.amdis.net/). Retention times were recalibrated using fatty acid methyl esters (FAME) standards, and compound identification was aided by the Agilent Fiehn GC/MS Metabolomics Retention Time Locking Library (G1676AA).

Metabolites can appear as multiple peaks in the chromatogram, so the software grouped together related MS signals into one ‘component’ and assigned it a retention time, a peak area, and a composite mass spectrum. The mass spectrum was then compared against the spectral library (FiehnLib), and based on the fragmentation pattern, retention time, and mass accuracy, a component became a ‘target’ (metabolite) match if it matched these criteria, otherwise it was tagged as an ‘unknown’. Tentative identifications were assigned based on the highest-scoring spectral match for each feature.

Summary reports were generated for all *C. reinhardtii* and *Daphnia* extract samples and manually curated. Peaks with retention time shifts greater than 30 s were removed, duplicates were checked and eliminated, and metabolites with ≤ 10 hits (a “hit” being detection above the limit and blank in a sample) were manually verified against the library. Features with only a single hit across all samples were removed. Data were normalised to the abundance of internal standard (d_4-Alanine or d_{27}-Myristic acid) in each sample. Final relative abundance values were calculated by subtracting the average relative abundance of each metabolite in the blanks from its relative abundance in the sample, thereby removing background solvent contaminants.

4.2.6 Preliminary trials – Method development

Untargeted metabolomics was conducted on *Daphnia* extract, *C. reinhardtii* cultures self-aggregated in response to *Daphnia* extract, and control cultures without extract. Three preliminary trials compared the efficiencies of MCF and TMS derivatisation techniques and assessed biomass requirements.

4.2.6.1 Trial 1: *Daphnia* extracts with MCF derivatisation

Trial 1 assessed the number of metabolites detectable in freeze-dried MPS *Daphnia*, extracts prepared from freeze-dried and frozen *Daphnia*, and *D. thomsoni* culture filtrate. As this trial was intended only to evaluate metabolite detectability, not all samples were replicated. Liquid samples (500 µL, freeze-dried) and 10 mg of freeze-dried MPS *Daphnia* were derivatised using the MCF method.

4.2.6.2 Trial 2: *C. reinhardtii* with MCF derivatisation

Samples from aggregated (*Daphnia* extract-treated) and unicellular control *C. reinhardtii* cultures were used to determine the minimum biomass required for metabolite detection. While Smart et al. (2010) recommends 10 mg dry biomass for microorganisms, 1 mg per replicate was used, as Lee and Fiehn (2008) reported that 0.2 mg of microalgae is sufficient for GC/MS analysis. Therefore, two biomass levels were tested 48 h after treatment: 2.28 and 0.59 mg for the 5% *Daphnia* extract group, and 3.73 and 0.35 mg for controls.

4.2.6.3 Trial 3: *C. reinhardtii* with TMS derivatisation

Following advice from Prof. Oliver Fiehn (University of California, Davis), TMS derivatisation was tested due to its versatility and larger compound libraries, enabling more compound annotations. Samples from the 5% *Daphnia* extract treatment (2.11 and 0.42 mg) and controls (2.16 and 0.48 mg), collected at 48 h, were processed with either 50 µL or 200 µL of the 1 mL supernatant transferred to GC vials during extraction (see **Section 4.2.2**, Step 8).

4.2.6.4 Metabolite filtering and statistical analyses

No statistical analyses were performed on preliminary trial data as there were no replicates. Therefore, data were not filtered, transformed, or imputed. For Trials 2–3, relative abundances were normalised to biomass concentration and multiplied by a factor of 1000 for ease of reporting.

4.2.7 Full analysis of *C. reinhardtii* and *Daphnia* extract using TMS derivatisation

4.2.7.1 Method selection

Based on the method development data presented in **Section 4.3.2**, the following parameters were selected for further analysis: TMS derivatisation, using 200 µL of metabolite supernatant extracted from 1 mg algal biomass. TMS derivatisation was chosen because it yielded more metabolites than MCF (see **Section 4.3.2**). A 200 µL of supernatant volume provided sufficient peak abundance counts while remaining below ~1 × 10^6 peaks, thereby avoiding column overloading (see **Section 4.3.3.4**).

Algal samples collected at -0.5, 1, 2, 12, 14, 20, and 36 h post-*Daphnia* extract addition were analysed for the control and both treatments (5% and 10% v/v *Daphnia* extract). Three biological replicates per treatment were used, unless otherwise stated. From each biological replicate, ~1 mg aliquots were weighed to create three technical replicates; where biomass was insufficient, duplicate or triplicate derivatisation replicates were generated by splitting 200 µL of extracted metabolites from a single sample into multiple GC vials and drying. **Table L.1** (**Appendix L**) summarises biological, technical, and total replicate numbers for each sample.

For *Daphnia* extract analysis, approximate concentrations in the algal biomass at each time point were calculated and used to select the volumes 13, 73, and 133 µL (as an approximate relevant range) to run for GC-MS. This analysis was intended to identify compounds potentially originating from the extract rather than to provide a comprehensive *Daphnia* metabolite profile.

4.2.7.2 Metabolite filtering and statistical analyses

Daphnia extract

For the full GC-MS analysis, *C. reinhardtii* and *Daphnia* extract data were processed and analysed separately. For the *Daphnia* extract, relative abundances were normalised to the initial extract volume (13, 73, or 133 µL), and metabolites with few hits were removed. As there were only nine samples (three groups in triplicate), the data were visually inspected to remove samples with high missing hit rates or highly skewed distributions. Remaining missing hits were imputed with the median value across groups. Multivariate analysis was performed using unsupervised principal component analysis (PCA) to provide an overview of variance among *Daphnia* extract samples (Chen et al., 2022).

C. reinhardtii

Relative abundance values for each metabolite were normalised to biomass concentration, i.e., the freeze-dried *C. reinhardtii* weight (~1 mg) for each sample. Across the three treatments (5% and 10% v/v *Daphnia* extract and control) and seven timepoints, with up to ten replicates per group, a total of 149 samples were analysed.

Metabolites were excluded if detected in fewer than 10% of all samples. Within each treatment:time group, hits were removed if a metabolite was missing in more than 40% of samples, following a modified "80% rule" (Wei et al., 2018) to retain more features given the low number of metabolites identified prior to filtering. Remaining groups were cross-checked against raw peak area data to determine whether missing hits were removed during pre-processing or were undetected in the original samples; where appropriate, missing values were imputed with the group median, which performs reliably with non-normal data and extreme outliers (Wei et al., 2018).

Statistical tests were performed using R (v4.4.1). Data handling, manipulation, and fold-change calculations used **readxl**, **readr**, **tibble**, **dplyr**, **tidyr**, **stringr**, **forcats**, and **purr.** Assumption checks for normality and homogeneity of variances used **stats**, **car**, and **e1071**; two-way ANOVA and effect size calculations used **stats**, **broom**, **effectsize**, and **rstatix**; post-hoc comparisons used **PMCMRplus** and **rstatix.** Data visualisation (heatmaps and PCA) was carried out with **ggplot2**, and skewness was calculated using **e1071::skewness()** function. The significance level for all tests was set at 0.05.

Data were transformed to stabilise variance and reduce skew. A two-way ANOVA was performed on transformed data to assess main effects of treatment, time, and their interaction on metabolite abundance (Chen et al., 2022). Residuals were tested for normality using Shapiro-Wilk tests, and cube-root transformed data were tested for homogeneity using Bartlett's and Levene's tests. As classical ANOVA assumptions were not met, Welch's one-way ANOVA was applied across treatment:time groups to verify results (Delacre et al., 2019). For metabolites with significant Welch's ANOVA results, pair-wise comparisons were performed using Games-Howell post-hoc tests to assess differences between treatments at the same timepoint and within treatments over time (Lee and Lee, 2018). *p*-values were adjusted for multiple testing using the Benjamini-Hochberg method (Chen et al., 2022). Multivariate analysis by unsupervised PCA was conducted to explore variance between *C. reinhardtii* experimental and QC samples (Chen et al., 2022).

4.2.7.3 Fold-change analysis

A fold-change analysis was conducted on *C. reinhardtii* metabolites to compare abundances between the 5% and 10% *Daphnia* extract treatments and the control at each timepoint. Fold-change was calculated as the $\log_2$ ratio of the mean relative abundance in the treatments to that in the control. Two-sample *t*-tests were performed, with *p*-values adjusted using the Benjamini-Hochberg method. Results were visualised as heatmaps, with metabolites detected in only one or neither group at a given timepoint indicated accordingly.

4.2.7.4 Pathway enrichment analysis

Metabolites showing significant differences in relative abundance between treatments (identified by Welch's ANOVA) were analysed for pathway and enrichment analyses using MetaboAnalyst (www.metabolanalyst.ca accessed June 2025) as discussed by (Chen et al., 2022). Pathway analysis parameters were visualised by scatter plot, with significant features identified via hypergeometric testing. Pathway topology was assessed using relative-betweenness centrality, and the *C. reinhardtii* pathway library selected as the reference metabolome. Enrichment analysis used the Global Test method to assess associations between metabolite sets and outcomes, based on KEGG human metabolic pathways.

4.3 Results and discussion

4.3.1 *C. reinhardtii* cell concentration, pH, and colony formation

As reported in **Chapter 3**, only the *Daphnia* extract treatments formed palmelloid colonies. No self-aggregation was detected at one hour in any treatment. By 12 hours, *C. reinhardtii* exposed to *Daphnia* extract formed four-, eight-, and 16-celled palmelloids, whereas controls remained unicellular. From 24–42 hours, the 10% treatment maintained the largest mean colony size; the 5% treatment peaked at 20 hours, then declined, and was significantly smaller than the 10% treatment at 36 hours (Tukey HSD, $p < 0.05$).

Cell concentration and pH curves in **Chapter 3** confirm that both parameters increased over the 42 hour experiment in all treatments with no between-treatment differences at any timepoint (two-way ANOVA with Tukey HSD, $p > 0.05$). As growth rate and pH were comparable across treatments, this indicates that increased colony formation in *Daphnia* treatments was not an artefact of increased cell division or a response to pH changes and was indeed in response to the *Daphnia* infochemicals.

4.3.2 Preliminary trials

4.3.2.1 MCF derivatisation (Preliminary trials 1-2)

In *Daphnia* extracts, 59 compounds were detected, with 26 retained after filtering for match quality and blank abundance (Trial 1, full breakdown in **Table 4.1**; metabolites and relative abundances shown in **Table M.1**, **Appendix M**). In *C. reinhardtii* samples, 83 compounds were detected, of which 35 remained after filtering (Trial 2, **Table 4.1** and **Table M.2**, **Appendix M**). Eighteen metabolites were shared between *C. reinhardtii* and *Daphnia* extract (highlighted in bold in tables). The raw data are provided in **Supplementary Data File S2**.

Relative abundances were broadly consistent across extract types, with the highest levels observed in the Sera extract and the lowest in *D. thomsoni* filtrate. The same metabolites were consistently detected in all *C. reinhardtii* samples, with only five metabolites unique to larger biomass samples (2–3 mg) and absent from smaller ones (0.3–0.5 mg), indicating minimal loss

of coverage at lower biomass. After normalisation, smaller samples showed inflated relative abundances, underscoring the need to maintain consistent sample mass.

4.3.2.2 TMS derivatisation (Preliminary trial 3)

In *C. reinhardtii* samples, 137 compounds were detected, of which 38 remained after filtering for match quality and blank abundance (**Table 4.1** and **Table M.3**). Raw data and metabolite filtering are shown in **Supplementary Data File S2**. Three metabolites (succinic acid, putrescine, and azelaic acid) were also detected with MCF derivatisation (Trial 2).

Detection was influenced by extraction volume and biomass: more metabolites were found using 200 µL extracts compared with 50 µL, and in samples with higher initial biomass (~2 mg vs ~0.5 mg). Although MCF used the full biomass sample and TMS analysed only 200 µL of a 1 mL supernatant, the overall coverage was comparable. This consistency likely reflects the broader compound scope accessible through TMS derivatisation.

4.3.3 Full analysis of *C. reinhardtii* and *Daphnia* extract using TMS derivatisation

4.3.3.1 Metabolites classes

GC-MS analysis identified a range of metabolites, including amino acids, organic acids, polyamines, sugars and polyols, nucleotides and vitamins, and several fatty acids. The fatty acids were reported in the library as methyl esters (e.g., methyl caprate, methyl palmitate), however, given the use of TMS derivatisation, these were interpreted as the corresponding free acids (see **Supplementary Data File S2**).

4.3.3.2 *Daphnia* extract results and filtering

Of 139 compounds detected in *Daphnia* extracts, 62 remained after filtering for match quality and blank abundance, of which, nine had three or fewer hits across nine samples and were also removed (summary in **Table 4.1**, full process shown in **Supplementary Data File S2**).

The entire 13 µL dataset was excluded, due to inconsistencies which were unlikely related to the biomass: after normalisation, smaller-volume extracts (73 or 13 µL) showed higher relative abundances than the 130 µL samples, with extreme outliers in the 13 µL group (e.g., glycerol at 1409 vs a mean of 195 across other samples); 22 metabolites present in the 130 and 73 µL groups were missing in one or several of the 13 µL replicates. These inconsistencies were possibly due to low sample size and metabolite concentrations too close to the detection limit. The remaining dataset had only two missing values, which were imputed with the group median.

Mean abundances of metabolites in the 130 and 73 µL groups are given in **Table 4.2**; metabolites previously identified in preliminary trials in *Daphnia* extract using the MCF method are bolded.

4.3.3.3 *C. reinhardtii* results and filtering

Of 133 compounds detected in *C. reinhardtii* (all of which were also detected in the *Daphnia* extracts), 35 remained after filtering for match quality and blank abundance, of which, 13 occurred in < 10% of all samples and were also removed (full breakdown in **Table 4.1**). The remaining 22 underwent group-level filtering: where > 40% of a group's values were missing, hits were removed; where ≥ 60% were present, missing values were imputed with the group median (see **Supplementary Data File S2**). A heatmap of relative abundances for the final 22 metabolites is provided in **Table 4.3**.

Table 4.1. Summary of metabolite filtering outcomes for *C. reinhardtii* and *Daphnia* extract datasets from MCF and TMS trials, and the full TMS analysis. Values indicate the number of compounds retained or excluded at each step. "Final metabolites" indicates those retained for analysis.

Analysis	Sample	Compound matches	Split peaks	Weak IDs	Higher blank	Low hits	Final metabolites
Trial 1 – MCF	*Daphnia* extract	59	7	26			26
Trial 2 – MCF	*C. reinhardtii*	83	15	33			35
Trial 3 – TMS	*C. reinhardtii*	137	13	56	30		38
Full analysis – TMS	*Daphnia* extract	139		52	25	9	53
Full analysis – TMS	*C. reinhardtii*	133		35	63	13	22

Table 4.2. Mean relative abundances of the 53 metabolites identified in the full GC-MS analysis of *Daphnia* extract (TMS derivatisation) following normalisation, filtering, and imputation. Colour intensity reflects relative abundance. Metabolites in **bold** were also detected in Trial 1 using MCF derivatisation.

Metabolite	Mean Relative Abundance		Metabolite	Mean relative Abundance	
	Daphnia extract			*Daphnia* extract	
	130 µL	73 µL		130 µL	73 µL
L-(+) lactic acid	59.38	176.59	1,3-diaminopropane	0.28	0.58
L-alanine	41.83	84.75	Beta-glycerolphosphate	0.04	0.14
Caprylic acid	0.03	0.13	Putrescine	1.79	3.52
L-leucine	3.01	12.72	Glycerol 1-phosphate	3.24	5.70
N-methylalanine	1.56	2.68	10-hydroxydecanoic acid	4.24	8.89
L-valine	20.89	36.54	Galactose	0.02	0.04
Urea	1.30	2.90	Fructose	0.39	0.96
Benzoic acid	0.16	0.37	D-glucose	1.33	3.82
Ethanolamine	5.51	12.39	D (+)altrose	1.59	3.48
Phosphoric acid	0.72	2.61	Tyramine	2.89	5.90
Glycerol	78.67	249.98	**L-lysine**	8.40	17.18
DL-isoleucine	13.54	24.62	D-sorbitol	0.52	1.23
L-proline	13.72	22.18	Palmitic acid	0.32	0.22
Glycine	12.47	28.71	**L-tyrosine**	7.65	15.42
Succinic acid	3.30	8.02	Pantothenic acid	0.13	0.31
Capric acid	0.11	0.26	Xanthine	0.28	0.97
Glyoxylic acid	0.01	0.05	Stearic acid	1.32	0.09
L-serine	4.25	7.62	Eicosanoic acid	3.68	0.18
L-threonine	4.21	7.41	Docosanoic acid	3.56	0.12
Beta- alanine	1.33	3.08	Inosine	9.95	18.99
Adipic acid	0.91	1.73	Lactose	0.10	0.36
L-methionine	0.06	0.10	Maltose	0.95	1.93
Aspartic acid	2.87	5.22	Lignoceric acid	2.88	0.17
L-pyroglutamic acid	10.46	23.38	Guanosine	2.73	14.04
Threonic acid	0.28	0.66	Hexacosanoic acid	2.44	0.09
L-glutamic acid	5.12	9.64	Octacosanoic acid	1.73	0.07
5-aminovaleric acid	0.60	1.28			

Table 4.3. Mean relative abundances of final 22 metabolites identified in the full GC-MS analysis of *C. reinhardtii* using TMS derivatisation, after normalisation, filtering, imputation, and multiplied by a factor of 1000. Colour intensity reflects relative abundance. Missing values indicate non-detection.

Metabolite	Mean Relative Abundance (x1000)																	
	Initial	Control						5% v/v *Daphnia* Extract					10% v/v *Daphnia* Extract					
	-0.5h	1h	2h	12h	14h	20h	36h	1h	2h	14h	20h	36h	1h	2h	12h	14h	20h	36h
L-alanine	3.3	13.8	3.0	6.6	5.4	6.0	7.1	8.0	6.7	5.8	19.4	8.7	50.2	25.2	17.6	8.5	13.6	12.8
L-leucine							0.7	1.0	0.6	0.6	1.6	0.6	3.7	2.6	1.3	0.8	1.0	1.2
N-methylalanine													2.4	1.0	0.2			
L-valine	0.5		0.3	0.8	1.0	1.1	2.8	4.0	2.7	2.3	7.5	2.5	23.3	11.5	6.7	3.6	4.8	4.5
Ethanolamine	4.5	58.1	19.3	23.7	12.6	14.0	29.4	17.7	22.6	24.4	25.8	29.0	16.1	18.2	31.6	28.1	31.0	31.7
Phosphoric acid	342.9	204.7																
DL-isoleucine						0.3	1.1	1.9	1.4	0.9	3.4	1.2	13.3	5.9	3.1	1.7	2.5	2.3
L-proline											2.4		6.3	3.2	1.4	0.5	1.1	0.9
Decanoic acid (capric acid)	4.8	8.2	5.5	9.1	4.5	2.4	11.2	8.3	6.4	11.2	10.7	8.4	6.7	3.8	6.1	5.6	3.7	5.7
Glyoxylic acid	60.8	87.4	77.4	116.5	57.2	30.5	171.2	126.7	97.2	170.0	191.6	124.6	93.4	52.9	76.9	79.5	37.2	80.7
L-serine							0.3		0.3		0.5	0.3	3.1	1.3	0.8			0.6
Adipic acid	2609	2335	2051		360.7													
L-pyroglutamic acid											3.2		14.3	7.2	2.8		1.9	
Threonic acid	3.0	3.5	2.4	3.4	1.6	1.3	0.7	0.6	0.6	0.4	1.5	0.6	2.0	1.9	0.8		0.9	1.0
L-glutamic acid	2.3		1.6			1.8			0.7	0.9	2.6		7.5	2.7	2.3	0.4		
1,3-diaminopropane	2.3	3.9	2.7	0.4	1.2								1.9	0.6				
Putrescine	60.8	118.4	52.3	79.6	37.9	55.7	54.4	113.5	57.6	101.1	124.6	58.1	100.1	92.9	85.0	83.8	80.8	62.1
Galactose						1.9		0.4	0.9	3.9	4.7	1.6		0.9	5.3	6.0	8.2	2.7
Fructose													1.0					
Tyramine													2.3	0.8				
L-lysine							0.8			0.5	0.4	0.5	4.1	1.6	1.1	0.4		1.2
L-tyrosine							0.4						3.7	1.2	0.7			0.7

4.3.3.4 Comparison to trials and literature

The full TMS analysis of *C. reinhardtii* narrowed 133 detected metabolites to 22, consistent with Trial 3 (138 reduced to 38). Other studies have reported higher metabolite counts, but often with larger sample sizes or different extraction approaches. For example, Zhu et al. (2021) detected 321 metabolites in *Tetradesmus obliquus* (10 mg dry biomass, 400 µL extract, TMS/GC-MS) but did not specify filtering outcomes; only 54 metabolites differed significantly between treatments. Similarly, Lee and Fiehn (2008) reported ~750 chromatogram peaks in *C.* reinhardtii, which yielded 334 reproducible signals but only 80 unique metabolites.

Untargeted LC-MS studies show even wider variation. Apostolopoulou et al. (2022) identified 58 significant metabolites across four algal species (5 mL culture), whereas Zhang et al. (2023) reported > 1000 differentially accumulated metabolites in *C. reinhardtii* exhibiting self-aggregation under perchlorate stress, though methods and sample sizes were not detailed. This reflects the different chemistries captured by each technique: LC detects larger, polar, thermally unstable compounds (e.g., lipids, secondary metabolites), while GC is suited to volatile, heat-stable compounds (e.g., organic acids, amino acids).

Overall, increasing biomass or extract volume can improve metabolite detection, but abundance peaks must remain below ~1×10^6 counts to avoid overload. In this study, MCF derivatisation sometimes exceeded this threshold (some > 7×10^6), whereas TMS with 200 µL extract provided robust peak counts within acceptable limits. This supports the use of TMS at this volume for subsequent analysis.

4.3.3.5 Library matching constraints

A major factor in the low number of identified metabolites was limited matching to the Fiehn library, despite many chromatographic peaks. The analysis of *C. reinhardtii* and *Daphnia* extract samples yielded significantly more components (peaks) than metabolite matches to the library. For example, two *C. reinhardtii* samples yielded 103 and 143 components but only 13 and 18 matches; a 130 µL *Daphnia* extract yielded 560 components and 135 matches, while a 13 µL sample yielded 237 components and 41 matches. Therefore, the low number of metabolites identified in these analyses were not due to a low number of peaks/detected compounds, but rather due to the components not matching with the library used. The Fiehn

library, curated for primary and some secondary metabolites, is widely accepted for GC-MS metabolomics but may not contain lipids, phenolics, or unusual algal secondary metabolites. Technical factors (GC conditions, calibration, derivatisation, deconvolution thresholds) can also reduce match rates.

4.3.3.6 Statistical analyses – *C. reinhardtii*

The *C. reinhardtii* metabolite relative abundance data (from 1–36 hours) were transformed to reduce skewness prior to statistical analysis. A $\log_2$ transformation did not improve skewness, but cube root-transformation reduced skewness for most metabolites and was therefore used for all statistical analyses (**Supplementary Data File S2**).

A two-way ANOVA was run to evaluate main effects of treatment, time, and their interaction on metabolite levels (groups being each treatment at each timepoint; **Table N.1**, **Appendix N**). However, the Shapiro-Wilk test indicated that residuals were not normally distributed, and Bartlett's and Levene's tests indicated unequal variances (**Table N.2**), meaning the classical ANOVA assumptions were not met. Since this could make the standard two-way ANOVA results unreliable, a Welch one-way ANOVA across groups was conducted as a robust check against heteroscedasticity to verify results of the two-way ANOVA (**Table N.2**).

Of the 22 *C. reinhardtii* metabolites detected, three showed no significant effect of treatment, time, or their interaction in the two-way ANOVA (ethanolamine, capric acid, glyoxylic acid), and for the latter two the Welch's ANOVA also found no significant difference between any group means. The Welch's ANOVA identified significant differences across groups for 18 metabolites (**Table N.2**). Groups where the two-way ANOVA indicated significance, but Welch's ANOVA did not, were likely false positives due to unmet assumptions.

For the 18 metabolites significant by Welch's ANOVA, pairwise comparisons were performed using Games-Howell post-hoc testing. A heatmap of the pairwise comparisons between treatments at the same timepoints (e.g., 5% *Daphnia* extract vs control at 1 h) for each metabolite is shown in **Figure 4.1** and full Games-Howell results are provided in **Supplementary Data File S2**. Of the 18 metabolites, three showed no significant differences between any treatments at any timepoint (**Figure 4.1** shows only metabolites with at least one significant pair; the rest -L-alanine, ethanolamine, putrescine- are shown in **Figure N.1**). In such cases, the significant Welch's ANOVA result was likely driven by temporal changes within

treatments rather than treatment effects. This is consistent with Lee and Fiehn (2008), who reported that metabolite profiles in *C. reinhardtii* can vary greatly depending on harvest time.

4.3.3.7 PCA

The first three principal components (PCs) explained ~73% of the total variance within the *C. reinhardtii* and QC samples, indicating most biological variation was captured by the PCA (**Figure 4.2**–**Figure 4.4**; PCA scores provided in **Supplementary Data File S2**). PC1 primarily represented variance between treatments, PC2 captured within-treatment variance across timepoints, particularly for the control and 10% *Daphnia* extract treatment. PC3 highlighted potential outlier samples, within-treatment variation, and possible treatment-time interaction effects. QC samples clustered tightly, confirming data quality and supporting the transformation and imputation methods used.

For the *Daphnia* extract samples, the first two PCs explained 89% of the variance, with PC3 accounting for only 5.9% (**Figure 4.5**–**Figure 4.7**; PCA scores provided in **Supplementary Data File S2**). The 130 µL and 73 µL sample groups each formed tight clusters, whereas the 13 µL group displayed greater variability-supporting the decision to exclude the latter from analysis. A clear separation remained between the 130 µL and 73 µL groups, indicating that sample volume strongly influenced the GC-MS results.

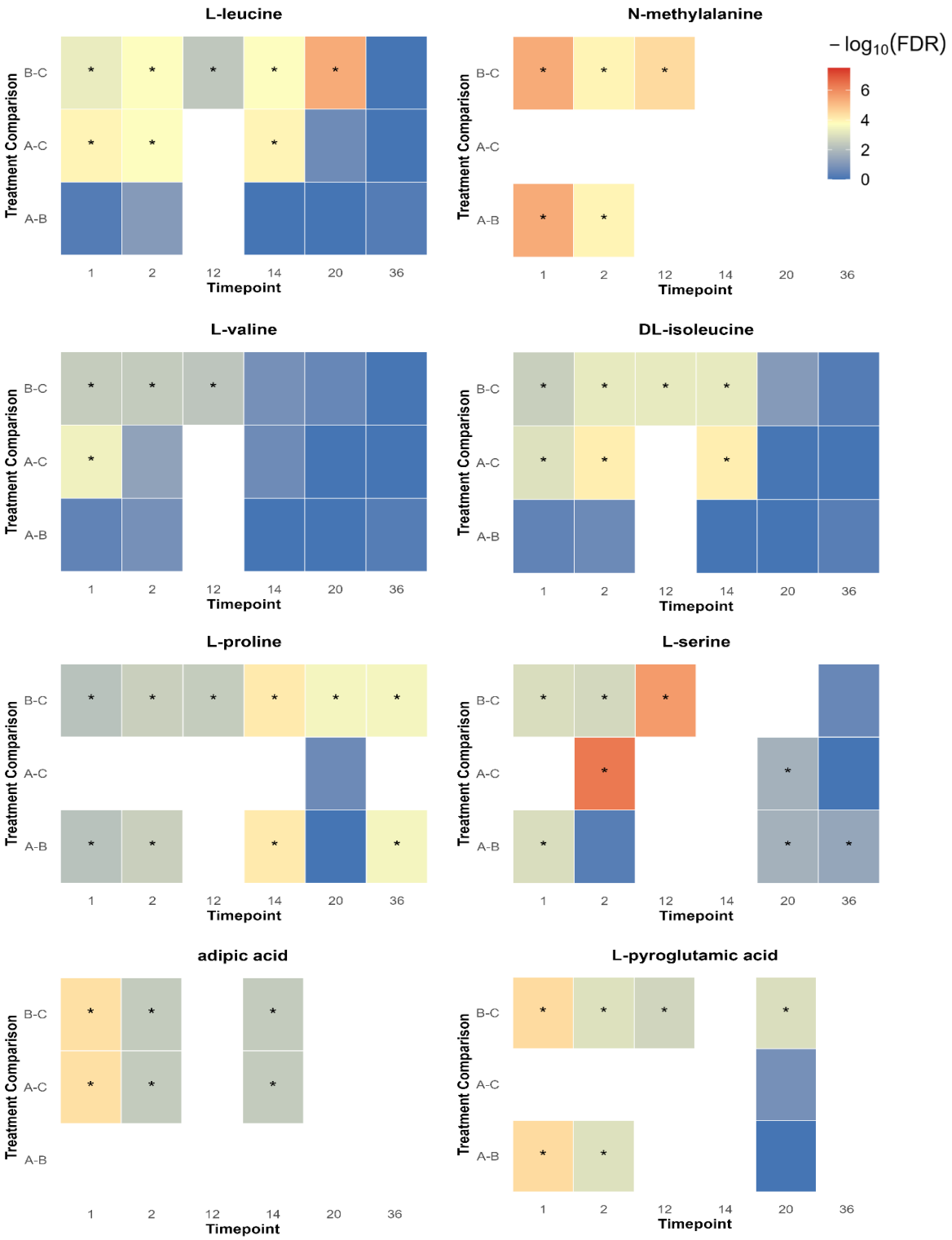

Figure 4.1. Games-Howell post-hoc pairwise tests for each metabolite between treatments (A: 5% *Daphnia* extract; B: 10% *Daphnia* extract; C: Control). Colour scale reflects -$\log_{10}$FDR; white cells indicate that the metabolite was absent in one or both treatments, except for pairs with A_12 h, which was not tested. Asterisks denote significance ($p < 0.05$).

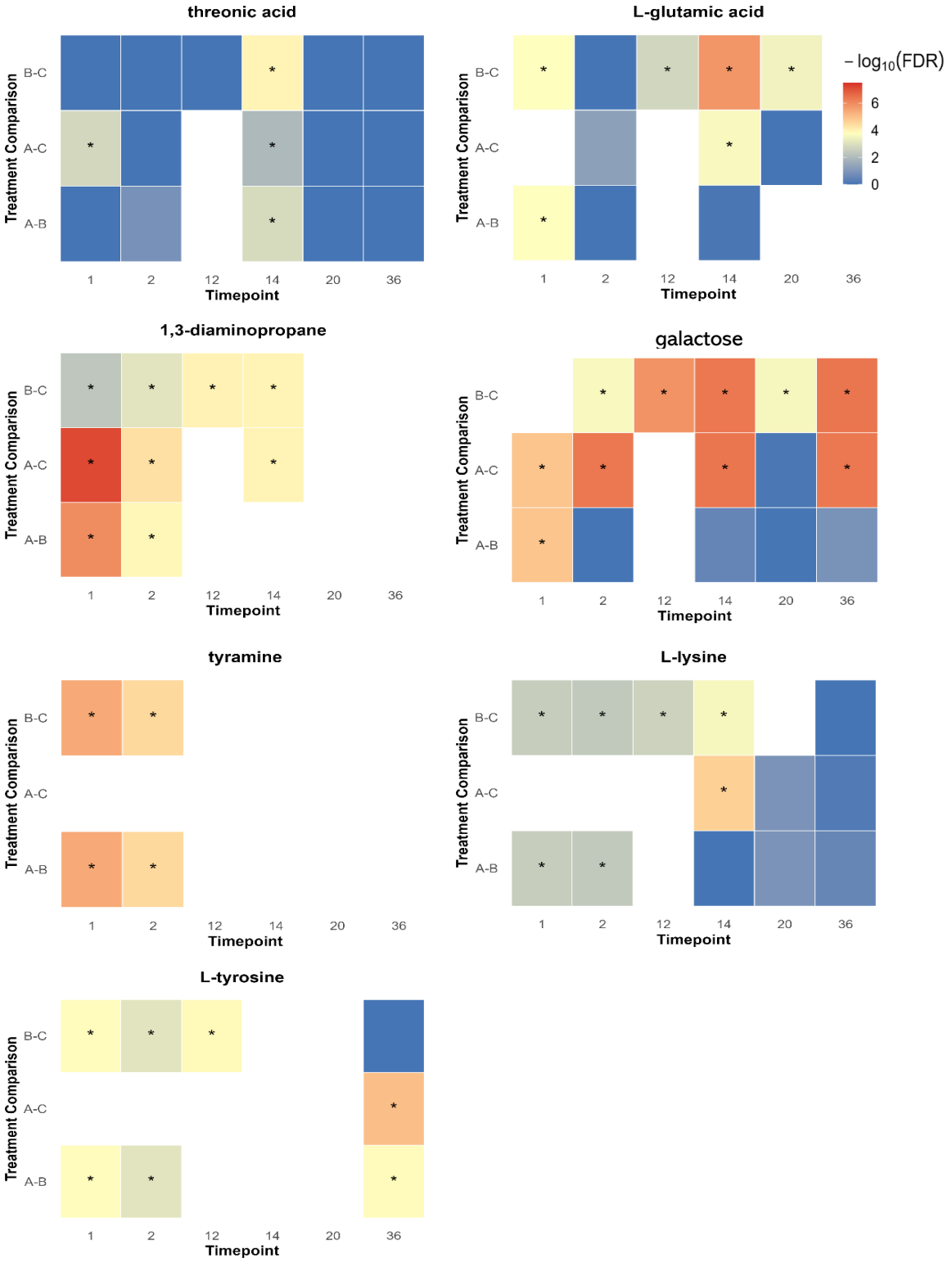

Figure 4.1. (*Continued*).

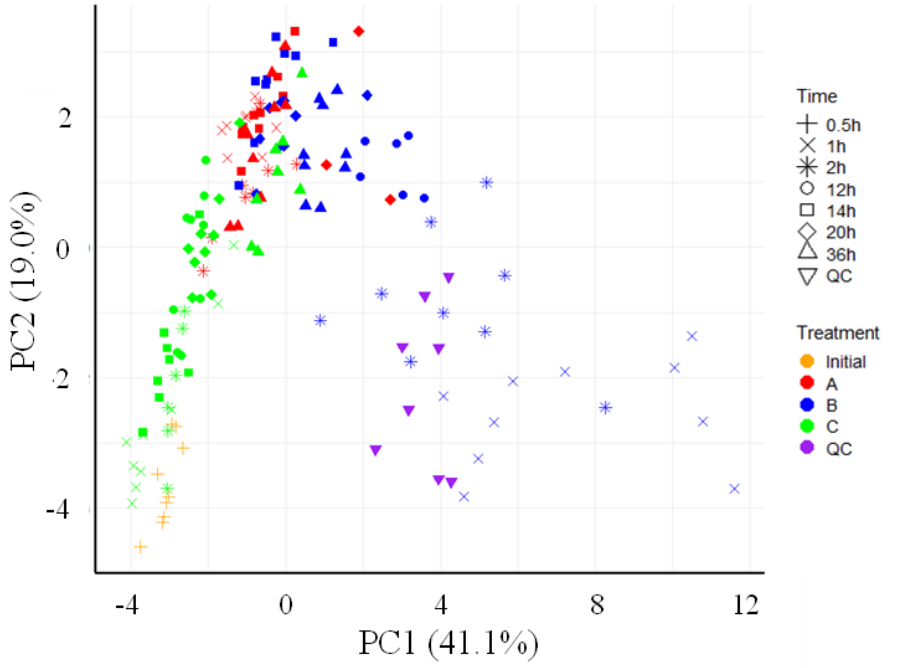

Figure 4.2. PCA of *C. reinhardtii* cube-root transformed metabolite data, showing PC1 vs PC2. Points represent individual samples, coloured by treatment (Initial: -0.5 h data, A: 5% *Daphnia* extract, B: 10% *Daphnia* extract, C: Control, QC: Quality controls).

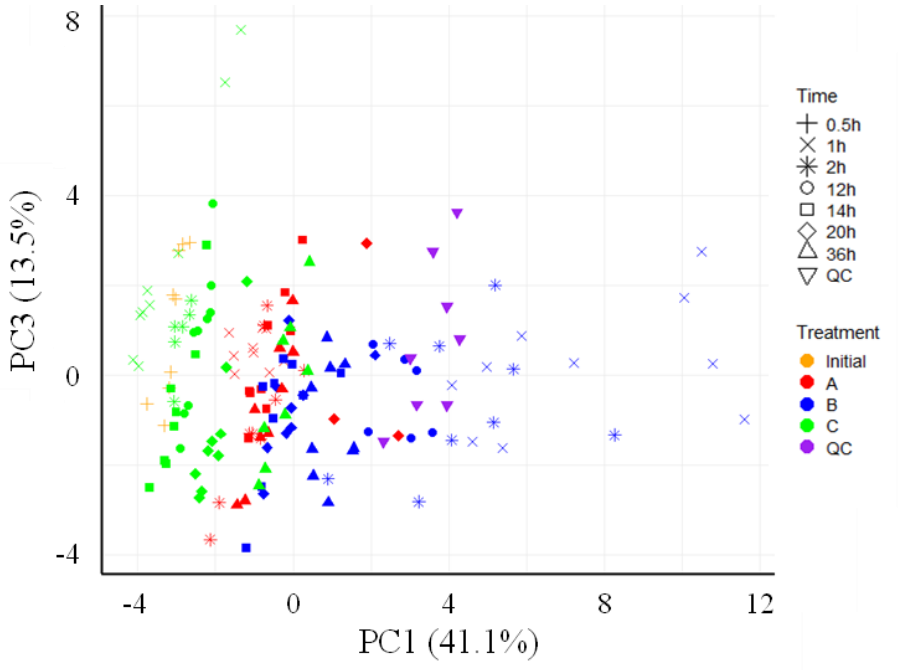

Figure 4.3. PCA of *C. reinhardtii* cube-root transformed metabolite data, showing PC1 vs PC3. Points represent individual samples, coloured by treatment (Initial: -0.5 h data, A: 5% *Daphnia* extract, B: 10% *Daphnia* extract, C: Control, QC: Quality controls).

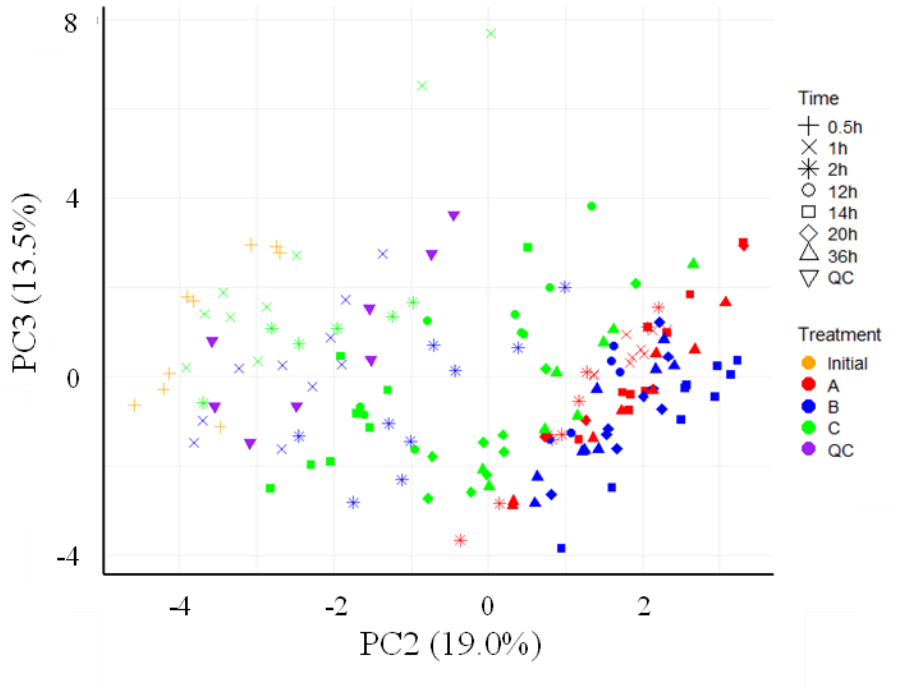

Figure 4.4. PCA of *C. reinhardtii* cube-root transformed metabolite data, showing PC2 vs PC3. Points represent individual samples, coloured by treatment (Initial: -0.5 h data, A: 5% *Daphnia* extract, B: 10% *Daphnia* extract, C: Control, QC: Quality controls).

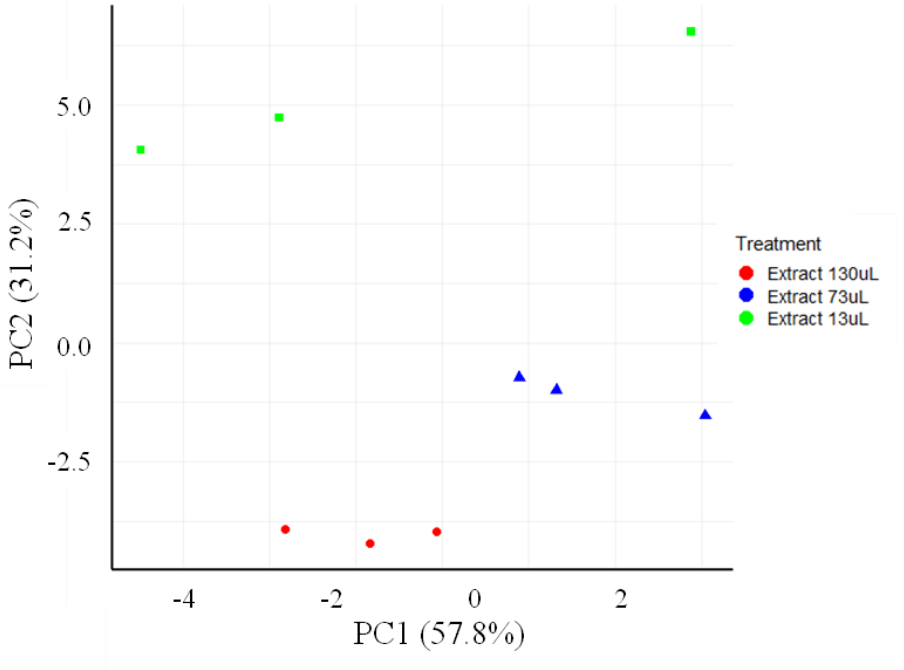

Figure 4.5. PCA of *Daphnia* extract cube-root transformed metabolite data, showing PC1 vs PC2. Points represent individual samples, coloured by sample volume (130 µL, 73 µL, 13 µL).

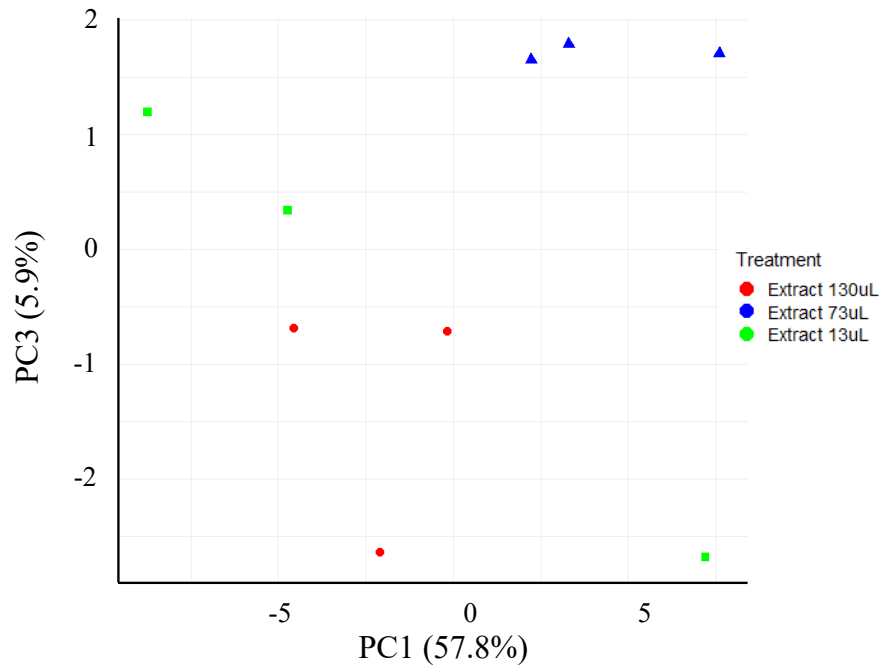

Figure 4.6. PCA of *Daphnia* extract cube-root transformed metabolite data, showing PC1 vs PC3. Points represent individual samples, coloured by sample volume (130 µL, 73 µL, 13 µL).

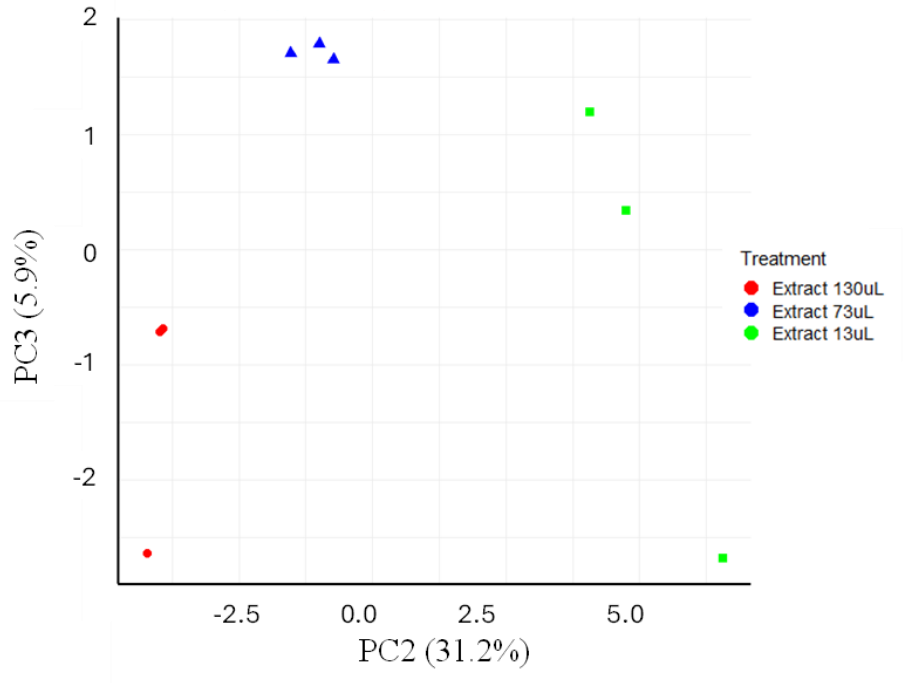

Figure 4.7. PCA of *Daphnia* extract cube-root transformed metabolite data, showing PC2 vs PC3. Points represent individual samples, coloured by sample volume (130 µL, 73 µL, 13 µL).

4.3.3.8 Fold change analysis – *C. reinhardtii*

The log_2-fold changes (log_2-FC) of metabolite abundances in *Daphnia* extract treatments relative to the control are shown in **Figure 4.8**. Most metabolites were either unique to the treatments or the control or exhibited a marked increase or decrease in abundance relative to the control group. Significantly different means between treatment and control are indicated by * in the fold-change heatmap. These should, however, be interpreted with caution and considered alongside the results of previous statistical analyses. The full fold-change analysis data is provided in **Supplementary Data File S2**.

All 22 metabolites were included in the fold-change analysis, regardless of statistical significance in earlier tests. For example, the abundances of alanine, ethanolamine, and putrescine were not significant in Games-Howell post-hoc tests between treatments and controls yet appeared significant in the fold-change analysis. This discrepancy arises because the fold-change analysis applies multiple-testing correction within each timepoint but does not account for overall group variance. Consequently, such differences in abundance may not be statistically robust. Similarly, capric acid and glyoxylic acid were not significant in either ANOVA.

4.3.3.9 Pathway and enrichment analysis – *C. reinhardtii*

The 18 metabolites that showed significant differences in relative abundance between treatments (Welch's ANOVA) were used in pathway and enrichment analyses in MetaboAnalyst. Only one enriched KEGG pathway, *valine, leucine and isoleucine biosynthesis*, was significant for both the adjusted *p*-value and the false discovery rate (FDR), likely reflecting the small number of metabolites available for analysis. Nevertheless, all enriched terms from the pathway and enrichment analyses are shown in **Figure 4.9** and **Table O.1**. Notably, alanine, aspartate and glutamate metabolism was also enriched among upregulated genes in the transcriptomics dataset (**Chapter 3**).

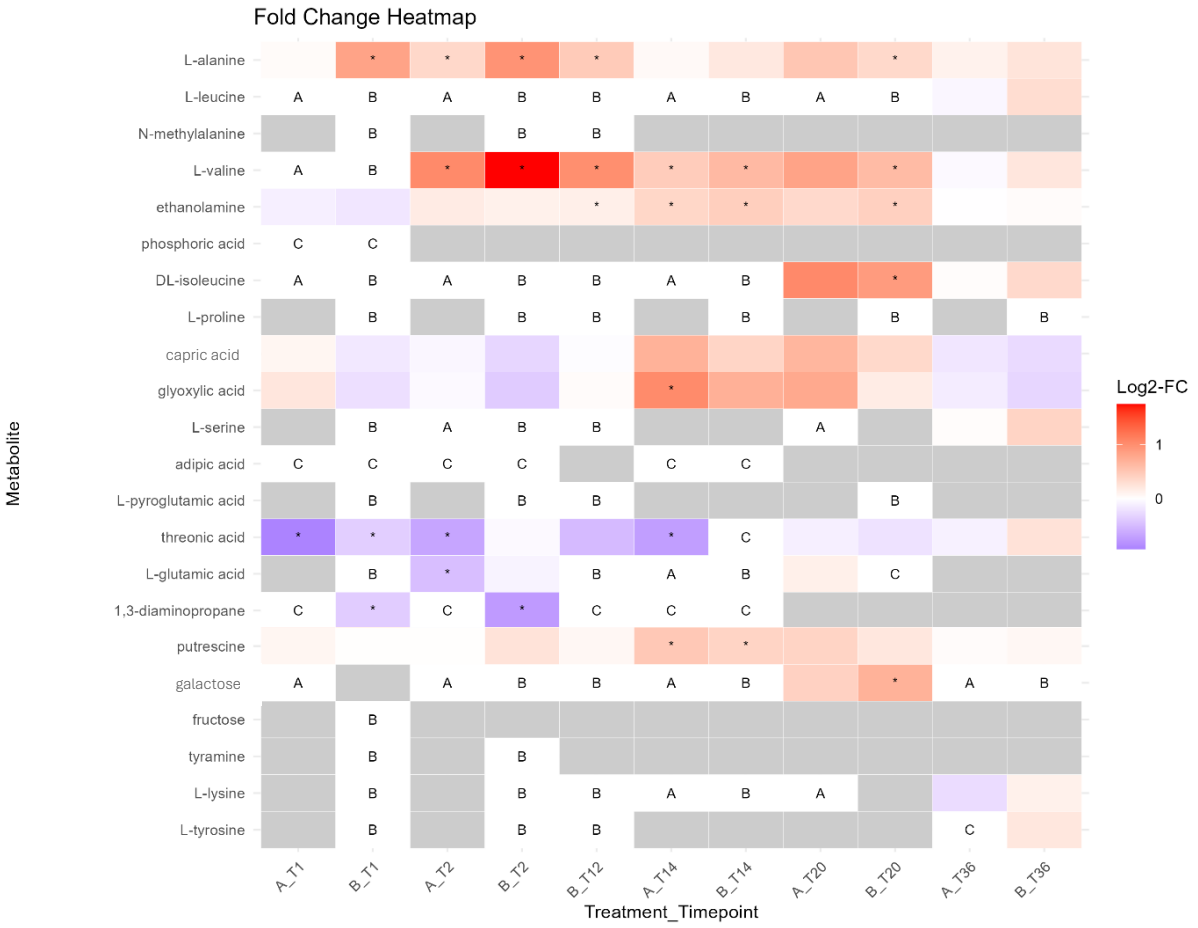

Figure 4.8. Heatmap of $\log_2$-fold change in metabolite abundance between *C. reinhardtii* 5% (A) and 10% (B) *Daphnia* extract treatments and the control (C) at each timepoint. Significant changes (p adj. < 0.05) are marked with *. White tiles containing a letter indicate that the metabolite is present only in the indicated treatment. Grey tiles indicate that the metabolite was absent from both groups. Note: some metabolites shown did not reach significance in the ANOVA model and/or Games-Howell post-hoc tests but are included here to illustrate overall trends.

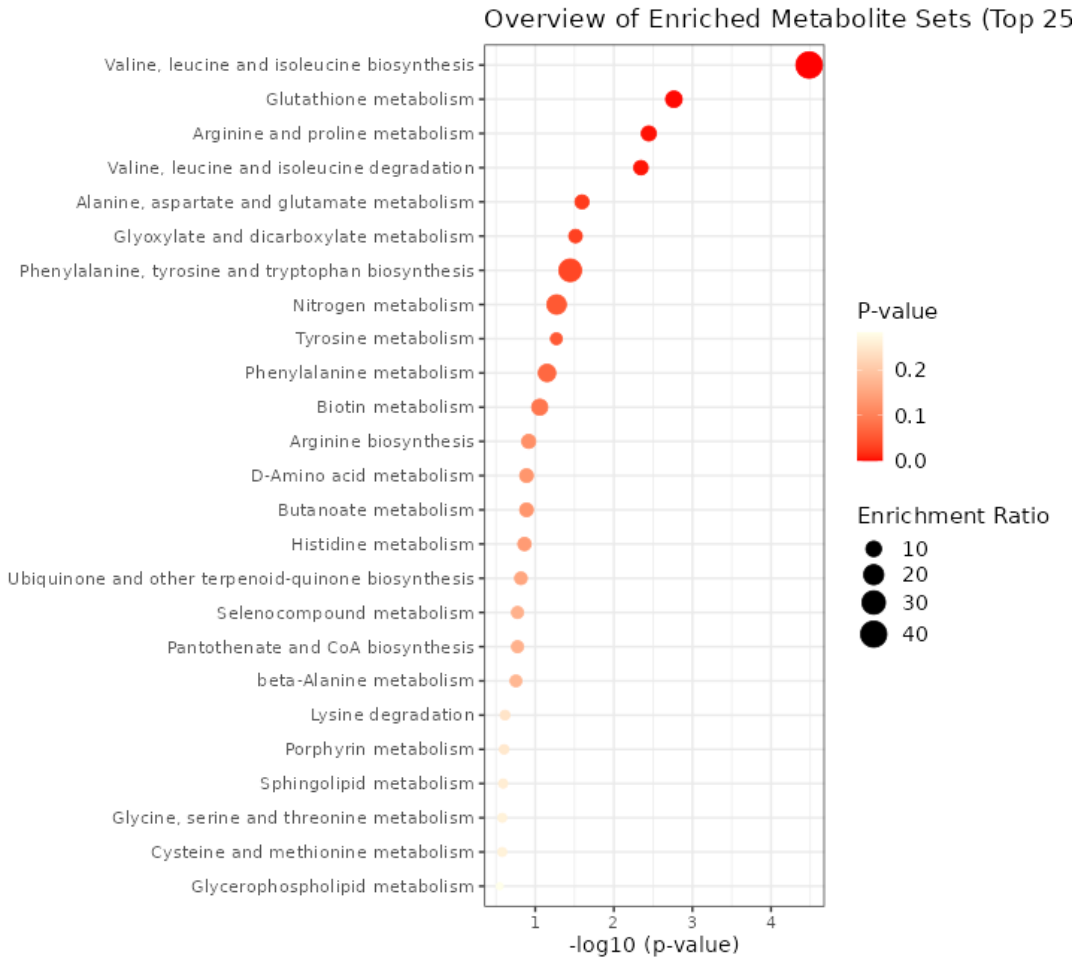

Figure 4.9. Overview of enriched metabolite sets identified in *C. reinhardtii* using MetaboAnalyst enrichment analysis. Analysis was performed on 18 metabolites showing significant differences in relative abundance between treatments (Welch's ANOVA). Enrichment was assessed using the hypergeometric test with the *C. reinhardtii* pathway library and KEGG human metabolic pathways as the reference set.

4.3.3.10 Origin of metabolites

Chlamydomonas or *Daphnia?*

All metabolites detected in *C. reinhardtii* cultures were also present in the *Daphnia* extract, making it difficult to determine whether they were algal products or originated from the extract itself. Metabolites could have been taken up by the algae or simply remained in the medium. Given the initial ratios of algal biomass to *Daphnia* extract volume (~2:1 mg:mL in 5% treatments; ~1:1 in 10%), only metabolites that were significantly more abundant in *C. reinhardtii* than in *Daphnia* extract, or higher in controls than treatments, can be confidently attributed to algal metabolism. In this dataset, only adipic acid met this criterion (though it was likely a contaminant; see below); all others were significantly more abundant in the *Daphnia* extract.

This finding means that under the current design, the metabolomic responses of *C. reinhardtii* during self-aggregation cannot be fully disentangled from metabolites originating from the *Daphnia* extract. While origins are yet unknown, the subsequent statistical analyses were nonetheless valuable for identifying relative differences between treatments, generating candidate infochemicals, and guiding future designs that isolate algal-specific metabolites.

Possible contaminants

An added complication is the detection of compounds unlikely to be true biological metabolites, suggesting possible contamination or derivatisation artefacts. A heatmap of raw peak areas for the 22 metabolites detected in *C. reinhardtii* was generated across all sample types, including blanks and standards (**Figure 4.10**), and several compounds showed similar peak intensities across nearly all samples, suggesting they may have originated from sample processing or consumables rather than as true metabolites. For example, phosphoric acid and adipic acid are seen in the blanks and standard mixes and are therefore likely contaminants or artefacts. Indeed, adipic acid can leach from plasticware, and phosphoric acid can be a derivatisation artefact from TMS or a possible contaminant from buffers or glassware. Capric acid and myristic acid were also detected across most samples and may have been carried over from the FAMEs standards.

These observations indicate that some of the detected metabolites likely reflect background contamination or derivatisation artefacts, rather than genuine biological products. Recognising

these signals is crucial to avoid misattributing contaminants as predator cues or algal metabolites.

4.3.3.11 Aggregation signalling molecules

Daphnia infochemicals

Having filtered out probable contaminants, the next step is to consider which metabolites detected here could plausibly act as *Daphnia*-derived infochemicals, as there is very little known about their identity. Based on metabolites detected in *Daphnia* extract, the following could be potential infochemical candidates:

- **Tyramine**, detected in *Daphnia* extract and some *C. reinhardtii* samples, has been reported to have an algicidal effect on some cyanobacteria and green algae (Yi et al., 2015), however, its effect on *C. reinhardtii* has not been studied, therefore, this could be a possible candidate infochemical. Tyramine is also a derivative of tyrosine.
- **Tyrosine** plays a role in signalling in *Chlamydomonas*. For example, tyrosine-phosphorylated proteins such as DYRKP have been found to regulate expression of matrix metalloproteinases (MMPs) for cell wall degradation (**Chapter 3**) (Haring et al., 1995; Kim et al., 2024). Therefore, as tyrosine was detected in *Daphnia* extract and some *C. reinhardtii* samples, it may also be a possible infochemical candidate.
- Other **amino acids**, such as lysine, serine, threonine, alanine, glutamic acid, proline, valine, methionine, isoleucine, and leucine, were all detected in the *Daphnia* extracts in this study. Many have been reported in both *Daphnia magna* and *C. reinhardtii* extracts (Jeong and Simpson, 2019; Liu et al., 2022). Although they may act as chemical cues, no direct evidence currently links them to grazer-microalgae signalling.
- **Urea** was detected in the *Daphnia* extract but absent from *C. reinhardtii*. As a nitrogenous waste product, urea is well known to be released by grazers and has been shown to induce colony formation in *Tetradesmus obliquus* (Wiltshire and Lampert, 1999).

Algal chemical signals

Microalgae employ chemical communication within their populations in response to environmental changes. Most studies to date have focused on chemical cues in the context of

sexual reproduction (Venuleo et al., 2017). However, many reports remain speculative, often lacking identification of the active compounds or their mechanisms of action (e.g., Amaral et al. (2023); Venuleo et al. (2017)).

There is evidence that microalgae release signals capable of inducing aggregation in non-stressed cells. For example, de Carpentier et al. (2022) characterised the secretome of aggregating *C. reinhardtii* mutants, which was able to trigger aggregation in other cells. However, this analysis did not differentiate between proteins directly involved in cell aggregation and those acting as extracellular cues for conspecifics.

By contrast, allelopathy, the production of compounds that affect the growth and survival of other species, has been much more extensively studied in microalgae. Allelochemicals typically include secondary metabolites such as aldehydes, glycolipids, fatty acids, phenolic compounds, alkaloids, oligopeptides and cyclic peptides, lactones, and amino acids (Bacellar Mendes and Vermelho, 2013).

The compounds identified in this study provide a basis for hypothesising intraspecific “alarm” signals in *C. reinhardtii*, as they include several classes with known signalling functions in plants and microorganisms. Their extracellular accumulation could warn the population of predator presence and promote defensive aggregation. Examples include:

- **Amino acids**: Although direct evidence for their role in intraspecific signalling is lacking, their activity as allelochemicals in interspecific interactions suggests they may also elicit responses in conspecifics.
- **Polyamines**: Compounds such as putrescine regulate growth, cell cycle progression, and resistance to stress in microalgae (Lavandosque and Vischi Winck, 2025), making them plausible modulators of aggregation or stress signalling.
- **Tyramine**: Reported to have algicidal effects (Yi et al., 2015). Given the species-specific nature of chemical signalling, tyramine could function as a stress signal within *C. reinhardtii*.
- **Fatty acids**: Decanoic and capric acid could act as extracellular messengers, consistent with the documented allelopathic roles of fatty acids and oxylipins in algae.

If these metabolites indeed originated from *C. reinhardtii*, they represent plausible candidates for intracellular stress signals with roles in aggregation. Testing these compounds in controlled bioassays will be necessary to confirm whether they possess aggregation-inducing activity. If

validated, such molecules could be harnessed as alternative biological flocculants for microalgal harvesting.

Figure 4.10. Heatmap of *C. reinhardtii* metabolite raw peak area. Metabolites showing similar abundances across samples may represent contaminants introduced during sample processing. Colour intensity reflects the relative raw peak area (white: low; purple: high).

4.4 Conclusions

This study applied untargeted GC-MS to profile metabolites in *Chlamydomonas reinhardtii* palmelloids formed in response to *Daphnia* infochemicals. TMS derivatisation of 1 mg dry weight samples provided adequate coverage, detecting hundreds of peaks, though only a fraction could be annotated using the Fiehn library. This limited annotation constrained mechanistic interpretation of self-aggregation.

A key finding was that all metabolites detected in *C. reinhardtii* cultures were also present in the *Daphnia* extract. As a result, no compound could be confidently attributed to algal metabolism as either a cause or consequence of palmelloid formation. This highlights a major challenge in predator-prey metabolomics: disentangling algal and grazer metabolites.

Future work should therefore prioritise experimental designs that separate algal and grazer metabolite production, or apply alternative aggregation triggers (e.g., light or temperature stress; see **Chapter 5**) that avoid introducing external metabolites. Improved metabolite coverage improved through expanded reference libraries and targeted approaches will also be critical for resolving the *C. reinhardtii* metabolome during palmelloid formation.

Despite these challenges, several metabolites identified here, including, tyramine, tyrosine, other amino acids, and urea, could be possible candidates for *Daphnia*-derived infochemicals, but these require targeted bioassays to confirm their role in triggering palmelloid formation. At the same time, several of the same compounds, including amino acids, polyamines, and fatty acids, are well-known signalling metabolites, raising the possibility that they also act as algal-derived intraspecific stress signals. Their accumulation during palmelloid formation could provide population-level cues that amplify aggregation responses.

If validated, such compounds could serve a dual purpose: enabling controlled induction of palmelloids for mechanistic studies and offering a biologically based, food-safe alternative to chemical flocculants for biomass harvesting.

References

Amaral, R., Duci, D., Cotta, F. C., Bacellar, F. L., Oliveira, S., Verret, F., Asadi, K., Vandamme, L. K. J., Reis, N. M., Bryant, L. D., Tosh, D., Mouget, J.-L., Perkins, R., & Rocha, P. R. F. (2023). Ion-driven communication and acclimation strategies in microalgae. *Chemical Engineering Journal*, *473*, 144985. https://doi.org/10.1016/j.cej.2023.144985

Apostolopoulou, N. G., Smeti, E., Lamorgese, M., Varkitzi, I., Whitfield, P., Regnault, C., & Spatharis, S. (2022). Microalgae show a range of responses to exometabolites of foreign species. *Algal Research*, *62*, 102627. https://doi.org/10.1016/j.algal.2021.102627

Bacellar Mendes, L. B., & Vermelho, A. B. (2013). Allelopathy as a potential strategy to improve microalgae cultivation. *Biotechnology for Biofuels*, *6*, 152. https://doi.org/10.1186/1754-6834-6-152

Beale, D., Pinu, F., Kouremenos, K., Poojary, M., Narayana, V., Boughton, B., Kanojia, K., Dayalan, S., Jones, O., & Dias, D. (2018). Review of recent developments in GC–MS approaches to metabolomics-based research. *Metabolomics*, *14*. https://doi.org/10.1007/s11306-018-1449-2

Chen, Y., Li, E. M., & Xu, L. Y. (2022). Guide to metabolomics analysis: A bioinformatics workflow. *Metabolites*, *12*. https://doi.org/10.3390/metabo12040357

de Carpentier, F., Maes, A., Marchand, C. H., Chung, C., Durand, C., Crozet, P., Lemaire, S. D., & Danon, A. (2022). How abiotic stress-induced socialization leads to the formation of massive aggregates in *Chlamydomonas*. *Plant Physiology*, *190*, 1927-1940. https://doi.org/10.1093/plphys/kiac321

Delacre, M., Leys, C., Mora, Y. L., & Lakens, D. (2019). Taking parametric assumptions seriously: Arguments for the use of Welch's F-test instead of the classical F-test in one-way ANOVA. *International Review of Social Psychology*.

Haring, M. A., Siderius, M., Jonak, C., Hirt, H., Walton, K. M., & Musgrave, A. (1995). Tyrosine phosphatase signalling in a lower plant: cell-cycle and oxidative stress-regulated expression of the *Chlamydomonas eugametos* VH-PTP13 gene. *Plant J*, *7*, 981-988. https://doi.org/10.1046/j.1365-313x.1995.07060981.x

Jeong, T.-Y., & Simpson, M. J. (2019). *Daphnia magna* metabolic profiling as a promising water quality parameter for the biological early warning system. *Water Research*, *166*, 115033. https://doi.org/10.1016/j.watres.2019.115033

Kim, M., Jorge, G. L., Aschern, M., Cuiné, S., Bertrand, M., Mekhalfi, M., Putaux, J.-L., Yang, J.-S., Thelen, J. J., Beisson, F., Peltier, G., & Li-Beisson, Y. (2024). The DYRKP1 kinase regulates cell wall degradation in *Chlamydomonas* by inducing matrix metalloproteinase expression. *The Plant Cell*, *36*, 4988-5003. https://doi.org/10.1093/plcell/koae271

Lavandosque, L. L., & Vischi Winck, F. (2025). Polyamine-mediated growth regulation in microalgae: integrating redox balance and amino acids pathway into metabolic engineering. *SynBio*, *3*, 8. https://doi.org/10.3390/synbio3020008

Lee, D. Y., & Fiehn, O. (2008). High quality metabolomic data for *Chlamydomonas reinhardtii*. *Plant Methods*, *4*, 7. https://doi.org/10.1186/1746-4811-4-7

Lee, S., & Lee, D. K. (2018). What is the proper way to apply the multiple comparison test? *Korean J Anesthesiol*, *71*, 353-360. https://doi.org/10.4097/kja.d.18.00242

Liu, W., Li, M., Li, W., Keller, A. A., & Slaveykova, V. I. (2022). Metabolic alterations in alga *Chlamydomonas reinhardtii* exposed to nTiO2 materials. *Environmental Science: Nano*, *9*, 2922-2938. https://doi.org/10.1039/D2EN00260D

Smart, K. F., Aggio, R. B., Van Houtte, J. R., & Villas-Bôas, S. G. (2010). Analytical platform for metabolome analysis of microbial cells using methyl chloroformate derivatization followed by gas chromatography-mass spectrometry. *Nat Protoc*, *5*, 1709-1729. https://doi.org/10.1038/nprot.2010.108

Venuleo, M., Raven, J. A., & Giordano, M. (2017). Intraspecific chemical communication in microalgae. *215*, 516-530. https://doi.org/10.1111/nph.14524

Wei, R., Wang, J., Su, M., Jia, E., Chen, S., Chen, T., & Ni, Y. (2018). Missing value imputation approach for mass spectrometry-based metabolomics data. *Scientific Reports*, *8*, 663. https://doi.org/10.1038/s41598-017-19120-0

Wiltshire, K. H., & Lampert, W. (1999). Urea excretion by *Daphnia*: A colony-inducing factor in *Scenedesmus*? *Limnology and Oceanography*, *44*, 1894-1903. https://doi.org/10.4319/lo.1999.44.8.1894

Yi, Y.-L., Yu, X.-B., Zhang, C., & Wang, G.-X. (2015). Growth inhibition and microcystin degradation effects of *Acinetobacter guillouiae* A2 on *Microcystis aeruginosa*. *Research in Microbiology*, *166*, 93-101. https://doi.org/10.1016/j.resmic.2014.12.013

Zarate, E., Boyle, V., Rupprecht, U., Green, S., Villas-Boas, S. G., Baker, P., & Pinu, F. R. (2016). Fully automated trimethylsilyl (TMS) derivatisation protocol for metabolite profiling by GC-MS. *Metabolites*, *7*. https://doi.org/10.3390/metabo7010001

Zhang, X., Zhang, Y., Chen, Z., Gu, P., Li, X., & Wang, G. (2023). Exploring cell aggregation as a defense strategy against perchlorate stress in *Chlamydomonas reinhardtii* through multi-omics analysis. *Science of The Total Environment*, *905*, 167045. https://doi.org/10.1016/j.scitotenv.2023.167045

Chapter 5.

From defence to design: Harnessing self-aggregation for harvesting of microalgae

---

Preface

This chapter places the insights from **Chapters 2**–**4** into a biotechnological context. The objective was to evaluate how predator-induced self-aggregation could be applied as a scalable harvesting strategy, with emphasis on the culture conditions, aggregation stability, and process dynamics that determine feasibility. **Chapter 5** linked ecological responses to the practical integration of self-aggregation into a harvesting workflow, highlighting the potential to develop a cleaner and more sustainable strategy compared to flocculation.

Abstract

The high cost of biomass recovery remains a major barrier to large-scale microalgal production. Conventional flocculation typically uses aluminium or ferric salts or synthetic polymers, which risk contaminating biomass and effluent. Self-aggregation could offer a sustainable alternative by exploiting natural self-aggregation, as *Daphnia* infochemicals can induce aggregation at significantly lower concentrations than conventional flocculants. This chapter investigated palmelloid formation in *Chlamydomonas reinhardtii* triggered by *Daphnia*-derived infochemicals, in the context of biomass harvesting.

The aggregation dynamics were strongly strain- and environment-dependent. The aggregate size and rate of formation varied with cell density, while wild-type CC-1690 and mutant background strain CC-5325 showed distinct light thresholds for palmelloid formation. Reported *Daphnia* infochemical sodium octyl sulphate failed to induce palmelloids in *C. reinhardtii*, indicating trigger specificity between algal species. These results highlighted the importance of screening multiple strains and identifying reliable infochemicals. Synthetic infochemicals with broad activity could be the most practical option for cost-effective and scalable harvesting.

Based on these results, a design framework was proposed: candidate strains and chemical triggers should first be screened for reliable aggregation; cultures could then be diverted to induction tanks where synthetic infochemicals are added under controlled light and temperature conditions; biomass is subsequently recovered using thickening and dewatering methods compatible with aggregate morphology.

This is the first study to evaluate predator-induced palmelloid formation in *C. reinhardtii* for industrial harvesting. By linking self-aggregation with established technologies, this provides a promising alternative to chemical flocculation, with the potential to reduce costs, eliminate harmful residues, and lower the environmental footprint of algal biomass recovery.

5.1 Introduction

Harvesting microalgae remains one of the largest barriers to making algal biotechnology sustainable and cost competitive. While cultivation at scale is feasible, recovering biomass from dilute cultures is expensive, energy-intensive, and often detrimental to product quality. Overcoming this step is essential to unlock the commercial potential of microalgae for food, feed, and biofuel industries.

In large-scale production, biomass concentrations typically reach only 0.5–0.75 g L^{-1} (dry weight) in open ponds and up to 2 g L^{-1} in closed photobioreactors, meaning that very large volumes must be processed relative to the recovered biomass (Davis et al., 2011; Fasaei et al., 2018). Harvesting is therefore carried out in multiple stages: pre-concentration (~0.5% total solids, TS), thickening (2–7% TS), dewatering (10–25% TS), and drying (90–95% TS) or further processing such as extraction (Muir et al., 2025). Pre-concentration and thickening are particularly important, as these steps reduce the volume for subsequent dewatering and drying, thereby lowering overall energy demand, cost, and carbon footprint.

Conventional harvesting methods face significant challenges: the small size and low density of cells, presence of negatively charged surface groups, and motility of some species (e.g., *Chlamydomonas*) leads to very slow natural settling or filtration, making biomass concentration technically challenging and energy intensive. Sedimentation is the simplest and most cost-effective thickening method; however, it is slow, can cause biomass degradation, and has poor recovery efficiency (Muir et al., 2025). Flocculation is therefore often required to accelerate settling, yet this typically relies on aluminium, ferric salts, or synthetic polymers, which are costly and risk contaminating biomass and effluent (Muir et al., 2025; Wei et al., 2025). Filtration efficiency is limited by membrane fouling and low flux when small pores are required to retain algal cells (Hashmi et al., 2025; Xiao et al., 2019). Centrifugation provides fast separation and a high recovery efficiency at a very high energy cost (Muir et al., 2025). In all cases, the trade-off lies between cost, recovery efficiency, biomass quality, and environmental burden of treatment for water recycling and discharge.

Mimicking natural biological cues to trigger self-aggregation could be a sustainable alternative to conventional flocculation. Predator-derived infochemicals can induce colony formation or aggregation via cell adhesion. *C. reinhardtii* formed palmelloid colonies in response to *Daphnia* infochemicals, with transcriptomic evidence suggesting delayed flagella regeneration

(**Chapters 2** and **3**). Such structures settle more rapidly than single cells (Wei et al., 2025) and could improve sedimentation, filtration, and even centrifugation without contaminating the biomass or effluent. Self-aggregation could therefore act as a form of "biological flocculation," reducing both the energy demand and chemical burden of harvesting.

This chapter discusses how self-aggregation triggered by predator-derived infochemicals can be optimised and integrated into conventional harvesting processes, by addressing microalgal traits, trigger strategies, environmental influences, and operational parameters that determine its scalability and sustainability.

5.2 Microalgal phenotypes

To make self-aggregation viable as a harvesting strategy, the formation of aggregates must genuinely aid thickening and dewatering of biomass relative to single cells. This requires designing the process around strain-specific traits to ensure compatibility with subsequent sedimentation, filtration, or centrifugation stages. Both the dynamics of colonies and aggregates in culture, and the culture as a whole, are therefore critical considerations.

5.2.1 Morphology

Self-aggregation responses vary widely between microalgal species (see **Chapter 2**). Key morphological traits (i.e., size, shape, density, motility, and extracellular polymer production) would influence how well aggregates perform in sedimentation, filtration, and centrifugation. These traits should therefore guide the selection of strains for harvesting applications.

5.2.1.1 Colonies

Colonies form when daughter cells remain together after cell division, as in *Scenedesmus* (coenobia) and *Chlamydomonas* (palmelloids). By increasing particle size, the formation of large colonies generally improves settleability under gravity and centrifugal force. While colonies typically retain a net negative surface charge, their surface-to-volume ratio is lower meaning gravitational forces dominate more strongly over electrostatic repulsion.

However, some colony traits can reduce settling. For example, *Chlamydomonas* palmelloids are non-motile, but colonies of *Gonium* possess flagella on all cells that beat in unison, making them motile and resistant to sedimentation or centrifugation (Herron and Nedelcu, 2015). Similarly, *Scenedesmus* colonies may bear spines that deter grazers but can increase buoyancy, slowing settling (Conway and Trainor, 1972).

Colonies may be well-suited to filtration because of their larger particle size. Microfiltration membranes (≤ 1-2 µm pores) typically achieve fluxes < 150 L m^{-2} h^{-1} due to small pores and fouling (Xiao et al., 2019). In contrast, macrofiltration membranes (5 µm pores) achieved fluxes up to 770 L m^{-2} h^{-1} with *S. acuminatus* (Xiao et al., 2019). Colonial cultures have larger particles and could therefore be filtered with larger pore sizes, achieving greater flux. Features

such as spines or flagella may further increase effective particle size but could also promote cake layer build-up and reduce flux. Colonies may also shear during filtration, releasing smaller cells that pass through pores, however, palmelloids may be more resistant to shearing than loosely adhered aggregates due to their rigid cell wall. Optimising pore size, backwashing, and operational mode is therefore essential.

Case example – *C. reinhardtii* palmelloids

Cultures treated with *Daphnia* extract (see **Chapter 3**) formed palmelloids much larger than unicells (**Figure 5.1**), improving potential for sedimentation, filtration, and centrifugation. The cell and colony size distributions, measured using ImageJ, of untreated cultures and those treated with *Daphnia* extract, are shown in **Figure 5.1**. The individual cells inside colonies were not significantly different in size to single cells, so the volume increased exponentially with each doubling of cell number inside a palmelloid. For example, while single cells were up to 12 μm in diameter and 630 μm^3 in volume, 32–celled palmelloids reached 46 μm diameter and 51,000 μm^3 (**Table 5.1**) The resulting colonies were large and non-motile, making them more amenable to sedimentation and centrifugation, and potentially suitable for coarser filtration (**Table 5.1**)

5.2.1.2 Aggregates

Some species aggregate though adhesion mediated by extracellular polymers (EPS) rather than colony formation (**Chapter 1**). *Chlorella vulgaris*, for example, does not form colonies but instead forms large aggregates through adhesion (**Chapter 2**) (Aljuboori et al., 2016). Such aggregates can improve harvesting by increasing particle size. EPS can also neutralise surface charges, reducing electrostatic repulsion.

Like colonies, settleability and filterability, are dependent on aggregate morphology. If EPS-rich aggregates are highly irregular or porous, they may have low density and high drag, which could counteract the benefits of increased size. EPS also promotes severe membrane fouling (Muir et al., 2025). Dense, compact aggregates would therefore be more suitable for sedimentation, filtration, and centrifugation, than loose, EPS-heavy flocs. During chemical flocculation, the shear rate influences floc characteristics which in turn influence the settling velocity and concentration factor (Zhang et al., 2019); similar effects are likely to be seen in

EPS-mediated aggregation, therefore, the mixing dynamics in the aggregation tank will require optimisation.

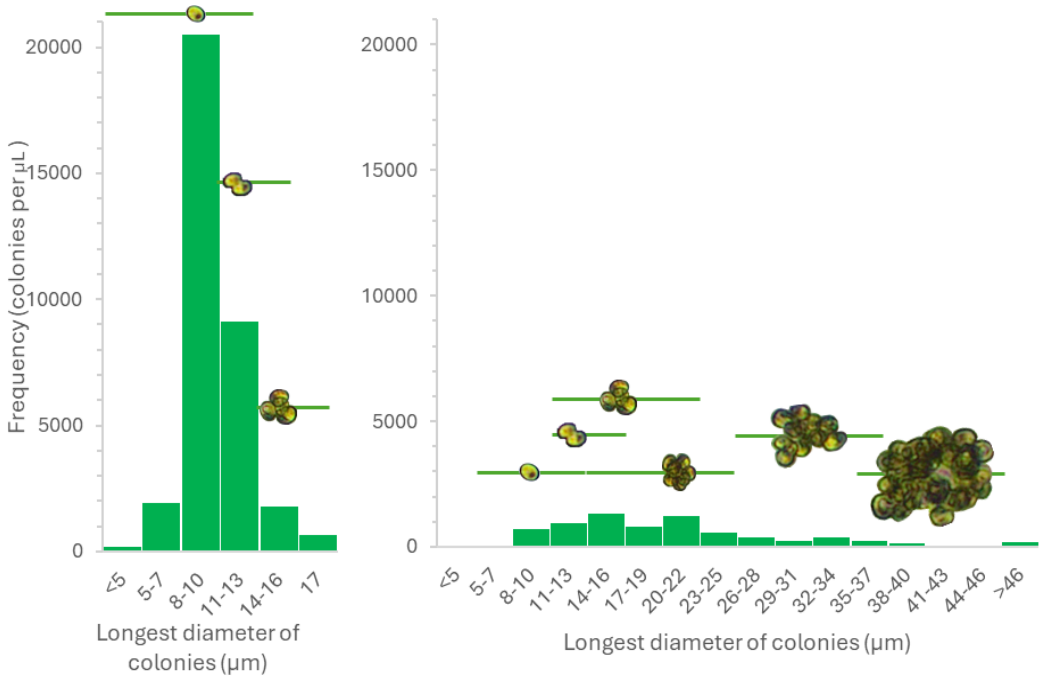

Figure 5.1. Diameter (µm) and abundance of *C. reinhardtii* single cells and colonies in the untreated control and culture treated with *Daphnia* extract (10% v/v). Photographs of colonies were captured using microscopy at 10× magnification. Horizontal lines indicate the diameter ranges for unicellular and paired cells and palmelloids, and images are positioned at the mean diameter for their respective categories.

5.2.2 Culture-wide response

Aggregation responses vary not only between species but also between strains, making strain selection critical for harvesting applications. Variation in culture-wide behaviour was evident even in untreated mutants (

Figure 5.2), affected in candidate self-aggregation genes (see **Chapter 3**). One strain contained a mixture of aggregates and single cells, whereas another formed exclusively palmelloids that did not adhere together. In CC-1690, cells formed palmelloids in that also adhered together to form large clusters. Even closely related strains can diverge: *C. reinhardtii* wild-type CC-1690 and background strain CC-5325 (CC-4533) are often compared due to their phenotypic

similarity, yet they showed markedly different light-dependent aggregation responses to *Daphnia* infochemicals (see **Section 5.4.1**).

For harvesting, it is critical that aggregation involves nearly all cells in culture. Partial aggregation, where large aggregates coexist with free cells, reduces settling and filtration efficiency and complicates downstream processing. This behaviour was observed in *C. vulgaris* (see **Chapter 2**). By contrast, colony formation tends to produce a more uniform response. For example, in *C. reinhardtii* wild-type CC-1690, up to ~90% of cells formed palmelloids in response to *Daphnia* infochemicals, and palmelloids also adhered together to form large clusters (**Chapter 2**).

Table 5.1. Measured dimensions and estimated volumes of *C. reinhardtii* cells and palmelloids in the untreated control and culture treated with *Daphnia* extract (10% v/v), with predicted implications for settling (sedimentation or centrifugation) and filtration efficiency.

Morphology /Treatment	**Cell diameter (µm)**	**Estimated volume (µm^3)**	**Motility**	**Predicted settling impact**	**Predicted filtration impact**
Single cells	5 × 6 to 10 × 12	78–630	Motile	Low settling due to small size and active swimming	Suitable only for microfiltration (≤ 10 µm); low flux
Paired cells	11–14	700–1,440	Non-motile	Similar to single cells	Similar to single cells
4-celled palmelloids	11–22 (colony)	700–5575	Non-motile	Higher settling velocity	Suitable for macrofiltration
8-celled palmelloids	15–25 (colony)	1,770–8,180	Non-motile	Significantly higher settling velocity	Suitable for macrofiltration; higher flux
16-celled palmelloids	26–36 (colony)	9,205–24,430	Non-motile	Much faster settling	Ideal for macrofiltration; reduced membrane fouling risk
32-celled palmelloids	36–46 (colony)	24,430–50,965	Non-motile	Very rapid settling	Optimal for coarse filtration

5.2.3 Culture manipulation

Beyond strain selection, mixed- or monocultures can be manipulated over time to select for effective aggregation phenotypes.

5.2.3.1 Prolonged stress to drive constitutive aggregation

For example, prolonged exposure to predator cues can induce persistent multicellularity: in a previous study, Herron et al. (2019) cultured five *C. reinhardtii* strains with *Paramecium tetraurelia* for 50 weekly transfers, after which two strains had evolved multicellularity, forming clusters that persisted without predation. This highlights both the diversity of strain-specific behaviours and the potential for long-term predator exposure to produce stable colonial cultures, though reversions to unicellularity remain possible.

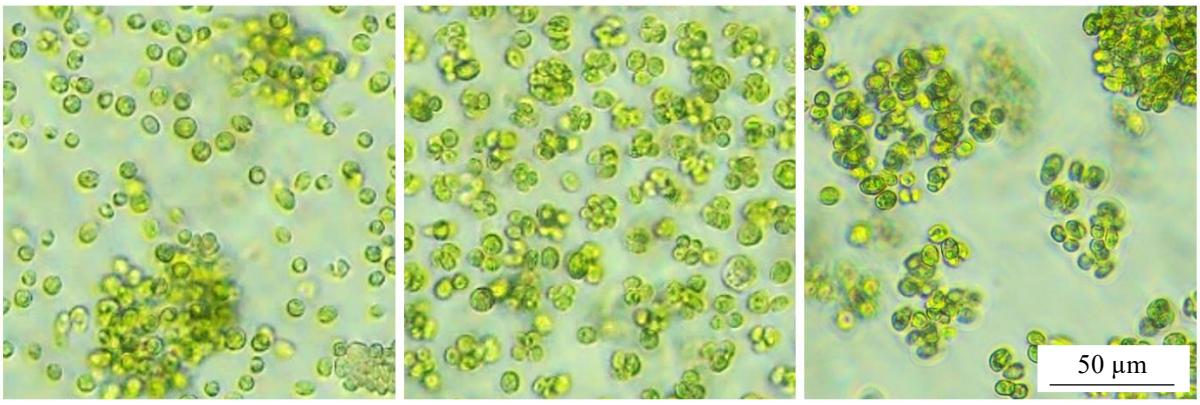

FAP199 mutant MMP13 mutant CC-1690 wildtype

Figure 5.2. Example of aggregation completeness in *C. reinhardtii* cultures: Left: FAP199 mutant with large aggregates and a substantial proportion of planktonic cells; Middle: MMP13 mutant with most biomass in palmelloids; Right: CC-1690 wild-type, with most biomass in palmelloid colonies that adhere together. Cultures were photographed at 20× magnification.

5.2.3.2 Recycling algal stress cues

The recycling of medium from aggregated cultures could be integrated to reuse both the added chemical cues and the algal aggregation cues. Previous studies have reported that the medium of cultures aggregated through non-chemical cues was capable of inducing aggregation in non-stressed cells, suggesting that algae release stress-cues capable of inducing aggregation (de Carpentier et al., 2022). Reuse of medium could also lead to constitutively colonial cultures (see above) or reduce the required dose of chemical cues for aggregation.

5.2.3.3 Recycling algal biomass

Similarly, regular recycling of settled algae biomass back into the culture system can increase the settleability over time. This was demonstrated in a previous study by Park et al. (2011), where recycling harvesting algae back to the HRAP increased the dominance of a readily settleable species and increasing the average colony size. These authors proposed that the increase in average colony size was due to an increase in the mean residence time resulting from algal recycling. However, in a self-aggregation context, recycling the settled biomass represents artificial selection of colonies with a higher settleability compared to planktonic cells remaining in the medium, leading to dominance of constitutive colonies and cells that are more responsive to aggregation cues. This would work in much the same way that filtration can lead to dominance of shorter *Spirulina* trichomes over time (Kurpan et al., 2024), an example which also highlights that recycling culture medium containing unicells could also lead to dominance of non-aggregating cells or simply smaller colonies. Therefore, recycling algal biomass after aggregation could be beneficial to not only increase the aggregation efficiency but also to prevent dominance of non-aggregating cells.

5.2.4 Genetic engineering

Alternatively, strains predisposed to remain in palmelloid form can be engineered. For instance, *C. reinhardtii* mutants with flagella defects often remain colonial (Brown et al., 2015; Hou et al., 2007; Lechtreck et al., 2009). Transcriptomic analysis in **Chapter 3** confirmed downregulation of flagella-related genes in palmelloids, suggesting impaired flagella

regeneration underpins colony persistence. Such strains could reduce or eliminate the need to trigger aggregation at every harvest (see **Section 5.5**).

5.2.5 Summary

Further work screening diverse strains, characterising specific phenotypes, and exploring responses to predator cues will be key to identifying cultures that aggregate rapidly, completely, and stably. The mode of aggregation (i.e., colony formation or adhesion via EPS) and size distribution throughout a culture influence the settleability and filterability, thus determining suitable harvesting methods. The production of algal allelochemicals or EPS can influence the suitability for mixed-species cultures or reuse of culture medium. The development of strains with reliable self-aggregation traits, through culture manipulation or genetic engineering, could lower dependence on added flocculants/infochemicals, reduce energy inputs during dewatering, and contribute to more sustainable and economically viable algal production systems.

5.3 Trigger selection

The induction of self-aggregation for harvesting requires a reliable trigger that can be applied at scale, induce a rapid response, and is economically viable. Previous work (**Chapter 2**) demonstrated that while some predator cues induce aggregation across multiple algal species, others do not. Developing a broadly effective trigger would improve economic feasibility, but in practice, strain-specific responses must be considered.

For sustainability, predator- or infochemical-based triggers must also be cost-competitive with conventional flocculants, introduce no harmful residues, require minimal water treatment for recycling or discharge, and be compatible with downstream biomass processing. Several approaches have been explored at laboratory scale (**Chapter 2**), including direct use of live grazers, predator culture filtrates, extracted infochemicals, and synthetic cues. Each of these approaches presents unique biological, technical, and economic challenges.

5.3.1 Live grazer co-culture

Live grazers, such as *Daphnia*, *Brachionus*, *Ochromonas* and *Peranema* can induce self-aggregation in microalgae (**Chapter 1**). Theoretically, direct grazer addition could serve as an on-demand induction step. While cost estimates are limited for *Daphnia*, production of *Brachionus calyciflorus* was reported at USD $0.23 per million rotifers per day (Rojo and Ibarra, 2017). At effective doses of 300–1000 rotifers L^{-1}, this corresponds to $0.069–0.23 per m^3 of algal culture (Lorusso, 2018; Lurling and Beekman, 2006; Yang et al., 2006), a cost comparable to commercial flocculants ($0.01–0.4 m^{-3}; see **Chapter 1**).

However, practical challenges are substantial. Some grazers exhibit rapid mortality in algal cultures (as shown for *Daphnia* in **Chapter 2**), limiting exposure time and making aggregation inconsistent. Co-cultivation could extend infochemical exposure but requires balancing different nutritional needs, increases risk of culture crashes, and introduces potential for overgrazing. Predator residues in the harvested biomass may also be undesirable. Finally, grazer-induced aggregation is inherently less reproducible than controlled chemical dosing, with cultures not aggregating every time, and forming aggregates of varying sizes due to the influence of bacteria or other contaminants (**Chapter 1**).

5.3.2 Predator culture filtrate

Filtrates from predator cultures can induce aggregation, sometimes more rapidly than live grazers themselves (Sathe and Durand, 2015). However, the economics and logistics may be problematic. For instance, filtrate from *Peranema trichophorum* costs ~USD \$1 L^{-1} and is effective at 10 L per m^3 of algal culture (Sathe and Durand, 2015), making it 10–100× more expensive than common flocculants (\$0.01–0.4 m^{-3}, see **Chapter 1**). Operationally, maintaining dense predator cultures is resource-intensive and prone to variability. Culture crashes, contamination, and disease reduce reliability and alter infochemical profiles. These difficulties mean that filtrates would require concentration and standardisation to avoid large variation in the self-aggregation efficiency. Media formulation also matters; specialised formulations like COMBO can boost grazer productivity (Sreevidya et al., 2025), but introduce additional chemicals into algal cultures, potentially affecting aggregation dynamics or leaving unwanted residues.

5.3.3 Extracted infochemicals

A more controlled approach is to extract the active infochemicals from grazers. **Chapters 2** and **3** showed that extracts from *Daphnia* can rapidly and effectively trigger palmelloid formation in *C. reinhardtii*. Infochemicals from dried *Daphnia* were extracted with a solvent of methanol, chloroform, and water (5:2:2, v:v:v), and evaporated and resuspended in water; this extract used 250 g dried *Daphnia*, 2.8 L of methanol, and 1.1 L of chloroform to produce 1 L of extract. Based on the materials costs only, dosing this extract at 5% v/v could cost NZD \$6.50 per litre of culture (Dried *Daphnia*[1] NZD \$220 kg^{-1}; MeOH[2] \$15 L^{-1}; chloroform[3] \$39 L^{-1}); this would need to be substantially reduced to be economically feasible.

Recovering the solvent for reuse could cut this cost down by ~10× and using methanol only would further reduce it, as chloroform is expensive and also not suitable for food or feed applications. Further, while a dosage of 5% v/v induced aggregation, this was not optimised and using different *Daphnia* biomass gave a more concentrated extract (see **Chapter 4**), so this could also be reduced. Identifying active compounds would also allow for a more targeted

[1] **Freeze Dried Daphnia** – maximumpets.co.nz
[2] **Methanol** ≥99.85% (GC), for synthesis – sigmaaldrich.com
[3] **Chloroform** for analysis EMPARTA® ACS – sigmaaldrich.com

extraction based on the properties of the target compounds. Therefore, production and dosage optimisation would substantially reduce the cost of this extraction, and extracts could be produced in bulk, standardised, and dosed precisely, providing greater reproducibility than live grazers or raw filtrates.

However, a significant challenge remains the availability and cost of *Daphnia* (or similar grazers). For example, based off the above extract, 1 kg of *Daphnia* could be required to harvest 80 L of culture, to recover ~40 g of *Chlorella* (assuming 0.5 g DW L^{-1}). As the cost of dried *Daphnia* is similar to that of *Chlorella*, this extract and dosage would not be feasible. However, to our knowledge there is not currently a large scale industry for *Daphnia* production, rather there are only suppliers of live or dried *Daphnia* or eggs for aquarists. Therefore, using extracts for harvesting microalgae could create new market potential for the grazer industry, which would reduce the cost.

Overall, using extracted infochemicals may be worthwhile if extracts produce robust, reproducible aggregation at significantly lower doses and if the *Daphnia* industry grows substantially. However, characterising and isolating active compounds instead could open up the possibility of synthesising chemical cues directly, likely providing a simpler and more cost effective system.

5.3.4 Synthetic infochemicals

Synthetic cues are the most scalable long-term option. Yasumoto et al. (2005) identified *Daphnia*-derived infochemicals that induced colony formation in *Scenedesmus gutwinskii* after ten days, including sodium octyl sulphate (SOS). The surfactant sodium dodecyl sulphate (SDS; not grazer-derived) also triggered aggregation. Both compounds were active at microgram-per-litre doses, equating to costs as low as USD $\$2 \times 10^{-5}$ m^{-3}, significantly cheaper than conventional flocculants (see **Chapter 1**).

However, infochemical activity is highly species specific. In this study, neither SOS nor SDS induced aggregation in *C. reinhardtii* or *Tetradesmus obliquus* when tested at concentrations reported to be active in *S. gutwinskii* (Yasumoto et al., 2005). In *C. reinhardtii* and *T. obliquus* cultures treated with 10 ng mL^{-1} SDS, the proportion of single cells did not differ significantly from controls at any time over four days (ANOVA and Tukey HSD, $p > 0.05$, **Appendix P**), and colony size distributions were similar between treatments and controls (**Figure 5.3**).

Likewise, *T. obliquus* cultures treated with SOS (10–10^3 ng mL^{-1}) showed no change in single-cell abundance compared to controls over ten days (**Figure 5.4**; ANOVA and Tukey HSD, $p > 0.05$, **Appendix P**). For *C. reinhardtii*, single-cell abundance also appeared unchanged in cultures treated with SDS (10^2, 10^3, 10^4 ng mL^{-1}) or SOS (10, 10^2, 10^3 ng mL^{-1}) over nine days (**Figure P.1**). For example, after two days, controls contained 60.4% single cells and treatments contained 54.2–56.7% single cells.

Together, these results confirm that SOS and SDS lack cross-species activity and do not trigger colony formation in *C. reinhardtii* or *T. obliquus*. Moreover, the ten day induction time reported for *S. gutwinskii* is impractical for biomass harvesting, where aggregation must occur within hours to a day to be viable. This underscores both the promise and the limitation of synthetic cues: although they can be highly cost effective, their utility depends on identifying molecules with rapid and broad activity across multiple taxa.

Future research must therefore still identify infochemicals capable of eliciting rapid, robust, and species-relevant responses. The characterisation and subsequent testing of active compounds may allow for the selection of those which are deemed food safe or unlikely to interfere with downstream processing. Since the compounds would be grazer-derived they are unlikely to introduce harmful residues into the biomass unlike conventional flocculants. They also may not need complex additional treatment to be removed prior to medium recycling, as our work (**Chapter 3**) and other studies (Wu et al., 2013) have shown that infochemicals degrade over time and lose their activity.

5.3.5 Summary

Each trigger strategy offers distinct advantages and limitations. Live grazers and culture filtrates can induce aggregation but are difficult to culture and require standardisation, while extracted infochemicals provide greater reproducibility but still depend on grazer cultivation. Synthetic cues offer the greatest potential for cost-effective and scalable harvesting, but only if active compounds can be identified that work rapidly across target species. These comparisons are summarised in **Table 5.2**.

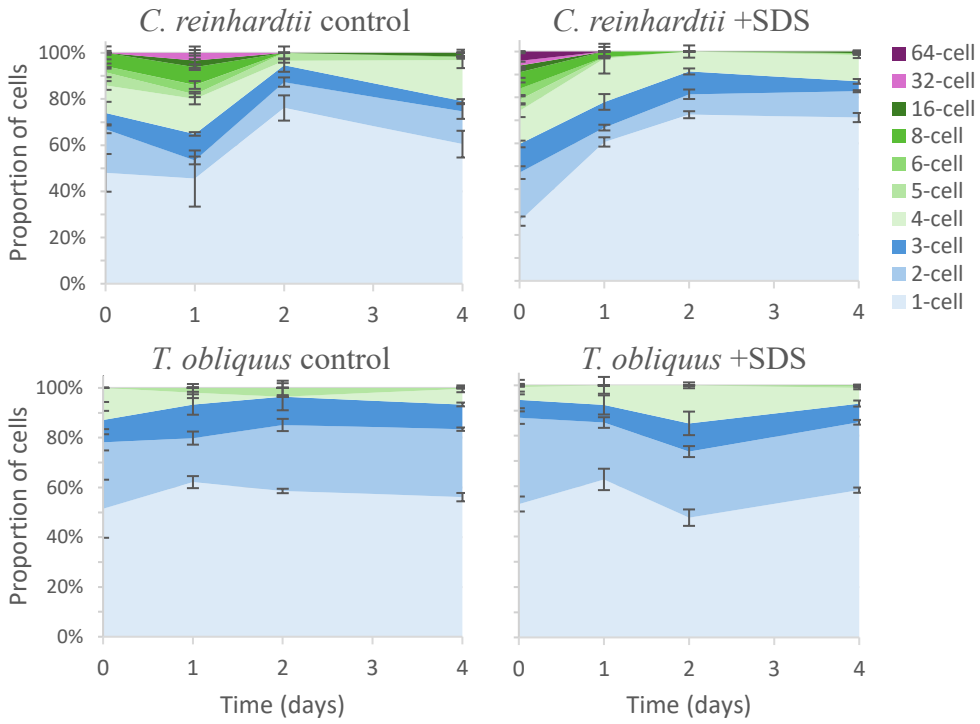

Figure 5.3. Proportion of *C. reinhardtii* and *T. obliquus* cells, unicellular and in colonies, over four days, in the controls and cultures treated with sodium dodecyl sulphate (10 ng mL^{-1}). Error bars represent the standard errors ($N = 3$ biological replicates).

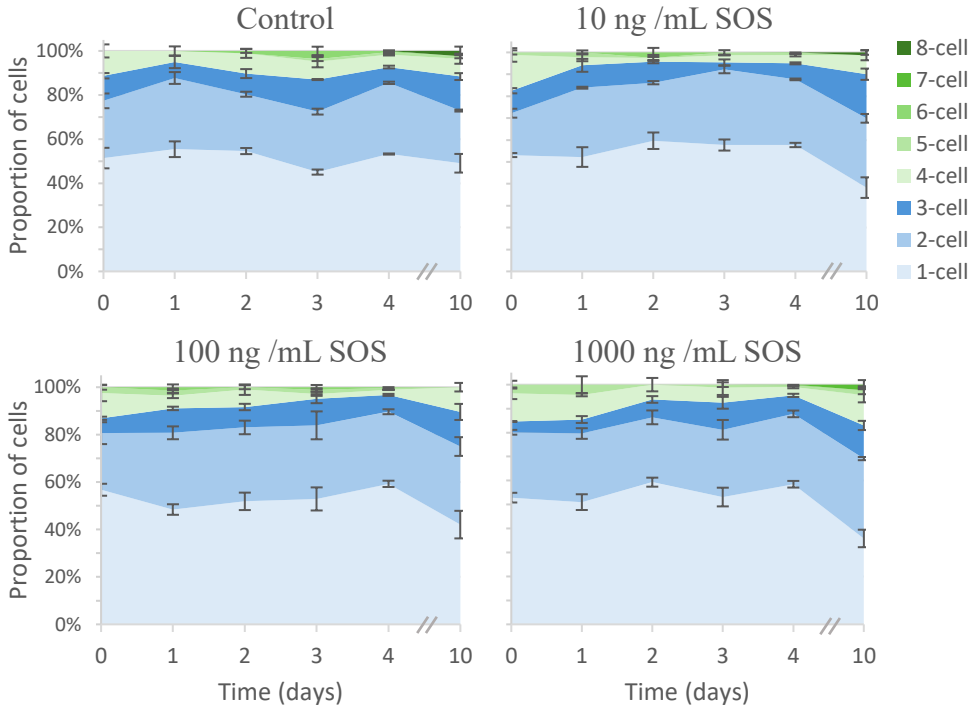

Figure 5.4. Proportion of *T. obliquus* cells, single and in colonies, over 10 days, in the controls and cultures treated with sodium octyl sulphate (10, 10^2, and 10^3 ng mL^{-1}). Error bars represent the standard errors ($N = 3$ biological replicates).

Table 5.2. Comparison of potential predator-derived trigger types for inducing self-aggregation in microalgae harvesting, summarising their main advantages, limitations, and relative suitability for scale-up.

Trigger type	Advantages	Limitations	Scale-up potential
Live grazers (e.g., *Daphnia*, *Brachionus*)	- Natural, proven induction of aggregation across species - Potentially low-cost (e.g., rotifer production USD \$0.069–0.23 m^{-3})	- No current large-scale suppliers - Grazer mortality reduces reliability - Risk of overgrazing biomass - Grazer culture crashes common - Predator residues may contaminate biomass	Low – biological variability and contamination risks limit industrial feasibility
Predator culture filtrate	- Faster induction than live grazers (Sathe & Durand, 2015) - No contamination with whole grazers	- No current large-scale suppliers - Higher cost (up to USD \$10 m^{-3} $_{culture}$) - Requires maintaining dense predator cultures - Variable infochemical composition - Media additives may affect algal physiology	Low – economically uncompetitive and operationally complex
Extracted infochemicals	- More controlled than live cultures - Rapid induction in *C. reinhardtii* (**Chapters 2–3**)	- No current large-scale suppliers - Extraction adds cost and complexity	Low – high grazer biomass demand for low microalgae yield
Synthetic infochemicals	- Potentially very low cost (USD \$2 × 10^{-5} m^{-3}) - Precise, reproducible dosing - Avoids grazer culture and residues - Food-safe options may be selected	- Active compounds identified for few species - Strong species-specific responses	High – if active, rapid response cues can be validated across target species

5.4 Environmental factors

Optimising culture conditions is essential to maximise aggregation efficiency and improve the subsequent settleability or filterability of biomass. Light and temperature are two key environmental parameters known to influence self-aggregation responses (**Chapter 1**) and, therefore, must be considered in harvesting applications.

5.4.1 Light intensity

To test the influence of light intensity, *C. reinhardtii* CC-1690 and CC-5325 cultures were incubated at 22 °C, without shaking, under continuous light ranging from 8.2 to 188.6 µmol m^{-2} s^{-1}. *Daphnia* extract (described in **Chapter 3**) was added at 5–10% v/v.

Light intensity had a strong effect on palmelloid formation (**Table 5.3** and **Table Q.1** and **Table Q.2** in **Appendix Q**). Under low light (8.2 µmol m^{-2} s^{-1}), CC-1690 did not aggregate in either *Daphnia*-treated or control cultures. At 19.0 µmol m^{-2} s^{-1}, palmelloids formed in *Daphnia* treatments by 48 h but disappeared by 72 h. Under higher light levels (56.1, 78.4, and 188.6 µmol m^{-2} s^{-1}), both treatments were dominated by palmelloids, indicating that excess light stress alone was sufficient to drive aggregation. Stock culture flasks of CC-1690 maintained a persistent palmelloid state at ≥ 56.1 µmol m^{-2} s^{-1}. At an intermediate "sweet spot" (37.8 µmol m^{-2} s^{-1}), palmelloids formed only in the *Daphnia* extract treatment, showing that infochemicals can induce aggregation within a specific light window.

In contrast, CC-5325 displayed much greater tolerance to high light: cultures remained unicellular and actively growing up to 188.6 µmol m^{-2} s^{-1}, while CC-1690 under the same conditions was entirely in palmelloid form. **Figure 5.5** shows CC-1690 and CC-5325 cultures incubated under 120 µmol m^{-2} s^{-1}, where CC-1690 was almost completely in palmelloids and settled rapidly, while CC-5325 was unicellular and motile. These results demonstrate for the first time that palmelloid formation is highly sensitive to light intensity and strongly strain dependent. Recycling settled biomass would help to maintain dominance of aggregating strains within a system.

Table 5.3. CC-1690 and CC-5325 cells in control and *Daphnia* extract treatments at 48 h, at varying light intensities. Images were taken at 10× magnification; each image is 0.25 mm.

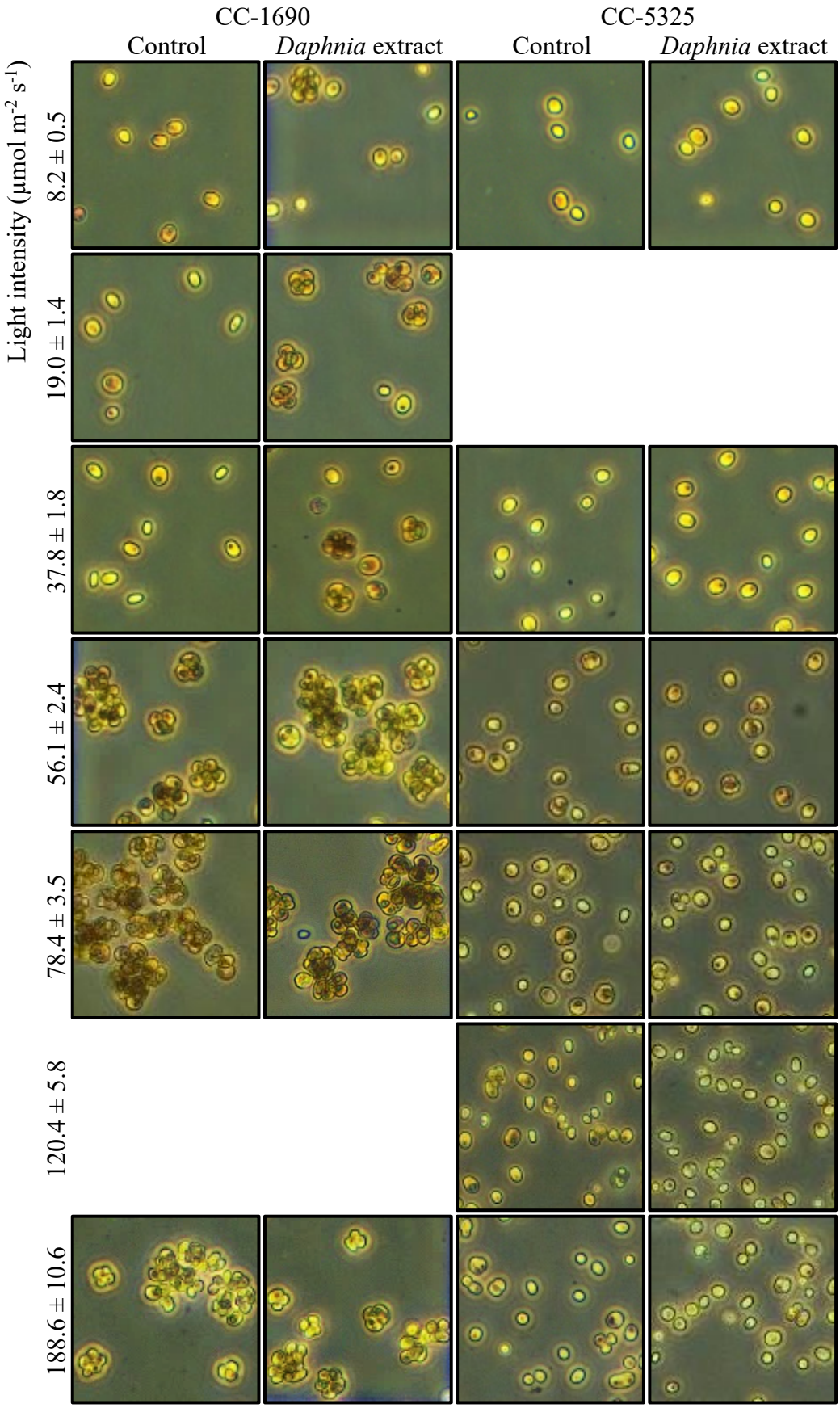

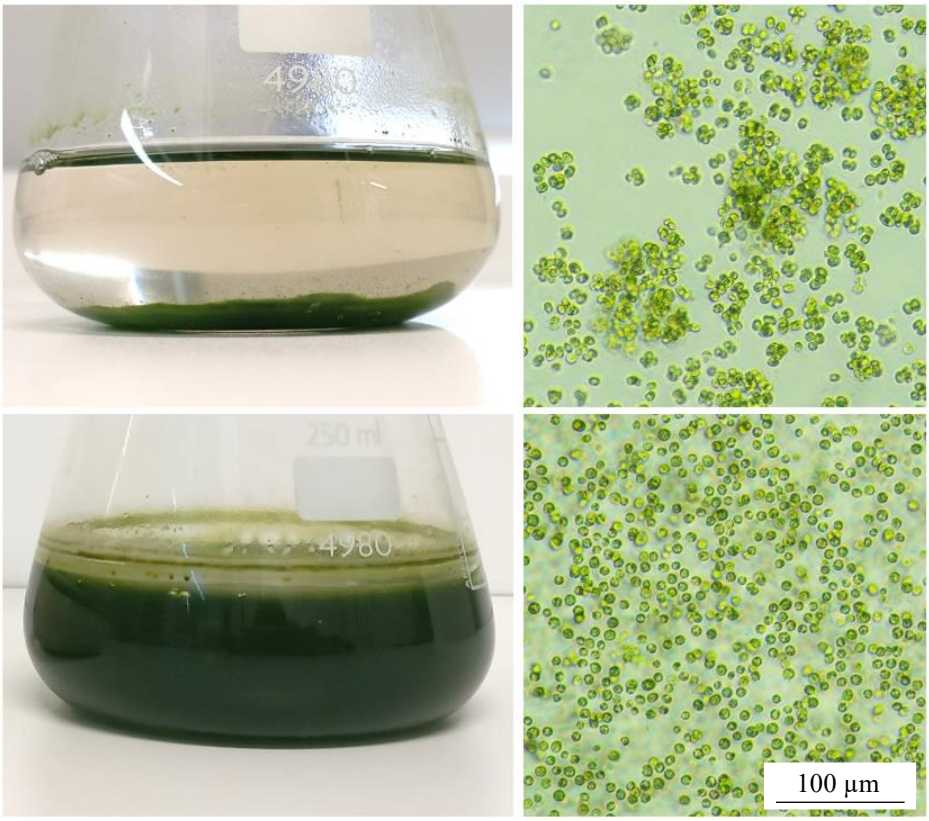

Figure 5.5. 250 mL flasks of *C. reinhardtii* CC-1690 (top) and CC-5325 (bottom) cultures incubated for six days at 78 µmol m^{-2} s^{-1} followed by five days at 120 µmol m^{-2} s^{-1}, where CC-1690 was almost completely in palmelloids and settled rapidly, while CC-5325 was unicellular and motile. Microscope images were taken at 20× magnification with no staining.

5.4.2 Temperature

Although temperature effects were not directly tested in this study, previous reports reviewed in **Chapter 1** indicated that aggregation in *C. reinhardtii* and related species can be temperature dependent. Colony formation and EPS-mediated aggregation are typically enhanced at moderate temperatures that support active metabolism, while high temperatures can reduce aggregation (Zhang et al., 2021; Zhu et al., 2019). In practice, the fluctuating temperatures in commercial cultures may influence aggregation, though temperature control would be easier in a dedicated aggregation tank rather than an open pond.

5.4.3 Implications for harvesting

These findings suggest that strategically adjusting light intensity and temperature, in combination with infochemicals, could help to optimise aggregation. Environmental parameters must be tailored to each strain, ensuring cultures are maintained within conditions that promote strong and reproducible aggregation without compromising growth or biomass quality.

Aggregation generally occurs most efficiently at temperatures that also promote active growth, meaning temperature adjustments may not be necessary to trigger aggregation. However, light intensity plays a more variable role. While our results show that there is an optimal light intensity range for palmelloid formation, light requirements vary greatly with culture depth and density; large-scale cultures may require five to ten times the light intensity of laboratory flasks (Lavens and Sorgeloos, 1996). Consequently, pilot-scale light trials would be essential to determine the feasible intensity range for aggregation under production conditions.

Short, controlled bursts of high light or temperature could also serve as practical induction tools, either to trigger aggregation directly or enhance responses when combined with infochemicals. This approach could serve as a rapid “shock-and-settle” protocol that is more energy-efficient and compatible with downstream processes.

Strain selection is a critical factor. Strains like CC-1690 readily shift into persistent palmelloid states under moderate light, whereas CC-5325 requires additional or alternative cues to aggregate. Designing harvesting protocols will therefore require careful matching of strains with their light and temperature thresholds, alongside chemical triggers, to achieve consistent performance at scale. For large-scale mixed-species cultures, strain choice becomes even more crucial: harvesting strategies will only succeed if all species respond reliably to the same cues. Interestingly, species that secrete abundant EPS may even promote aggregation of less responsive taxa.

5.5 Timing and integration

The timing of infochemical addition is critical for effective induction of self-aggregation. Because colonies and aggregates typically remain suspended under mechanical mixing, premature aggregation is unlikely to cause growth inhibition as a result of settling and lower light exposure. In laboratory tests, *C. reinhardtii* growth was either enhanced or unaffected when aggregation was induced by *Daphnia* extracts (**Chapters 2** and **3**). Therefore, aggregation could be triggered in the main culture, however, at larger scales, this relationship may differ, as light penetration can become a limiting factor. Additional paddlewheels may be required if aggregates are large and settle rapidly.

Species-specific factors and environmental conditions further influence aggregation dynamics. In *C. reinhardtii*, for example, initial cell concentration strongly affected responses to *Daphnia* infochemicals: cultures at ~5 × 10^5 cells mL^{-1} aggregated within 12 h, whereas cultures at ~5 × 10^4 cells mL^{-1} required 24–48 h to begin aggregating (see **Chapter 2**). Interestingly, delayed aggregation resulted in larger colonies, with palmelloids of up to 32 cells compared with four or eight cells in denser cultures.

It may also be necessary to harvest cultures before colonies become too large. This sounds counterintuitive, but as discussed in **Section 5.2.2**, a uniform colony size distribution throughout a culture is important for efficient harvesting; if some colonies begin to adhere into larger aggregates this could lead to complications such as increased fouling of membranes.

These results emphasise the need for timing trials to identify the most effective point of trigger addition. If aggregation occurs rapidly, dosing shortly before harvest may be sufficient. If aggregation is slower or enhanced at lower cell densities, earlier addition may be preferable, allowing colonies to reach optimal size before biomass recovery.

At scale, harvesting is often semi-continuous or continuous to minimise storage and reduce equipment size/costs. Integration of self-aggregation into such systems may require staging. One strategy is to divert a fraction of culture into a smaller induction tank, trigger aggregation under optimised conditions, and then transfer the aggregated biomass to sedimentation tanks, filtration units, or centrifuges. This approach enables precise control over timing and environmental conditions while maintaining compatibility with continuous large-scale culture systems.

5.6 Proposed design

Laboratory-, pilot-, and large-scale testing are essential to identify microalgae-predator/infochemical systems that induce aggregation efficiently for harvesting. However, translating this concept into a practical protocol requires careful process design to ensure economic competitiveness with conventional flocculation.

Building on the findings of **Chapters 3** and **4** and the parameters identified as critical for enhancing aggregation, we propose the following design framework:

- **Strain selection**: Following aggregation trials, one or more algal species should be chosen that rapidly, uniformly, and consistently produce colonies or aggregates with properties (e.g., size, density, motility, EPS content) that enhance sedimentation, filtration, and/or centrifugation. Strain improvement through genetic engineering could be explored to develop "palmelloid-prone" or rapidly aggregating strains.
- **Trigger selection**: Grazer-derived infochemicals should be extracted, characterised, and tested across algal strains. From these, synthetic analogues or chemical cues effective across multiple species should be selected as scalable triggers.
- **Mode of aggregation**: A fraction of the culture volume would be diverted into a smaller "aggregation tank" where the trigger is added at the strain-specific optimal dosage. The timing of this transfer should account for cell concentration and aggregation kinetics.
- **Environmental parameters**: Light and temperature should be tightly controlled in the aggregation tank within ranges that promote strong aggregation but remain technically and economically feasible. Short, controlled bursts of extreme light or temperatures may also be applied to enhance induction.
- **Harvesting**: Aggregated biomass should be thickened and dewatered after an optimal holding period. Sedimentation (in the aggregation tank or a separate unit) could be followed by filtration or centrifugation. Clarified water may be recycled directly or after treatment. The dewatered biomass can then be dried or further processed.

Optional strategies include:

- Reusing aggregation culture medium containing infochemicals and allelochemicals to drive stable aggregation responses,

- Recycling a fraction of harvested biomass back into the main culture to maintain dominance of colonial cells or aggregation prone phenotypes.

A simplified process flow diagram for integrating infochemical-induced self-aggregation into harvesting systems is shown in **Figure 5.6.**

This proposed design represents the first integrated framework for applying predator-derived infochemicals to drive self-aggregation in microalgae. By linking ecological defence strategies with biotechnological harvesting, it establishes a novel foundation for developing sustainable, low-cost alternatives to chemical flocculation.

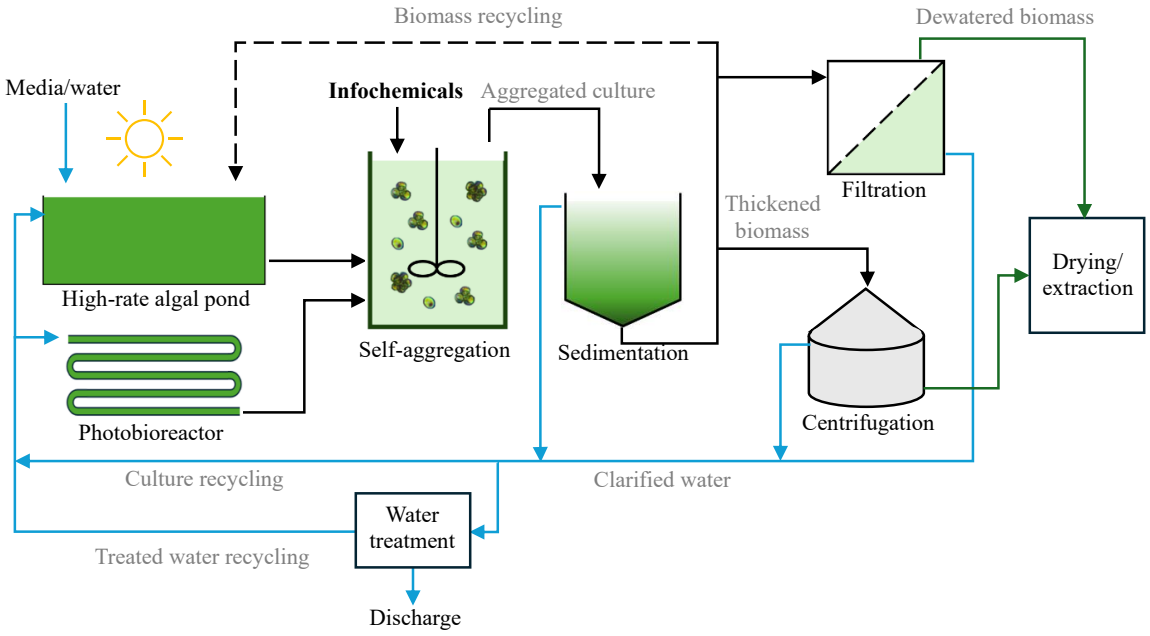

Figure 5.6. Conceptual process flow for harvesting microalgal biomass using infochemical-induced self-aggregation, prior to thickening via sedimentation and dewatering via filtration or centrifugation. Biomass or culture recycling can encourage dominance of colonial cells and reuse infochemicals and allelochemicals. The dewatered biomass can be dried or processed further, and the clarified water can be treated and recycled.

5.7 Conclusions

This work demonstrates that harnessing microalgae's natural ecological defence mechanism of self-aggregation could offer a promising alternative to overcome both the cost and technical barriers associated with chemical flocculation for biomass harvesting. However, further research is required to design protocols and evaluate their technical and economic feasibility through a long term study at scale.

The mechanistic insights revealed by the transcriptomic data highlight new opportunities for developing engineered strains with heightened or persistent aggregation capacity. Key operational parameters identified that influence aggregation included light intensity, temperature, initial cell density, timing of infochemical addition, and aggregation rate.

Predator-derived infochemicals, once identified and characterised, could be synthesised and used as reproducible, on-demand aggregation triggers, with lower costs and risk compared to methods that require considerable volumes of zooplankton biomass. However, the lack of aggregation in *Chlamydomonas reinhardtii* exposed to *Daphnia* infochemical sodium octyl sulphate, which previously induced colony formation in *Scenedesmus gutwinskii*, highlighted the species-specificity of chemical cues.

Strain-specific phenotypes are also critical: *C. reinhardtii* cultures varied in the proportion of cells aggregating, the dominant mode of aggregation (colony formation vs extracellular polymeric adhesion), and the resulting colony size distribution. These traits directly affect settling velocity, filterability, and compatibility with downstream dewatering processes.

Optimising strain selection, trigger selection, and process design could therefore yield a novel harvesting strategy that enhances sedimentation, filtration, and centrifugation performance, while reducing costs, and avoiding harmful residues. Self-aggregation could lower the chemical burden of harvesting, simplify water recycling, and improve biomass quality for food, feed, and bioproduct applications.

Ultimately, reducing harvesting costs is essential for unlocking the full commercial potential of microalgae. A well-optimised self-aggregation system has the potential to transform a longstanding bottleneck into a sustainable, scalable, and economically viable solution.

References

Aljuboori, A. H. R., Uemura, Y., & Thanh, N. T. (2016). Flocculation and mechanism of self-flocculating lipid producer microalga *Scenedesmus quadricauda* for biomass harvesting. *Biomass and Bioenergy*, *93*, 38-42. https://doi.org/10.1016/j.biombioe.2016.06.013

Brown, J. M., Cochran, D. A., Craige, B., Kubo, T., & Witman, G. B. (2015). Assembly of IFT trains at the ciliary base depends on IFT74. *Curr Biol*, *25*, 1583-1593. https://doi.org/10.1016/j.cub.2015.04.060

Conway, K., & Trainor, F. R. (1972). *Scenedesmus* morphology and flotation. *Journal of Phycology*, *8*, 138-143. https://doi.org/10.1111/j.1529-8817.1972.tb04014.x

Davis, R., Aden, A., & Pienkos, P. T. (2011). Techno-economic analysis of autotrophic microalgae for fuel production. *Applied Energy*, *88*, 3524-3531. https://doi.org/10.1016/j.apenergy.2011.04.018

de Carpentier, F., Maes, A., Marchand, C. H., Chung, C., Durand, C., Crozet, P., Lemaire, S. D., & Danon, A. (2022). How abiotic stress-induced socialization leads to the formation of massive aggregates in *Chlamydomonas*. *Plant Physiology*, *190*, 1927-1940. https://doi.org/10.1093/plphys/kiac321

Fasaei, F., Bitter, J. H., Slegers, P. M., & van Boxtel, A. J. B. (2018). Techno-economic evaluation of microalgae harvesting and dewatering systems. *Algal Research*, *31*, 347-362. https://doi.org/10.1016/j.algal.2017.11.038

Hashmi, Z., Idriss, I. M., Zaini, J., Abu Bakar, M. S., Wibisono, Y., Abdullah, R., & Bilad, M. R. (2025). Advancements in membrane modifications for enhanced microalgae harvesting: A comprehensive review. *Separation and Purification Technology*, *360*, 131012. https://doi.org/10.1016/j.seppur.2024.131012

Herron, M., & Nedelcu, A. (2015). Volvocine algae: From simple to complex multicellularity. In Ruiz-Trillo, I., & Nedelcu, A. (Eds.) Evolutionary transitions to multicellular life. *Advances in marine genomics* (Vol. 2, pp. 129-152). Springer, Dordrecht. https://doi.org/10.1007/978-94-017-9642-2_7

Herron, M. D., Borin, J. M., Boswell, J. C., Walker, J., Chen, I. C. K., Knox, C. A., Boyd, M., Rosenzweig, F., & Ratcliff, W. C. (2019). De novo origins of multicellularity in response to predation. *Scientific Reports*, *9*, 2328. https://doi.org/10.1038/s41598-019-39558-8

Hou, Y., Qin, H., Follit, J. A., Pazour, G. J., Rosenbaum, J. L., & Witman, G. B. (2007). Functional analysis of an individual IFT protein: IFT46 is required for transport of outer dynein arms into flagella. *J Cell Biol*, *176*, 653-665. https://doi.org/10.1083/jcb.200608041

Kurpan, D., Idà, A., Körner, F. G., Bombelli, P., da Silva Aguiar, J. P., Marinho, L. M., do Valle, A. F., Acién, F. G., Trasatti, S. P., & Schievano, A. (2024). Long-term evaluation of productivity and harvesting efficiency of an industrial Spirulina (*Arthrospira platensis*) production facility. *Bioresource Technology Reports*, *25*, 101741. https://doi.org/10.1016/j.biteb.2023.101741

Lavens, P., & Sorgeloos, P. (Eds.). (1996). Manual on the production of live fish food for aquaculture. FAO Fisheries Technical Paper. No. 361. Rome, FAO. 295p.

Lechtreck, K. F., Johnson, E. C., Sakai, T., Cochran, D., Ballif, B. A., Rush, J., Pazour, G. J., Ikebe, M., & Witman, G. B. (2009). The *Chlamydomonas reinhardtii* BBSome is an IFT cargo required for export of specific signaling proteins from flagella. *J Cell Biol*, *187*, 1117-1132. https://doi.org/10.1083/jcb.200909183

Lorusso, N. (2018). *Consequences of an inducible defence: The ecological and evolutionary repercussions of temporary colony formation in Clamydomonas reinhardtii.* (Dissertation). Rutgers, The State University of New Jersey.

Lurling, M., & Beekman, W. (2006). Palmelloids formation in *Chlamydomonas reinhardtii*: Defence against rotifer predators? *International Journal of Limnology*, *42*, 65-72. https://doi.org/10.1051/limn/2006010

Muir, E., Guieysse, B., & Plouviez, M. (2025). Large-scale harvesting of microalgae. In I. A. Severo, J. C. Ordóñez, A. B. Mariano, & J. V. C. Vargas (Eds.), *Microalgae Horizons: Fundamentals, Innovations, and Industrial Applications* (pp. 377-399). Springer Nature Switzerland. https://doi.org/10.1007/978-3-031-84282-5_13

Park, J. B. K., Craggs, R. J., & Shilton, A. N. (2011). Recycling algae to improve species control and harvest efficiency from a high rate algal pond. *Water Research*, *45*, 6637-6649. https://doi.org/10.1016/j.watres.2011.09.042

Rojo, A., & Ibarra, L. (2017). Pilot-scale production of the rotifer *Brachionus* sp. under different culture systems. *Revista de Biologia Marina Y Oceanografia*, *52*.

Sathe, S., & Durand, P. M. (2015). A low cost, non-toxic biological method for harvesting algal biomass. *Algal Research*, *11*, 169-172. https://doi.org/10.1016/j.algal.2015.06.021

Sreevidya, C. P., V, A., T.M, M. K., M.A, A., Aliyas, A. T., Sarasan, M., S.P, S., Singh, I. S. B., & Puthumana, J. (2025). Design and optimization of a recirculating aquaculture system (RAS) for live feed production in aquaculture: A case study using *Daphnia magna*. *Aquaculture International*, *33*, 217. https://doi.org/10.1007/s10499-025-01893-1

Wei, X., Rao, N. R. H., Tyagi, S., Thielemans, W., Cao, W., Guo, L. J., & Muylaert, K. (2025). Performance of different flocculants for harvesting Chlorella vulgaris by dissolved air flotation and sedimentation. *Bioresource Technology*, *433*, 132743. https://doi.org/10.1016/j.biortech.2025.132743

Wu, X., Zhang, J., Qin, B., Cui, G., & Yang, Z. (2013). Grazer density-dependent response of induced colony formation of *Scenedesmus obliquus* to grazing-associated infochemicals. *Biochemical Systematics and Ecology*, *50*, 286-292. https://doi.org/10.1016/j.bse.2013.05.001

Xiao, J., Liu, R., Yang, L., Hu, Q., & Zhang, X. (2019). Macrofiltration-a leap towards high efficiency microalgal harvesting: A case study using *Scenedesmus acuminatus*. *Algal Research*, *37*, 1-10. https://doi.org/10.1016/j.algal.2018.11.001

Yang, Z., Kong, F., Shi, X., & Cao, H. (2006). Morphological response of *Microcystis aeruginosa* to grazing by different sorts of zooplankton. *Hydrobiologia*, *563*, 225-230. https://doi.org/10.1007/s10750-005-0008-9

Yasumoto, K., Nishigami, A., Yasumoto-Hirose, M., Kasai, F., Okada, Y., Kusumi, T., & Ooi, T. (2005). Aliphatic sulfates released from *Daphnia* induce morphological defense of phytoplankton: Isolation and synthesis of kairomones. *Tetrahedron Letters*, *46*, 4765-4767. https://doi.org/10.1016/j.tetlet.2005.05.027

Zhang, H., Yang, L., Zang, X., Cheng, S., & Zhang, X. (2019). Effect of shear rate on floc characteristics and concentration factors for the harvesting of *Chlorella vulgaris* using coagulation-flocculation-sedimentation. *Science of The Total Environment*, *688*, 811-817. https://doi.org/10.1016/j.scitotenv.2019.06.321

Zhang, L., Sun, Y., Cheng, J., Cui, G., Huang, Y., & Yang, Z. (2021). Warming mitigates the enhancement effect of elevated air CO_2 on anti-grazer morphological defense in *Scenedesmus obliquus*. *Science of The Total Environment*, *770*, 145341. https://doi.org/10.1016/j.scitotenv.2021.145341

Zhu, X., Wang, Y., Hou, X., Kong, Q., Sun, Y., Wang, J., Huang, Y., & Yang, Z. (2019). High temperature promotes the inhibition effect of Zn^{2+} on inducible defense of *Scenedesmus obliquus*. *Chemosphere*, *216*, 203-212. https://doi.org/10.1016/j.chemosphere.2018.10.116

Chapter 6.

Conclusions and future prospects

6.1 Conclusions

Microalgae have a vast biotechnological potential, but their biomass is inherently difficult to harvest, creating a major bottleneck for large-scale applications. Biomass recovery through sedimentation, filtration, and centrifugation can be aided by chemical flocculation, but low-cost flocculants are often unsuitable for food or feed applications.

Self-aggregation offers a sustainable biological alternative, but the critical literature review revealed that most previous reports of self-aggregation were limited to morphological observations at the lab scale (**Chapter 1**). A few studies investigated the transcriptomic changes during aggregation in *Chlamydomonas reinhardtii*, *Tetradesmus obliquus*, and *Microcystis aeruginosa*, in response to *Daphnia* or *Brachionus calyciflorus* (Berger, 2017; Harke et al., 2017; Lorusso, 2018; Sun et al., 2020), demonstrating changes in pathways linked to mobility, cell-to-cell adhesion, cell wall synthesis, and the production of EPS and the extracellular matrix, but it is not clear whether these mechanisms are conserved across all microalgae. Given the highly variable responses of different species to environmental stressors, a deeper understanding of the mechanisms by which algae sense cues and initiate aggregation is essential for controlled, scalable application.

As a first step in this endeavour, it was necessary to develop a reliable bioassay that could induce a significant reliable self-aggregation response (combined with a stable control) in green microalgae, because no such protocol had been well described in the literature. Consequently, and for the first time, a series of bioassays were conducted to systematically study the self-aggregation responses of *Chlamydomonas reinhardtii*, *Tetradesmus obliquus*, and *Chlorella vulgaris* to various predator cues. This study revealed divergent responses to *Daphnia* cues (**Chapter 2**), and while past studies largely focused on filtrate from *Daphnia* cultures, a concentrated and reproducible extract from dried *Daphnia* was produced that enabled precise dosing of infochemicals into algal cultures. *C. reinhardtii* treated with this extract formed palmelloid colonies, within 24 hours, that contained 4–32 cells each and further adhered into macroscopic aggregates.

While the three species all exhibited some aggregation under different treatments, the *C. reinhardtii* + *Daphnia* extract system demonstrated rapid and reproducible palmelloid formation involving nearly the entire culture, while controls remained unicellular. This uniform

aggregation and reproducibility enabled the subsequent downstream transcriptomic and metabolomic profiling of aggregated versus unicellular cultures.

Transcriptomic analysis of *C. reinhardtii* thus provided new insights into the molecular pathways that regulate palmelloid formation (**Chapter 3**). In palmelloid cultures, there was widespread downregulation of flagella-related genes, including those encoding flagella-associated proteins (FAPs), tubulin proteins, centrosomal proteins, radial spoke proteins, and intraflagellar transport (IFT) components. There was also mixed regulation of genes encoding pherophorins (ECM glycoproteins) and matrix metalloproteinases (MMP) involved in cell wall degradation and remodelling. Changes in signalling pathways were also observed, including calcium signalling, cyclin-dependent kinases, ubiquitin-proteasome components, and transient receptor potential (TRP) channels. The combined downregulation of several TRP and VDCC genes also suggests that *C. reinhardtii* may intentionally dampen Ca^{2+}-mediated signalling while in palmelloids. These results support a new hypothesis that flagella regeneration does not occur following cell division, thereby preventing degradation of the mother cell wall and encapsulating daughter cells in a palmelloid colony.

Mutant studies confirmed MMP13 as a candidate enzyme for cell wall degradation, as loss of *MMP13* was associated with a strong palmelloid phenotype. These assays also established TRP13 as a new candidate involved in external signal sensing. By contrast, knock-out mutants of *PHC18* (encoding a pherophorin) and *FAP199* aggregated significantly under *Daphnia*-extract treatment, likely reflecting functional overlap within the PHC and FAP gene families, or their indirect association with aggregation.

These transcriptomic changes point to a mechanistic model where *Daphnia* infochemicals activate TRP channels, triggering an influx of Ca^{2+} and activating signalling cascades. These cascades regulate ubiquitin-mediated degradation of flagella proteins and the simultaneous downregulation of degradative enzymes (PHCs and MMPs). The basal bodies remain in a centrosome role, driving mitosis and not flagella reassembly. Without flagella, ectosomal delivery of degradative enzymes to the cell wall does not occur, and cells remain trapped in palmelloids as they continue to divide. Interestingly, a clear divergence in responses was observed between *C. reinhardtii* CC-5325 (mutant background strain) and CC-1690: CC-1690 formed palmelloids under *Daphnia* infochemicals and high light stress, whereas CC-5325 did not, demonstrating strain-specific variation and the importance of strain choice in functional studies and application.

Untargeted metabolomic profiling of *C. reinhardtii* was then carried out to investigate the molecular pathways during palmelloid formation (**Chapter 4**). This identified 22 consistent metabolites, including 15 that differed significantly in abundance between aggregated and control cultures. However, most were also abundant in the *Daphnia* extract, making it difficult to distinguish between transferred predator metabolites and true algal responses. This highlights the need for refined experimental designs to resolve algal metabolomes reliably. Nonetheless, the study provides a basis for future works, describing methods which were able to detect metabolites while pointing to the mapping of compounds to reference libraries as a crucial step where information is currently being lost due to low mapping rates. The metabolomics analysis also revealed amino acids, including tyrosine, tyramine, and urea as potential candidates for *Daphnia*-derived infochemicals capable of inducing aggregation, and allowed for identification of candidate compounds acting as intracellular "alarm" signals in *C. reinhardtii*, including amino acids, polyamines, and fatty acids. These compounds will require targeted bioassays to confirm their role in triggering or amplifying aggregation responses.

Looking at the practical implications of this research, palmelloid formation increased particle volume exponentially with each cell division, making colonies inherently more amenable to sedimentation and filtration than unicells. Morphology and aggregation dynamics varied between *C. reinhardtii* strains and under different culture conditions (e.g., light intensity, initial cell density), indicating that successful application of self-aggregation for harvesting will require designs tailored to strain-specific dynamics and environmental parameters.

Among potential induction strategies, identifying, characterising, and ultimately synthesising grazer-derived infochemicals appears most practical and economically feasible (**Chapter 5**). Using live zooplankton or producing concentrated extracts would require significant volumes of biomass that are not yet produced at scale and would be prohibitively expensive. Consequently, identifying and synthesising active infochemicals could provide a lower cost option. The extremely low reported active concentrations of *Daphnia* infochemicals would make the induction of self-aggregation more economically sustainable compared to chemical flocculation, and the natural origin may remove the barrier that exists for common flocculants in food and feed applications.

Overall, this thesis developed an aggregation assay protocol and provided the first combined transcriptomic and metabolomic study of *Daphnia*-induced self-aggregation in *C. reinhardtii*, establishing likely molecular mechanisms and discussing the influence of aggregation

dynamics on the potential of self-aggregation to reduce costs and the chemical burden of biomass recovery. Exposure to *Daphnia* extracts reproducibly induced aggregation in multiple microalgae. The transcriptomics analyses provided strong evidence towards flagella suppression as the primary driver of palmelloid formation in *C. reinhardtii*, although candidate genes require confirmation using mutants with a responsive background strain. Unfortunately, metabolomic insights remain low, as there was no clear evidence to distinguish between *Daphnia* and algal metabolites. However, the results provided a basis for future work by identifying limitations with the experimental design: a non-chemical (or known chemical) trigger, such as light stress, may be more suitable for a metabolomics study, and annotating compound peaks to multiple libraries may increase the number of detected compounds.

6.2 Future prospects

This work highlights clear directions for future research to gain a more complete understanding of the molecular pathways regulating *Chlamydomonas reinhardtii* self-aggregation and applying aggregation at an industrial scale.

First, molecular mechanisms require further validation: *MMP13* and *TRP13* were identified as strong candidates regulating palmelloid formation; future research should extend to other candidate genes, including members of the large MMP, PHC, and FAP gene families, as well as TRP channels and IFT-related genes. Because these gene families are directly involved in flagella function and cell wall degradation, they are strong candidates for controlling aggregation and should be studied in responsive background strains that reliably form palmelloids.

The identification of key genes is also crucial to investigating evolutionary trends among different microalgae species. The phylogeny could be studied to find out if key genes, such as receptors, are conserved, and investigate regulators involved in self-aggregation.

Signalling cascades involved in palmelloid formation could be confirmed by studying post-translational regulation through proteomics, to complement the transcriptomics datasets. This study found mixed transcriptional regulation of calcium signalling, protein kinases, and MAPK pathways, sometimes diverging from reports in other species. Proteomics could determine whether these pathways are up- or downregulated at the protein level, providing clearer insights into the signalling events driving palmelloid formation.

Additionally, targeted bioassays should confirm the activity of candidate compounds, whether derived from *Daphnia* or *C. reinhardtii*. Isolating and characterising grazer-derived infochemicals would allow their direct testing and help to distinguish algal metabolic responses from predator-derived compounds. In parallel, studying palmelloid formation under non-chemical stressors (e.g., light or temperature) could reveal algal-derived metabolites acting as alarm signals with potential as “self-flocculants”. Developing synthetic analogues of these cues could enable reliable induction while maintaining suitability for food and feed applications.

An alternative approach to identifying active *Daphnia* infochemicals could involve investigating analogous or orthologous receptors shared between *Daphnia* and *C. reinhardtii*. This comparative receptor-based strategy would aim to identify chemical signals that both

organisms respond to. A similar approach was demonstrated by Phan et al. (2022), who identified ortholog GPCRs common to the parasite *Schistosoma mansoni* and its snail host *Biomphalaria glabrata*, and then tested the bioactivity of putative ligands to narrow down biomolecules potentially involved in parasite-host interactions. Applying this strategy to *Daphnia*-microalgae interactions would combine functional gene annotation, data mining, and *in silico* receptor modelling using AI-based tools (e.g., AlphaFold 3.0). Analogous/orthologous receptors with conserved features in *Daphnia* and *C. reinhardtii* could highlight potential chemical classes involved in cross-species signalling. From these candidate receptors, putative ligands could be identified and tested for their ability to induce self-aggregation in *C. reinhardtii*.

Following identification of effective chemical triggers, applied studies should determine the most efficient induction conditions, including timing, light intensity, mixing, and cell density. Pilot-scale trials should evaluate whether induction tanks or continuous dosing strategies are more effective when integrated into sedimentation, filtration, or centrifugation workflows.

These trials could also serve to screen natural isolates for favourable aggregation traits: the mode of aggregation, proportion of culture responding, and size distribution of colonies or aggregates ultimately determine harvesting efficiency by affecting settling velocity, filterability, and compatibility with downstream processes. Engineered strains predisposed to palmelloid formation or aggregation may also be viable in some contexts, though their use could be constrained in “natural product” markets.

Life-cycle assessments (LCA) will be essential to compare self-aggregation against chemical-flocculation. Analyses should consider energy demand, chemical inputs, water recycling compatibility, and biomass quality. Such assessments will clarify whether self-aggregation offers environmental and economic benefits at scale.

While *C. reinhardtii* is a robust model, industrial relevance must be tested in other strains used in aquaculture, nutraceuticals, and other industries. Exploring cues from different grazers and tailoring induction strategies to strain-specific responses will be necessary. Engineering strains predisposed to palmelloid formation may further broaden the applicability of this approach.

Overall, this thesis generated hypotheses and provided a mechanistic basis for palmelloid formation, while demonstrating the harvesting potential of chemically triggered self-aggregation in *C. reinhardtii*. With refined triggers, informed strain selection, and careful

process integration, self-aggregation could reduce costs, eliminate harmful residues, and significantly lower the environmental footprint of algal biomass recovery.

References

Phan, P., Liang, D., Zhao, M., Wyeth, R. C., Fogarty, C., Duke, M. G., McManus, D. P., Wang, T., & Cummins, S. F. (2022). Analysis of rhodopsin G protein-coupled receptor orthologs reveals semiochemical peptides for parasite (Schistosoma mansoni) and host (Biomphalaria glabrata) interplay. *Scientific Reports*, *12*, 8243. https://doi.org/10.1038/s41598-022-11996-x

Appendices

List of Appendix Illustrations

List of Appendix Tables

Appendix A. Cultivation media

A.1. TAP (Tris acetate phosphate) media

Stock solutions for 1 L of TAP media (adjust final pH to 7.0)

1 M Tris base	20.0 mL
Phosphate buffer II	1.0 mL
Nutrient stock	10.0 mL
Hutner's trace elements	1.0 mL
Glacial acetic acid	1.0 mL

Tris base

Trizma base 12.1 g into 100 mL

Phosphate buffer (for 100 mL)

K_2HPO_4	10.8 g
KH_2PO_4	5.6 g

Nutrient stock (for 500 mL)

NH_4Cl	20 g
$MgSO_4.7H_2O$	5 g
$CaCl_2.2H_2O$	2.5 g

A.2. BG-11 media

Stock solutions for 1 L of BG-11 media (adjust final pH to 7.0)

Solution A	50.0 mL
Solution B	10.0 mL
Solution C	10.0 mL
Solution D	1.0 mL
Hutner's trace elements	1.0 mL

Solution A (for 1 L)

$NaNO_3$	30 g
K_2HPO_4	62 g
KH_2PO_4	30.4 g

Solution B (for 500 mL)

$MgSO_4.7H_2O$	3.75 g

Solution C (for 500 mL)

$CaCl_2.2H_2O$	1.8 g

Solution D (for 100 mL)

Citric acid	0.6 g
Ferric ammonium citrate	0.6 g
Na_2EDTA	0.098 g

Appendix B. Microalgae growth monitoring

In most experiments, the microalgae culture growth was measured using both optical density and cell counts, due to the simplicity of these methods. The growth profile of *C. reinhardtii* under typical culturing conditions (in an incubator at 22 °C, 115 rpm orbital shaking and 24 ± 1 µmol m^{-2} s^{-1} light) was monitored using optical density (**Figure B.1**). The dry weight of *C. reinhardtii* was also measured during culturing to relate optical density to dry weight (**Figure B.2**). During a bioassay experiment with 5% and 10% v/v resuspended *Daphnia* MPS extract, the optical density and cell counts were measured ten times from each of three biological replicates over 36 hours, which are plotted in **Figure B.3**. This relationship should be linear and was most closely correlated between 0.24 and 1.0 optical density (optical density above 1.0 was calculated from appropriately diluted cultures).

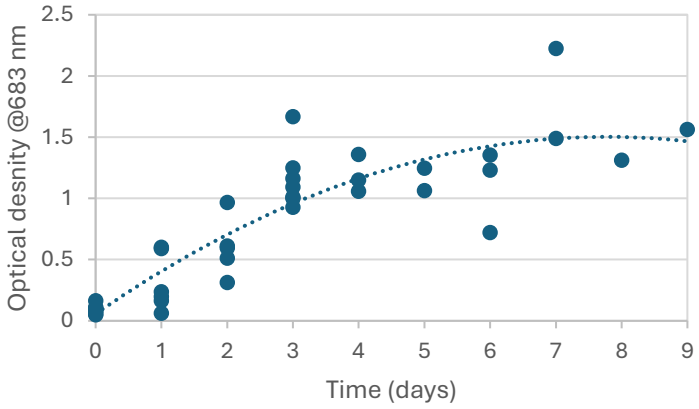

Figure B.1. *C. reinhardtii* culture optical density over 8 days incubation in flasks (115 rpm, 22 °C, 24 ± 1 µmol m^{-2} s^{-1} light).

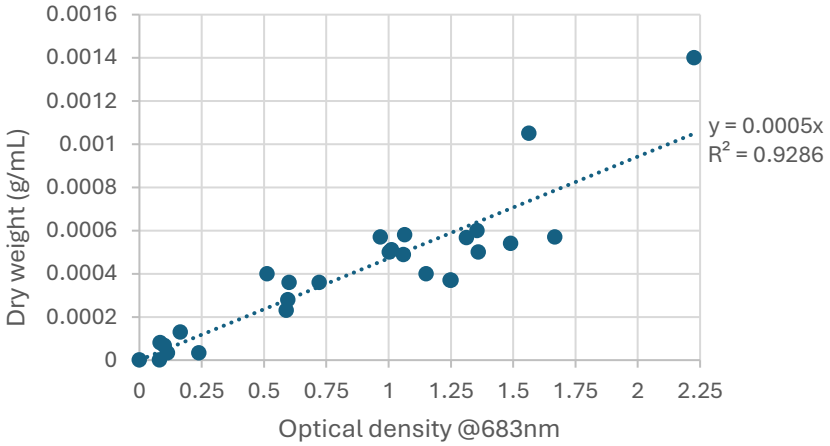

Figure B.2. *C. reinhardtii* dry weight and optical density relationship.

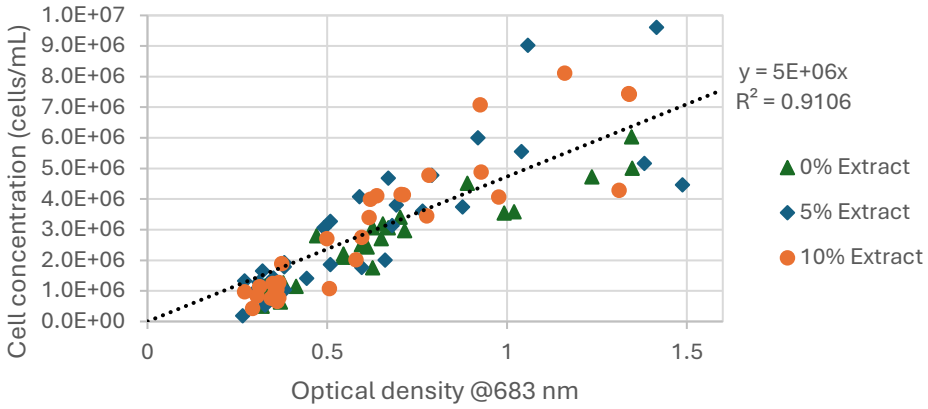

Figure B.3. *C. reinhardtii* cell concentration and optical density relationship.

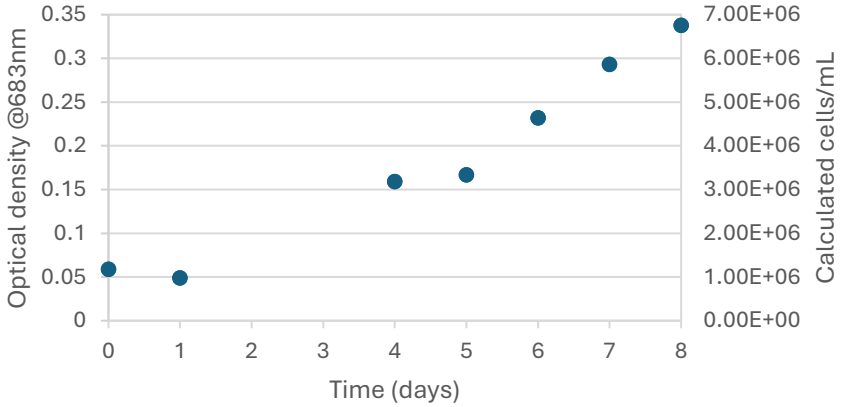

Figure B.4. *C. vulgaris* optical density over 8 days incubation in flasks (115 rpm, 22 °C, 24 ± 1 µmol m^{-2} s^{-1} light).

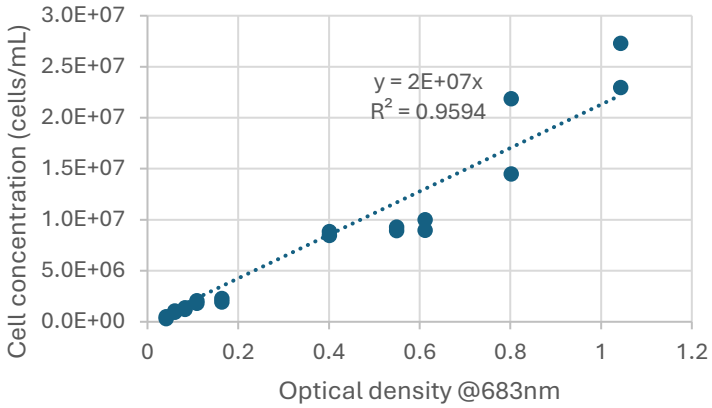

Figure B.5. *C. vulgaris* cell concentration and optical density relationship.

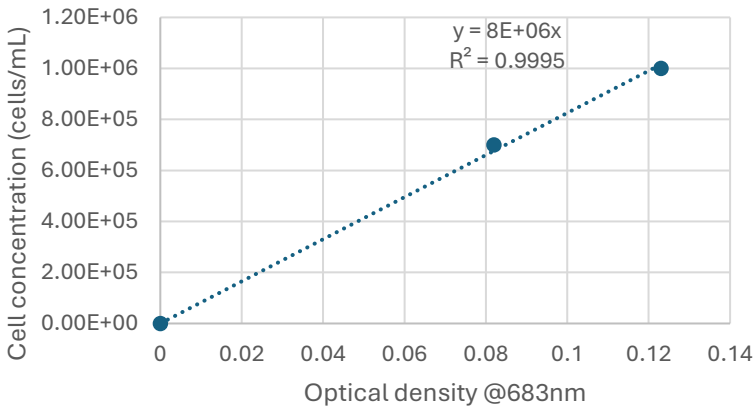

Figure B.6. *T. obliquus* cell concentration and optical density relationship.

Appendix C. Bioassay results

The following results are from bioassays described in **Chapter 2**.

C.1. *Chlorella vulgaris*

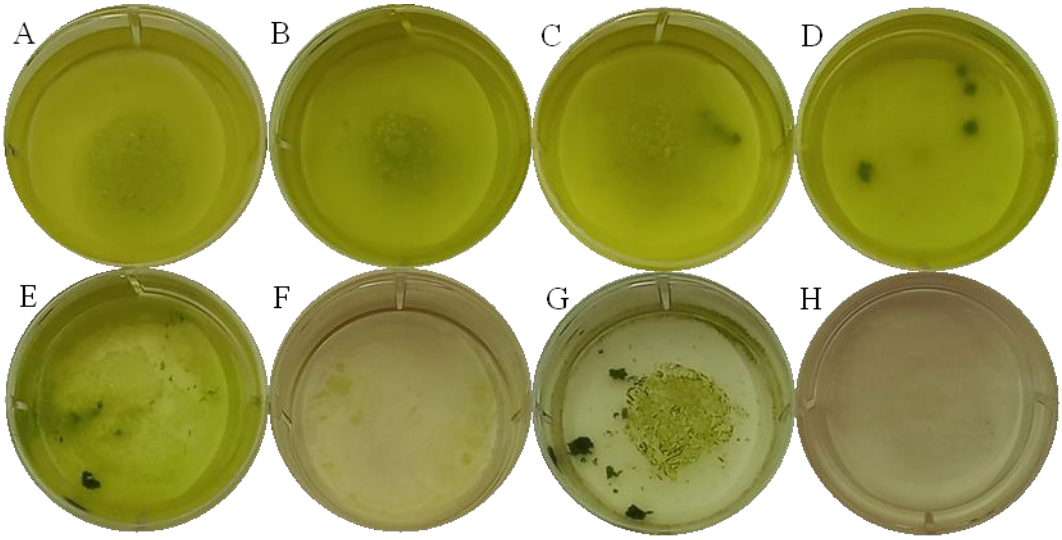

Figure C.1. Photographs of *C. vulgaris* bioassay wells at 24 h in control (A) and cultures treated with live *D. magna* at 1.25 mL^{-1} (B), 37% v/v *D. magna* filtrate (C), 1% v/v *Daphnia* water extract (D), 1% v/v solvent (E), 2% v/v solvent (F), 1% v/v *Daphnia* solvent extract (G), and 2% v/v *Daphnia* solvent extract (H).

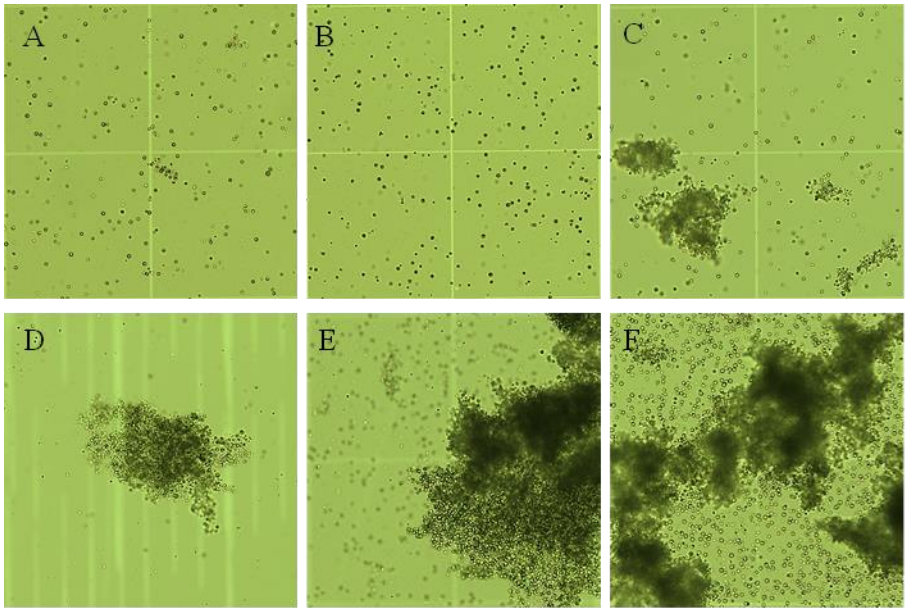

Figure C.2. *C. vulgaris* cells at 24 h, in control (A) and cultures treated with live *D. magna* at 1.25 mL^{-1} (B), *D. magna* filtrate at 37% v/v (C), *Daphnia* water extract at 1% v/v (D), *Daphnia* solvent extract at 1% v/v (E), and solvent at 1% v/v (F). Images were taken in brightfield at 10× magnification; each image is 500 × 500 µm.

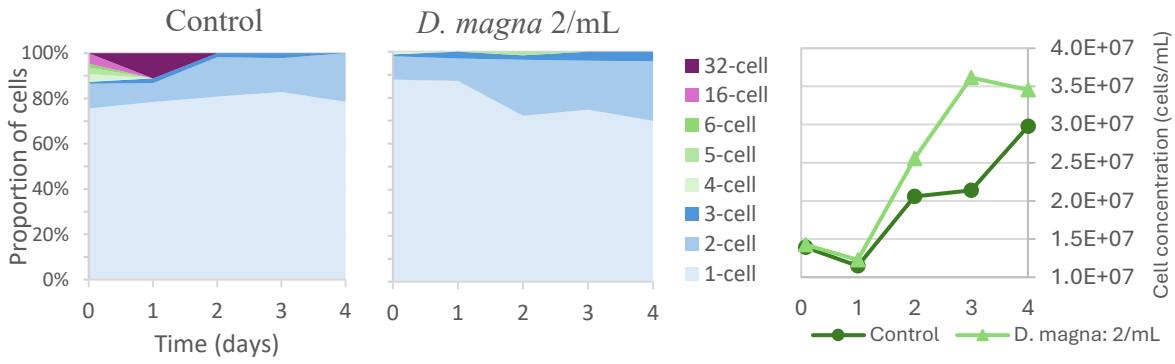

Figure C.3. Proportion of *C. vulgaris* cells, unicellular and in colonies, and cell concentration over four days, in control and culture treated with live *D. magna*.

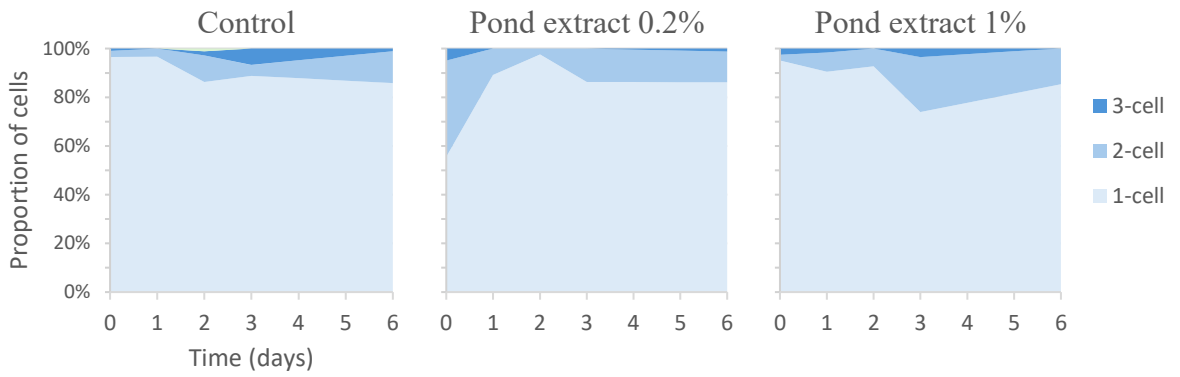

Figure C.4. Proportion *C. vulgaris* cells, unicellular and in colonies, over six days, in control, and cultures treated with pond organism extract at 0.2% v/v and 1% v/v.

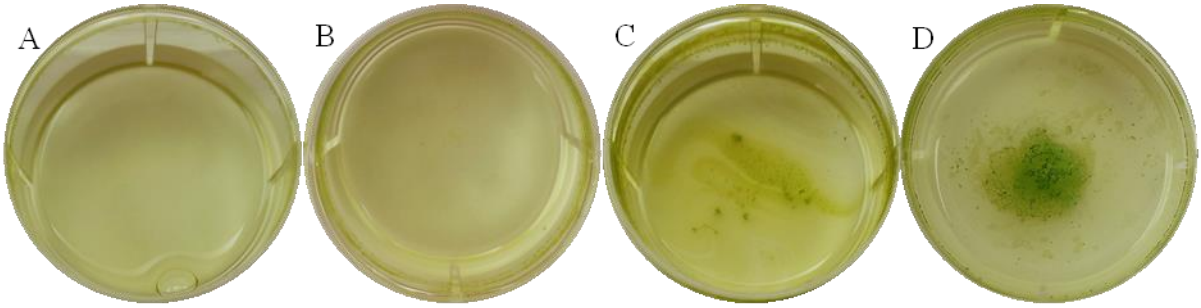

Figure C.5. Photographs of *C. vulgaris* bioassay wells, at 24, 24, and 19 h, respectively, in control (A), and cultures treated with resuspended frozen extract at 1% v/v (B), 5% v/v (C), and 10% v/v (D).

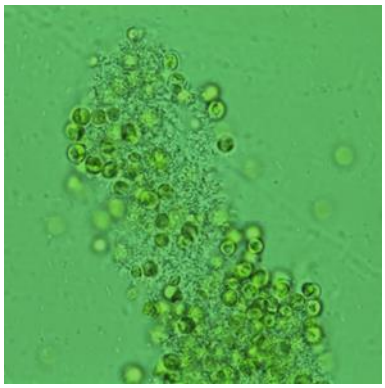

Figure C.6. *C. vulgaris* aggregate in culture treated with resuspended frozen extract, imaged at 100x magnification.

C.2. *Tetradesmus obliquus*

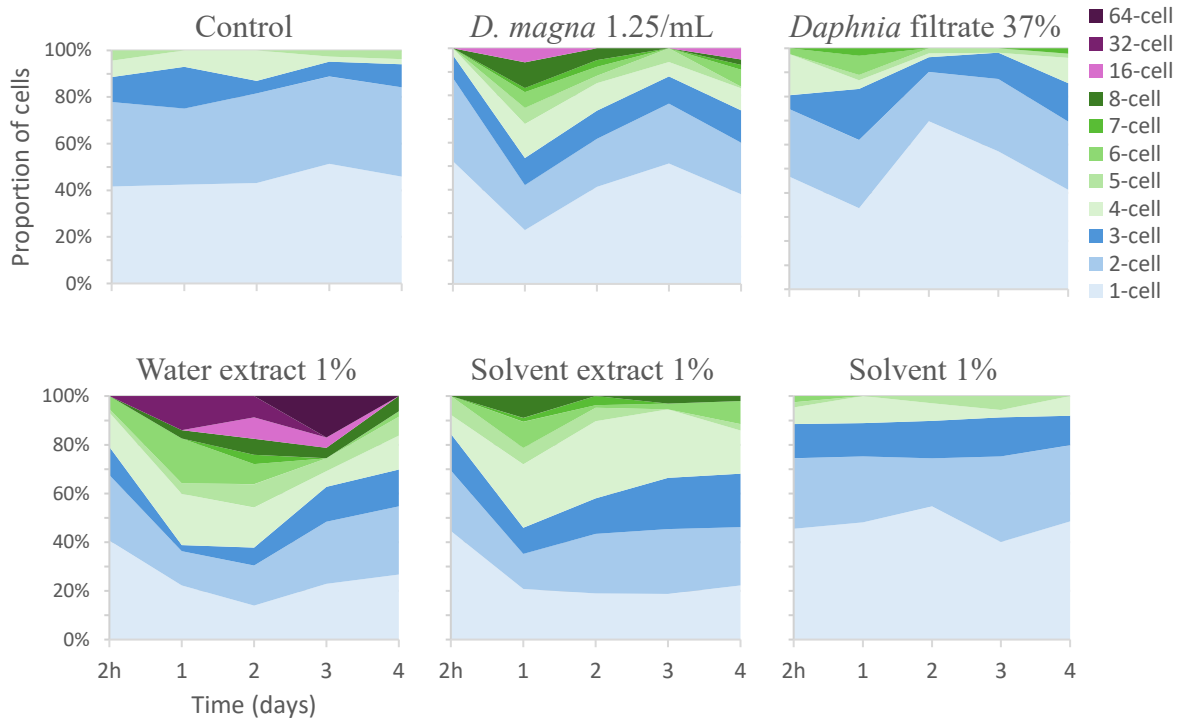

Figure C.7. Proportion of *T. obliquus* cells, single and in colonies, over four days, in the control and cultures treated with live *D. magna* 1.25 mL^{-1}, *D. magna* filtrate 37% v/v, *Daphnia* water extract 1% v/v, *Daphnia* solvent extract 1% v/v, and solvent 1% v/v. Note: these were carried out in triplicate but only sampled from one bioassay culture for analysis.

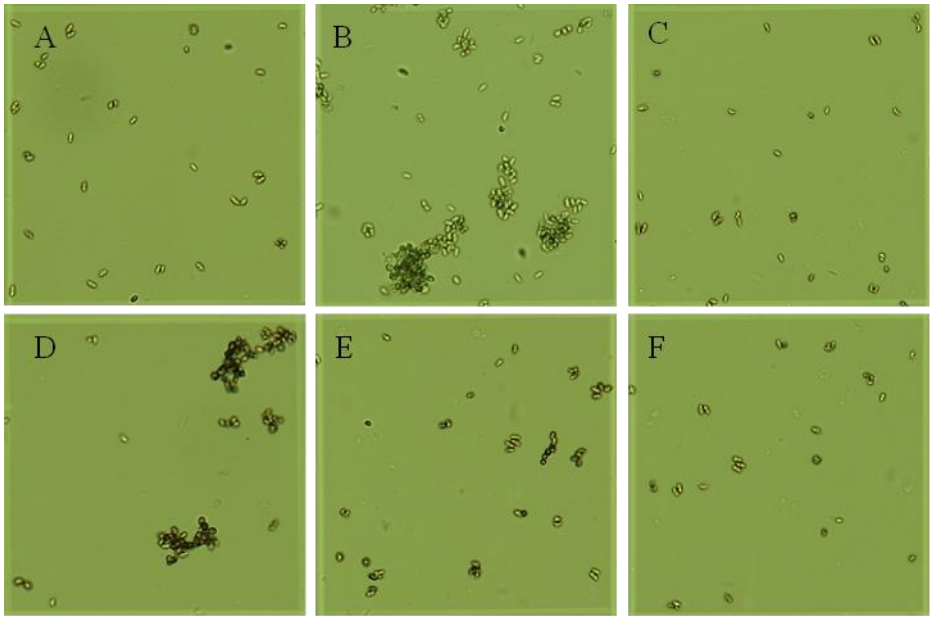

Figure C.8. *T. obliquus* cells imaged in Brightfield at 10× magnification after 48h, in the control (A) and cultures treated with live *D. magna* 1.25 mL^{-1} (B), *D. magna* filtrate 37% (C), *Daphnia* water extract 1% v/v (D), *Daphnia* solvent extract 1% v/v (E), and solvent 1% v/v (F). Scale: each image is 250 × 250 µm.

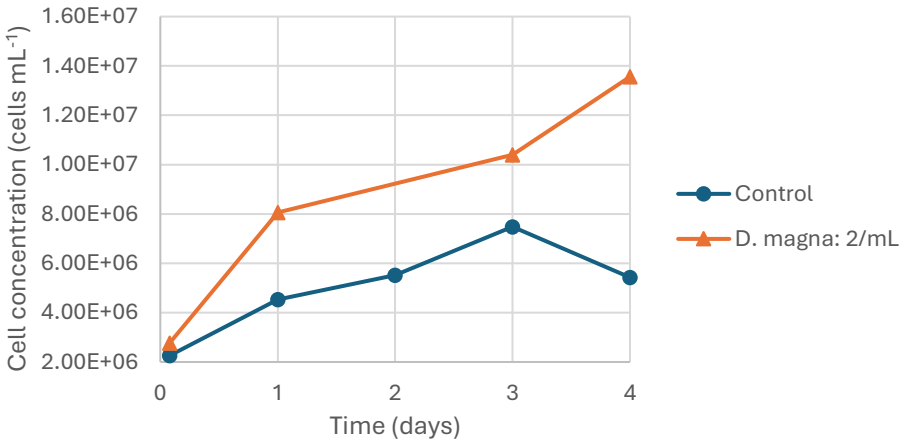

Figure C.9. *T. obliquus* cell concentrations over four days in the control and culture treated with live *D. magna* (2 mL^{-1}). Note: not sampled in replicate.

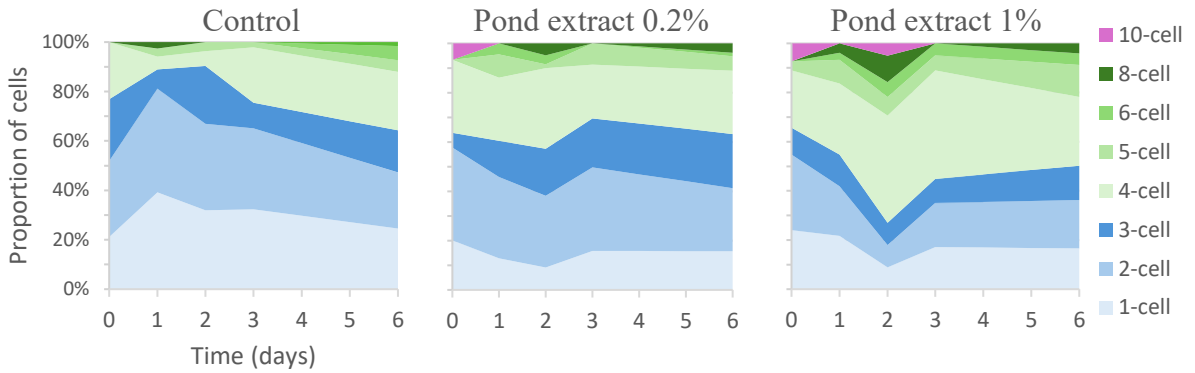

Figure C.10. Proportion of *T. obliquus* cells, single and in colonies, over six days, in the control and cultures treated with pond organism extract at 0.2% v/v and 1% v/v.

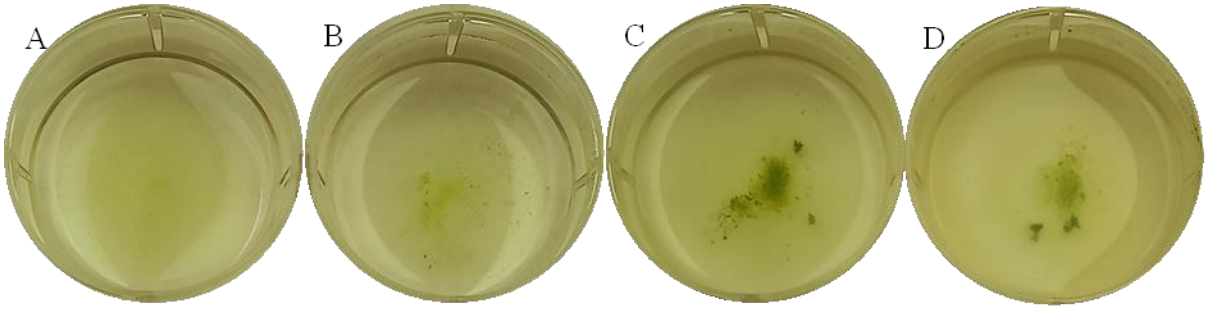

Figure C.11. Photographs of *T. obliquus* bioassay wells, at 24 h, in the control (A), and cultures treated with resuspended frozen extract at 1% v/v (B), 5% v/v (C), and 10% v/v (D).

C.3. *Chlamydomonas reinhardtii*

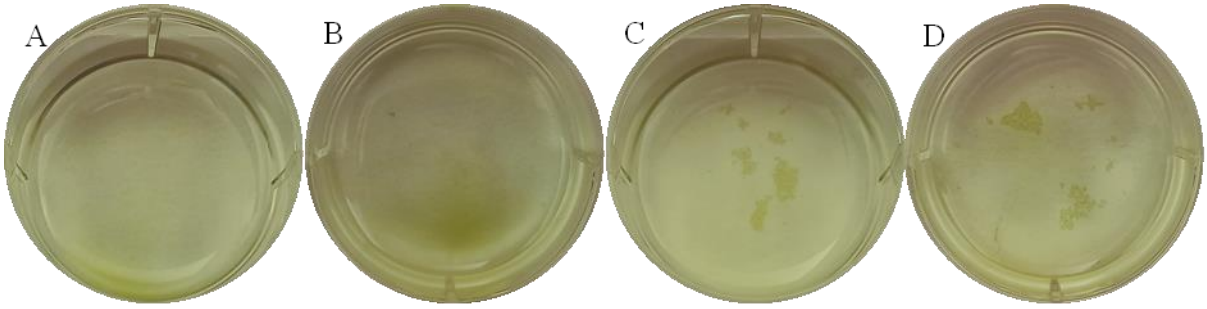

Figure C.12. Photographs of *C. reinhardtii* bioassay wells, at 24 h, in the control (A), and cultures treated with resuspended frozen extract at 1% v/v (B), 5% v/v (C), and 10% v/v (D).

Appendix D. TEM

Samples from the 5% treatment at -0.5 h and 14 h were imaged using a transmission electron microscope (TEM); however, no extracellular matrices, palmelloids/parent cell walls, or flagella were observed, and most of the cells in the prepared samples were individual. It is possible that the colonies present in the sample may have been disrupted by the sample preparation process; consequently, this method was not pursued further.

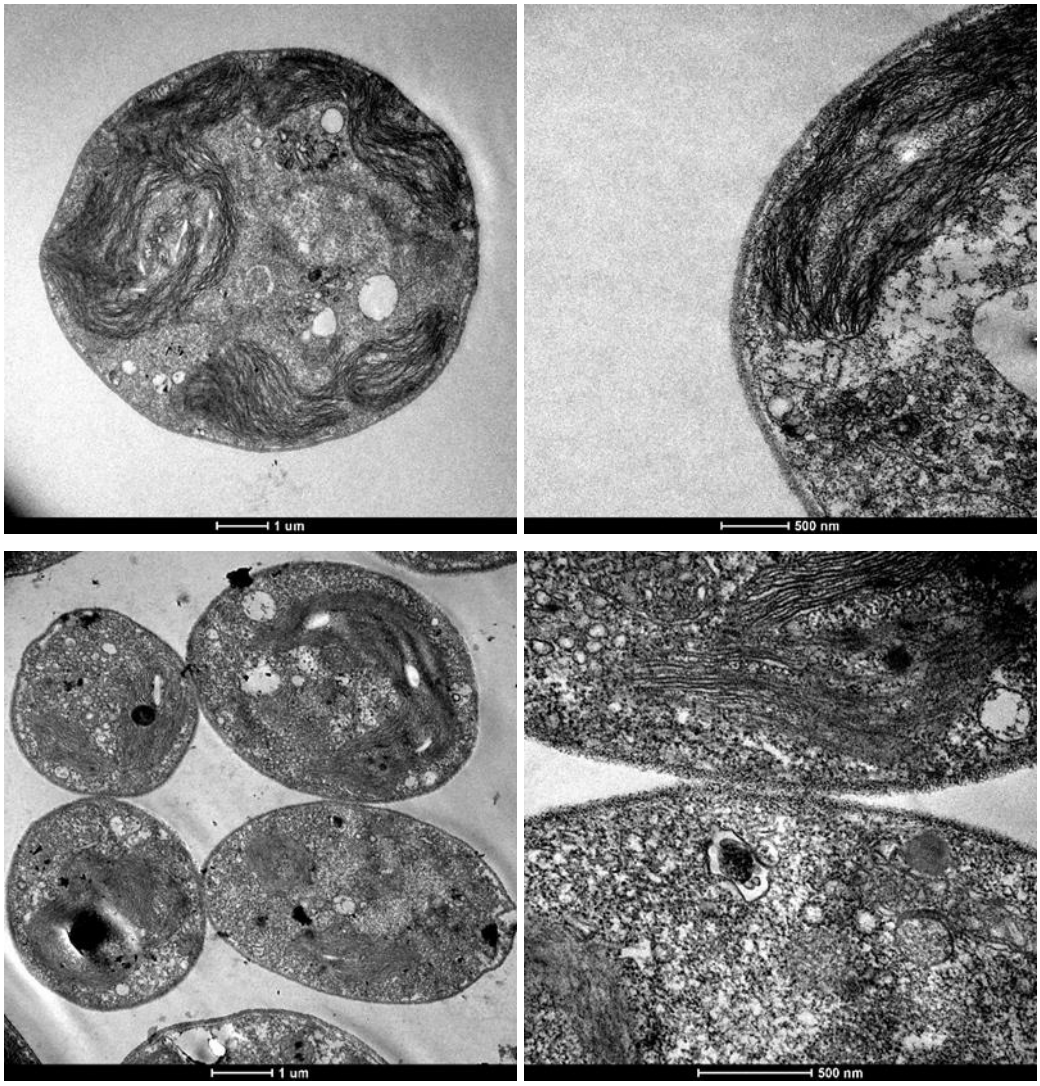

Figure D.1. *C. reinhardtii* cells from the 5% *Daphnia* extract treatment at -0.5 h (top) and 14 h (bottom), imaged under the FEI Tecnai G2 Biotwin transmission electron microscope.

Appendix E. RNA sequencing

E.1. RNA agarose gel and RNA concentration

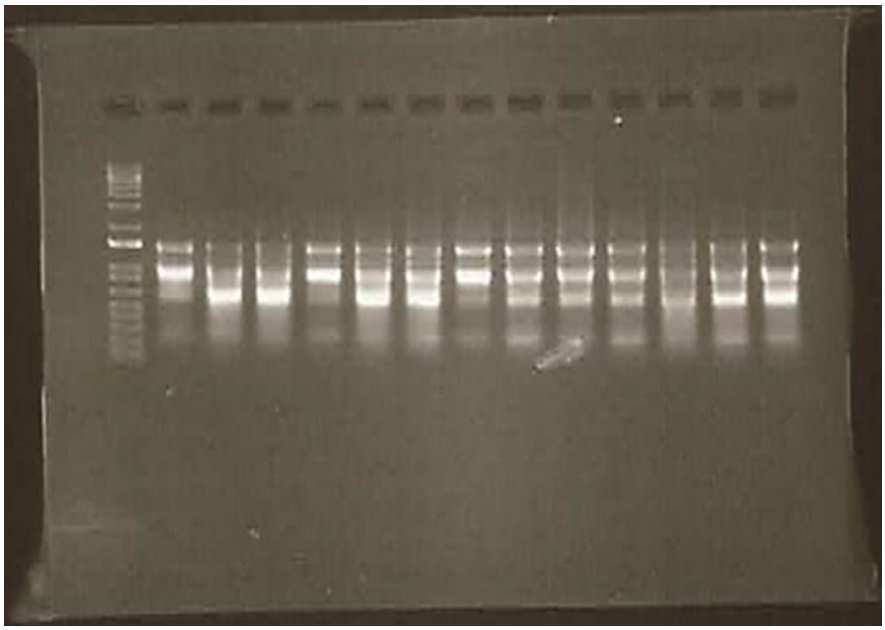

Figure E.1. Agarose gel electrophoresis, on RNA from 15 *C. reinhardtii* treated and control samples.

E.2. RNA concentration

Table E.1. Concentration of extracted *C. reinhardtii* RNA, from nanodrop absorbance readings, and concentration of diluted RNA following drying and resuspension, measured using Qubit fluorometer. Sample names represent Treatment_Time.Replicate, where A = 5% *Daphnia* treatment, B = 10% *Daphnia* treatment, and C = control.

	Nanodrop absorbance following extraction										Qubit	
	Before DNase treatment			After DNase treatment			Concentration	260/230	260/280	Volume used for	Concentration	Amount
Sample	230 nm	260 nm	280 nm	230 nm	260 nm	280 nm	(ng uL^{-1})	ratio	ratio	seq (uL)	(ng µL^{-1})	(µg)
A_1.1	1.035	1.917	0.967	0.954	1.882	0.979	752.8	1.97	1.92	5	73.0	2.19
A_1.2	0.63	1.367	0.62	0.531	1.125	0.541	450	2.12	2.08	10	81.8	2.454
A_1.3	1.139	1.815	0.873	0.703	1.474	0.701	589.6	2.10	2.10	5	52.4	1.572
A_12.1	0.867	1.714	0.803	0.967	1.87	0.96	748	1.93	1.95	5	102.0	3.06
A_12.2	0.751	1.616	0.744	1.079	1.956	1.056	782.4	1.81	1.85	5	124.0	3.72
A_12.3	1.16	1.998	1.105	1.074	1.947	1.041	778.8	1.81	1.87	5	260.0	7.8
A_20.1	0.944	1.802	0.869	1.167	2.001	1.131	800.4	1.71	1.77	5	120.0	3.6
A_20.2	1.36	2.057	1.285	0.995	1.901	0.983	760.4	1.91	1.93	5	123.0	3.69
A20.3	1.616	2.083	1.464	1.376	2.068	1.343	827.2	1.50	1.54	5	98.8	2.964
A_36.1	0.941	1.877	0.931	1.063	1.934	1.025	773.6	1.82	1.89	5	49.4	1.482
A_36.2	1.28	2.03	1.189	1.406	2.062	1.321	824.8	1.47	1.56	5	82.8	2.484
A_36.3	1.05	1.487	0.671	0.86	1.787	0.894	714.8	2.08	2.00	5	46.4	1.392
B_1.1	0.407	0.927	0.422	0.553	1.235	0.577	494	2.23	2.14	10	115.0	3.45
B_1.2	0.741	1.589	0.735	0.774	1.59	0.761	636	2.05	2.09	5	51.4	1.542
B_1.3	0.795	1.667	0.782	0.841	1.693	0.824	677.2	2.01	2.05	5	48.0	1.44
B_12.1	1.397	2.066	1.31	1.344	2.038	1.274	815.2	1.52	1.60	5	104.0	3.12
B_12.2	1.207	1.97	1.044	0.985	1.884	0.956	753.6	1.91	1.97	5	71.8	2.154
B_12.3	1.224	2.027	1.185	1.289	2.034	1.231	813.6	1.58	1.65	5	140.0	4.2

Table E.1. (*Continued*).

	Nanodrop absorbance following extraction										Qubit	
	Before DNase treatment			After DNase treatment			Concentration	260/230	260/280	Volume used for	Concentration	Amount
Sample	230 nm	260 nm	280 nm	230 nm	260 nm	280 nm	(ng uL^{-1})	ratio	ratio	seq (uL)	(ng µL^{-1})	(µg)
B_20.1	1.479	2.067	1.384	1.224	2	1.173	800	1.63	1.71	5	83.8	2.514
B_20.2	1.298	2.053	1.233	1.262	2.011	1.206	804.4	1.59	1.67	5	78.0	2.34
B_20.3	1.064	1.964	1.035	0.917	1.792	0.898	716.8	1.95	2.00	5	55.8	1.674
B_36.1	0.619	1.379	0.623	0.545	1.283	0.557	513.2	2.35	2.30	10	62.0	1.86
B_36.2	1.328	1.96	1.02	1.167	2.003	1.13	801.2	1.72	1.77	5	68.2	2.046
B_36.3	1.117	1.939	0.995	1.027	1.951	1.04	780.4	1.90	1.88	5	68.0	2.04
C_1.1	0.581	1.297	0.585	0.567	1.226	0.566	490.4	2.16	2.17	10	67.4	2.022
C_1.2	0.77	1.47	0.67	0.613	1.324	0.632	529.6	2.16	2.09	5	42.8	1.284
C_1.3	0.691	1.363	0.614	0.556	1.197	0.566	478.8	2.15	2.11	10	64.6	1.938
C_12.1	0.817	1.732	0.815	0.688	1.466	0.697	586.4	2.13	2.10	5	34.2	1.026
C_12.2	0.804	1.479	0.664	0.643	1.395	0.656	558	2.17	2.13	5	37.4	1.122
C_12.3	1.505	2.06	1.226	1.209	2.035	1.231	814	1.68	1.65	5	72.2	2.166
C_20.1	0.945	1.879	0.932	0.811	1.684	0.805	673.6	2.08	2.09	5	65.2	1.956
C_20.2	1.061	1.965	1.026	1	1.903	0.994	761.2	1.90	1.91	5	51.8	1.554
C_20.3	1.655	2.073	1.53	1.187	1.994	1.137	797.6	1.68	1.75	5	83.8	2.514
C_36.1	1.384	2.055	1.318	1.227	2.003	1.166	801.2	1.63	1.72	5	91.8	2.754
C_36.2	1.212	2.023	1.159	1.116	1.972	1.083	788.8	1.77	1.82	5	59.8	1.794
C_36.3	1.19	1.968	1.018	1.075	1.987	1.105	794.8	1.85	1.80	5	49.4	1.482

Appendix F. Validation of RNAseq by RT-qPCR

F.1. RT-qPCR materials and methods

Reverse-transcription quantitative polymerase chain reaction (RT-qPCR) was carried out to estimate gene expression to validate RNA sequencing results. Strongly differentially expressed genes, *MMP13* and *FAP199*, were selected, along with *CBLP* (*RACK1*), which is constitutively expressed in *C. reinhardtii* and therefore was used as the endogenous reference, or 'housekeeping' gene. These genes were tested using RNA extracted from the control and 5% *Daphnia* treatments, at 0 h and 36 h.

RNA concentration and purity were measured using a NanoPhotometer® N60/N50 (Implen GmbH, Munich, Germany). First-strand cDNA synthesis was conducted using 1 µg of total RNA extract with random hexamers, according to the SuperScript™ IV First-Strand Synthesis System (Invitrogen, Auckland, NZ) protocol. Samples were stored at −20 °C until RT-qPCR analyses.

The target positions for the forward and reverse primers were designed manually using Geneious Prime version 2020.2 and RNA transcript sequences from the Phytozome database (matrix metalloproteinase: Phytozome gene identifier Cre03.g144564; lipase-domain containing flagellar-associated protein 199: Phytozome gene identifier Cre09.g399400). For the housekeeping gene (*Chlamydomonas* beta subunit-like polypeptide) forward and reverse primers from Aksoy et al. (2014) were used. RT-qPCR assays were validated by assessing optimal annealing temperatures of the primers, optimal primer concentration, and reaction efficiency using decreasing ten-fold dilutions of cDNA (from 25 ng L^{-1} to 0.0025 ng L^{-1}). Reactions were performed in 20 µL volumes containing 10 µL PowerUp™ SYBR™ Green Master Mix, 7 µL DNase-free water, 1 µL cDNA diluted 1:10, and 1 µL of each primer diluted in the final reaction concentration to 0.5 µM. The PCR conditions were as follows: an initial denaturation at 95 °C for 2 min, followed by 45 cycles: 95 °C for 30 seconds, 60 °C for 30 seconds, and 72 °C for 15 seconds using a QuantStudio Real-Time PCR System (Applied Biosystems). Each sample was analysed in triplicate and included no template control reactions. Data were reported as normalized relative expression (fold change) to control samples. This was done by recording the Ct values and calculating the ΔΔCt value as $2^{-\Delta\Delta Ct}$.

ΔΔCt = ΔCt (treated sample) – ΔCt (control sample) and ΔCt = Ct (gene of interest) – Ct (housekeeping gene).

F.2. RT-qPCR results

RT-qPCR was carried out on two strongly differentially expressed genes, *MMP13* and *FAP199*, on samples from the control and 5% *Daphnia* extract treatments taken at 0 h and 36 h. The $\log_2$-fold change was calculated from the ratio of the quantification cycle values between the 5% treatment and the control and compared against the RNAseq data (**Figure 3.7**). The qPCR and the RNAseq demonstrated similar trends (*MMP13* downregulated and *FAP199* upregulated, at 1 h and 36 h), although there was high variability in the qPCR data. This was due to compounding variability from the target gene values and the housekeeping gene, as some variability was seen between biological and technical replicates (**Figure F.1**).

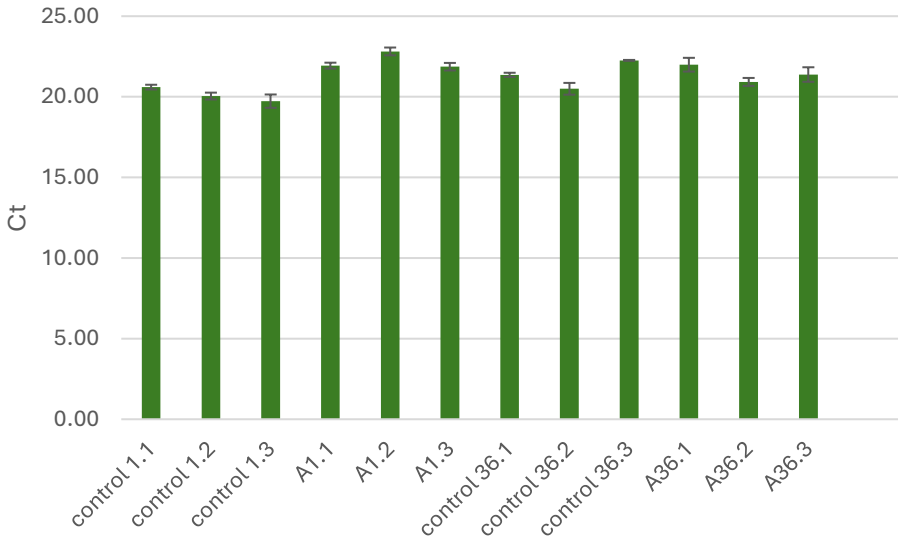

Figure F.1. Quantification cycle (Ct) values for the housekeeping gene, *CBLP*, across the biological and technical replicates. Bars represent individual sample means, with error bars representing the standard deviation. Control is the control treatment and A is the 5% *Daphnia* extract treatment; 1 and 36 are the timepoints samples (h), and 1–3 are the biological replicates.

Appendix G. Self-aggregation experimental data.

G.1. Optical density

Table G.1. Raw data – Optical density in 5% *Daphnia* treatment (A), 10% *Daphnia* treatment (B), and control (C).

	Optical density											
Time (h)		-0.5	0	1	2	12	14	16	20	24	36	42	48
Flask	A1	0.27	0.327	0.32	0.35	0.509	0.59	0.67	0.791	1.04	1.416	1.532	1.444
	A2	0.381	0.265	0.294	0.31	0.509	0.491	0.596	0.68	0.876	1.382	1.452	1.456
	A3	0.443	0.359	0.38	0.38	0.661	0.692	0.765	0.919	1.058	1.488	1.564	1.574
	B1	0.36	0.361	0.373	0.355	0.616	0.638	0.783	0.925	1.16	1.338	1.414	
	B2	0.312	0.292	0.305	0.27	0.506	0.499	0.62	0.712	0.928	1.312	1.376	
	B3	0.365	0.344	0.348	0.365	0.58	0.596	0.705	0.777	0.977	1.34	1.438	
	C1	0.319	0.353	0.328	0.315	0.47	0.545	0.655	0.626	0.89	1.346	1.4	1.456
	C2	0.339	0.37	0.344	0.328	0.544	0.611	0.65	0.715	1.02	1.348	1.526	1.526
	C3	0.413	0.36	0.378	0.356	0.626	0.595	0.703	0.67	0.992	1.236	1.34	1.738
Mean	A	0.365	0.317	0.331	0.347	0.560	0.591	0.677	0.797	0.991	1.429	1.516	1.491
SE		0.051	0.028	0.025	0.02	0.051	0.058	0.049	0.069	0.058	0.031	0.033	0.041
Mean	B	0.346	0.332	0.342	0.33	0.567	0.578	0.703	0.805	1.022	1.33	1.409	
SE		0.017	0.021	0.02	0.03	0.032	0.041	0.047	0.063	0.071	0.009	0.018	
Mean	C	0.357	0.361	0.35	0.333	0.547	0.584	0.669	0.67	0.967	1.31	1.422	1.573
SE		0.029	0.005	0.015	0.012	0.045	0.02	0.017	0.026	0.040	0.037	0.055	0.085

G.2. Cell concentration

Table G.2. Raw data – cell concentration, in cells per mL, in 5% *Daphnia* treatment (A), 10% *Daphnia* treatment (B), and control (C).

		Cell concentration (cells mL^{-1})											
Time (h)		-0.5	0	1	2	12	14	16	20	24	36	42	48
Flask	A1	1329082	528061	1650510	1415816	3275510	4076531	4686224	4778061	5548469	9604592	10030612	7522959
	A2	1033163	183673	928571	1280612	1857143	3066327	1760204	3135204	3739796	5165816	7994898	5117347
	A3	1408163	1022959	1788265	1918367	2005102	3806122	3609694	6000000	9025510	4459184	8400510	7892857
	B1	1058673	653061	1890306	954082	3400510	4109694	4778061	7081633	8117347	7446429	7785714	
	B2	1140306	426020	829082	974490	1071429	2701531	3989796	4140306	4885204	4283163	4941327	
	B3	1278061	762755	1237245	770408	2015306	2750000	4147959	3443878	4066327	7423469	6852041	
	C1	497449	724490	1170918	1058673	2801020	2198980	3191327	3066327	4520408	6028061	5122449	4956633
	C2	997449	635204	959184	941327	2099490	2436224	2704082	2966837	3589286	5007653	5660714	4727041
	C3	1147959	897959	1265306	982143	1750000	2507653	3408163	3061224	3545918	4724490	5071429	4168367
Mean	A	1256803	578231	1455782	1538265	2379252	3649660	3352041	4637755	6104592	6409864	8808673	6844388
SE		114126	243576	266588	194017	450160	301932	854437	829966	1550983	1610336	622088	870097
Mean	B	1159014	613946	1318878	899660	2162415	3187075	4305272	4888605	5689626	6384354	6526361	
SE		64019	99155	309056	64894	676359	461522	240763	1114791	1236664	1050616	837095	
Mean	C	880952	752551	1131803	994048	2216837	2380952	3101190	3031463	3885204	5253401	5284864	4617347
SE		196613	77138	90508	34394	309025	93294	208188	32346	317849	395861	188501	234069

G.3. pH

Table G.3. Raw data – pH in 5% *Daphnia* treatment (A), 10% *Daphnia* treatment (B), and control (C).

	pH											
Time (h)		-0.5	0	1	2	12	14	16	20	24	36	42	48
Flask	A1	7.65	7.64	7.65	7.66	7.88	7.88	7.87	7.95	8.08	8.36	8.32	8.39
	A2	7.66	7.62	7.61	7.68	7.86	7.86	7.86	7.92	8.05	8.34	8.30	8.39
	A3	7.69	7.65	7.67	7.72	7.92	7.91	7.91	8.01	8.10	8.37	8.35	8.38
	B1	7.69	7.61	7.65	7.63	7.89	7.88	7.90	7.96	8.09	8.35	8.34	
	B2	7.65	7.59	7.61	7.65	7.82	7.84	7.83	7.91	8.04	8.33	8.27	
	B3	7.68	7.61	7.66	7.64	7.83	7.86	7.88	7.95	8.05	8.33	8.27	
	C1	7.67	7.69	7.71	7.70	7.90	7.88	7.88	7.97	8.08	8.29	8.31	8.40
	C2	7.70	7.65	7.69	7.69	7.89	7.92	7.92	7.97	8.08	8.31	8.33	8.42
	C3	7.71	7.71	7.71	7.71	7.93	7.93	7.91	8.00	8.12	8.31	8.33	8.40
Mean	A	7.67	7.64	7.64	7.69	7.89	7.88	7.88	7.96	8.08	8.36	8.32	8.39
SE		0.01	0.01	0.02	0.02	0.02	0.01	0.02	0.03	0.01	0.01	0.01	0.00
Mean	B	7.67	7.60	7.64	7.64	7.85	7.86	7.87	7.94	8.06	8.34	8.29	
SE		0.01	0.01	0.02	0.01	0.02	0.01	0.02	0.02	0.02	0.01	0.02	
Mean	C	7.69	7.68	7.70	7.70	7.91	7.91	7.90	7.98	8.09	8.30	8.32	8.41
SE		0.01	0.02	0.01	0.01	0.01	0.02	0.01	0.01	0.01	0.01	0.01	0.01

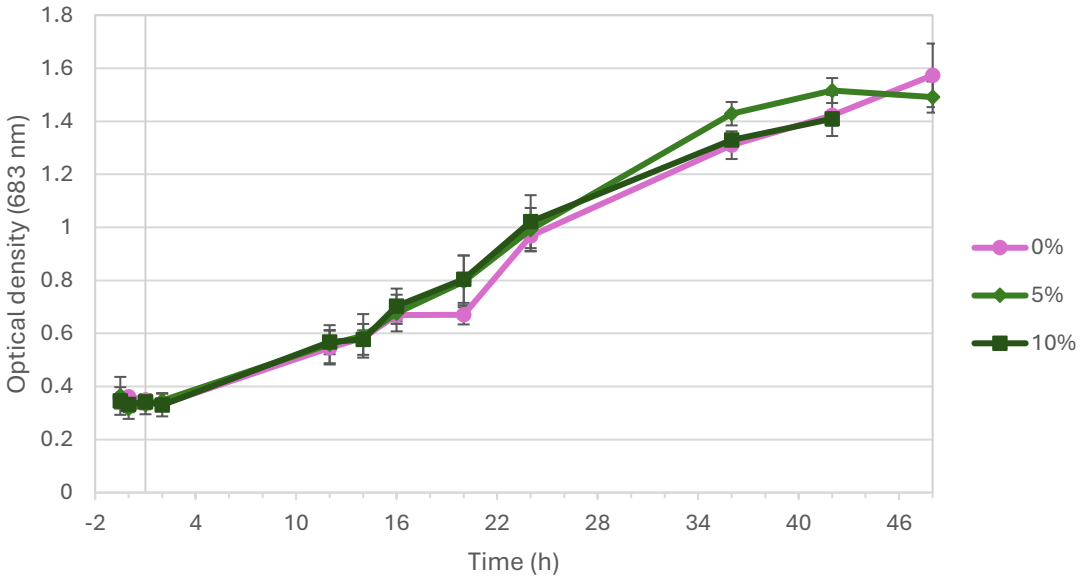

Figure G.1. Optical density of the 5% and 10% *Daphnia* extract treatments and the control. Error bars represent the standard errors ($N = 3$).

G.4. Mean colony size

Table G.4. Raw data – mean colony size, in average number of cells per colony, in 5% *Daphnia* treatment (A), 10% *Daphnia* treatment (B), and control (C).

		Mean colony size (number of cells per colony)										
Time (h)		-0.5	0	1	2	12	14	16	20	24	36	42
Flask	A1	1.0611	1.1500	1.1492	1.1034	1.9603	2.2412	2.3020	2.2869	1.9612	1.6853	1.5817
	A2	1.0465	1.4400	1.2133	1.2184	1.9676	2.2679	2.4820	2.4629	1.7494	1.5411	1.5546
	A3	1.0636	1.5305	1.6115	1.3333	1.8322	2.4992	2.5268	2.8337	3.1505	1.3721	1.4513
	B1	1.0950	1.1852	1.2350	1.1873	2.0699	2.4633	2.6306	2.4480	2.9906	3.2578	3.1660
	B2	1.0347	1.0637	1.1444	1.1105	2.1212	2.5956	2.6067	2.1992	2.8412	2.2628	2.2896
	B3	1.0351	1.3591	1.1659	1.1439	1.6844	1.7672	2.2773	1.9231	2.1001	2.5729	2.3276
	C1	1.0428	1.1181	1.0432	1.0668	1.3987	1.1744	1.1130	1.0713	1.0649	1.1136	1.0524
	C2	1.1045	1.0289	1.0621	1.0365	1.3832	1.1437	1.2802	1.0680	1.0675	1.0827	1.0384
	C3	1.1111	1.4606	1.3589	1.1257	1.1787	1.2934	1.3360	1.0840	1.0842	1.1231	1.1081
Mean	A	1.0571	1.3735	1.3247	1.2184	1.9200	2.3361	2.4369	2.5279	2.2870	1.5328	1.5292
SE		0.0053	0.1148	0.1446	0.0664	0.0440	0.0819	0.0687	0.1612	0.4360	0.0905	0.0397
Mean	B	1.0549	1.2027	1.1817	1.1472	1.9585	2.2754	2.5049	2.1901	2.6440	2.6979	2.5944
SE		0.0200	0.0857	0.0273	0.0222	0.1378	0.2569	0.1140	0.1516	0.2753	0.2939	0.2860
Mean	C	1.0861	1.2025	1.1547	1.0764	1.3202	1.2038	1.2431	1.0744	1.0722	1.1065	1.0663
SE		0.0218	0.1316	0.1022	0.0262	0.0709	0.0457	0.0670	0.0049	0.0061	0.0122	0.0213

G.5. Proportion of single cells, and cells in pairs and in colonies

Table G.5. Raw data – proportion of single cells, in 5% *Daphnia* treatment (A), 10% *Daphnia* treatment (B), and control (C).

		Proportion of cells which are single										
Time (h)		-0.5	0	1	2	12	14	16	20	24	36	42
Flask	A1	0.9155	0.8068	0.8114	0.8595	0.3474	0.2691	0.2564	0.2483	0.3444	0.4513	0.5041
	A2	0.9309	0.5833	0.7527	0.7530	0.3516	0.2596	0.2058	0.2075	0.4243	0.5358	0.5175
	A3	0.9058	0.5212	0.4779	0.6463	0.3842	0.2091	0.2113	0.1565	0.1029	0.6121	0.5700
	B1	0.8699	0.7734	0.7274	0.7754	0.3128	0.2228	0.1853	0.2205	0.1163	0.0928	0.1094
	B2	0.9463	0.9162	0.8277	0.8639	0.3143	0.2106	0.1905	0.2693	0.1520	0.2734	0.2762
	B3	0.9401	0.6388	0.7979	0.8212	0.4557	0.4193	0.2583	0.3556	0.2986	0.2055	0.2569
	C1	0.9282	0.8521	0.9259	0.8892	0.6175	0.7958	0.8529	0.8985	0.9029	0.8451	0.9143
	C2	0.8721	0.9518	0.9149	0.9295	0.6233	0.8220	0.6906	0.9020	0.9005	0.8767	0.9360
	C3	0.8578	0.5682	0.6290	0.8338	0.7872	0.6846	0.6497	0.8783	0.8719	0.8326	0.8521
Mean	A	0.9174	0.6371	0.6807	0.7529	0.3611	0.2459	0.2245	0.2041	0.2905	0.5331	0.5305
SE		0.0073	0.0867	0.1028	0.0615	0.0116	0.0186	0.0160	0.0266	0.0966	0.0465	0.0201
Mean	B	0.9188	0.7761	0.7843	0.8202	0.3609	0.2842	0.2114	0.2818	0.1890	0.1906	0.2142
SE		0.0245	0.0801	0.0297	0.0255	0.0474	0.0676	0.0235	0.0395	0.0558	0.0526	0.0527
Mean	C	0.8860	0.7907	0.8233	0.8842	0.6760	0.7675	0.7311	0.8929	0.8918	0.8515	0.9008
SE		0.0215	0.1149	0.0972	0.0278	0.0556	0.0421	0.0621	0.0074	0.0099	0.0131	0.0251

Table G.6. Raw data – proportion of cells in pairs, in 5% *Daphnia* treatment (A), 10% *Daphnia* treatment (B), and control (C).

		Proportion of cells in pairs										
Time (h)		-0.5	0	1	2	12	14	16	20	24	36	42
Flask	A1	0.0230	0.0580	0.0464	0.0468	0.0545	0.0401	0.0359	0.0406	0.0395	0.0388	0.0351
	A2	0.0296	0.0278	0.0385	0.0239	0.0440	0.0416	0.0348	0.0472	0.0437	0.0533	0.0421
	A3	0.0435	0.0499	0.0542	0.0612	0.0611	0.0429	0.0367	0.0340	0.0300	0.0881	0.0595
	B1	0.0434	0.0547	0.0567	0.0428	0.0660	0.0372	0.0395	0.0187	0.0277	0.0178	0.0177
	B2	0.0268	0.0120	0.0123	0.0105	0.0381	0.0227	0.0524	0.0431	0.0251	0.0262	0.0279
	B3	0.0439	0.0268	0.0371	0.0331	0.0582	0.0390	0.0381	0.0281	0.0439	0.0261	0.0343
	C1	0.0513	0.0211	0.0566	0.0819	0.0255	0.0278	0.0384	0.0383	0.0474	0.0567	0.0578
	C2	0.0051	0.0321	0.0213	0.0705	0.0462	0.0314	0.0566	0.0396	0.0455	0.0642	0.0442
	C3	0.0267	0.0341	0.0565	0.0519	0.0321	0.0387	0.0539	0.0550	0.0734	0.0637	0.0533
Mean	A	0.0320	0.0452	0.0463	0.0440	0.0532	0.0415	0.0358	0.0406	0.0377	0.0601	0.0456
SE		0.0060	0.0090	0.0045	0.0109	0.0050	0.0008	0.0006	0.0038	0.0041	0.0146	0.0073
Mean	B	0.0380	0.0311	0.0354	0.0288	0.0541	0.0330	0.0434	0.0300	0.0322	0.0234	0.0266
SE		0.0056	0.0125	0.0128	0.0096	0.0083	0.0052	0.0046	0.0071	0.0059	0.0028	0.0048
Mean	C	0.0277	0.0291	0.0448	0.0681	0.0346	0.0326	0.0496	0.0443	0.0554	0.0615	0.0518
SE		0.0133	0.0040	0.0118	0.0087	0.0061	0.0032	0.0057	0.0054	0.0090	0.0024	0.0040

Table G.7. Raw data – proportion of cells in four-celled colonies, in 5% *Daphnia* treatment (A), 10% *Daphnia* treatment (B), and control (C).

		Proportion of cells in four-celled colonies										
Time (h)		-0.5	0	1	2	12	14	16	20	24	36	42
Flask	A1	0.0614	0.1353	0.1422	0.0937	0.4860	0.5657	0.5727	0.6385	0.5499	0.4781	0.4283
	A2	0.0395	0.3889	0.2088	0.2231	0.4725	0.5857	0.6783	0.6542	0.4720	0.3121	0.4020
	A3	0.0507	0.4289	0.4565	0.2926	0.4936	0.6086	0.5767	0.6361	0.7292	0.2815	0.3462
	B1	0.0867	0.1719	0.2159	0.1818	0.4771	0.5760	0.6257	0.6715	0.7781	0.7633	0.7208
	B2	0.0268	0.0719	0.1600	0.1257	0.4571	0.5401	0.5780	0.6235	0.6768	0.5527	0.5059
	B3	0.0160	0.3344	0.1649	0.1457	0.3848	0.4750	0.5904	0.5867	0.5872	0.6282	0.5719
	C1	0.0205	0.1268	0.0174	0.0289	0.3206	0.1578	0.1023	0.0632	0.0497	0.0982	0.0279
	C2	0.1228	0.0161	0.0638	0.0000	0.2819	0.1466	0.2453	0.0585	0.0540	0.0591	0.0198
	C3	0.1156	0.3977	0.3145	0.1143	0.1808	0.2767	0.2784	0.0667	0.0547	0.1037	0.0946
Mean	A	0.0506	0.3177	0.2692	0.2031	0.4840	0.5867	0.6092	0.6429	0.5837	0.3572	0.3922
SE		0.0063	0.0919	0.0956	0.0583	0.0062	0.0124	0.0345	0.0057	0.0761	0.0611	0.0242
Mean	B	0.0432	0.1927	0.1803	0.1511	0.4397	0.5304	0.5980	0.6272	0.6807	0.6481	0.5995
SE		0.0220	0.0765	0.0179	0.0164	0.0280	0.0296	0.0143	0.0245	0.0552	0.0616	0.0636
Mean	C	0.0863	0.1802	0.1319	0.0477	0.2611	0.1937	0.2087	0.0628	0.0528	0.0870	0.0474
SE		0.0329	0.1134	0.0923	0.0343	0.0417	0.0416	0.0540	0.0024	0.0016	0.0140	0.0237

Table G.8. Raw data – proportion of cells in eight-celled colonies, in 5% *Daphnia* treatment (A), 10% *Daphnia* treatment (B), and control (C).

		Proportion of cells in eight-celled colonies										
Time (h)		-0.5	0	1	2	12	14	16	20	24	36	42
Flask	A1					0.1121	0.1252	0.1350	0.0726	0.0662	0.0191	0.0244
	A2					0.1319	0.1131	0.0812	0.0911	0.0600	0.0356	0.0281
	A3			0.0114		0.0611	0.1394	0.1753	0.1531	0.1379	0.0183	0.0194
	B1					0.1440	0.1639	0.1495	0.0836	0.0779	0.1041	0.1258
	B2					0.1905	0.2266	0.1790	0.0641	0.1462	0.1286	0.1322
	B3					0.1013	0.0668	0.1132	0.0296	0.0703	0.0687	0.0655
	C1					0.0364	0.0186	0.0064				
	C2					0.0486		0.0075				
	C3							0.0180				
Mean	A			0.0038		0.1017	0.1259	0.1305	0.1056	0.0881	0.0243	0.0240
SE				0.0038		0.0211	0.0076	0.0273	0.0243	0.0250	0.0056	0.0025
Mean	B					0.1453	0.1524	0.1472	0.0591	0.0981	0.1005	0.1078
SE						0.0258	0.0465	0.0190	0.0158	0.0241	0.0174	0.0212
Mean	C					0.0283	0.0062	0.0106				
SE						0.0146	0.0062	0.0037				

Table G.9. Raw data – proportion of cells in 16-celled colonies, in 5% *Daphnia* treatment (A), 10% *Daphnia* treatment (B), and control (C).

		Proportion of cells in 16-celled colonies										
Time (h)		-0.5	0	1	2	12	14	16	20	24	36	42
Flask	A1										0.0127	0.0081
	A2										0.0632	0.0102
	A3								0.0204			0.0049
	B1								0.0058		0.0219	0.0262
	B2										0.0191	0.0578
	B3										0.0715	0.0715
	C1											
	C2											
	C3											
Mean	A								0.0068		0.0253	0.0077
SE									0.0068		0.0193	0.0016
Mean	B								0.0019		0.0375	0.0518
SE									0.0019		0.0170	0.0134
Mean	C											
SE												

Table G.10. Raw data – proportion of cells in colonies, in 5% *Daphnia* treatment (A), 10% *Daphnia* treatment (B), and control (C).

		Proportion of cells in 4, 8, or 16-celled colonies										
Time (h)		-0.5	0	1	2	12	14	16	20	24	36	42
Flask	A1	0.0614	0.1353	0.1422	0.0937	0.5981	0.6909	0.7077	0.7112	0.6161	0.5100	0.4608
	A2	0.0395	0.3889	0.2088	0.2231	0.6044	0.6988	0.7594	0.7453	0.5321	0.4109	0.4403
	A3	0.0507	0.4289	0.4679	0.2926	0.5547	0.7480	0.7519	0.8095	0.8672	0.2998	0.3705
	B1	0.0867	0.1719	0.2159	0.1818	0.6212	0.7399	0.7752	0.7608	0.8561	0.8893	0.8729
	B2	0.0268	0.0719	0.1600	0.1257	0.6476	0.7668	0.7570	0.6876	0.8230	0.7004	0.6959
	B3	0.0160	0.3344	0.1649	0.1457	0.4861	0.5417	0.7036	0.6163	0.6575	0.7684	0.7089
	C1	0.0205	0.1268	0.0174	0.0289	0.3570	0.1763	0.1087	0.0632	0.0497	0.0982	0.0279
	C2	0.1228	0.0161	0.0638	0.0000	0.3305	0.1466	0.2528	0.0585	0.0540	0.0591	0.0198
	C3	0.1156	0.3977	0.3145	0.1143	0.1808	0.2767	0.2964	0.0667	0.0547	0.1037	0.0946
Mean	A	0.0506	0.3177	0.2730	0.2031	0.5857	0.7126	0.7397	0.7553	0.6718	0.4069	0.4239
SE		0.0063	0.0919	0.0993	0.0583	0.0156	0.0179	0.0161	0.0288	0.1007	0.0607	0.0273
Mean	B	0.0432	0.1927	0.1803	0.1511	0.5850	0.6828	0.7453	0.6882	0.7788	0.7860	0.7592
SE		0.0220	0.0765	0.0179	0.0164	0.0500	0.0710	0.0215	0.0417	0.0614	0.0552	0.0569
Mean	C	0.0863	0.1802	0.1319	0.0477	0.2894	0.1999	0.2193	0.0628	0.0528	0.0870	0.0474
SE		0.0329	0.1134	0.0923	0.0343	0.0549	0.0394	0.0567	0.0024	0.0016	0.0140	0.0237

G.6. Concentration of single cells

Table G.11. Raw data – single cell concentration, in cells per mL, in 5% *Daphnia* treatment (A), 10% *Daphnia* treatment (B), and control (C).

		Concentration of single cells (single cells per mL)										
Time (h)		-0.5	0	1	2	12	14	16	20	24	36	42
Flask	A1	1192500	417500	1312500	1192500	1115000	1075000	1177500	1162500	1872500	4247500	4955000
	A2	942500	105000	685000	945000	640000	780000	355000	637500	1555000	2712500	4055000
	A3	1250000	522500	837500	1215000	755000	780000	747500	920000	910000	2675000	4692500
	B1	902500	495000	1347500	725000	1042500	897500	867500	1530000	925000	677500	835000
	B2	1057500	382500	672500	825000	330000	557500	745000	1092500	727500	1147500	1337500
	B3	1177500	477500	967500	620000	900000	1130000	1050000	1200000	1190000	1495000	1725000
	C1	452500	605000	1062500	922500	1695000	1715000	2667500	2700000	4000000	4992500	4590000
	C2	852500	592500	860000	857500	1282500	1962500	1830000	2622500	3167500	4302500	5192500
	C3	965000	500000	780000	802500	1350000	1682500	2170000	2635000	3030000	3855000	4235000
Mean	A	1128333	348333	945000	1117500	836667	878333	760000	906667	1445833	3211667	4567500
SE		94388	125386	188950	86494	143071	98333	237518	151701	283160	518030	267219
Mean	B	1045833	451667	995833	723333	757500	861667	887500	1274167	947500	1106667	1299167
SE		79600	34950	195370	59184	217672	166235	88612	131627	133985	236873	257635
Mean	C	756667	565833	900833	860833	1442500	1786667	2222500	2652500	3399167	4383333	4672500
SE		155512	33114	84068	34681	127745	88416	243186	24023	303028	330846	279467

G.7. Concentration of colonies

Table G.12. Raw data – colony concentration (4, 8 and 16-celled colonies), in colonies per mL, in 5% *Daphnia* treatment (A), 10% *Daphnia* treatment (B), and control (C).

		Concentration of colonies (colonies per mL)										
Time (h)		-0.5	0	1	2	12	14	16	20	24	36	42
Flask	A1	20000	17500	57500	32500	435000	627500	735000	790000	792500	1155000	1087500
	A2	10000	17500	47500	70000	245000	482500	310000	537500	460000	437500	820000
	A3	17500	107500	202500	137500	257500	632500	587500	1055000	1765000	317500	735000
	B1	22500	27500	100000	42500	457500	662500	820000	1240000	1625000	1497500	1507500
	B2	7500	7500	32500	30000	145000	432500	652500	665000	897500	652500	710000
	B3	5000	62500	50000	27500	215000	342500	657500	507500	620000	1237500	1045000
	C1	2500	22500	5000	7500	232500	90000	82500	47500	55000	145000	35000
	C2	30000	2500	15000	0	157500	87500	165000	42500	47500	72500	27500
	C3	32500	87500	97500	27500	77500	170000	240000	50000	47500	120000	117500
Mean	A	15833	47500	102500	80000	312500	580833	544167	794167	1005833	636667	880833
SE		3005	30000	50083	30721	61356	49188	124585	149404	391531	261472	106207
Mean	B	11667	32500	60833	33333	272500	479167	710000	804167	1047500	1129167	1087500
SE		5465	16073	20224	4640	94681	95277	55019	222609	299656	249872	231197
Mean	C	21667	37500	39167	11667	155833	115833	162500	46667	50000	112500	60000
SE		9610	25658	29309	8207	44752	27093	45484	2205	2500	21262	28831

Appendix H. Self-aggregation experiment statistical analyses results

H.1. Data transformations, and Shapiro-Wilk and Levene's test results

Table H.1. Shapiro-Wilk normality test results for residuals of two-way ANOVA model across all measured parameters. *P*-values above 0.05 indicate no significant deviation from normality; adjusted *p*-values used the Benjamini-Hochberg correction to control false discover rate across multiple tests. Where necessary, data was transformed to improve normality, as indicated.

Parameter	Shapiro *p* (raw)	Transformation	Shapiro *p*	*p* adj
Cell concentration	1.11E-05	Cube root	0.135374	0.291104
pH	0.138512	log1p	0.207932	0.291104
Mean colony size (MCS)	1.54E-05	Box-Cox (lambda=-1)	0.119802	0.291104
Proportion of cells single	0.080257	log1p	0.142138	0.291104
Proportion cells in colonies	0.168591	Raw	0.168591	0.291104
Single cell concentration	0.049026	Square root	0.795682	0.795682
Colony concentration	1.14E-08	Cube root	0.468376	0.546438

Table H.2. Levene's test results assessing homogeneity of variances across treatment and time combinations for each parameter. *P*-values above 0.05 suggest equal variances, meeting the ANOVA assumption of variance homogeneity; adjusted *p*-values used the Benjamini-Hochberg correction to control false discover rate across multiple tests.

Parameter	statistic	*p* value	df	df.residual	*p* adj
Cell concentration	0.736873	0.82709	32	66	0.99981
pH	0.301215	0.99981	32	66	0.99981
Mean colony size (MCS)	0.622502	0.928595	32	66	0.99981
Proportion of cells single	0.609068	0.937243	32	66	0.99981
Proportion cells in colonies	0.676834	0.88643	32	66	0.99981
Single cell concentration	0.499083	0.983392	32	66	0.99981
Colony concentration	0.535810	0.972489	32	66	0.99981

H.2. Two-way ANOVA

Table H.3. Summary of two-way ANOVA results showing effects of treatment, time, and their interaction on each (transformed) measured *C. reinhardtii* parameter. *p*-values and BH adjusted *p*-values are reported for each main effect and interaction term. Statistically significant results ($p < 0.05$) are bolded.

Parameter	Term	df	df residual	statistic	*p* value	*p* adj
Cell concentration	Treatment	2	66	6.8741	0.001942	0.001942
	Time	10	66	57.6029	1.08E-28	3.78E-28
	Treatment:Time	20	66	0.8855	0.605050	0.605050
pH	Treatment	2	66	81.3577	1.54E-18	2.70E-18
	Time	10	66	36.0367	6.30E-23	1.10E-22
	Treatment:Time	20	66	4.7739	7.20E-07	1.01E-06
Mean colony size	Treatment	2	66	163.5714	2.66E-26	9.31E-26
	Time	10	66	32.7375	8.46E-22	8.46E-22
	Treatment:Time	20	66	9.8596	5.45E-13	9.54E-13
Proportion of cells single	Treatment	2	66	166.7510	1.57E-26	9.31E-26
	Time	10	66	34.7972	1.63E-22	2.29E-22
	Treatment:Time	20	66	10.0356	3.65E-13	8.52E-13
Proportion of cells in colonies	Treatment	2	66	21.7334	5.61E-08	6.54E-08
	Time	10	66	886.0057	3.02E-66	2.12E-65
	Treatment:Time	20	66	1.6093	0.076871	0.089683
Single cell concentration	Treatment	2	66	77.7081	4.50E-18	6.30E-18
	Time	10	66	49.3825	9.29E-27	2.17E-26
	Treatment:Time	20	66	10.5025	1.29E-13	8.52E-13
Colony concentration	Treatment	2	66	158.4591	6.35E-26	1.48E-25
	Time	10	66	33.5908	4.24E-22	4.94E-22
	Treatment:Time	20	66	10.2038	2.50E-13	8.52E-13

H.3. Post-hoc Tukey HSD pairwise comparisons

Table H.4. Pairwise comparisons of estimated means for cell concentration, from Tukey's HSD post-hoc test following two-way ANOVA. A = 5% *Daphnia* extract treatment; B = 10% *Daphnia* extract treatment; C = control. *p*-values reflect adjusted significant levels for multiple comparisons; statistically significant results ($p < 0.05$) are bolded.

Parameter	Time	Contrast	Estimate	SE	df	t ratio	*p* value
Cell concentration	-0.5h	A - B	97789.12	894225.5	66	0.109356	1
		A - C	375850.3	894225.5	66	0.420308	1
		B - C	278061.2	894225.5	66	0.310952	1
	0 h	A - B	-35714.3	894225.5	66	-0.03994	1
		A - C	-174320	894225.5	66	-0.19494	1
		B - C	-138605	894225.5	66	-0.155	1
	1 h	A - B	136904.8	894225.5	66	0.153099	1
		A - C	323979.6	894225.5	66	0.362302	1
		B - C	187074.8	894225.5	66	0.209203	1
	2 h	A - B	638605.4	894225.5	66	0.714144	1
		A - C	544217.7	894225.5	66	0.608591	1
		B - C	-94387.8	894225.5	66	-0.10555	1
	12 h	A - B	216836.7	894225.5	66	0.242486	1
		A - C	162415	894225.5	66	0.181626	1
		B - C	-54421.8	894225.5	66	-0.06086	1
	14 h	A - B	462585	894225.5	66	0.517302	1
		A - C	1268707	894225.5	66	1.418778	0.999918
		B - C	806122.4	894225.5	66	0.901476	1
	16 h	A - B	-953231	894225.5	66	-1.06599	1
		A - C	250850.3	894225.5	66	0.280522	1
		B - C	1204082	894225.5	66	1.346508	0.999971
	20 h	A - B	-250850	894225.5	66	-0.28052	1
		A - C	1606293	894225.5	66	1.796295	0.995127
		B - C	1857143	894225.5	66	2.076817	0.966531
	24 h	A - B	414966	894225.5	66	0.464051	1
		A - C	2219388	894225.5	66	2.48191	0.813254
		B - C	1804422	894225.5	66	2.01786	0.976298
	36 h	A - B	25510.2	894225.5	66	0.028528	1
		A - C	1156463	894225.5	66	1.293256	0.999988
		B - C	1130952	894225.5	66	1.264728	0.999992
	42 h	A - B	2282313	894225.5	66	2.552279	0.770597
		A - C	3523810	894225.5	66	3.940627	0.054466
		B - C	1241497	894225.5	66	1.388348	0.999947

Table H.5. Pairwise comparisons of estimated means for pH, from Tukey's HSD post-hoc test following two-way ANOVA. A = 5% *Daphnia* extract treatment; B = 10% *Daphnia* extract treatment; C = control. *p*-values reflect adjusted significant levels for multiple comparisons; statistically significant results ($p < 0.05$) are bolded.

Parameter	Time	Contrast	Estimate	SE	df	t ratio	*p* value
pH	-0.5h	A - B	-0.00667	0.020268	66	-0.32893	1
		A - C	-0.02667	0.020268	66	-1.31573	0.999982
		B - C	-0.02	0.020268	66	-0.9868	1
	0 h	A - B	0.033333	0.020268	66	1.644664	0.998792
		A - C	-0.04667	0.020268	66	-2.30253	0.901223
		B - C	-0.08	0.020268	66	-3.94719	0.053473
	1 h	A - B	0.003333	0.020268	66	0.164466	1
		A - C	-0.06	0.020268	66	-2.96039	0.478213
		B - C	-0.06333	0.020268	66	-3.12486	0.364679
	2 h	A - B	0.046667	0.020268	66	2.302529	0.901223
		A - C	-0.01333	0.020268	66	-0.65787	1
		B - C	-0.06	0.020268	66	-2.96039	0.478213
	12 h	A - B	0.04	0.020268	66	1.973596	0.982059
		A - C	-0.02	0.020268	66	-0.9868	1
		B - C	-0.06	0.020268	66	-2.96039	0.478213
	14 h	A - B	0.023333	0.020268	66	1.151264	0.999999
		A - C	-0.02667	0.020268	66	-1.31573	0.999982
		B - C	-0.05	0.020268	66	-2.467	0.821753
	16 h	A - B	0.01	0.020268	66	0.493399	1
		A - C	-0.02333	0.020268	66	-1.15126	0.999999
		B - C	-0.03333	0.020268	66	-1.64466	0.998792
	20 h	A - B	0.02	0.020268	66	0.986798	1
		A - C	-0.02	0.020268	66	-0.9868	1
		B - C	-0.04	0.020268	66	-1.9736	0.982059
	24 h	A - B	0.016667	0.020268	66	0.822332	1
		A - C	-0.01667	0.020268	66	-0.82233	1
		B - C	-0.03333	0.020268	66	-1.64466	0.998792
	36 h	A - B	0.02	0.020268	66	0.986798	1
		A - C	0.053333	0.020268	66	2.631462	0.718204
		B - C	0.033333	0.020268	66	1.644664	0.998792
	42 h	A - B	0.03	0.020268	66	1.480197	0.999815
		A - C	3.12E-17	0.020268	66	1.54E-15	1
		B - C	-0.03	0.020268	66	-1.4802	0.999815

Table H.6. Pairwise comparisons of estimated means for mean colony size (MCS), from Tukey's HSD post-hoc test following two-way ANOVA. A = 5% *Daphnia* extract treatment; B = 10% *Daphnia* extract treatment; C = control. *p*-values reflect adjusted significant levels for multiple comparisons; statistically significant results ($p < 0.05$) are bolded.

Parameter	Time	Contrast	Estimate	SE	df	t ratio	*p* value
Mean colony size (MCS)	-0.5h	A - B	0.002121	0.204926	66	0.010349	1
		A - C	-0.02907	0.204926	66	-0.14187	1
		B - C	-0.03119	0.204926	66	-0.15222	1
	0 h	A - B	0.170855	0.204926	66	0.833739	1
		A - C	0.170973	0.204926	66	0.834314	1
		B - C	0.000118	0.204926	66	0.000575	1
	1 h	A - B	0.142932	0.204926	66	0.697482	1
		A - C	0.169932	0.204926	66	0.829235	1
		B - C	0.027	0.204926	66	0.131753	1
	2 h	A - B	0.071151	0.204926	66	0.347204	1
		A - C	0.142025	0.204926	66	0.693053	1
		B - C	0.070873	0.204926	66	0.345849	1
	12 h	A - B	-0.03849	0.204926	66	-0.18784	1
		A - C	0.599809	0.204926	66	2.926955	0.502589
		B - C	0.638303	0.204926	66	3.114799	0.371235
	14 h	A - B	0.060739	0.204926	66	0.296395	1
		A - C	1.132267	0.204926	66	5.525249	**0.000266**
		B - C	1.071528	0.204926	66	5.228854	**0.000796**
	16 h	A - B	-0.06793	0.204926	66	-0.33149	1
		A - C	1.193874	0.204926	66	5.825881	**8.48E-05**
		B - C	1.261804	0.204926	66	6.157367	**2.34E-05**
	20 h	A - B	0.337787	0.204926	66	1.648336	0.998746
		A - C	1.453444	0.204926	66	7.092532	**5.53E-07**
		B - C	1.115657	0.204926	66	5.444196	**0.00036**
	24 h	A - B	-0.35695	0.204926	66	-1.74187	0.996948
		A - C	1.214815	0.204926	66	5.928069	**5.72E-05**
		B - C	1.571769	0.204926	66	7.669934	**5.24E-08**
	36 h	A - B	-1.16503	0.204926	66	-5.68513	**0.000145**
		A - C	0.426352	0.204926	66	2.08052	0.965831
		B - C	1.591382	0.204926	66	7.765646	**3.54E-08**
	42 h	A - B	-1.0652	0.204926	66	-5.19799	**0.00089**
		A - C	0.462867	0.204926	66	2.258702	0.917772
		B - C	1.52807	0.204926	66	7.456691	**1.25E-07**

Table H.7. Pairwise comparisons of estimated means for the proportion of single cells, from Tukey's HSD post-hoc test following two-way ANOVA. A = 5% *Daphnia* extract treatment; B = 10% *Daphnia* extract treatment; C = control. *p*-values reflect adjusted significant levels for multiple comparisons; statistically significant results ($p < 0.05$) are bolded.

Parameter	Time	Contrast	Estimate	SE	df	t ratio	*p* value
Proportion of single cells	-0.5h	A - B	-0.00137	0.075865	66	-0.01801	1
		A - C	0.031368	0.075865	66	0.413466	1
		B - C	0.032734	0.075865	66	0.431479	1
	0 h	A - B	-0.13904	0.075865	66	-1.83268	0.993462
		A - C	-0.1536	0.075865	66	-2.02469	0.975296
		B - C	-0.01457	0.075865	66	-0.19201	1
	1 h	A - B	-0.10365	0.075865	66	-1.36625	0.999961
		A - C	-0.14259	0.075865	66	-1.87956	0.990649
		B - C	-0.03894	0.075865	66	-0.51331	1
	2 h	A - B	-0.06725	0.075865	66	-0.88641	1
		A - C	-0.13125	0.075865	66	-1.73	0.997257
		B - C	-0.064	0.075865	66	-0.84358	1
	12 h	A - B	0.000138	0.075865	66	0.00182	1
		A - C	-0.31492	0.075865	66	-4.15108	**0.029595**
		B - C	-0.31506	0.075865	66	-4.1529	**0.029434**
	14 h	A - B	-0.03831	0.075865	66	-0.50504	1
		A - C	-0.52156	0.075865	66	-6.87486	**1.34E-06**
		B - C	-0.48325	0.075865	66	-6.36982	**1.01E-05**
	16 h	A - B	0.013132	0.075865	66	0.173101	1
		A - C	-0.50656	0.075865	66	-6.67714	**2.96E-06**
		B - C	-0.51969	0.075865	66	-6.85025	**1.47E-06**
	20 h	A - B	-0.07769	0.075865	66	-1.024	1
		A - C	-0.68887	0.075865	66	-9.08017	**1.54E-10**
		B - C	-0.61118	0.075865	66	-8.05617	**1.07E-08**
	24 h	A - B	0.101559	0.075865	66	1.338684	0.999975
		A - C	-0.60128	0.075865	66	-7.92566	**1.83E-08**
		B - C	-0.70284	0.075865	66	-9.26435	**6.84E-11**
	36 h	A - B	0.342492	0.075865	66	4.5145	**0.009479**
		A - C	-0.31842	0.075865	66	-4.19716	**0.025761**
		B - C	-0.66091	0.075865	66	-8.71166	**7.23E-10**
	42 h	A - B	0.316364	0.075865	66	4.170092	**0.027954**
		A - C	-0.37028	0.075865	66	-4.88081	**0.002752**
		B - C	-0.68665	0.075865	66	-9.0509	**1.75E-10**

Table H.8. Pairwise comparisons of estimated means for the proportion of cells in colonies, from Tukey's HSD post-hoc test following two-way ANOVA. A = 5% *Daphnia* extract treatment; B = 10% *Daphnia* extract treatment; C = control. *p*-values reflect adjusted significant levels for multiple comparisons; statistically significant results ($p < 0.05$) are bolded.

Parameter	Time	Contrast	Estimate	SE	df	t ratio	*p* value
Proportion of cells in colonies	-0.5h	A - B	0.007363	0.07663	66	0.096092	1
		A - C	-0.03573	0.07663	66	-0.46622	1
		B - C	-0.04309	0.07663	66	-0.56231	1
	0 h	A - B	0.124968	0.07663	66	1.630797	0.998952
		A - C	0.13751	0.07663	66	1.794472	0.9952
		B - C	0.012542	0.07663	66	0.163676	1
	1 h	A - B	0.092672	0.07663	66	1.209347	0.999997
		A - C	0.141038	0.07663	66	1.84051	0.993048
		B - C	0.048366	0.07663	66	0.631163	1
	2 h	A - B	0.052062	0.07663	66	0.679398	1
		A - C	0.155384	0.07663	66	2.027728	0.974839
		B - C	0.103322	0.07663	66	1.348329	0.99997
	12 h	A - B	0.000795	0.07663	66	0.010368	1
		A - C	0.296322	0.07663	66	3.866924	0.066779
		B - C	0.295527	0.07663	66	3.856556	0.068691
	14 h	A - B	0.029757	0.07663	66	0.388317	1
		A - C	0.512684	0.07663	66	6.690405	**2.81E-06**
		B - C	0.482928	0.07663	66	6.302088	**1.32E-05**
	16 h	A - B	-0.0056	0.07663	66	-0.07303	1
		A - C	0.520363	0.07663	66	6.790609	**1.88E-06**
		B - C	0.525959	0.07663	66	6.863635	**1.4E-06**
	20 h	A - B	0.067095	0.07663	66	0.875573	1
		A - C	0.692547	0.07663	66	9.037562	**1.85E-10**
		B - C	0.625452	0.07663	66	8.161989	**6.95E-09**
	24 h	A - B	-0.10707	0.07663	66	-1.39719	0.999939
		A - C	0.618985	0.07663	66	8.077603	**9.83E-09**
		B - C	0.726051	0.07663	66	9.474791	**2.43E-11**
	36 h	A - B	-0.37918	0.07663	66	-4.94826	**0.002174**
		A - C	0.319883	0.07663	66	4.1744	**0.027594**
		B - C	0.699067	0.07663	66	9.122658	**1.28E-10**
	42 h	A - B	-0.33533	0.07663	66	-4.37603	**0.014796**
		A - C	0.376455	0.07663	66	4.912642	**0.002463**
		B - C	0.711789	0.07663	66	9.288675	**6.12E-11**

Table H.9. Pairwise comparisons of estimated means for the concentration of single cells, from Tukey's HSD post-hoc test following two-way ANOVA. A = 5% *Daphnia* extract treatment; B = 10% *Daphnia* extract treatment; C = control. *p*-values reflect adjusted significant levels for multiple comparisons; statistically significant results ($p < 0.05$) are bolded.

Parameter	Time	Contrast	Estimate	SE	df	t ratio	*p* value
Concentration of single cells	-0.5h	A - B	82500	278956	66	0.295746	1
		A - C	371666.7	278956	66	1.332349	0.999977
		B - C	289166.7	278956	66	1.036603	1
	0 h	A - B	-103333	278956	66	-0.37043	1
		A - C	-217500	278956	66	-0.77969	1
		B - C	-114167	278956	66	-0.40926	1
	1 h	A - B	-50833.3	278956	66	-0.18223	1
		A - C	44166.67	278956	66	0.158328	1
		B - C	95000	278956	66	0.340555	1
	2 h	A - B	394166.7	278956	66	1.413007	0.999924
		A - C	256666.7	278956	66	0.920097	1
		B - C	-137500	278956	66	-0.49291	1
	12 h	A - B	79166.67	278956	66	0.283796	1
		A - C	-605833	278956	66	-2.17179	0.944897
		B - C	-685000	278956	66	-2.45558	0.828119
	14 h	A - B	16666.67	278956	66	0.059747	1
		A - C	-908333	278956	66	-3.25619	0.284938
		B - C	-925000	278956	66	-3.31593	0.252543
	16 h	A - B	-127500	278956	66	-0.45706	1
		A - C	-1462500	278956	66	-5.24276	**0.000757**
		B - C	-1335000	278956	66	-4.7857	**0.003822**
	20 h	A - B	-367500	278956	66	-1.31741	0.999982
		A - C	-1745833	278956	66	-6.25845	**1.57E-05**
		B - C	-1378333	278956	66	-4.94104	**0.002229**
	24 h	A - B	498333.3	278956	66	1.786423	0.995512
		A - C	-1953333	278956	66	-7.0023	**7.97E-07**
		B - C	-2451667	278956	66	-8.78872	**5.26E-10**
	36 h	A - B	2105000	278956	66	7.545993	**8.7E-08**
		A - C	-1171667	278956	66	-4.20018	**0.025526**
		B - C	-3276667	278956	66	-11.7462	**0**
	42 h	A - B	3268333	278956	66	11.7163	**0**
		A - C	-105000	278956	66	-0.3764	1
		B - C	-3373333	278956	66	-12.0927	**0**

Table H.10. Pairwise comparisons of estimated means for the concentration of colonies, from Tukey's HSD post-hoc test following two-way ANOVA. A = 5% *Daphnia* extract treatment; B = 10% *Daphnia* extract treatment; C = control. *p*-values reflect adjusted significant levels for multiple comparisons; statistically significant results ($p < 0.05$) are bolded.

Parameter	Time	Contrast	Estimate	SE	df	t ratio	*p* value
Concentration of colonies	-0.5h	A - B	4166.667	185232.7	66	0.022494	1
		A - C	-5833.33	185232.7	66	-0.03149	1
		B - C	-10000	185232.7	66	-0.05399	1
	0 h	A - B	15000	185232.7	66	0.080979	1
		A - C	10000	185232.7	66	0.053986	1
		B - C	-5000	185232.7	66	-0.02699	1
	1 h	A - B	41666.67	185232.7	66	0.224942	1
		A - C	63333.33	185232.7	66	0.341912	1
		B - C	21666.67	185232.7	66	0.11697	1
	2 h	A - B	46666.67	185232.7	66	0.251935	1
		A - C	68333.33	185232.7	66	0.368905	1
		B - C	21666.67	185232.7	66	0.11697	1
	12 h	A - B	40000	185232.7	66	0.215945	1
		A - C	156666.7	185232.7	66	0.845783	1
		B - C	116666.7	185232.7	66	0.629838	1
	14 h	A - B	101666.7	185232.7	66	0.548859	1
		A - C	465000	185232.7	66	2.510356	0.796504
		B - C	363333.3	185232.7	66	1.961497	0.983425
	16 h	A - B	-165833	185232.7	66	-0.89527	1
		A - C	381666.7	185232.7	66	2.060471	0.969498
		B - C	547500	185232.7	66	2.955742	0.481586
	20 h	A - B	-10000	185232.7	66	-0.05399	1
		A - C	747500	185232.7	66	4.035465	**0.041582**
		B - C	757500	185232.7	66	4.089451	**0.035528**
	24 h	A - B	-41666.7	185232.7	66	-0.22494	1
		A - C	955833.3	185232.7	66	5.160176	**0.001021**
		B - C	997500	185232.7	66	5.385118	**0.000448**
	36 h	A - B	-492500	185232.7	66	-2.65882	0.699223
		A - C	524166.7	185232.7	66	2.829774	0.574561
		B - C	1016667	185232.7	66	5.488592	**0.000305**
	42 h	A - B	-206667	185232.7	66	-1.11571	1
		A - C	820833.3	185232.7	66	4.431363	**0.012404**
		B - C	1027500	185232.7	66	5.547077	**0.000245**

Appendix I. *Daphnia e*xtract characterisation.

The *Daphnia* extracts were transparent, yellow/orange, and had surfactant-like properties (increased surface tension and significant foaming during rotary evaporation). The nitrogen concentration, measured as ammonia (AQUAfast ammonia LR reaction tubes), was < 0.04 mg L^{-1}, and the phosphate concentration (ACD095 AQUAfast phosphate (total) digestion tubes) was 5.9 mg L^{-1}.

Following freeze-drying, the dry weight was 183.2 g L^{-1}.

The concentration of carbohydrates in the *Daphnia* extract was quantified using the phenol-sulfuric acid method, as described by Yang 2007, Chen 2023, and Yue 2022. The method measures methylated sugars, pentoses, and polysaccharides, whilst being unaffected by proteins (Yue 2022). A glucose standard was created in the range of 0 to 80 µg mL^{-1}, as recommended by Yue (2022), using the peak absorbance detected at 488 nm. *Daphnia* extract was diluted x40 with distilled water to bring the carbohydrate content within range. The absorbance of triplicate samples were measured against a blank of distilled water treated the same. The total carbohydrate concentration was 0.929 ± 0.048 g L^{-1}.

Appendix J. RNA sequencing

J.1. Mapping rate

Table J.1. Number of filtered and mapped reads, and mapping rate, in each sample.

Treatment	Timepoint	Filtered Reads	Mapped reads	Mapping Rate %
5% Daphnia extract	1 h	21848462	16291999	74.57
		21384496	16270921	76.09
		25595788	17311212	67.63
	12 h	23263970	17395396	74.77
		19416857	14552625	74.95
		20192384	15553107	77.02
	20 h	23083643	16972940	73.53
		23559099	18151168	77.05
		31023392	22433304	72.31
	36 h	23329983	17836371	76.45
		25109747	17789818	70.85
		23530634	17199518	73.09
10% Daphnia extract	1 h	23918001	18608217	77.8
		25050408	19040556	76.01
		23797377	17199169	72.27
	12 h	20066929	14981525	74.66
		18400611	12712844	69.09
		23588571	18085982	76.67
	20 h	18084106	13165296	72.8
		18610627	14214356	76.38
		19068843	14047808	73.67
	36 h	20322773	15565257	76.59
		20517867	14986539	73.04
		17225620	13134836	76.25
Control	1 h	22028035	15725468	71.39
		22786057	13784015	60.49
		18573182	14367324	77.36
	12 h	19039169	13874228	72.87
		18791989	13835690	73.63
		20481848	15543716	75.89
	20 h	23208380	17554222	75.64
		18889952	14878749	78.77
		19336555	14597621	75.49
	36 h	22720855	16966908	74.68
		25458225	19562524	76.84
		18616478	14333116	76.99

J.2. PCA plot

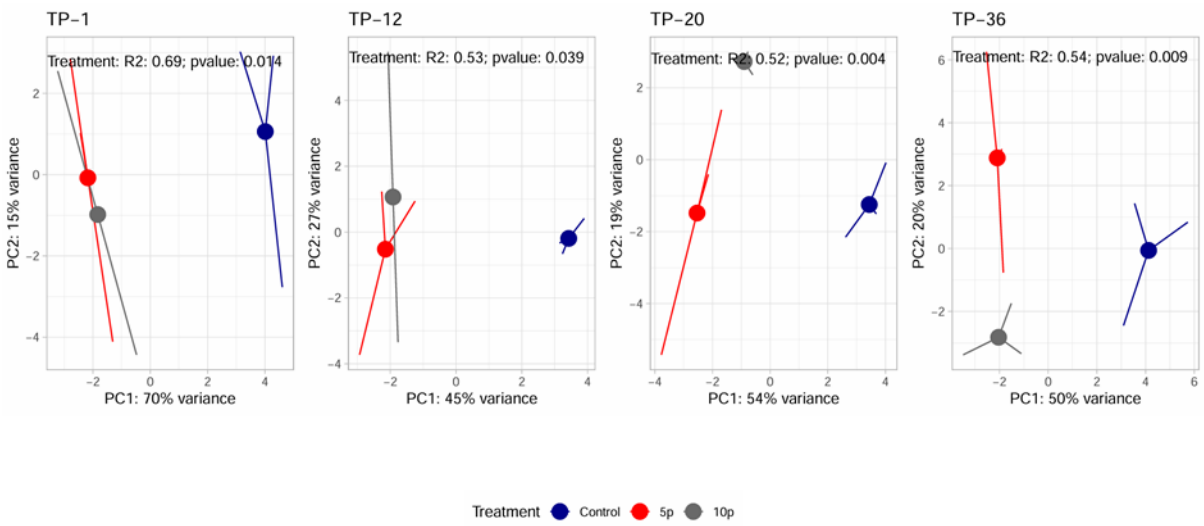

Figure J.1. Principal Component Analysis (PCA) plot of the variance for control and treatments at each timepoint for RNA sequencing data.

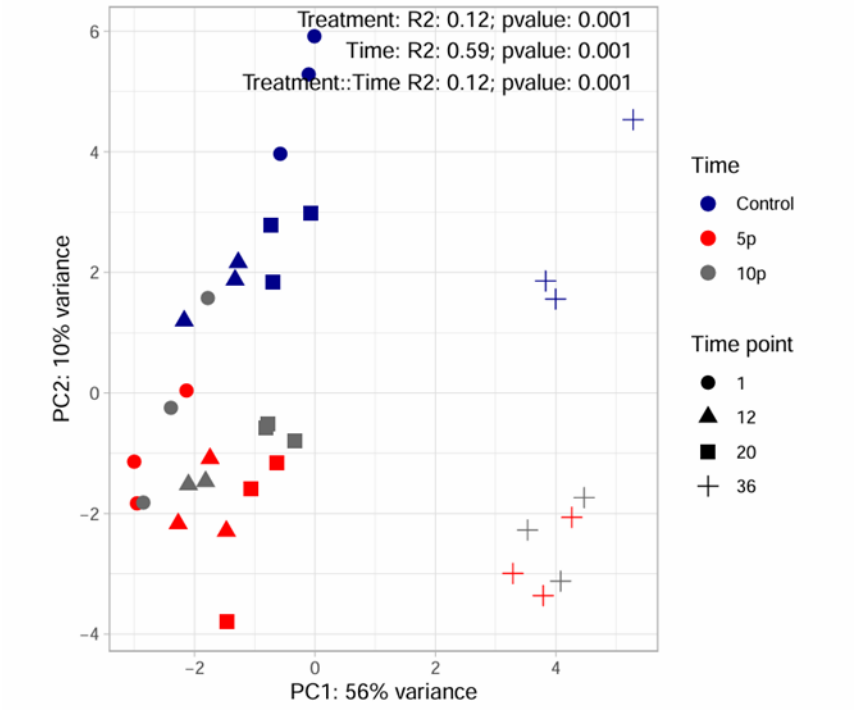

Figure J.2. Principal Component Analysis (PCA) plot of the variance for control and treatments for RNA sequencing data.

J.3. Distribution of DEGs across treatments and timepoints

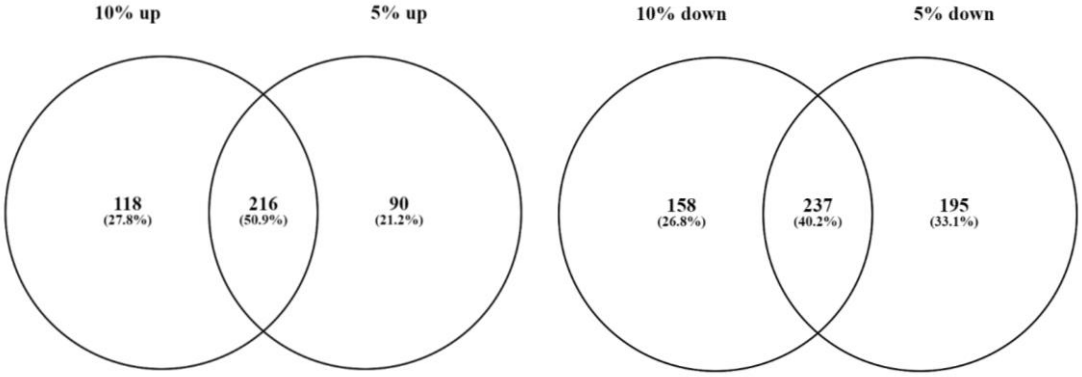

Figure J.3. Venn diagram of *C. reinhardtii* genes significantly upregulated (left) and downregulated (right) in *Daphnia* extract 5% and 10% treatments.

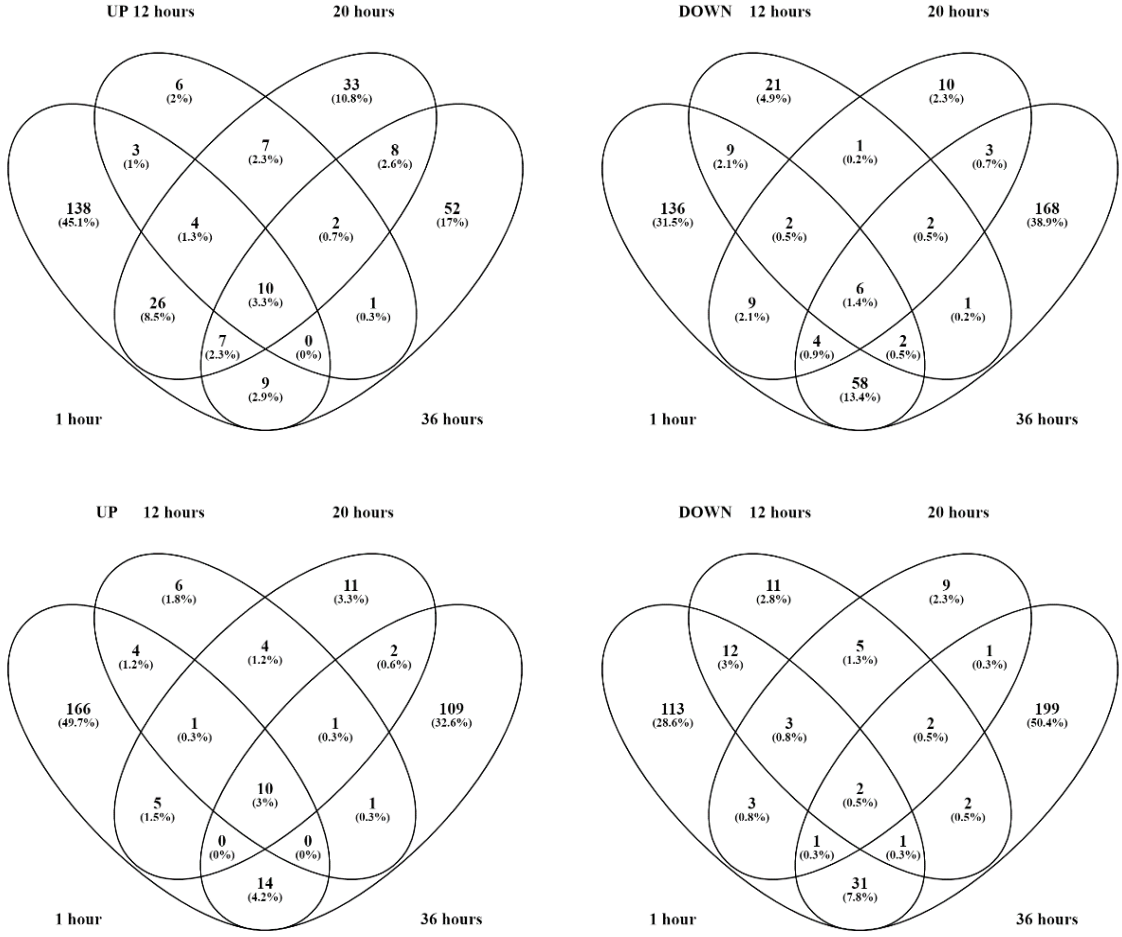

Figure J.4. Venn diagram of *C. reinhardtii* genes significantly upregulated (left) and downregulated (right) in *Daphnia* extract 5% (top) and 10% v/v (bottom) treatments at 1, 12, 20, and 36 h.

J.4. Top 200 DEGs in *Daphnia* treatments relative to control

Table J.2. 100 most upregulated (left) and 100 most downregulated (right) genes, showing their log2-fold change in each treatment and timepoint.

Gene	Log2FC								Gene	Log2FC							
	5%				10%					5%				10%			
	1h	12h	20h	36h	1h	12h	20h	36h		1h	12h	20h	36h	1h	12h	20h	36h
IFR1	1.77	4.69	7.27	6.33	1.68	4.35	7.58	6.46	*FMG1A*	-4.14	-6.05	-5.20	-3.98	-2.38	-5.82	-5.25	-4.16
FAP199	4.75	2.96	3.22	4.07	4.42	3.32	3.59	3.91	*PHC36*	-3.13	-6.50	-4.81	-6.46	-3.90		-3.74	-6.15
TRP13	3.91	3.51	3.42	3.61	3.73	3.59	3.83	3.80	*THI4*		-3.03	-3.20	-1.35		-3.41	-3.64	-1.93
FAP41	3.99	1.82	2.93	3.05	3.73	1.87	3.24	2.71	*FAP319*				-6.55			3.64	-6.10
MOT22	2.44	3.65	2.24	2.50	2.79	3.49	3.61	2.33	*FAP320*				-8.37				-7.18
PHC18	3.30	2.33	2.99	2.88	2.78	2.36	2.91	2.40	*CYCD5*	-3.55	-2.50	-1.11		-4.49	-1.93	-1.81	
FEA1	2.68	3.33	2.23	2.14	3.03	3.93	2.71	1.85	*SLT1*	-4.19	-1.88			-4.96	-2.62		1.72
LTH3	2.90	2.42	2.00	2.11	2.90	2.37	2.51	2.19	*FAP344*	-2.00	-1.54	-1.59	-2.35	-2.31	-1.75	-1.49	-1.87
RWP4	1.20	2.53	2.58	2.19	1.78	2.74	3.39	2.90	*METE1*		-3.06				-6.85	-4.20	
CAD1	3.38	2.47	1.19		4.62	4.16	2.63		*CAH1*	-1.91		-2.08		-2.88	-3.42	-3.62	
FAP79	2.10	2.48	2.09	1.88	1.56	2.50	2.50	1.48	*FXL8*	-2.06	-1.91	-2.14		-2.59	-1.94	-3.00	
PHC66	-1.64	1.96	3.53		-1.36	1.81	2.70	1.20	*FAP359*				-6.54				-7.07
GGH1	1.51	1.06	2.46	2.36	1.70	1.06	2.23		*FAP175*	-2.14	-1.64	-1.76	-1.58	-1.88	-1.68	-1.18	-1.74
FTR1	0.86	1.83	1.68	1.43	0.98	1.65	1.48	1.71	*HCP1*			3.29	-3.37			2.75	-3.47
MMP4		2.19	3.52	-2.12			3.23		*THB1*	1.65			-4.74	2.83			-3.46
CPLD27	1.31		1.76	2.52	1.38		1.09	2.61	*THB8*				-7.40				-4.99
HSP70C	2.63		1.33	1.43	3.07		0.96	1.19	*AMT1A*	-5.37				-6.70			
HCP4	1.55		2.40	-2.62	1.41		2.31		*DUR3A*	-5.92				-5.90			
CYP744C1			3.80	2.75				3.41	*FMG1B*	-1.49	-1.39	-1.50	-1.63	-1.20	-1.32	-1.18	-1.93
COQ8	2.09	2.20	1.79		1.97	1.84			*FAP317*			2.34	-3.98	1.86			-3.39
EFT2	3.33		2.03		2.95		1.56		*MMP13*	-1.42		-1.97	-3.23	-0.75		-1.16	-2.98
CLPB5	1.67	1.37	2.24	1.54	1.56			1.46	*FAP170*	-2.73	-1.33	-1.15	-1.58	-1.99	-1.41		-1.24
PGA6	2.01		1.93	2.39	1.28			2.23	*CGL154*	-2.83		1.67	-3.09	-1.70			-2.02
GPX5	1.36		1.22	1.72	1.67		1.07	2.39	*RRM4*	-2.84		1.40	-2.46	-2.42			-1.97
FOX1		1.24	1.14	1.95	0.93	1.36	1.03	1.62	*FAP322*				-4.87				-5.81
HSP22E	-1.13	-1.40		2.14		-1.65		2.90	*FAP248*	-2.31		-1.06	-2.63	-1.98			-2.22
GSTS1	1.23			1.29	2.42	1.08	0.95	2.21	*DHC11*	-1.18	-1.12	-1.56	-1.77	-0.95	-0.93	-1.27	-1.25
ATM2	1.42	1.44	2.99	1.21			2.02		*VIPP2*	-0.96	-1.67		1.83	-1.34	-1.60		2.61
FAP413	1.40	1.44	0.82	0.87	1.22	1.68	1.15	0.50	*FAP242*				-4.09				-5.91
CGL113	1.33	1.10		0.83	1.74	2.05	1.10	0.78	*FAP366*	-2.38	-1.18	-1.46	-1.58	-2.10			-1.30
MSF1	1.75	1.13	1.24		2.27	0.92	0.76	-0.74	*HEN2*	-1.73	-1.77	-1.60	-2.86				-1.98
PTA3	1.89		1.29	1.87	1.64			2.07	*PTB3*	-0.81	-0.67	-1.26	-1.88		-1.32	-1.15	-2.78
LCI33		1.19	2.12	1.13		0.99	1.96	1.14	*FBB5*	-0.86	-1.42	-1.55	-1.38	-0.68	-1.46	-1.56	-0.95
ycf12				2.40	-2.31			3.78	*DEG1C*	-1.39	-1.84		1.50	-1.65	-1.47		1.86
PHO1	4.22				4.06				*GFY4*				-7.60				-2.04
UPM1	-1.84		2.43		-2.13		1.88		*POB22*	-2.87	-1.34			-3.60	-1.08		0.73
AST4	2.46		1.26	1.28	2.32		0.90		*FAP234*	-1.50	-1.08	-1.52	-1.85	-1.18		-0.84	-1.64
MMP19	1.13	1.12	1.16	0.61	1.34	1.01	1.30	0.55	*DHC10*	-1.33	-1.03	-1.22	-1.80	-1.10	-0.95	-0.74	-1.38
CNS1	1.49	1.07	1.79	1.37	1.42			0.99	*DHC1*	-1.50	-1.05	-1.20	-1.75	-1.03	-0.94	-0.75	-1.19
BAG6	2.09			-2.47	3.50				*SULTR2*	-3.51	-1.51			-4.26			
SELU1			2.20	2.48				3.34	*NSG13*	-3.40	-1.56			-2.70	-1.56		
FAP211			2.74	1.11			2.31	1.84	*FIP37B*		-2.26	-3.43				-3.49	
AGG3	2.47	0.61	0.85		2.88		1.06		*LCI1*				2.70		-6.43		
PAO5			1.23	2.56			1.28	2.76	*FAP381*	-1.48	1.12		-1.97	-2.11			-2.39
CFA1			2.37	2.20			1.06	1.90	*TTL7*	-1.23	-1.19	-1.01	-1.18	-0.88	-1.30	-1.33	-0.89
FAP380	1.27		0.92	1.53	1.60			2.20	*AGG2*	-1.24	-0.76	-1.12	-2.08	-0.64	-0.78	-0.76	-1.60
VLE1	1.61		0.95	-1.34	1.46		1.00	1.12	*rtl*	-3.11				-3.28			2.53
DGAT3	1.21	1.58	2.07		1.01		1.59		*FAP17*	-2.40	-0.97	-1.17	-1.24	-2.07			-1.06
PHT3A	1.80	0.72	1.29		1.82	0.84	0.92		*PHC5*	-1.28	-0.82	-0.97	-1.59	-1.13	-0.61	-0.64	-1.84
GSP1			1.68	1.99			1.17	2.34	*SBD1*	-3.12	-1.25			-3.25	-1.22		

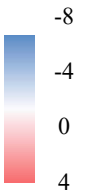

Table J.2. (*Continued*).

Gene	Log$_2$-FC								Gene	Log$_2$-FC							
	5%				10%					5%				10%			
	1h	12h	20h	36h	1h	12h	20h	36h		1h	12h	20h	36h	1h	12h	20h	36h
GPM3				3.43				3.67	*ARS73A*	-2.93	-1.69			-2.85	-1.28		
CNX6			2.39	2.56				2.13	*FDX5*		-3.56		-5.18				
MMP29		1.28	1.15	-2.28	1.10		1.28		*THIC1*	-0.68	-1.17	-1.47		-0.70	-1.53	-2.26	-0.93
HSP22F		-1.12		1.67		-1.69		2.53	*DHC9*	-1.30	-0.81	-1.19	-1.94	-1.14		-0.65	-1.69
CPLD66			1.51	1.83	-1.37			2.24	*PTB12*	-2.57		-1.10		-3.09			-1.80
CGL143	1.39	1.38	1.69	1.06	1.39				*DHC14*	-1.14	-0.95	-1.10	-1.73	-0.76	-0.81	-0.70	-1.32
HSP90B	1.25	1.03		-1.15	1.29	0.95		-1.21	*CGL53*	-4.72				-3.79			
CGL150	1.63			1.74	1.47			2.00	*XDH1*	-2.51		-2.10		-1.59		-2.26	
PDC3	1.82		0.99	0.84	1.82			1.36	*IFT140*	-1.64	-0.82	-0.90	-1.61	-1.23	-0.81		-1.31
TEF22		1.48	1.07	1.68		1.52		1.02	*DHC7*	-1.34	-0.74	-1.11	-1.88	-1.01		-0.63	-1.57
MSD3		1.90	1.73			1.27	1.84		*LCI23*		-3.14			-5.08			
CPLD58	1.99		1.06	1.08	1.79			0.79	*SLT2*	-3.82				-4.31			
OPR125	1.65		1.91		1.43		1.70		*AMX2*	-3.24			-1.65	-2.07			-1.12
MRPL16	1.50			1.95	0.98			2.17	*TPM1*	-1.38		-0.93	-1.98	-1.41			-2.37
MRPS106	1.19	1.11	1.06	-0.85	1.37		1.02		*TUB1*	-1.45	-1.00	-0.96	-1.12	-1.20	-0.99	-0.77	-0.57
GSL1	-0.95	1.56	1.48			1.36	1.22		*TMEM107*	-1.67		-1.31	-1.43	-1.38		-2.26	
SEC14		1.03	1.05	0.81		1.32	1.59	0.73	*COQD2*	-1.93	-1.16	0.76		-2.34	-0.99		0.82
MAS1	1.69			-2.18	1.68			-0.94	*ARS9*	-1.51	-1.05		1.29	-1.69	-1.38		1.06
ARB1	1.58	1.38	2.24		1.25				*RYR1*	-1.58	-0.84	-1.03	-1.60	-1.39			-1.52
SULTR3	1.46	0.82	0.78	-1.20	1.25		0.92		*AGL1*	-3.25			0.94	-2.87			0.88
RHP1	0.77			2.22	0.78			2.60	*FAP181*	-1.87		-1.09	-1.56	-1.57			-1.74
NEP1	1.43	1.00	1.62		1.30		1.00		*FAP321*				-2.99				-4.82
TSI2	1.59		1.35	1.14	1.39			0.81	*MMP6*	-1.42			-2.41	-0.90		0.94	-2.09
icreI				3.18				3.01	*DII1*	-1.36	-0.75	-0.91	-1.37	-1.07	-0.69	-0.63	-0.97
RWP5	1.10	1.36			1.51	1.38		-0.82	*RJL1*	-0.99		-1.48	-1.44	-0.97		-1.02	-1.78
EIF3G	1.48	0.99	1.32		1.49		0.90		*GOX5*	-1.12		-0.89	-1.33	-0.86		-0.97	-2.42
CGL120	1.03		1.23	1.72				2.19	*POB15*	-1.83		-1.88		-1.76			-2.11
HCS1	1.71			1.33	1.65			1.44	*LHCSR3A*	-1.95				-2.81	-2.82		
CHLI2		1.27	1.33	0.81		1.02	0.93	0.73	*SAH1*	-1.06	-1.40			-0.85	-1.35	-1.36	-1.55
EIF3D	1.68	1.24	1.52		1.64				*HCP3*			1.47	-2.91			1.28	-1.91
TSF1	1.34	0.74	0.88	1.01	1.30			0.79	*DHC6*	-1.38	-0.91	-1.09	-1.80	-1.03			-1.34
PUF4	2.10		2.16		1.74				*PBGD2*	-1.30	-1.16	-0.92	-0.69	-1.62	-1.11	-0.72	
LASPO1	1.93		1.02		1.99		1.06		*CAT2*	-2.07	-0.83		0.57	-2.06	-1.00		0.94
EFG3	1.55	0.75	0.71	0.67	1.37	0.91			*TBA1*	-1.75			-2.14	-0.91	-1.00		-1.68
TOC34	1.52		0.84	1.03	1.53			1.02	*FAP393*	-1.52	-1.03	-1.23		-1.25	-1.24	-1.17	
GLDH1	0.99		0.74	1.36	1.02		0.81	0.98	*ABCA1*	-1.51	-1.68	-1.32		-1.30	-1.62		
TOM40	1.93		1.03	0.84	2.01				*TTLL3*	-1.80		-1.00	-1.68	-1.06			-1.83
EFG8	2.27		1.05		2.45				*CMD1*				-7.33				
EIF2A	1.32	1.04	1.07		1.44	0.88			*FAP265*	-1.94			-1.89	-1.68			-1.80
CRB3	1.29	0.85	1.13	1.29	1.16				*DHC4*	-0.93	-0.80	-1.27	-1.00	-0.91	-0.65	-0.79	-0.95
TIM17	1.88		1.44		1.51			0.89	*FAP272*	-1.19	-0.67	-1.08	-1.66	-1.18			-1.48
SELW1	2.33				3.36				*PF22*	-1.25		-1.10	-1.33	-1.01		-1.00	-1.55
TTL12	0.79	0.93	1.33	1.33				1.27	*FAP308*	-1.39	-1.36	-1.06	-1.34	-0.87			-1.22
TIM44	1.37		1.22	0.88	1.25			0.89	*DRC11*	-0.99	-0.80	-0.90	-1.36	-1.02	-0.71		-1.33
FKB53	1.32	0.93	1.30	0.82	1.18				*LHCBM9*	-1.50			-1.85	-1.64		-1.99	
HNR1	1.57	0.90	1.17		1.87				*EBG1*	-1.91			-2.24	-1.46			-1.25
LTH1		0.74	0.89	0.84		0.89	1.32	0.83	*LCI35*	-0.91		-1.03	-1.91	-0.79			-2.19
CGL42	1.08		1.41	1.47				1.55	*AMX3*					-3.22			-3.60
TSH1	1.40	0.78	1.01		1.45		0.85		*FAS1*	-1.79			-1.89	-1.75			-1.32
PURB1	1.25	0.96	1.05		1.36		0.84		*DHC16*	-1.30	-0.73	-0.71	-1.87	-0.62			-1.48

J.5. Gene ontology enrichment

Table J.3. Enriched *biological process* GO terms of upregulated (top) and downregulated (bottom) *C. reinhardtii* DEGs in 5% and 10% *Daphnia* extract treatments. Numbers indicated the count of DEGs per GO term; colour intensity reflects enrichment level (-log FDR < 0.05, $p < 0.05$).

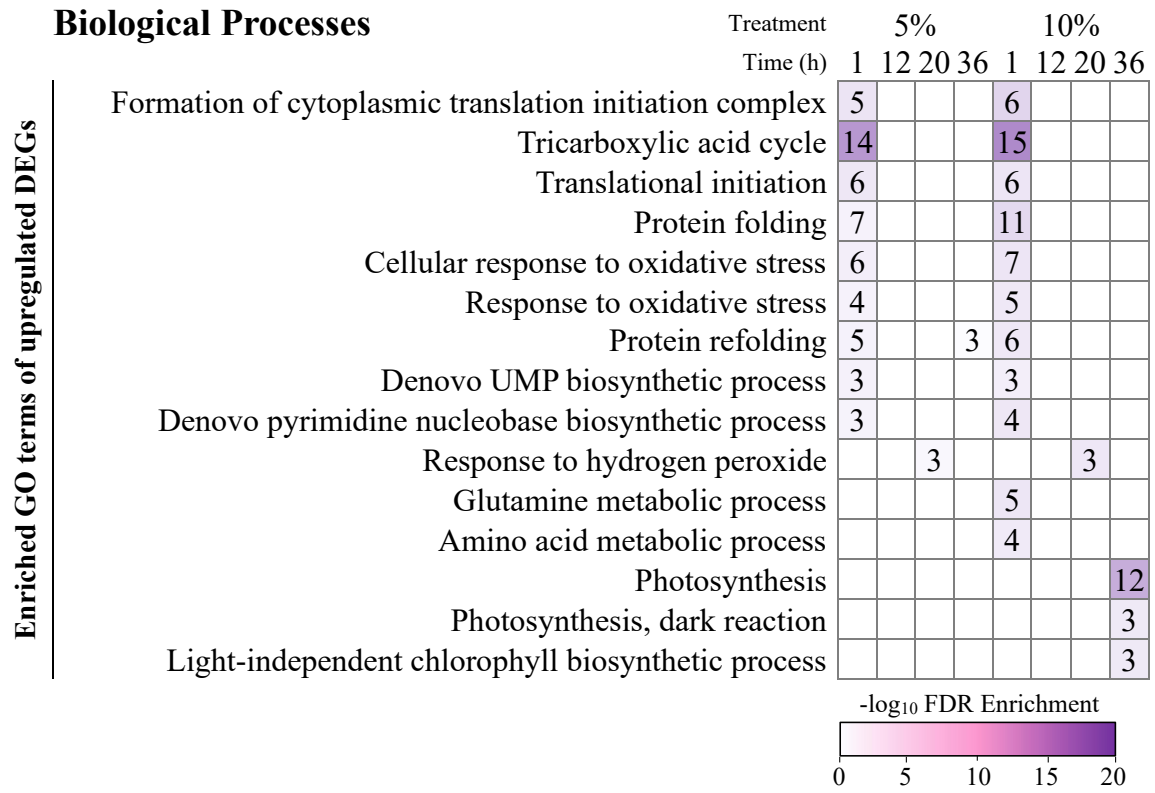

Table J.3. (*Continued*).

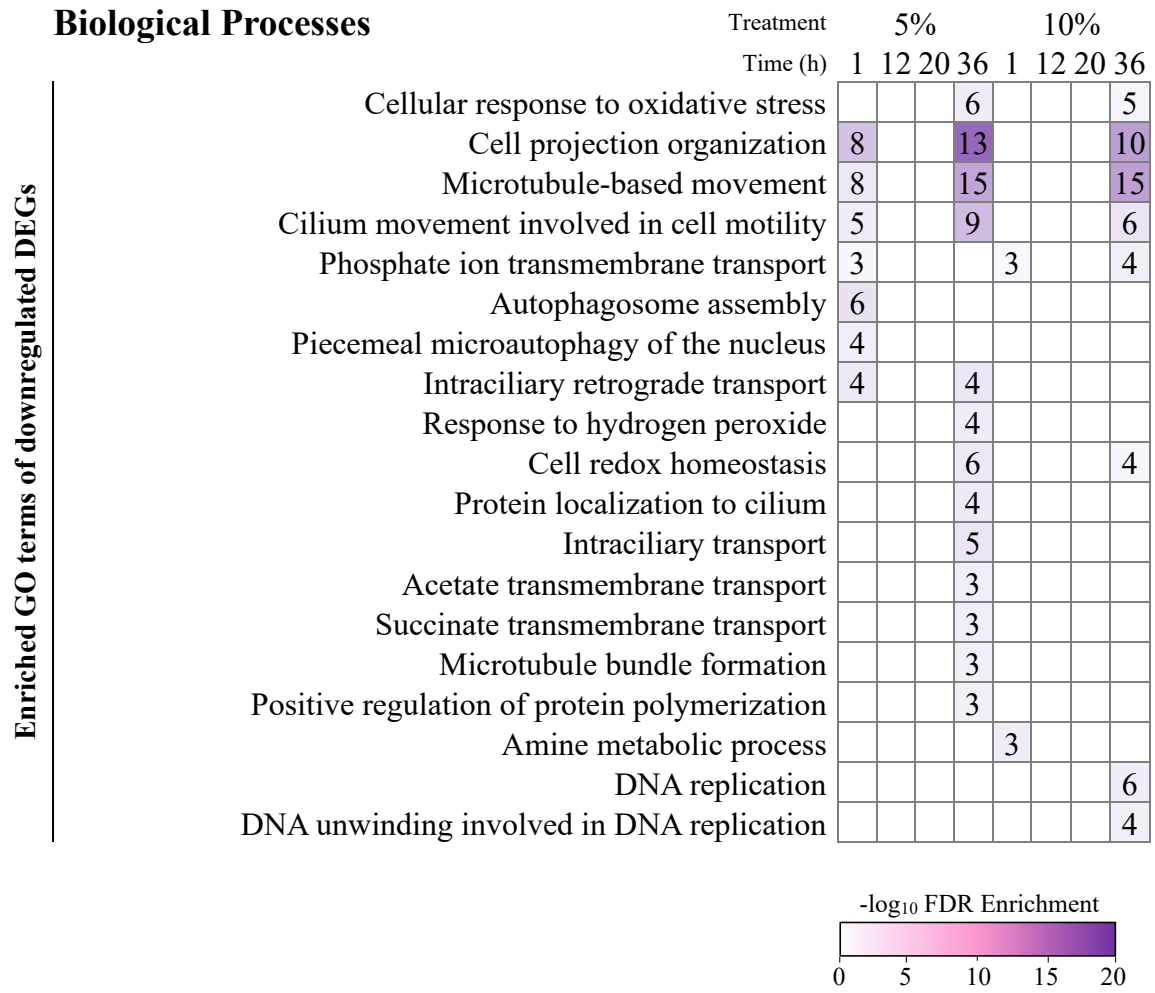

Table J.4. Enriched *molecular function* GO terms of upregulated (top) and downregulated (bottom) *C. reinhardtii* DEGs in 5% and 10% *Daphnia* extract treatments. Numbers indicated the count of DEGs per GO term; colour intensity reflects enrichment level (-log FDR < 0.05, $p < 0.05$).

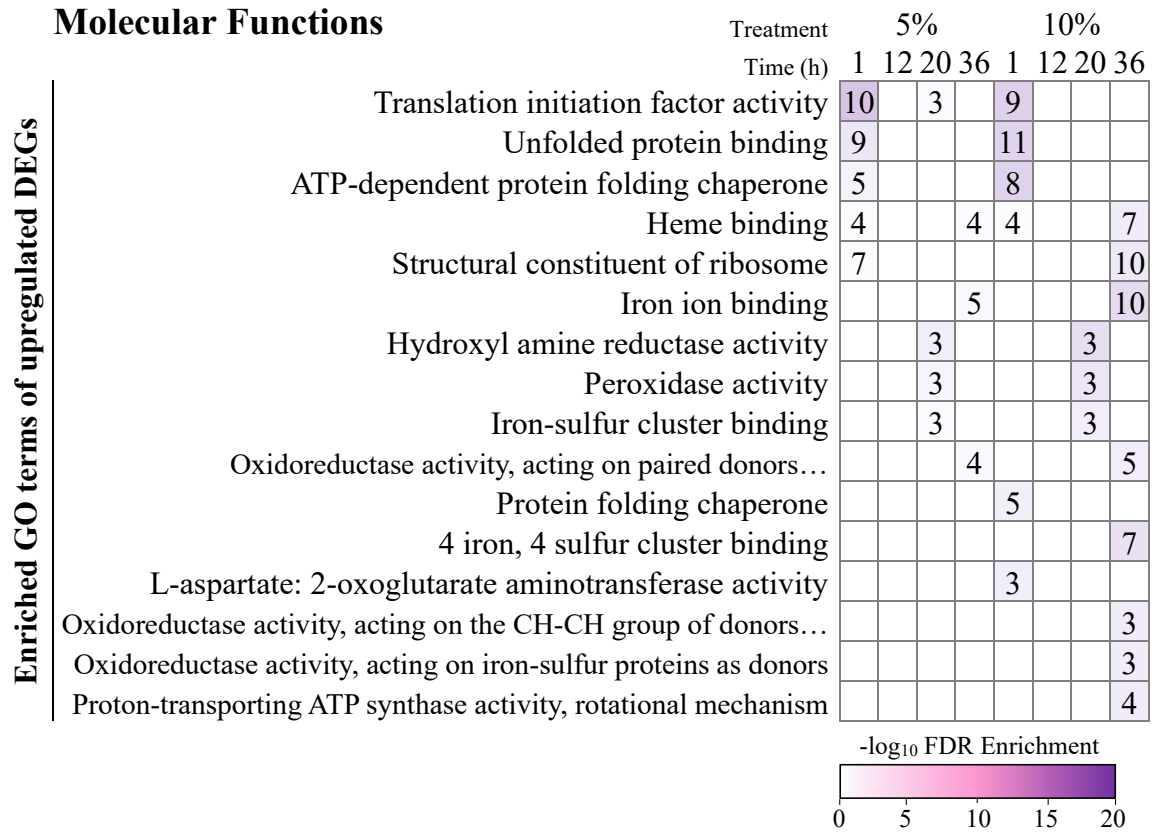

Table J.4. (*Continued*).

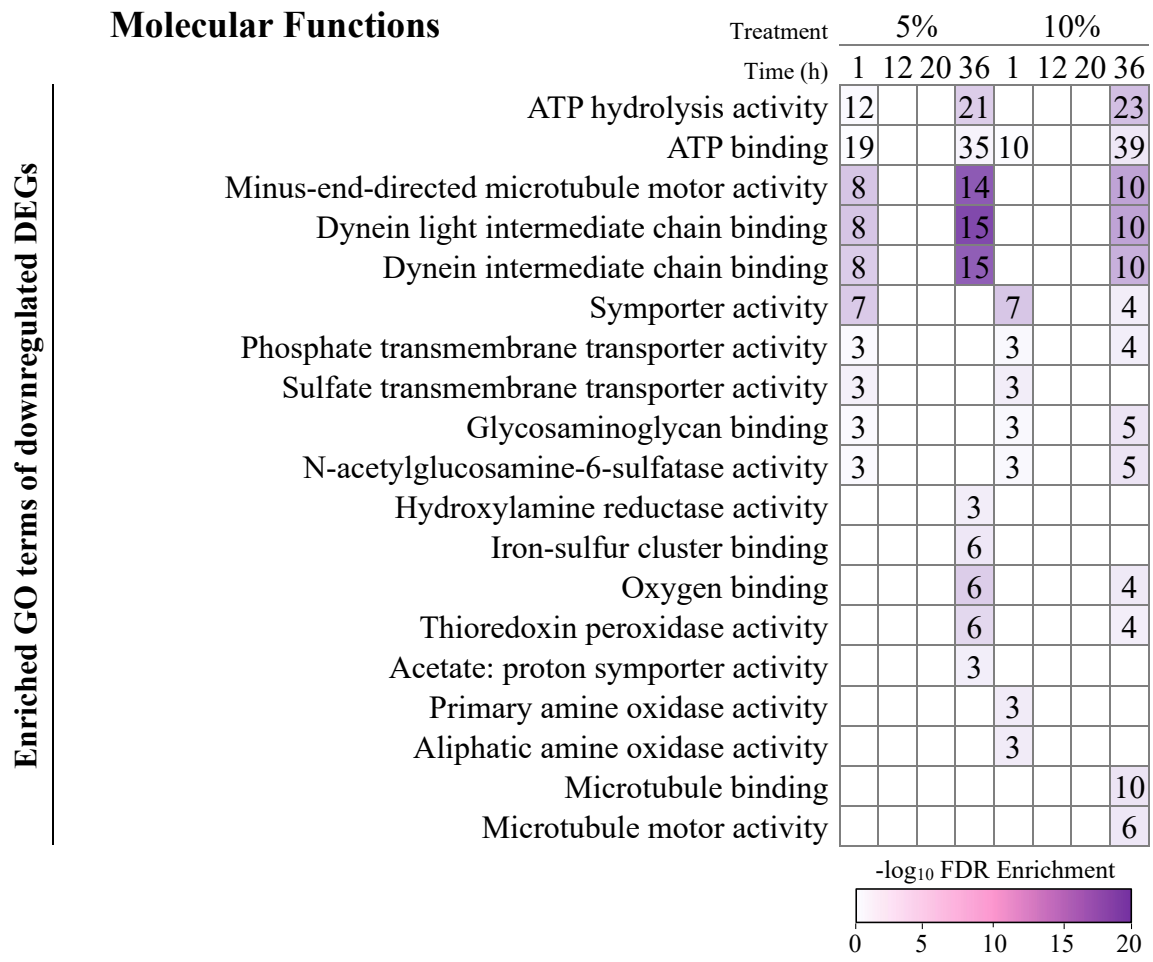

J.6. Signalling cascades

Table J.5. Signalling-related DEGs ($p < 0.05$) in *Daphnia* treatments relative to controls.

	Gene		Log$_2$-FC							
			5%				10%			
			1h	12h	20h	36h	1h	12h	20h	36h
Transient receptor-potential channels	*TRP13*	Cre03.g175050	3.9	3.5	3.4	3.6	3.7	3.6	3.8	3.8
	TRP11	Cre07.g341350				1.3				1.6
	TRP2	Cre16.g655950							0.6	
	TRP1	Cre10.g452950	-1.0			-1.1	-0.7			-1.1
	TRP6	Cre07.g334300	-1.0		-0.6	-0.9	-0.5			-1.0
	TRP22	Cre02.g112200	-0.4			-0.6				-0.4
Voltage-dependent calcium channels	*CAV1*	Cre17.g720600				-0.7	-0.6			-1.0
	CAV2	Cre16.g665050	-0.7			-0.9				-0.6
	CAV3	Cre16.g665100	-0.8				-0.6			-0.5
	CAV4	Cre11.g467528	-1.0		-0.8	-1.3				-1.9
	CAV5	Cre17.g702850				-1.2				
	CAV6	Cre16.g667350	-0.5			-1.0				
	CAV7	Cre10.g444850	-1.0			-0.8				
Ca^{2+} binding proteins	*CRT2*	Cre01.g038400	1.5				1.4			-1.4
	CAS1	Cre12.g497300		-0.6		0.6				
	MOT6	Cre03.g197500				-0.7				-0.5
Aurora-like kinases	*ALK1*	Cre12.g529550	-0.5							-0.5
	ALK2	Cre04.g220700					-1.4			-1.4
	ALK3	Cre12.g498650				-1.7				-1.8
Calmodulin-related	*DLE2*	Cre11.g468450			-0.5	-0.9				-0.8
	RSP20	Cre03.g178150			-0.4	-1.1				-1.1
	POC6	Cre06.g283550	-1.1		-0.7	-1.1	-0.8			-1.1
	GLC2B	Cre17.g725350	0.6				0.6			0.5
	FAP223	Cre17.g705000				-0.5	-0.3			-0.7
	FAP272	Cre03.g178350	-1.2	-0.7	-1.1	-1.7	-1.2			-1.5
Calcium-dependent protein kinases	*CDPK10*	Cre03.g144484	-1.1				-0.9			
	CDPK12	Cre06.g265550	-0.5		-0.5	-0.5	-0.7			
	CDPK13	Cre08.g382800	-0.3			-0.2				
	CDPK2	Cre19.g750597	-0.6			-1.1				-1.0
	CDPK3	Cre07.g328900	0.3			-0.7	0.3			-0.9
	CDPK4	Cre02.g114750	-0.8				-0.7			-0.7
	CDPK5	Cre01.g009500			-0.7					-0.7
	CDPK7	Cre02.g106650		0.7	0.6	-1.0		0.7	0.9	-0.6
	CDPK8	Cre02.g074370	-1.1			-1.5	-0.7			-1.7
	CDPK9	Cre13.g571700								-0.3

Table J.5. (*Continued*).

	Gene		Log2-FC							
			5%				10%			
			1h	12h	20h	36h	1h	12h	20h	36h
Mitogen-activated protein kinase	*MAPK3*	Cre12.g509000				-0.4				-0.6
	SIK1	Cre07.g317300	-0.5			-0.5	-0.4			
Sucrose non-fermenting 1-related kinase	*SNRK2P*	Cre07.g329850	-1.0			-0.9	-0.7			-1.0
	SNRK2N	Cre13.g568050	-0.4			-0.7				-1.3
	SNRK2J	Cre17.g707800	-0.7			-0.9				-1.0
	SNRKB1	Cre10.g457500	-0.8			-0.6				-0.6
	SNRKBG1	Cre12.g484350	-0.4			-0.3				-0.4
	SNRK2M	Cre12.g485600				-1.2				
	SNRK1B	Cre13.g570250	-0.5			-0.6				
	SNRK1A	Cre04.g211600	-0.8							
	SNRK2F	Cre11.g481000	-0.5				-0.5			
	SNRK2L	Cre17.g707650				-0.4	-0.4			
	SNRK2I	Cre16.g657350	0.9		0.8					0.5
	SNRK2K	Cre02.g076000		0.9	0.6			0.7	0.7	
	SNRK2C	Cre02.g075900		0.4						
NIMA-related kinase	*CNK2*	Cre12.g560350	-1.0			-0.8	-0.6			
	CNK4	Cre05.g232750				-0.4				-0.5
	CNK5	Cre10.g443300	-0.4			-0.3				-0.4
	CNK6	Cre12.g514650	-0.8			-0.8	-0.5			-0.8
	CNK7	Cre12.g499850				-0.5				-0.5
	CNK9	Cre02.g107800	-1.1			-0.6	-0.9			-1.3
	FA2	Cre07.g351150				-0.7				
Cyclin-dependent kinase	*CDK1*	Cre01.g008650				-0.8				
	CDKA1	Cre10.g465900					-0.4			
	CDKB1	Cre08.g372550					-1.0			-1.7
	CDKC1	Cre08.g385850					0.4			-0.4
	CDKG1	Cre06.g271100	-1.3							
	CDKH1	Cre07.g355400					0.7			
	LF2	Cre12.g494500	-0.8				-0.8			-0.6
Cyclin-dependent kinase-like	*FLS1*	Cre12.g551250	0.4	0.6	0.4		0.4	0.5		
	FLS2	Cre03.g169500	-0.8				-0.6		0.5	0.4

Table J.6. DEGs ($p < 0.05$) involved in the ubiquitin proteasome pathway in *Daphnia* treatments relative to controls.

Gene		Log$_2$-FC							
		5%				10%			
		1h	12h	20h	36h	1h	12h	20h	36h
26s proteasome									
RPN1	Cre16.g676197					0.4			
RPN2	Cre17.g727950	0.4				0.6			
RPN3	Cre06.g275650	0.5				0.9			
RPN6	Cre02.g097650	0.4				0.7			
RPN7	Cre13.g581450	0.5				0.8			
RPN8	Cre06.g278256	0.7				0.9			
RPN9	Cre17.g734516					0.8			
RPN10	Cre16.g663500					0.4			0.5
RPN11	Cre01.g011500			-0.5		0.4		-0.7	
RPN12	Cre17.g708300	0.6				1.1			
RPT1	Cre14.g625400	0.8				1.1			
RPT2	Cre07.g329700	0.5				0.6			
RPT4	Cre17.g710150	0.6				1.0			
RPT5	Cre10.g439150	0.7				0.8			
RPT6	Cre04.g216600					0.4			
POA4	Cre01.g030850	0.6				0.7			
PBE1	Cre10.g461950					0.6	-0.7		0.9
EIF3F	Cre16.g654500	1.1	0.9	0.7		1.2	0.8		
Ubiquitin activating enzyme E1									
UBA1	Cre09.g386400	0.9				1.3			0.5
UBA3	Cre12.g491500		-0.5						
SAE2 (*UBA2*)	Cre06.g296983	1.0	0.6	0.6		0.7			
ATG7	Cre03.g165215	-2.1			-0.8	-1.6			-0.8

Table J.6. (*Continued*).

Gene		Log$_2$-FC						
		5%				10%		
			1h	12h	20h	36h	1h	12h	20h
Ubiquitin-conjugating enzyme E2									
UBC2	Cre05.g247600	0.6				0.7			
UBC9	Cre16.g693700	0.5			-0.5	0.8			
UBC10	Cre06.g294850	0.9	0.7	0.9	0.9	0.8	0.8	0.9	0.7
UBC11	Cre01.g026600					0.5			
UBC12	Cre01.g027200	-1.1			-0.7				
UBC13	Cre01.g046850	0.7			-1.0	0.7			-0.5
UBC14	Cre02.g141450				-1.5				
UBC17	Cre06.g292800	-0.8				-0.7			
UBC19	Cre08.g372400					0.4			
UBC20	Cre10.g430050	-0.4		-0.6	-0.5				-0.9
UBC21	Cre12.g510300				1.1	0.7			1.3
UBC22	Cre12.g515450	-1.6							
UBC23	Cre12.g546650				-1.4				
UBC34	Cre03.g202897		0.7					0.7	
UBC36	Cre06.g297650	-2.3				-2.4			1.4
UBC39	Cre10.g429000	-1.0	-1.5			-1.3			
SCE1	Cre02.g142000	0.4			-0.4	0.5			
SCE3 (*UBE2I*)	Cre01.g019450		1.0		1.1				
RCE1	Cre08.g370850			-0.7					
Ubiquitin protein ligase E3									
SDIR1	Cre12.g501450		0.6		0.9		0.9		1.3
SIZ1	Cre12.g500900				0.8				
PCOP1 (*RFWD2*)	Cre02.g085050	-0.6				-0.7			-0.6
SKP1	Cre12.g501200		-0.8						

J.7. Flagella-related genes

J.7.1 Matrix metalloproteinases (MMP)

Table J.7. All MMP DEGs ($p < 0.05$), showing log_2-fold change in *Daphnia* treatments relative to control.

Gene		Log_2-FC							
		5%				10%			
		1h	12h	20h	36h	1h	12h	20h	36h
MMP4	Cre07.g324500		2.2	3.5	-2.1			3.2	
MMP19	Cre03.g170850	1.1	1.1	1.2	0.6	1.3	1.0	1.3	0.5
MMP29	Cre13.g605200		1.3	1.1	-2.3	1.1		1.3	
MMP9	Cre16.g652200				-0.9	1.6	1.4		
MMP22	Cre07.g324500	1.2				1.2			-1.2
MMP13	Cre03.g144564	-1.4		-2.0	-3.2	-0.8		-1.2	-3.0
MMP6	Cre16.g692200	-1.4			-2.4	-0.9		0.9	-2.1
MMP21	Cre06.g292050	-1.0			-2.1				-2.3
MMP33	Cre17.g708450		0.8		-1.8		1.0		-1.6
MMP14	Cre08.g376950	-1.2			-0.9	-0.8			-1.3
MMP2	Cre17.g718450				-2.3				-1.4
MMP15	Cre16.g694200	-2.1				-1.5			
MMP23	Cre07.g333400	-1.1			-1.3				-0.8
MMP7	Cre07.g353600				-1.5				-1.7
MMP11	Cre09.g388350	-1.3				-1.6			
MMP25	Cre10.g421350				-1.2				-1.3
MMP1	Cre17.g718500				-1.1				-1.4
MMP31	Cre14.g621700				-0.9				-1.4
MMP3	Cre09.g393700				-0.5				-0.8
MMP32	Cre14.g625850					-1.1			
MMP17	Cre02.g078950								-1.0
MMP20	Cre03.g201550	-0.8							

J.7.2 Pherophorins (PHC)

Table J.8. All PHC DEGs ($p < 0.05$), showing log_2-fold change in *Daphnia* treatments relative to control.

Gene		Log_2-FC							
		5%				10%			
		1h	12h	20h	36h	1h	12h	20h	36h
PHC18	Cre24.g755997	3.3	2.3	3.0	2.9	2.8	2.4	2.9	2.4
PHC66	Cre02.g081700	-1.6	2.0	3.5		-1.4	1.8	2.7	1.2
PHC52	Cre01.g047265			1.2				0.9	1.3
PHC35	Cre05.g238687	0.6		0.8	0.9			0.8	
PHC56	Cre16.g654600		0.7	0.8				0.8	
PHC3	Cre06.g278162		-0.7		0.8				
PHC36	Cre05.g238600	-3.1	-6.5	-4.8	-6.5	-3.9		-3.7	-6.1
PHC5	Cre05.g238650	-1.3	-0.8	-1.0	-1.6	-1.1	-0.6	-0.6	-1.8
PHC6	Cre17.g718000	-1.4			-2.0	-1.0			-1.7
PHC30	Cre09.g404201	-1.8		1.8		-2.2			
PHC26	Cre06.g299150	-0.5	-0.5	-0.4	-0.7	-0.7	-0.6	-0.6	-0.9
PHC24	Cre14.g620702		-2.3				-2.4		
PHC38	Cre02.g094450		1.1		-1.2		1.2		-1.2
PHC47	Cre02.g118650	-1.1			-1.6				-1.9
PHC69	Cre03.g192250	-0.7			-1.8	-0.5			-1.2
PHC22	Cre17.g696700				-1.4				-2.0
PHC61	Cre16.g654700				-1.6				-1.8
PHC1	Cre17.g717900				-1.5				-1.6
PHC51	Cre03.g192201				-1.0				-2.0
PHC4	Cre12.g549000				-1.2				-1.4
PHC34	Cre09.g388353	-2.5							
PHC31	Cre17.g710300				-1.1				-1.3
PHC2	Cre14.g620600	-0.4	-0.5		-0.9				-0.6
PHC32	Cre09.g388351	-2.4							
PHC12	Cre02.g095095				-1.2				-1.1
PHC8	Cre17.g717850		-1.2				-1.0		
PHC19	Cre17.g696500				-1.0				-1.1
PHC33	Cre09.g388355	-2.0							
PHC7	Cre17.g718000								-1.5
PHC15	Cre09.g396100	-0.6			-0.9				
PPHC1	Cre12.g514700								-0.7

J.7.3 Flagella-associated proteins (FAPs)

Table J.9. Downregulated flagella-associated protein DEGs (only showing DEGs with log_2-FC < -1.25) in *Daphnia* treatments relative to controls.

Gene		Log$_2$-FC							
		5%				10%			
		1h	12h	20h	36h	1h	12h	20h	36h
FAP319	Cre08.g365103				-6.6			3.6	-6.1
FAP320	Cre08.g365150				-8.4				-7.2
FAP359	Cre08.g365300				-6.5				-7.1
FAP317	Cre08.g364950			2.3	-4.0	1.9			-3.4
FAP322	Cre08.g365205				-4.9				-5.8
FAP242	Cre08.g365100				-4.1				-5.9
FAP321	Cre08.g365200				-3.0				-4.8
FAP338	Cre17.g719600								-3.5
FAP386	Cre08.g358850	-4.6				-1.8			
FAP344	Cre08.g358564	-2.0	-1.5	-1.6	-2.4	-2.3	-1.7	-1.5	-1.9
FAP175	Cre05.g245500	-2.1	-1.6	-1.8	-1.6	-1.9	-1.7	-1.2	-1.7
FAP170	Cre02.g090050	-2.7	-1.3	-1.2	-1.6	-2.0	-1.4		-1.2
FAP248	Cre16.g665850	-2.3		-1.1	-2.6	-2.0			-2.2
FAP366	Cre12.g534050	-2.4	-1.2	-1.5	-1.6	-2.1			-1.3
FAP234	Cre01.g023550	-1.5	-1.1	-1.5	-1.8	-1.2		-0.8	-1.6
FAP381	Cre16.g681750	-1.5	1.1		-2.0	-2.1			-2.4
FAP17	Cre03.g146867	-2.4	-1.0	-1.2	-1.2	-2.1			-1.1
FAP181	Cre03.g212305	-1.9		-1.1	-1.6	-1.6			-1.7
FAP393	Cre06.g260150	-1.5	-1.0	-1.2		-1.3	-1.2	-1.2	
FAP265	Cre02.g147100	-1.9			-1.9	-1.7			-1.8
FAP272	Cre03.g178350	-1.2	-0.7	-1.1	-1.7	-1.2			-1.5
FAP308	Cre10.g430700	-1.4	-1.4	-1.1	-1.3	-0.9			-1.2
FAP291	Cre08.g367550	-0.6	-0.9	-1.0	-1.3	-0.8	-0.9	-1.1	
FAP362	Cre11.g475600	-1.4	-0.9	-1.1	-1.1	-1.0		-0.9	
FAP226	Cre17.g728300	-1.5		-1.0	-1.6	-1.0			-1.3
FAP141	Cre06.g307900	-1.4		-1.0	-1.3	-1.3			-1.3
FAP315	Cre02.g141700	-1.4		-0.7	-1.3	-1.2		-0.6	-1.1
FAP13	Cre17.g723450	-2.0		-0.7	-0.9	-1.4			-1.2
FAP139	Cre09.g387912	-1.4		-0.9	-1.1	-0.9			-1.8
FAP209	Cre02.g147750	-1.3		-1.0	-1.7	-0.8			-1.3
FAP282	Cre14.g617250	-1.4		-0.8	-1.2	-1.3			-1.2
FAP311	Cre04.g225200	-1.0		-0.9	-1.4	-0.9			-1.6
FAP201	Cre09.g397993	-1.0		-0.8	-1.3	-0.9			-1.5

Table J.9. (*Continued*).

Gene		Log$_2$-FC							
		5%				10%			
		1h	12h	20h	36h	1h	12h	20h	36h
FAP27	Cre14.g611100	-1.2		-0.6	-1.4	-1.0			-1.2
FAP138	Cre14.g632350	-1.7			-1.4	-1.3			-1.1
FAP89	Cre01.g039500	-1.4			-1.2	-1.1			-1.6
FAP297	Cre01.g029350	-1.4		-0.9	-1.3	-0.7			-1.0
FAP369	Cre13.g563700	-1.0		-0.8	-1.0	-0.9			-1.7
FAP67	Cre12.g558700	-1.3		-0.7	-1.4	-1.0			-1.0
FAP87	Cre01.g052150	-1.7			-1.2	-1.4			-0.9
FAP314	Cre12.g529150	-1.0		-0.9	-1.3	-0.8			-1.3
FAP309	Cre17.g718750	-1.3			-1.4	-1.0			-1.4
FAP35	Cre16.g657650	-1.5			-1.3	-0.9			-1.4
FAP221	Cre11.g476376	-1.1		-0.7	-1.4	-0.7			-1.2
FAP104	Cre05.g245701	-1.4			-1.7	-1.0			-1.0
FAP101	Cre02.g112100	-1.5			-1.2	-0.8			-1.5
FAP348	Cre16.g693204	-1.2			-1.6	-1.0			-1.3
FAP28	Cre09.g400923	-1.5			-1.1	-1.0			-1.3
FAP39	Cre02.g145100	-1.1		-0.6	-1.1	-0.8			-1.3
FAP256	Cre10.g431150	-0.8		-0.9	-1.1	-0.8			-1.3
FAP304	Cre01.g045150	-1.4				-2.0			1.2
FAP2	Cre17.g747247	-1.0			-1.4	-0.7			-1.6
FAP137	Cre16.g693600	-0.7			-1.6	-0.7			-1.7
FAP336	Cre17.g740700	-1.1			-1.3	-0.9			-1.4
FAP11	Cre09.g390578	-1.4		-0.7	-1.0	-0.8			-0.7
FAP356	Cre08.g384900	-0.9			-1.4	-0.7			-1.4
FAP152	Cre11.g468850	-1.4		-0.9	-1.1	-1.0			
FAP365	Cre17.g740261	-1.3			-1.3	-0.9			-0.8
FAP44	Cre09.g386736	-1.1		-0.5	-1.3	-0.7			-0.6
FAP208	Cre11.g482001	-1.0			-0.9	-0.9			-1.4
FAP113	Cre07.g321400	-1.1			-1.3	-0.7			-1.1
FAP215	Cre03.g180450	-0.8			-1.1				-2.2
FAP273	Cre03.g200950	-1.5			-0.9	-0.9			-0.9
FAP177	Cre09.g395769	-0.8			-1.4	-0.7			-1.2
FAP218	Cre03.g158400	-0.8			-1.2	-0.8			-1.3
FAP47	Cre17.g704300	-1.0		-0.6	-1.4				-0.8
FAP384	Cre01.g019900	-0.9			-0.9	-0.8			-1.3
FAP76	Cre09.g387689	-1.0			-1.3	-0.6			-0.8
FAP270	Cre09.g407250	-0.7			-1.3	-0.5			-1.3
FAP176	Cre08.g367250	-0.8		-0.8	-0.7				-1.3
FAP206	Cre04.g230340	-0.9		-0.6	-1.4				-0.6
FAP212	Cre02.g077850				-1.7				-1.8

Table J.9. (*Continued*).

Gene		Log2-FC							
		5%				10%			
		1h	12h	20h	36h	1h	12h	20h	36h
FAP78	Cre12.g536600	-0.9			-1.3	-0.6			-0.7
FAP165	Cre03.g211521	-1.2			-1.4	-0.8			
FAP161	Cre13.g564400	-0.9			-1.4				-1.0
FAP324	Cre08.g383101	-0.7			-1.3				-1.3
FAP325	Cre06.g263200	-1.5				-1.6			
FAP244	Cre08.g374700	-1.7			-1.5				
FAP230	Cre01.g012800	-1.3			-1.0	-0.8			
FAP392	Cre14.g627650	-1.4			-1.0	-0.6			
FAP385	Cre12.g495550	-1.5			-1.4				
FAP394	Cre17.g731500				-1.6				-1.3
FAP54	Cre12.g518550	-1.3			-1.4				
FAP364	Cre12.g543500	-1.4				-1.1			
FAP258	Cre07.g325751	-1.4				-0.9			
FAP341	Cre09.g399215	-1.4			-0.9				
FAP61	Cre03.g167600	-1.3			-0.9				
FAP376	Cre16.g658700				-1.5				
FAP233	Cre09.g393450								-1.4
FAP260	Cre17.g708000				-1.4				
FAP276	Cre04.g216203				-1.3				

Table J.10. Upregulated flagella-associated protein DEGs (only showing DEGs with log_2-FC > 1.25) in *Daphnia* treatments relative to controls.

Gene		Log2-FC							
		5%				10%			
		1h	12h	20h	36h	1h	12h	20h	36h
FAP199	Cre09.g399400	4.7	3.0	3.2	4.1		4.4	3.3	3.6
FAP41	Cre10.g452250	4.0	1.8	2.9	3.1		3.7	1.9	3.2
FAP79	Cre04.g217908	2.1	2.5	2.1	1.9		1.6	2.5	2.5
FAP413	Cre08.g364000	1.4	1.4	0.8	0.9		1.2	1.7	1.2
FAP211	Cre02.g077750			2.7	1.1				2.3
FAP380	Cre01.g010400	1.3		0.9	1.5		1.6		
FAP346	Cre12.g492600		1.5	1.0				1.3	1.3
FAP23	Cre01.g005850	0.7	0.8	1.5			1.1		
FAP224	Cre06.g298350	1.4					1.5		
FAP37	Cre17.g747297				2.0				

J.7.4 Structural flagellar proteins

Table J.11. Structural flagellar protein DEGs in *Daphnia* treatments relative to controls.

Gene		Log$_2$-FC							
		5%				10%			
		1h	12h	20h	36h	1h	12h	20h	36h
TUA1	Cre03.g190950	-0.7			-0.8	-0.7			
TUA2	Cre04.g216850	-0.5			-0.9				
TUB1	Cre12.g542250	-1.4	-1.0	-1.0	-1.1	-1.2	-1.0	-0.8	-0.6
TUB2	Cre12.g549550	-1.2	-0.6		-0.9	-1.0	-0.7		
CEP95	Cre12.g497250	-1.5			-1.1	-1.4			-1.3
CEP131	Cre09.g394732	-1.0				-1.8			-2.3
CEP83	Cre11.g467620	-0.9			-0.9	-0.6			-1.5
CEP19	Cre12.g487350				-0.5				-0.8
RSP1	Cre03.g201900	-1.3		-0.8	-1.4	-0.9			-0.7
RSP2	Cre10.g427300	-1.2			-0.7	-0.8			
RSP3	Cre06.g291700							0.8	
RSP4	Cre05.g242500	-0.8		-0.6	-1.0	-0.7			-0.6
RSP5	Cre12.g544000	-1.0			-1.0	-0.8			-0.6
RSP6	Cre05.g242550	-1.4			-1.2	-1.0			-0.7
RSP7	Cre07.g347050	-0.7		-0.5	-1.1	-0.6			-1.0
RSP8	Cre02.g078600	-0.6			-0.7				-0.6
RSP9	Cre07.g330200	-0.9		-0.6	-1.0	-0.9			-0.7
RSP10	Cre01.g005450	-0.8			-1.0				
RSP11	Cre10.g465250	-0.8			-1.0	-0.5			
RSP12	Cre02.g114700	-0.8			-1.3				-0.8
RSP14	Cre14.g617500	-1.0		-0.8	-0.9	-0.8			-0.9
RSP16	Cre12.g511050	-1.0			-0.8	-0.7			-0.6
RSP17	Cre07.g340400	-0.9			-0.8	-0.6			
RSP20	Cre03.g178150			-0.4	-1.1				-1.1

J.7.5 Intraflagellar transport (IFT)

Table J.12. All IFT DEGs ($p < 0.05$) in *Daphnia* treatments relative to controls.

Gene		Log_2-FC							
		5%				10%			
		1h	12h	20h	36h	1h	12h	20h	36h
IFT140	Cre08.g362650	-1.6	-0.8	-0.9	-1.6	-1.2	-0.8		-1.3
IFT144	Cre13.g572700	-1.4	-0.7	-1.0	-1.2	-1.0			-1.2
IFT121	Cre11.g475000	-1.4	-0.7	-0.9	-1.3	-0.9			-1.0
IFT122	Cre01.g065822	-1.4		-0.7	-1.4	-1.0			-1.3
IFT25	Cre10.g450350	-1.3			-1.6	-1.0			-1.3
IFT139	Cre06.g268800	-0.8		-0.6	-1.4	-0.7			-1.2
IFT43	Cre06.g251200	-0.9		-0.6	-1.0	-0.8			-1.3
IFT172	Cre17.g703900	-1.2			-1.5	-0.8			-1.1
IFT27	Cre01.g047950	-0.9			-1.2	-1.1			-1.4
IFT56	Cre11.g467616	-1.0			-1.2	-0.9			-1.2
IFT80	Cre03.g204150	-1.1			-1.3	-0.8			-1.1
IFT81	Cre17.g723600	-1.2			-1.2	-0.9			-0.9
IFT46	Cre05.g241637	-0.8			-1.3	-0.9			-1.2
IFT74	Cre01.g027950	-1.0			-1.2	-1.0			-1.1
IFT88	Cre07.g335750	-1.3			-1.1	-1.0			-0.8
IFT54	Cre11.g467739	-1.1			-1.0	-0.9			-1.0
IFT20	Cre02.g089950	-0.9			-1.2	-0.8			-1.0
IFT70	Cre07.g342200	-1.0			-1.0	-0.8			-0.9
IFT38	Cre17.g721250	-1.0			-0.9	-0.9			-0.7
IFT22	Cre01.g039200	-1.0			-0.8	-0.7			-0.7
IFT52	Cre04.g219250	-0.9			-1.0	-0.6			-0.7
IFT57	Cre10.g467000	-0.7			-0.6	-0.5			

Appendix K. Mutant bioassays - Phenotype at low and high light

All strains were cultured with regular transfers for three months under low light (8 µmol m^{-2} s^{-1}), before flasks were emptied, refilled with fresh media, and monitored over eight days. CC-5325 grew the fastest, consistent with literature reports (Tammana and Tammana, 2017), reaching ~9 × 10^6 cells mL^{-1} by day three and remaining above 8 × 10^6 cells mL^{-1} through to day eight. Mutant cultures all plateaued at ~8 × 10^6–10^7 cells mL^{-1} by day six to seven before declining (**Figure K.1**).

While cultured under high light (188 µmol m^{-2} s^{-1}), growth was greater than under low light (**Figure K.1**). CC-5325 again grew faster than mutants, reaching ~3.3 × 10^7 cells mL^{-1}, while mutants plateaued at ~2.5 × 10^7 cells mL^{-1}.

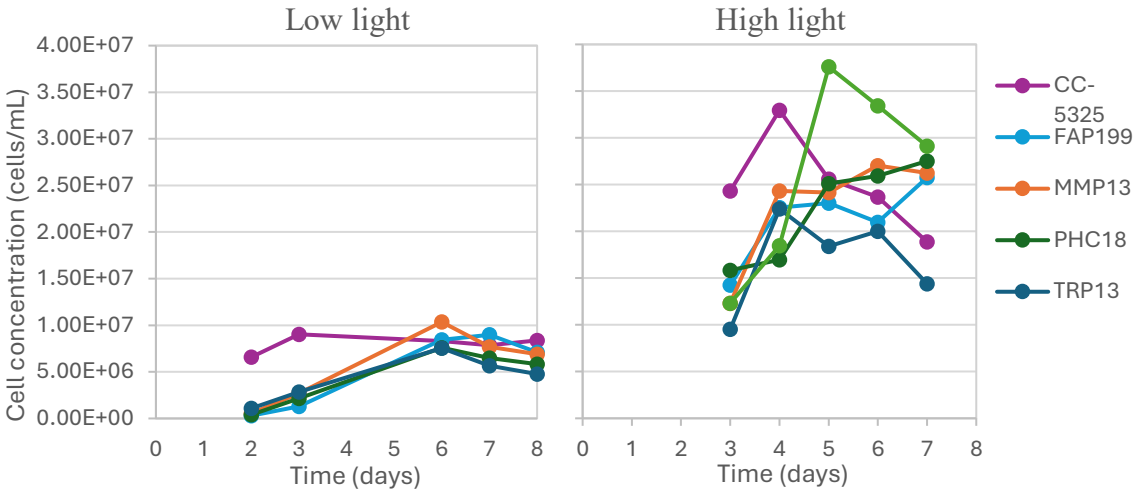

Figure K.1. Cell concentration over eight days in *C. reinhardtii* CC-1690, CC-5325 and mutants FAP199, MMP13, PHC18, and TRP13. Cultures were incubated under constant low light (8.2 ± 0.5 µmol m^{-2} s^{-1}) and high light (188.6 ± 10.6 µmol m^{-2} s^{-1}).

Under both low and high light, CC-5325 and TRP13 cultures remained predominantly unicellular, while the other strains exhibited different phenotypes at each light level. The colony size distributions are provided in **Figure K.2** and **Figure K.3**.

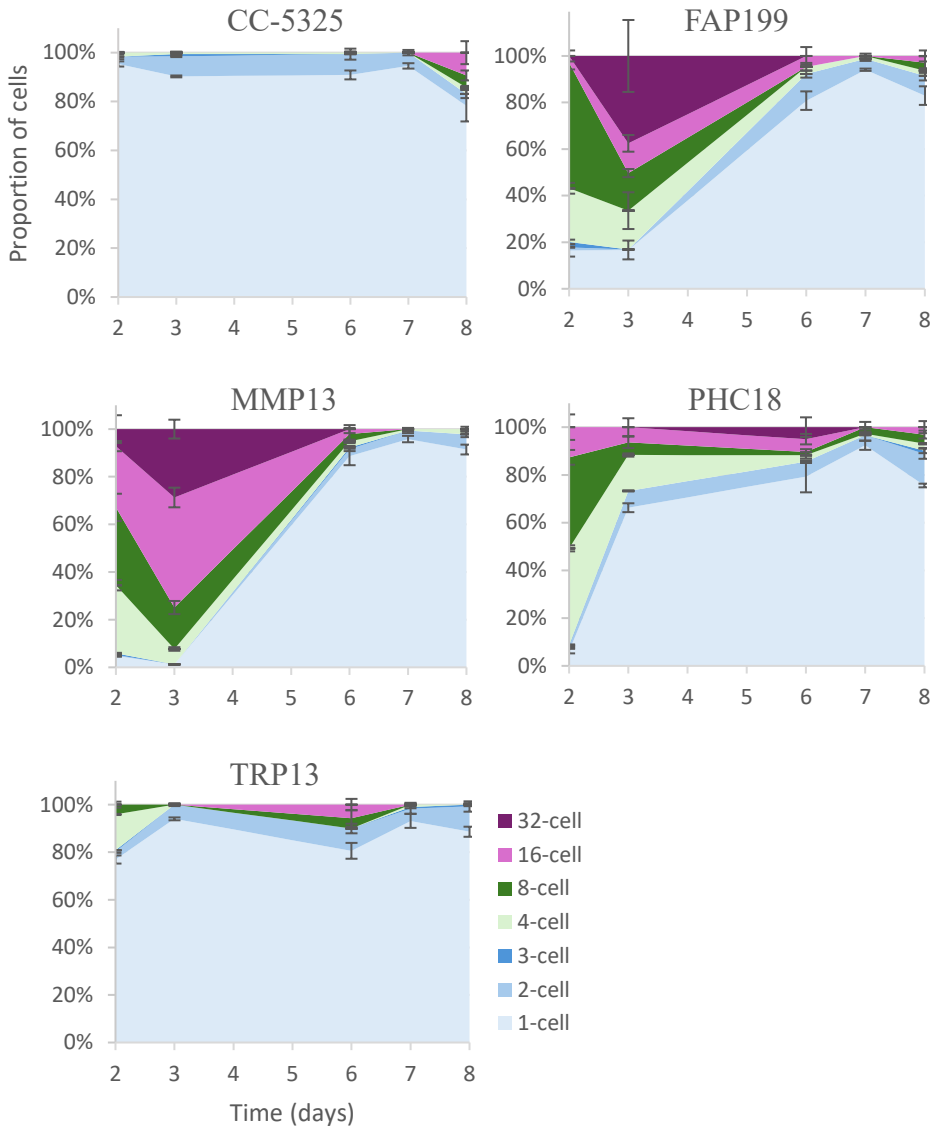

Figure K.2. Proportion of cells, single and in colonies, in *C. reinhardtii* CC-5325 and mutants FAP199, MMP13, PHC18, and TRP13, over eight days under constant low light (8.2 ± 0.5 µmol m^{-2} s^{-1}).

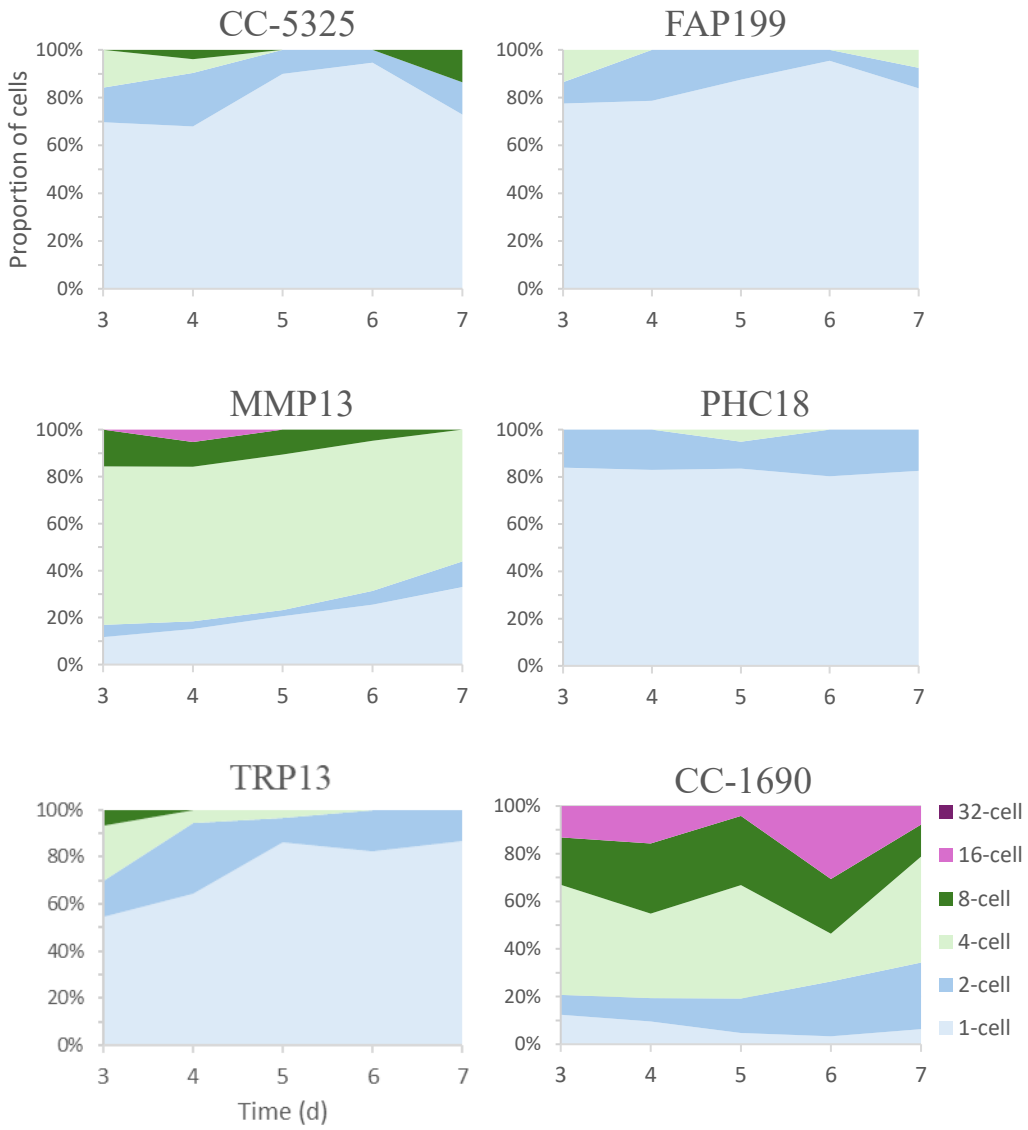

Figure K.3. Proportion of cells, single and in colonies, in *C. reinhardtii* CC-5325 and CC-1690, and mutants FAP199, MMP13, PHC18, TRP13, over seven days under constant high light (188.6 ± 10.6 µmol m^{-2} s^{-1}).

Appendix L. Metabolomics sample replicates

Table L.1. Number of *C. reinhardtii* sample replicates included in the full GC-MS analysis, by treatment and time point. Biological replicates represent independent culture flasks; technical replicates were generated from separate ~1 mg aliquots of the same biological replicate; extra derivatisation replicates were created by splitting the same extract into multiple GC vials when biomass was limited. Total replicates include both technical and extra derivatisation replicates.

Treatment	Time	Number of Replicates			
		Biological	Technical (total)	Extra derivatisation	Total
Control	-0.5 h	3	9		9
	1 h	3	3	6	9
	2 h	3	4	2	6
	12 h	3	4	5	9
	14 h	3	8		8
	20 h	3	7	2	9
	36 h	3	5	3	8
5% Extract	1 h	3	8	1	9
	2 h	3	9		9
	14 h	3	8	1	9
	20 h	1	3		3
	36 h	3	8	1	9
10% Extract	1 h	3	8	2	10
	2 h	3	9		9
	12 h	2	4	2	6
	14 h	3	9		9
	20 h	3	9		9
	36 h	3	8	1	9

Appendix M. Metabolomics trials

Table M.1. Relative abundances of metabolites detected in *Daphnia* extracts by GC-MS (MCF derivatisation; Trial 1). Columns correspond to extract type. Data are single runs used to assess detectability. Missing values indicate non-detection. Colour intensity reflects relative abundance. Metabolites in **bold** were detected in *C. reinhardtii* also.

Metabolite	Relative Abundance						
	Sera Extract	MPS Extract	MPS Extract	Frozen Extract	Frozen Extract	MPS *Daphnia*	*D. thomsoni* filtrate
	500 µL	500 µL	500 µL	500 µL	500 µL	10 mg	500 µL
Dodecane	5.28	0.06	0.09	0.19	0.19	4.30×10^{-3}	
Lactic acid	56.85	2.79	2.98	2.12	1.94	3.29×10^{-2}	2.67×10^{-4}
Caprylic acid	1.54	0.04	0.04	0.07	0.04	2.69×10^{-3}	
Benzoic acid	2.23	0.07	0.07	0.08	0.10	1.13×10^{-3}	1.37×10^{-5}
Nicotinic acid	1.27	0.01	0.01	0.04	0.04	4.10×10^{-3}	
Alanine	229.21	5.08	5.43	24.93	26.31	2.50	
Glycine	86.95	0.81	0.86	10.38	11.91	0.56	3.27×10^{-4}
Para-Toluic acid	0.86	3.18×10^{-3}	3.71×10^{-3}	0.03	0.03	3.21×10^{-3}	2.15×10^{-3}
Adipic acid	1.99	0.19	0.22	0.05	0.03	5.86×10^{-4}	1.88×10^{-5}
Caprinoic acid	0.44	0.01	0.01	0.03	0.02	4.74×10^{-3}	2.65×10^{-5}
Beta-Alanine	15.42	0.29	0.31	1.45	1.54	0.12	7.09×10^{-5}
Valine	163.23	3.43	3.70	19.84	21.20	1.78	1.61×10^{-4}
Isoleucine	52.68	1.17	1.29	6.85	7.33	0.74	2.12×10^{-4}
Proline	159.58	3.48	3.74	20.43	21.15	1.45	4.29×10^{-4}
Dodecanoic acid (C12_0)	1.66	0.06	0.07	0.05	0.05	0.01	3.24×10^{-4}
Threonine	46.98	0.56	0.59	6.96	7.92	0.32	3.37×10^{-4}
Aspartic acid	32.71	0.29	0.29	7.37	11.34	0.88	1.43×10^{-4}
Asparagine	2.29	0.10	0.10	2.24	2.85	0.11	1.36×10^{-4}
Glutamic acid	26.89	0.33	0.30	3.82	6.05	0.48	3.56×10^{-5}
Phenylalanine	65.68	0.96	1.06	12.85	13.65	1.12	1.33×10^{-4}
10,13-dimethyltetra-decanoic acid	5.52	0.01	0.02	0.05	0.04	0.50	2.23×10^{-3}
Stearic acid (C18_0)	1.10	0.01	0.01	0.03	0.03	0.05	1.82×10^{-3}
Ornithine	18.40	0.16	0.16	6.64	8.00	0.15	2.19×10^{-4}
Lysine	96.45	2.28	2.24	23.25	24.89	3.35	1.93×10^{-4}
Tyrosine	56.76	0.97	1.06	7.39	8.81	0.66	2.30×10^{-5}
Tryptophan	43.18	0.46	0.50	11.29	12.64	1.01	6.04×10^{-4}

Table M.2. Relative abundances of metabolites detected in *C. reinhardtii* by GC-MS (MCF derivatisation; Trial 2) normalized against biomass concentration and multiplied by a factor of 1000. Columns correspond to extract type and biomass amount. Data are single runs (no replicates) used to assess detectability. Missing values indicate non-detection. Missing values indicate non-detection. Colour intensity reflects relative abundance. Metabolites in **bold** were detected in *Daphnia* extracts also.

Metabolite	Relative Abundance			
	5% Extract Treatment		Control	
	0.59 mg	2.28 mg	0.35 mg	3.73 mg
Nicotinamide		0.26		
Succinic acid	3.34	2.75	7.32	3.74
Lactic acid	3.80	3.48	1.21	0.36
Caprylic acid		0.05		0.08
Dodecane		0.04		
2-Hydroxybutyric acid	0.02	0.06		0.06
Alanine	26.11	23.63	42.85	18.02
Valine	11.33	11.47	20.14	8.77
Leucine	10.66	12.15	21.91	9.75
Isoleucine	3.47	3.32	6.08	2.55
Proline	11.51	11.38	17.52	8.02
Malic acid	0.58	0.42	0.61	0.47
Dodecanoic acid (C12_0)		0.34		0.04
Threonine	1.34	1.63	2.42	1.30
Aspartic acid	3.25	4.04	5.43	3.63
Azelaic acid	0.48	0.40	0.40	0.20
Creatinine	0.86	1.01	1.78	0.70
Serine	0.32	0.42	0.61	0.32
Myristic acid (C14_0)	2.64	2.36	1.86	1.40
Glutamic acid	3.41	4.13	7.54	3.65
Glutathione	0.70	0.70	1.40	0.57
Pentadecanoic acid (C15_0)		0.09		0.05
Phenylalanine	4.50	5.50	10.20	4.59
Cysteine	0.23	0.27	0.63	0.27
Palmitelaidic acid (C16_1n-9c)	7.41	4.81	5.02	2.08
10,13-dimethyltetradecanoic acid (C17_0)	179.77	103.67	163.80	66.83
Putrescine	9.53	7.52	21.72	5.55
Alpha-Linolenic acid (C18_3n-3,6,9c)	22.10	22.69	16.12	8.33
Trans-Vaccenic acid	57.46	44.44	43.74	19.49
Oleic acid (C18_1n-9c)	26.19	20.54	21.76	9.63
Stearic acid (C18_0)	31.03	13.68	26.18	8.61
Ornithine	2.01	1.83	1.51	0.62
Lysine	9.16	13.66	14.63	9.00
Tyrosine	1.91	2.99	4.21	2.54
Tryptophan	0.90	2.43	2.62	2.20

Table M.3. Relative abundances of metabolites identified in *C. reinhardtii* by GC-MS (TMS derivatisation; Trial 3) normalized against biomass concentration and multiplied by a factor of 1000. Columns correspond to extract type and biomass amount. Data are single runs (no replicates). Missing values indicate non-detection.

Metabolite	Relative Abundance							
	5% Extract Treatment				Control			
	0.42 mg		2.11 mg		0.48 mg		2.16 mg	
	50 µL	200 µL	50 µL	200 µL	50 µL	200 µL	50 µL	200 µL
Glycolic acid				5.62		0.05		13.42
Oxalic acid								7.43
Caprylic acid				0.04		0.20		0.33
Urea				1.81				1.65
1,3-dihydroxyacetone								2.35
Ethanolamine	2.18	12.03	26.07	181.40	2.18	15.80	16.30	122.87
Phosphoric acid	25.58	144.30	107.16	1034.6	23.40	216.25	85.33	1187.2
DL-isoleucine 2	0.54	3.84	3.17	25.20	0.25	2.51	3.04	33.61
Glycine	3.54	9.85	13.70	79.64	2.35	4.20	10.22	80.45
Succinic acid		2.07		30.37		5.08		39.00
Capric acid		0.89		8.11		0.71		4.92
Uracil	0.48	2.27	1.62	13.16	0.43	1.68	1.29	11.10
L-serine 2	0.09	1.68	1.19	10.41	0.16	1.56	1.45	17.35
L-threonine 2				10.04				19.27
Aspartic acid 1				6.02		1.21		9.92
Capric acid				1.33				4.06
D-malic acid		0.71		13.32		2.72		20.27
4-guanidinobutyric acid 2	7.35		9.96		7.43		8.39	2.31
L-glutamic acid 2	0.45	3.30	1.95	18.77	0.18	1.29	1.88	23.23
Pyrophosphate				7.95				
5-aminovaleric acid 3	1.72		2.24		1.54		1.79	0.25
Putrescine	16.30	97.47	154.20	1260.9	7.61	43.64	20.97	200.94
Glycerol 1-phosphate		1.19		25.75		0.71		10.09
Azelaic acid				2.82				3.62
Citric acid		0.28		5.77		1.84		6.26
Galactose	1.40	8.31	8.49	52.64		0.10	0.09	0.93
Adenine 1		1.33	0.05	8.18		0.81	0.21	5.71
D (+)altrose 1		7.42		87.26		1.45		54.95
L-lysine 2	0.33	2.33	1.77	20.02	0.31	2.50	2.09	27.98
L-tyrosine 2	0.14	1.99	1.37	15.22	0.13	1.39	1.57	21.45
Palmitic acid		0.08		28.09				9.52
L-tryptophan 2		0.15	0.04	2.56		0.15	0.14	3.17
Elaidic acid				7.80				1.80
Stearic acid				10.90				2.86
6-phosphogluconic acid				3.22		0.93		8.18
Docosanoic acid		0.13		0.58		0.04		0.40
Alizarin		0.05	0.17	1.35				0.36
Guanosine 2		9.08		141.85		10.93		83.80

Appendix N. Results of statistical tests for *C. reinhardtii* metabolites

N.1. Two-way ANOVA

Table N.1. Results of two-way ANOVA for *C. reinhardtii* metabolites abundances across treatments (5% and 10% *Daphnia* extract, and control) and timepoints (1, 2, 12, 14, 20, and 36 h). *p*-values are shown both raw and FDR-adjusted. Metabolites in bold had statistically significant terms after FDR correction ($p < 0.05$).

Metabolite	term	df1	df2	statistic	*p*	*p* adj.	Eta $_{sq.}$ partial
L-alanine	Treatment	2	123	28.76	5.67E-11	1.70E-10	0.2502
L-alanine	Time	5	123	3.5	5.38E-03	5.38E-03	0.0762
L-alanine	Treatment:Time	9	123	3.54	6.13E-04	9.19E-04	0.1387
L-leucine	Treatment	2	123	314.96	4.07E-49	1.22E-48	0.6781
L-leucine	Time	5	123	9.41	1.29E-07	1.29E-07	0.0507
L-leucine	Treatment:Time	9	123	14.33	1.26E-15	1.89E-15	0.1389
N-methylalanine	Treatment	2	122	593.05	1.42E-63	2.13E-63	0.3146
N-methylalanine	Time	5	122	179.2	1.91E-54	1.91E-54	0.2376
N-methylalanine	Treatment:Time	9	122	174.02	3.32E-65	9.95E-65	0.4154
L-valine	Treatment	2	123	104.98	2.53E-27	7.58E-27	0.4481
L-valine	Time	5	123	1.04	4.00E-01	4.00E-01	0.0111
L-valine	Treatment:Time	9	123	14.49	9.01E-16	1.35E-15	0.2784
ethanolamine	Treatment	2	123	2.26	1.09E-01	1.63E-01	0.0299
ethanolamine	Time	5	123	2.53	3.24E-02	9.71E-02	0.0836
ethanolamine	Treatment:Time	9	123	1.23	2.85E-01	2.85E-01	0.073
phosphoric acid	Treatment	2	123	345.3	3.46E-51	3.46E-51	0.1248
phosphoric acid	Time	5	123	318.38	1.41E-68	2.11E-68	0.2876
phosphoric acid	Treatment:Time	9	123	347.79	5.19E-83	1.56E-82	0.5654
DL-isoleucine	Treatment	2	123	179.16	3.63E-37	1.09E-36	0.5749
DL-isoleucine	Time	5	123	7.16	6.52E-06	6.52E-06	0.0574
DL-isoleucine	Treatment:Time	9	123	11.79	3.12E-13	4.68E-13	0.1703
L-proline	Treatment	2	123	274.72	4.25E-46	1.27E-45	0.691
L-proline	Time	5	123	4.82	4.63E-04	4.63E-04	0.0303
L-proline	Treatment:Time	9	123	10.95	2.15E-12	3.22E-12	0.1239
capric acid	Treatment	2	123	1.77	1.74E-01	3.83E-01	0.0251
capric acid	Time	5	123	1.33	2.55E-01	3.83E-01	0.0471
capric acid	Treatment:Time	9	123	0.92	5.12E-01	5.12E-01	0.0584

Table N.1. (*Continued*).

Metabolite	term	df1	df2	statistic	*p*	*p* adj.	Eta $_{sq.}$ partial
glyoxylic acid	Treatment	2	123	3.24	4.25E-02	1.28E-01	0.0451
glyoxylic acid	Time	5	123	1.11	3.60E-01	4.69E-01	0.0385
glyoxylic acid	Treatment:Time	9	123	0.97	4.69E-01	4.69E-01	0.0607
L-serine	Treatment	2	123	144.58	5.03E-33	5.03E-33	0.2504
L-serine	Time	5	123	68.09	8.82E-34	1.32E-33	0.2948
L-serine	Treatment:Time	9	123	44.68	1.22E-34	3.66E-34	0.3482
adipic acid	Treatment	2	123	374.45	4.91E-53	7.36E-53	0.3155
adipic acid	Time	5	123	112.69	3.34E-44	3.34E-44	0.2374
adipic acid	Treatment:Time	9	123	104.28	3.17E-53	7.36E-53	0.3954
L-pyroglutamic acid	Treatment	2	123	371.03	7.96E-53	2.39E-52	0.4116
L-pyroglutamic acid	Time	5	123	63.27	2.29E-32	2.29E-32	0.1755
L-pyroglutamic acid	Treatment:Time	9	123	69.05	7.78E-44	1.17E-43	0.3447
threonic acid	Treatment	2	123	30.48	1.77E-11	2.65E-11	0.1769
threonic acid	Time	5	123	13.94	8.59E-11	8.59E-11	0.2023
threonic acid	Treatment:Time	9	123	10.11	1.57E-11	2.65E-11	0.2639
L-glutamic acid	Treatment	2	123	46.33	1.01E-15	1.01E-15	0.0943
L-glutamic acid	Time	5	123	42.8	2.31E-25	3.47E-25	0.2177
L-glutamic acid	Treatment:Time	9	123	61.46	2.70E-41	8.10E-41	0.5628
1,3-diaminopropane	Treatment	2	123	599.77	3.65E-64	5.48E-64	0.2737
1,3-diaminopropane	Time	5	123	391.34	1.01E-73	3.04E-73	0.4465
1,3-diaminopropane	Treatment:Time	9	123	122.54	4.81E-57	4.81E-57	0.2517
putrescine	Treatment	2	123	4.82	9.63E-03	1.45E-02	0.0585
putrescine	Time	5	123	3.83	2.95E-03	8.85E-03	0.116
putrescine	Treatment:Time	9	123	1.47	1.67E-01	1.67E-01	0.0801
galactose	Treatment	2	123	804.45	2.29E-71	6.87E-71	0.4169
galactose	Time	5	123	308.86	7.93E-68	1.19E-67	0.4001
galactose	Treatment:Time	9	123	64.8	1.93E-42	1.93E-42	0.1511
fructose	Treatment	2	123	148.06	1.80E-33	1.80E-33	0.1235
fructose	Time	5	123	143.39	1.44E-49	2.16E-49	0.299
fructose	Treatment:Time	9	123	140.19	2.80E-60	8.39E-60	0.5262
tyramine	Treatment	2	123	413.59	2.48E-55	3.72E-55	0.2462
tyramine	Time	5	123	179.86	8.53E-55	8.53E-55	0.2677
tyramine	Treatment:Time	9	123	167.74	1.17E-64	3.51E-64	0.4494
L-lysine	Treatment	2	123	141.96	1.11E-32	3.32E-32	0.3161
L-lysine	Time	5	123	37.43	3.54E-23	3.54E-23	0.2084
L-lysine	Treatment:Time	9	123	33.79	3.11E-29	4.67E-29	0.3386
L-tyrosine	Treatment	2	123	278.51	2.13E-46	6.40E-46	0.3777
L-tyrosine	Time	5	123	63.91	1.46E-32	1.46E-32	0.2167
L-tyrosine	Treatment:Time	9	123	52.78	4.65E-38	6.98E-38	0.3221

N.2. Shapiro-wilk, Bartlett's, Levene's, and Welch's one-way ANOVA tests

Table N.2. Results of Shapiro-Wilk normality test, Bartlett's and Levene's homogeneity of variance tests, and Welch's one-way ANOVA for *C. reinhardtii* metabolites abundances across treatments (5% and 10% *Daphnia* extract, and control) and timepoints (1, 2, 12, 14, 20, and 36 h). *n total* = total observations; *Groups* = number of treatment-timepoint combinations. Welch *p*-values are shown both raw and FDR-adjusted. "NA" indicates that the Welch test could not be performed due to insufficient variance structure. Metabolites in bold were statistically significant after FDR correction (Welch $p < 0.05$).

Metabolite	n total	Groups	Shapiro *p*	Bartlett *p*	Levene *p*	Welch *p*	Welch *p* FDR
L-alanine	140	17	5.00×10^{-7}	6.84×10^{-15}	1.07×10^{-6}	1.91×10^{-7}	6.68×10^{-7}
L-leucine	140	17	2.59×10^{-7}	0	1.98×10^{-7}	1.64×10^{-4}	2.29×10^{-3}
N-methylalanine	139	17	1.44×10^{-20}	0	3.25×10^{-10}	7.56×10^{-7}	1.76×10^{-6}
L-valine	140	17	2.57×10^{-8}	0	5.60×10^{-10}	3.25×10^{-14}	3.41×10^{-13}
Ethanolamine	140	17	1.78×10^{-10}	4.60×10^{-19}	1.42×10^{-3}	2.99×10^{-7}	8.97×10^{-7}
Phosphoric acid	140	17	1.63×10^{-23}	0	1.49×10^{-7}	NA	NA
DL-isoleucine	140	17	3.57×10^{-9}	0	1.01×10^{-11}	1.15×10^{-8}	6.04×10^{-8}
L-proline	140	17	9.07×10^{-17}	0	1.02×10^{-12}	0.0109	0.0120
Capric acid	140	17	1.37×10^{-3}	0.397	0.845	0.259	0.259
Glyoxylic acid	140	17	1.22×10^{-3}	0.386	0.801	0.134	0.140
L-serine	140	17	4.73×10^{-18}	0	9.83×10^{-15}	9.57×10^{-7}	2.01×10^{-6}
Adipic acid	140	17	2.88×10^{-20}	0	3.77×10^{-6}	3.46×10^{-4}	5.83×10^{-4}
L-pyroglutamic acid	140	17	7.27×10^{-18}	0	4.29×10^{-7}	1.91×10^{-3}	2.45×10^{-3}
Threonic acid	140	17	1.02×10^{-3}	0	0.0457	4.91×10^{-8}	2.06×10^{-7}
L-glutamic acid	140	17	1.67×10^{-14}	0	6.58×10^{-5}	4.29×10^{-7}	1.13×10^{-6}
1,3-diaminopropane	140	17	3.51×10^{-15}	0	3.57×10^{-10}	6.45×10^{-10}	4.51×10^{-9}
Putrescine	140	17	0.0374	0.277	0.916	2.12×10^{-3}	2.47×10^{-3}
Galactose	140	17	1.11×10^{-9}	0	2.92×10^{-4}	2.97×10^{-15}	6.25×10^{-14}
Fructose	140	17	8.09×10^{-24}	0	2.55×10^{-7}	NA	NA
Tyramine	140	17	8.79×10^{-22}	0	1.16×10^{-6}	6.45×10^{-4}	9.68×10^{-4}
L-lysine	140	17	1.85×10^{-15}	0	8.07×10^{-12}	1.99×10^{-3}	2.45×10^{-3}
L-tyrosine	140	17	2.33×10^{-18}	0	3.13×10^{-10}	3.61×10^{-4}	5.83×10^{-4}

N.3. Games-Howel post-hoc tests

Figure N.1 shows only metabolites with no significant ($p < 0.05$) pairs between treatments, from Games-Howel post-hoc pairwise tests. Heatmaps of significant metabolites are provided in **Chapter 4**, **Figure 4.1**. Full Games-Howell test results are provided in **Supplementary Data File S2**.

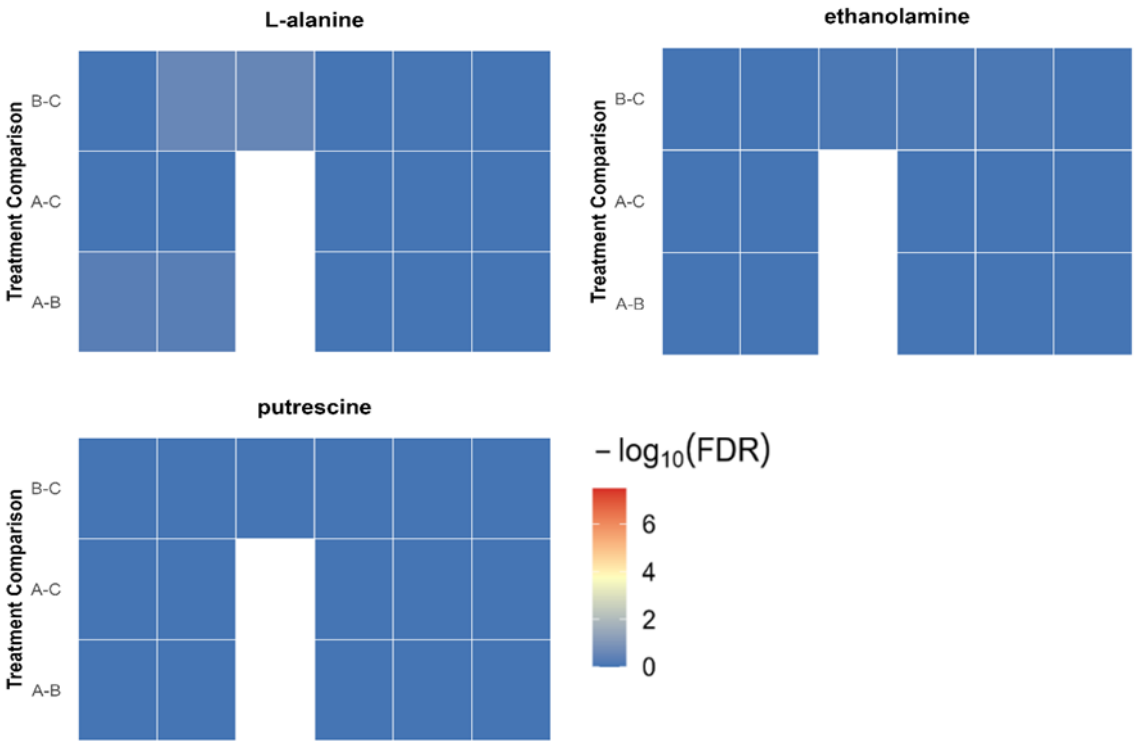

Figure N.1. Games-Howell post-hoc pairwise tests between treatments (A: 5% *Daphnia* extract, B: 10% *Daphnia* extract, C: Control), for metabolites with no significantly different pairs. Colour scale reflects -$\log_{10}$FDR; white cells indicate that the metabolite was absent in one or both treatments, except for pairs with A_12 h, which was not tested.

Appendix O. MetaboAnalyst pathway and enrichment analysis

Table O.1. Metabolic pathway and enrichment analysis results from *C. reinhardtii* using MetaboAnalyst. Analysis was performed on 18 metabolites showing significant differences in relative abundance between treatments (Welch's ANOVA). Pathway enrichment was assessed using the hypergeometric test, topology measured as relative-betweenness centrality, the *C. reinhardtii* pathway library, and KEGG human metabolic pathways as the reference. Significant pathways are bolded based on adjusted *p* values and false discovery rate (FDR).

	Enrichment			Pathway		
	p	*p* adj	FDR	*p*	*p* adj	FDR
Valine, leucine and isoleucine biosynthesis	**3.27E-05**	**0.0026**	**0.0026**	0.0024	0.19	0.063
Isoquinoline alkaloid biosynthesis				0.0023	0.18	0.063
Glucosinolate biosynthesis				0.0024	0.19	0.063
Glutathione metabolism	0.0017	0.14	0.069	0.0044	0.33	0.069
Arginine and proline metabolism	0.0036	0.28	0.090	0.0035	0.26	0.069
Valine, leucine and isoleucine degradation	0.0045	0.35	0.090	0.0072	0.52	0.080
Alanine, aspartate and glutamate metabolism	0.025	1	0.41	0.024	1	0.24
Glyoxylate and dicarboxylate metabolism	0.031	1	0.41	0.041	1	0.32
Phenylalanine, tyrosine and tryptophan biosynthesis	0.036	1	0.41	0.26	1	0.87
Nitrogen metabolism	0.053	1	0.48	0.14	1	0.71
Tyrosine metabolism	0.054	1	0.48	0.032	1	0.28
Phenylalanine metabolism	0.071	1	0.57			
Biotin metabolism	0.088	1	0.64			
Cyanoamino acid metabolism				0.052	1	0.35
Lysine biosynthesis				0.11	1	0.68
Arginine biosynthesis	0.12	1	0.73	0.21	1	0.87
D-Amino acid metabolism	0.13	1	0.73	0.0055	0.40	0.072
Butanoate metabolism	0.13	1	0.73			
Sulfur metabolism				0.1363	1	0.71
Histidine metabolism	0.14	1	0.73			
Ubiquinone and other terpenoid-quinone biosynthesis	0.15	1	0.74			
Selenocompound metabolism	0.17	1	0.74	0.19	1	0.87
Pantothenate and CoA biosynthesis	0.17	1	0.74	0.26	1	0.87
beta-Alanine metabolism	0.18	1	0.74	0.15	1	0.72
Lysine degradation	0.24	1	0.88			
Porphyrin metabolism	0.25	1	0.88	0.51	1	1
Sphingolipid metabolism	0.26	1	0.88	0.22	1	0.87
Glycine, serine and threonine metabolism	0.26	1	0.88	0.33	1	1
Cysteine and methionine metabolism	0.26	1	0.88	0.43	1	1
Glycerophospholipid metabolism	0.28	1	0.91	0.05	1	0.35
One carbon pool by folate				0.23	1	0.87
Carbon fixation by Calvin cycle				0.25	1	0.87

Appendix P. Infochemical bioassays

P.1. Microalgae culturing

C. reinhardtii CC-1690 was cultured and maintained in sterile tris-acetate-phosphate (TAP) liquid media and *C. vulgaris* 259 and *T. obliquus* UTEX 3155 in sterile BG-11 liquid media. The microalgae were cultured in conical flasks, closed with cotton stoppers, and incubated at 22 °C, on an orbital shaker at 115 rpm, and under continuous light 24 ± 1 μmol m^{-2} s^{-1}. To avoid nutrient limitation and significant pH decline, cultures were refreshed weekly by adding up to 5 mL culture to 100 mL of fresh media in a clean and sterile flask.

P.2. Bioassay set-up

To test the activity of reported *Daphnia* infochemicals for inducing self-aggregation in microalgae, bioassays were carried out in sterile 6-well Falcon tissue culture plates, where each well contained 5 mL total of microalgae and various treatments. Actively growing, recently refreshed microalgae cultures were used to ensure that nutrient availability was not a contributing factor to any response. The plates were covered with Parafilm to allow for gas transfer whilst keeping the cultures sterile. The plates were incubated under the same conditions as the stock cultures.

Sodium dodecyl sulphate (SDS) and sodium octyl sulphate (SOS) were purchased from Sigma-Aldrich. These were dissolved in distilled water and autoclaved (121 °C for 15 minutes). The solutions were appropriately diluted in sterile distilled water and added to *C. reinhardtii* CC-1690 and *T. obliquus*, at doses based on the active concentrations reported to induce colony formation in *S. gutwinskii* after 10 days (Yasumoto et al., 2005). Controls contained an equivalent volume of sterile distilled water, e.g., 10% v/v water in the control and 10% v/v infochemical solution in the treatments.

SDS was tested in *C. reinhardtii* at 10, 10^2, 10^3, and 10^4 ng mL^{-1}, and in *T. obliquus* at 10 ng mL^{-1}; SOS was tested in *C. reinhardtii* at 10, 10^2, and 10^3 ng mL^{-1}. SDS experiments were sampled at 0, 1, 2, and 4 days, and the SOS experiment was sampled at 0, 1, 2, 3, 4, and 10 days. Where treatments were run in triplicate, statistical analyses were carried out to determine if the proportion of single cells was significantly different between treatments or timepoints.

P.3. Morphological analysis

C. reinhardtii colony formation and cell concentration were monitored using light microscopy. 100 µL of each sample was fixed with Lugol's iodine at 2% v/v and 10 µL was placed on a haemocytometer and imaged in Brightfield at 10x magnification (Olympus U-LH100HG BX53); sample images of all four haemocytometer grid corners were later manually analysed by counting the number of single, paired, and aggregated cells, giving the total cell concentration, and the colony size distribution.

P.4. Statistical analyses

Two-way ANOVA tests were run using R-studio, on the proportion of single in each group, to test effects of treatment and time. All parameters had triplicate measurements for all timepoints. The ANOVA *p*-values were adjusted for multiple testing using the Benjamini-Hochberg method to control the false discovery rate. For each parameter, Levene's test and the Shapiro-Wilk test were used to check that residuals were normally distributed, and that the variance was equal across treatment and time groups. Where the residuals were not normally distributed, log and cube root transformations were used to improve it. The best transformation per parameter was selected based on the Shapiro-Wilk p-value. For parameters with significant ANOVA effects, post-hoc pairwise comparisons were carried out using Tukey's HSD test, on treatment, time, and their interactions, which adjusts *p*-values for multiple comparisons. R packages used in statistical analyses included **car**, **broom**, **emmeans**, and **ggplot2**.

P.5. Results

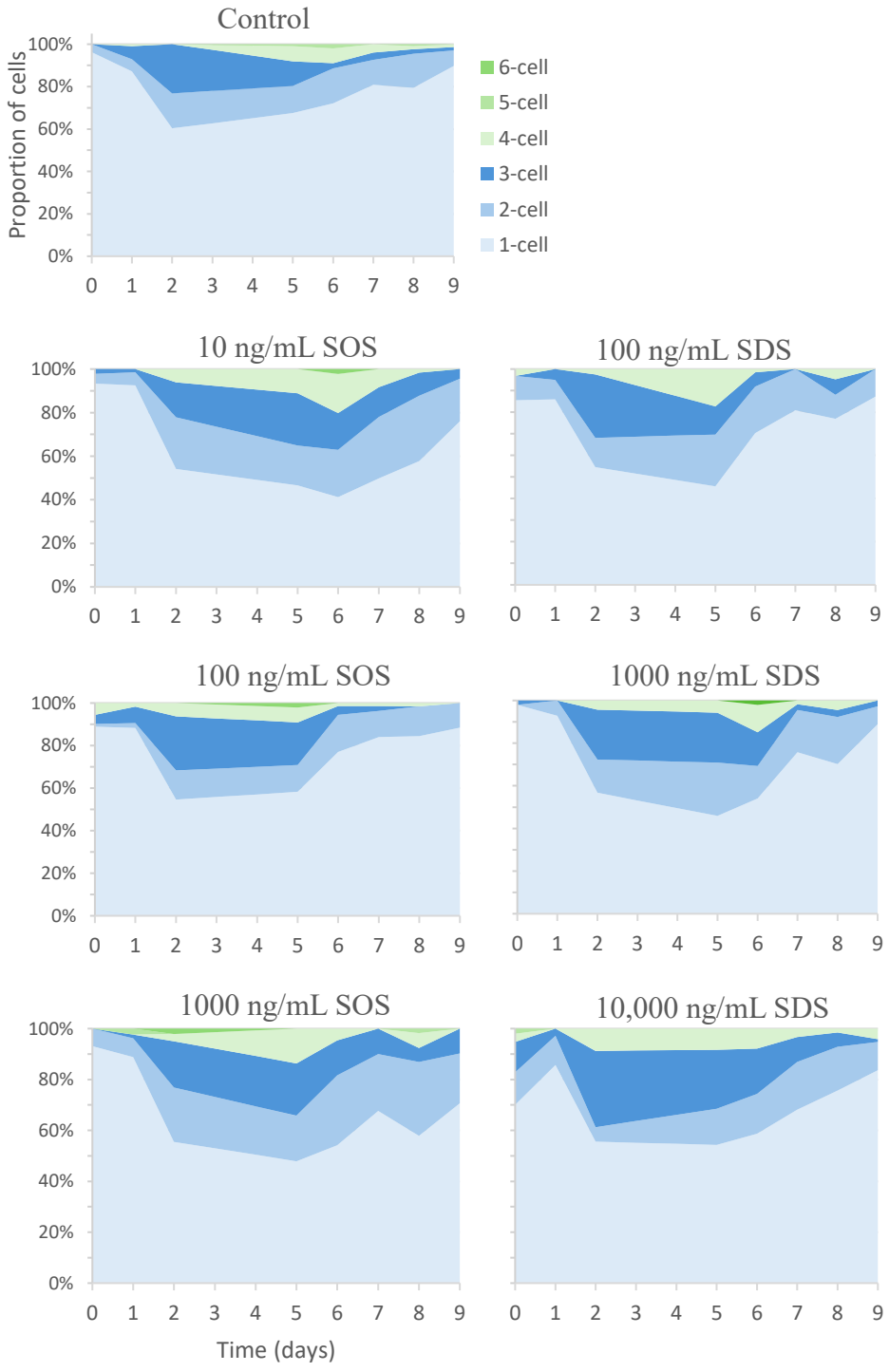

Figure P.1. Proportion of *C. reinhardtii* cells, single and in colonies, over nine days, in controls, and cultures treated with sodium octyl sulphate (10, 10^2, and 10^3 ng mL^{-1}) and sodium dodecyl sulphate (10^2, 10^3, and 10^4 ng mL^{-1}).

Table P.1. Summary of two-way ANOVA results showing effects of treatment, time, and their interaction on the (transformed) proportion of single cells in each experiment. *p*-values and BH adjusted *p*-values are reported for each main effect and interaction term. Statistically significant results ($p < 0.05$) are bolded.

Experiment	term	df	df residual	statistic	*p* value	*p* adj
T. obliquus - SOS	Treatment	3	48	0.144764	0.93254	0.946651
T. obliquus - SOS	Time	5	48	8.904497	4.91E-06	**1.47E-05**
T. obliquus - SOS	Treatment:Time	15	48	1.179183	0.319414	0.479122
C. reinhardtii - SDS	Treatment	1	16	0.00462	0.946651	0.946651
C. reinhardtii - SDS	Time	3	16	11.98406	0.00023	**0.000345**
C. reinhardtii - SDS	Treatment:Time	3	16	2.950676	0.06428	0.192839
T. obliquus - SDS	Treatment	1	16	0.129055	0.724111	0.946651
T. obliquus - SDS	Time	3	16	1.380732	0.284625	0.284625
T. obliquus - SDS	Treatment:Time	3	16	0.658334	0.589502	0.589502

Table P.2. Proportion of single cells in *C. reinhardtii* and *T. obliquus* cultures treated with SDS or SOS, over ten days.

Species	Treatment	Proportion of single cells at time (days)					
		0	1	2	3	4	10
C. reinhardtii	Control	0.41	0.24	0.86		0.51	
		0.64	0.36	0.79		0.55	
		0.32	0.72	0.64		0.74	
	SDS 10 ng mL^{-1}	0.26	0.60	0.76		0.76	
		0.19	0.56	0.71		0.69	
		0.25	0.65	0.70		0.68	
T. obliquus	Control	0.36	0.58	0.60		0.59	
		0.38	0.68	0.56		0.57	
		0.80	0.61	0.60		0.52	
	SDS 10 ng mL^{-1}	0.60	0.63	0.54		0.60	
		0.51	0.53	0.40		0.59	
		0.48	0.71	0.49		0.56	
T. obliquus	Control	0.41	0.60	0.58	0.43	0.53	0.50
		0.52	0.59	0.54	0.48	0.54	0.58
		0.61	0.47	0.52	0.45	0.53	0.40
	SOS 10 ng mL^{-1}	0.51	0.41	0.63	0.57	0.59	0.30
		0.55	0.56	0.66	0.53	0.55	0.36
		0.53	0.59	0.51	0.63	0.59	0.49
	SOS 100 ng mL^{-1}	0.54	0.50	0.43	0.48	0.56	0.35
		0.63	0.52	0.53	0.65	0.61	0.56
		0.54	0.43	0.59	0.46	0.61	0.35
	SOS 1000 ng mL^{-1}	0.57	0.59	0.55	0.44	0.57	0.41
		0.48	0.45	0.59	0.60	0.57	0.27
		0.53	0.49	0.63	0.56	0.62	0.39

Table P.3. Shapiro-Wilk normality test results for residuals of two-way ANOVA model across the proportion of single cells in each group. *P*-values above 0.05 indicate no significant deviation from normality; adjusted *p*-values used the Benjamini-Hochberg correction to control false discover rate across multiple tests. Where necessary, data was transformed to improve normality, as indicated. Note: while this test indicated minor deviation from normality for the T. obliquus – SDS experiment, given the equal sample sizes and by visual inspection of residuals, ANOVA was deemed robust.

Experiment	Transformation	Shapiro *p*	*p* adj
T. obliquus - SOS	Cube root	0.608537426	0.608537
C. reinhardtii - SDS	Raw	0.324792007	0.487188
T. obliquus - SDS	log1p	0.010025635	0.030077

Table P.4. Levene's test results assessing homogeneity of variances across treatment and time combinations for each parameter. *P*-values above 0.05 suggest equal variances, meeting the ANOVA assumption of variance homogeneity; adjusted *p*-values used the Benjamini-Hochberg correction to control false discover rate across multiple tests.

Experiment	df	df residual	statistic	*p* value	*p* adj
T. obliquus - SOS	23	48	0.476141	0.971868	0.971868
C. reinhardtii - SDS	7	16	0.881511	0.542214	0.971868
T. obliquus - SDS	7	16	0.700368	0.671844	0.971868

Table P.5. Pairwise comparisons of estimated means for the proportion of single cells in SDS and SOS treatments and controls, from Tukey's HSD post-hoc test following two-way ANOVA. *p*-values reflect adjusted significant levels for multiple comparisons; statistically significant results ($p < 0.05$) are bolded.

Experiment	*p* value	Comparison	Term	*p* adj_all
T. obliquus - SOS	0.946008	SOS10-Control	Treatment	0.999997
T. obliquus - SOS	0.999831	SOS100-Control	Treatment	0.999997
T. obliquus - SOS	0.999997	SOS1000-Control	Treatment	0.999997
T. obliquus - SOS	0.964686	SOS100-SOS10	Treatment	0.999997
T. obliquus - SOS	0.940236	SOS1000-SOS10	Treatment	0.999997
T. obliquus - SOS	0.999657	SOS1000-SOS100	Treatment	0.999997
C. reinhardtii - SDS	0.946651	SDS10-Control	Treatment	0.999997
T. obliquus - SDS	0.724111	SDS10-Control	Treatment	0.999997
T. obliquus - SOS	0.988333	1-0	Time	0.999997
T. obliquus - SOS	0.941709	2-0	Time	0.999997
T. obliquus - SOS	0.823926	4-0	Time	0.999997
T. obliquus - SOS	0.995631	3-0	Time	0.999997
T. obliquus - SOS	0.000378	10-0	Time	**0.002741**
T. obliquus - SOS	0.640956	2-1	Time	0.999997
T. obliquus - SOS	0.444417	4-1	Time	0.999997
T. obliquus - SOS	0.999996	3-1	Time	0.999997
T. obliquus - SOS	0.002768	10-1	Time	**0.011467**
T. obliquus - SOS	0.999587	4-2	Time	0.999997
T. obliquus - SOS	0.715301	3-2	Time	0.999997
T. obliquus - SOS	1.75E-05	10-2	Time	**0.000254**
T. obliquus - SOS	0.519396	3-4	Time	0.999997
T. obliquus - SOS	5.96E-06	10-4	Time	**0.000173**
T. obliquus - SOS	0.001911	10-3	Time	**0.010405**
C. reinhardtii - SDS	0.093394	1-0	Time	0.300938
C. reinhardtii - SDS	0.000209	2-0	Time	**0.002017**
C. reinhardtii - SDS	0.002153	4-0	Time	**0.010405**
C. reinhardtii - SDS	0.032684	2-1	Time	0.118479
C. reinhardtii - SDS	0.266944	4-1	Time	0.774138
C. reinhardtii - SDS	0.647326	4-2	Time	0.999997

Appendix Q. Light influence bioassays

Q.1. Microalgae culturing

C. reinhardtii CC-1690 and CC-5325 were cultured and maintained in sterile tris-acetate-phosphate (TAP) liquid media. The microalgae were cultured in conical flasks, closed with cotton stoppers, and incubated at 22 °C, with no shaking, and under continuous light of varying intensities (LED lights from all angles), ranging from 8.2 to 188.6 µmol m^{-2} s^{-1}. Cultures were refreshed regularly by emptying the flasks under a laminar flow cabinet and refilling with sterile TAP media.

Q.2. Bioassay set-up

Daphnia extract (described in **Chapter 3**) was added at 5% and 10% v/v to CC-1690 and CC-5325 at varying light intensities. These bioassays were carried out in sterile 6-well Falcon tissue culture plates, where each well contained 5 mL of culture and distilled water or *Daphnia* extract. Actively growing, recently refreshed microalgae cultures were used to ensure that nutrient availability was not a contributing factor to any response. The plates were covered with Parafilm to allow for gas transfer whilst keeping the cultures sterile.

CC-1690 was previously incubated at 54.0 ± 1.7 µmol m^{-2} s^{-1}, on an orbital shaker which had a green mat; cultures were only exposed to light from above and to the sides. CC-1690 aggregated in *Daphnia* extract cultures in these conditions (**Table Q.1**). CC-1690 was moved, along with the mutant strains, to an incubator with a wire rack and no shaker, with LED strips around the top, bottom, and two walls, and a florescent light at the top: this exposed cultures to light from every direction (**Figure Q.1**). Therefore, despite the following measured light intensities starting at a lower range, the light exposure to cells was significantly higher for the same measured light intensity.

- Cultures were kept at 8.2 ± 0.5 µmol m^{-2} s^{-1} for six months. CC-1690 aggregated in *Daphnia* treatments at first but stopped after 3–4 months.
- Increased to 19.0 ± 1.4 µmol m^{-2} s^{-1} for two weeks; bioassay done after 11 days.
- Increased to 56.1 ± 2.4 µmol m^{-2} s^{-1} for one week; bioassay done after five days.
- Decreased to 37.8 ± 1.8 µmol m^{-2} s^{-1} for six weeks; bioassay done after 5.5 weeks.

- Increased to 78.4 ± 3.5 µmol m^{-2} s^{-1} for one week; bioassay done after four days.
- Increased to 120.4 ± 5.8 µmol m^{-2} s^{-1} for one week; bioassay done after five days.
- Increased to 188.6 ± 10.6 µmol m^{-2} s^{-1}; bioassay done after 18 days.

Figure Q.1. Incubator where light bioassays took place. Cultures were incubated in flasks and Falcon plates on the top shelf. Light was measured in nine positions across the top shelf facing up, and the means were reported.

Q.3. Results

Light intensity influenced *C. reinhardtii* palmelloid formation in response to *Daphnia* extract. Images of cells and colonies in control and *Daphnia* treated cultures at varying light intensities are shown in **Table Q.1** (CC-1690) and **Table Q.2** (CC-5325).

Table Q.1. *C. reinhardtii* CC-1690 single cells and colonies in control and *Daphnia* extract treatments, at 48–72 h, at varying light intensities. Cultures which were dominated by palmelloids are marked with "C". Images were taken at 10× magnification; each image is 0.25 mm.

Light intensity (µmol m^{-2} s^{-1})	Extract dose (v/v)	48 h		72 h	
		Control	*Daphnia* extract	Control	*Daphnia* extract
54.0 ± 1.7 (Different incubator. See Section Q.2)	10%	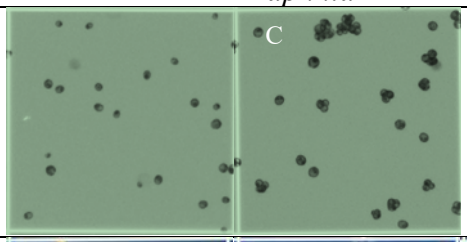			
8.2 ± 0.5	5%	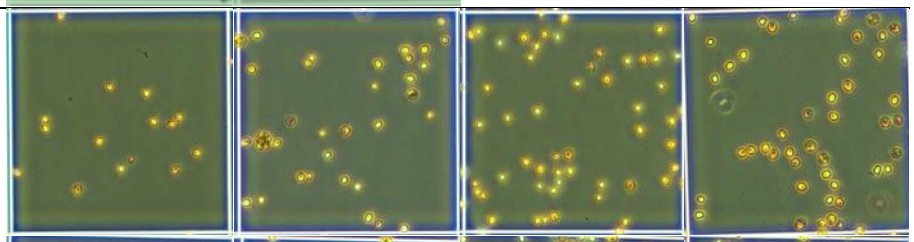			
19.0 ± 1.4	10%	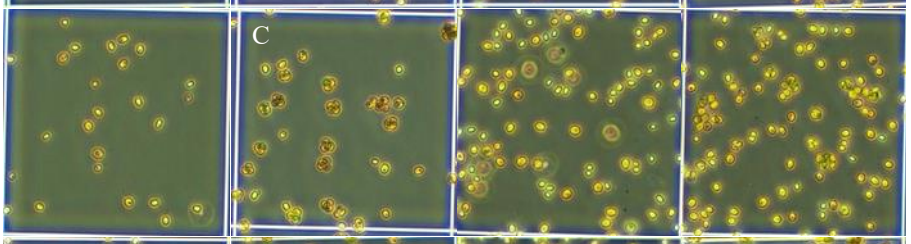			
37.8 ± 1.8	5%	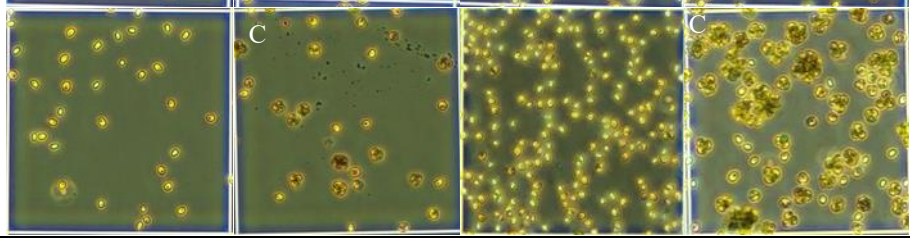			

Table Q.1. *Continued*).

Light intensity (µmol m^{-2} s^{-1})	Extract dose (v/v)	48 h		72 h	
		Control	*Daphnia* extract	Control	*Daphnia* extract
37.8 ± 1.8	10%	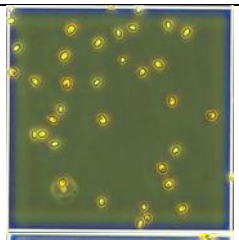	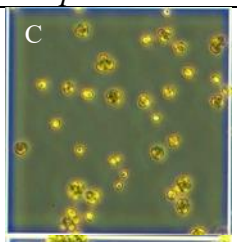	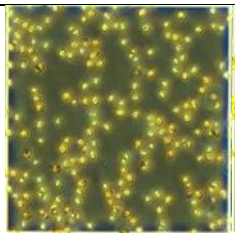	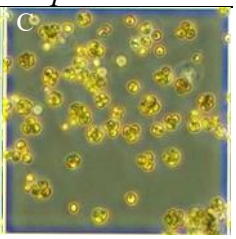
56.1 ± 2.4	10%	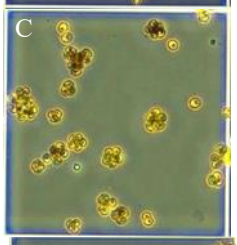	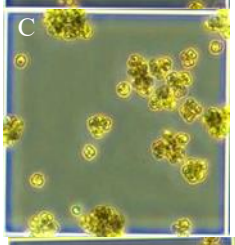		
78.4 ± 3.5	5%	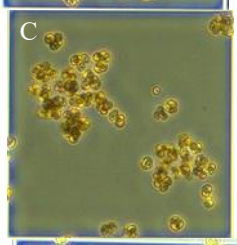	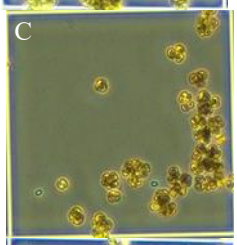		
188.6 ± 10.6	10%	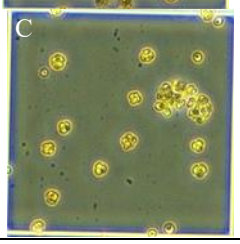	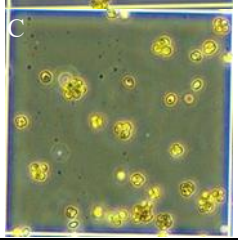	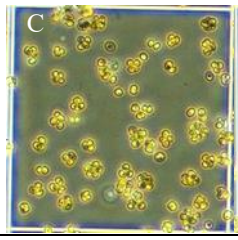	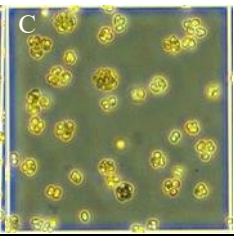

Table Q.2. *C. reinhardtii* CC-5325 single cells and colonies in control and cultures treated with *Daphnia* extract, at 48–72 h, at varying light intensities. All cultures were dominated by single cells. Images were taken at 10× magnification; each image is 0.25 mm.

Light intensity (µmol m^{-2} s^{-1})	Extract dose (v/v)	48 h		72 h	
		Control	*Daphnia* extract	Control	*Daphnia* extract
8.2 ± 0.5	5%	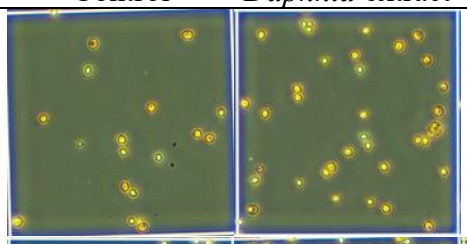			
37.8 ± 1.8	5%	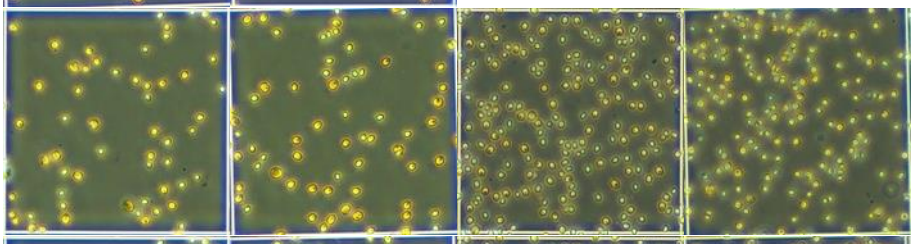			
37.8 ± 1.8	10%	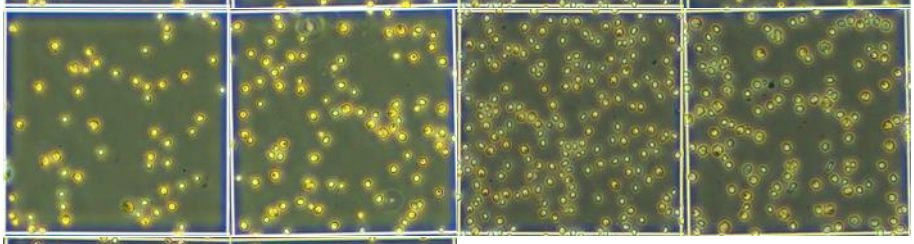			
56.1 ± 2.4	10%	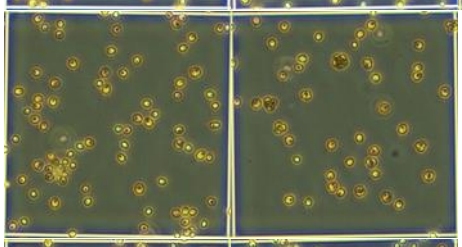			
78.4 ± 3.5	5%	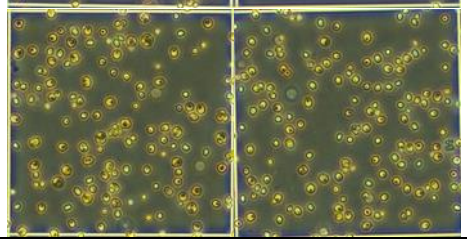			

Table Q.2. (*Continued*).

Light intensity (µmol m^{-2} s^{-1})	Extract dose (v/v)	48 h		72 h	
		Control	*Daphnia* extract	Control	*Daphnia* extract
120.4 ± 5.8	5%	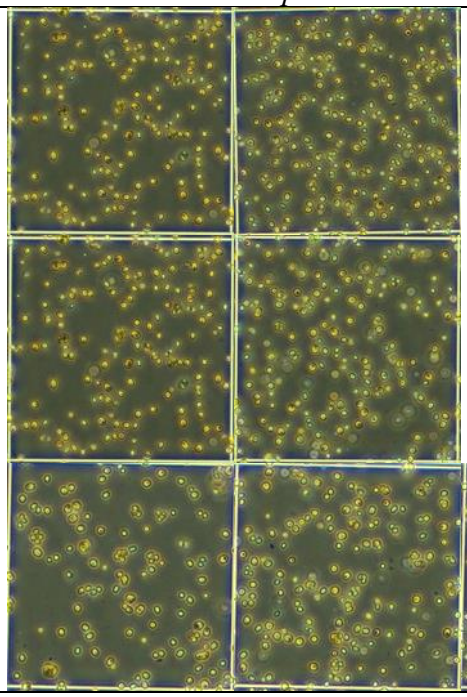			
120.4 ± 5.8	10%				
188.6 ± 10.6	10%				

Appendix R. Statements of contribution

MASSEY UNIVERSITY
TE KUNENGA KI PŪREHUROA
UNIVERSITY OF NEW ZEALAND

GRADUATE RESEARCH SCHOOL

STATEMENT OF CONTRIBUTION
DOCTORATE WITH PUBLICATIONS/MANUSCRIPTS

We, the student and the student's main supervisor, certify that all co-authors have consented to their work being included in the thesis and they have accepted the student's contribution as indicated below in the Statement of Originality.			
Student name:	Emma Muir		
Name and title of main supervisor:	A/Prof Nicola Brown		
In which chapter is the manuscript/published work?		Chapter 1	
Describe the contribution that the student and members of the supervisory team have made to the manuscript/published work:[4] Emma Muir was the main contributor of the literature review. Dr Guieysse, Dr Plouviez, and the other authors helped to edit the manuscript.			
Please select one of the following three options:			
◉	The manuscript/published work is published or in press Please provide the full reference of the research output: Muir, E., Grossman, A. R., Chisti, Y., Fedrizzi, B., Guieysse, B., Plouviez, M. (2024). Self-aggregation for sustainable harvesting of microalgae. Algal Research, 83, 103685. https:/doi.org/10.1016/j.algal.2024.103685.		
○	The manuscript is currently under review for publication Please provide the name of the journal:		
○	It is intended that the manuscript will be published, but it has not yet been submitted to a journal		
Student's signature:		Main supervisor's signature:	
This form should be placed at the beginning of each relevant thesis chapter.			

[4] Refer to the Massey University Publishing and Authorship guidelines (OneMassey for staff, Stream for students) and/ or Contributor Roles Taxonomy (CRediT) guidelines for guidance.

MASSEY UNIVERSITY
TE KUNENGA KI PŪREHUROA
UNIVERSITY OF NEW ZEALAND

GRADUATE RESEARCH SCHOOL

STATEMENT OF CONTRIBUTION
DOCTORATE WITH PUBLICATIONS/MANUSCRIPTS

We, the student and the student's main supervisor, certify that all co-authors have consented to their work being included in the thesis and they have accepted the student's contribution as indicated below in the Statement of Originality.			
Student name:	Emma Muir		
Name and title of main supervisor:	A/Prof. Nicola Brown		
In which chapter is the manuscript/published work?		Chapter 3	
Describe the contribution that the student and members of the supervisory team have made to the manuscript/published work:[5] Emma Muir designed and conducted all experiments, data analyses, and RNA extraction. Differential expression analyses were perform ed by Miss Muir and Dr. Olivier Laroche (Cawthron Institute, Nelson). Miss Muir carried out all functional analyses of DEGs, mutant experiments, and wrote and edited the chapter. RT-qPCR was carried out by Dr. Kirsty Smith (Cawthron Institute, Nelson). Dr. Plouviez, Dr. Guieysse, and A/Prof. Brown offered advice for editing the manuscript.			
Please select one of the following three options:			
○	The manuscript/published work is published or in press Please provide the full reference of the research output:		
○	The manuscript is currently under review for publication Please provide the name of the journal:		
◉	It is intended that the manuscript will be published, but it has not yet been submitted to a journal		
Student's signature:		Main supervisor's signature:	
This form should be placed at the beginning of each relevant thesis chapter.			

[5] Refer to the Massey University Publishing and Authorship guidelines (OneMassey for staff, Stream for students) and/ or Contributor Roles Taxonomy (CRediT) guidelines for guidance.

MASSEY UNIVERSITY
TE KUNENGA KI PŪREHUROA
UNIVERSITY OF NEW ZEALAND

GRADUATE RESEARCH SCHOOL

STATEMENT OF CONTRIBUTION
DOCTORATE WITH PUBLICATIONS/MANUSCRIPTS

We, the student and the student's main supervisor, certify that all co-authors have consented to their work being included in the thesis and they have accepted the student's contribution as indicated below in the Statement of Originality.			
Student name:	Emma Muir		
Name and title of main supervisor:	A/Prof. Nicola Brown		
In which chapter is the manuscript/published work?	Chapter 4		
Describe the contribution that the student and members of the supervisory team have made to the manuscript/published work:[6] Emma carried out the GC-MS analyses at University of Auckland with the support of Dr. Katryna van Leeuwen and Dr Jin Wang (University of Auckland). Dr. van Leeuwen carried out the data pre-processing. Emma carried out further analysis of the metabolite data, and wrote the chapter. Dr. Plouviez, Dr. Guieysse, and A/Prof. Brown helped to edit the manuscript.			
Please select one of the following three options:			
○	The manuscript/published work is published or in press Please provide the full reference of the research output:		
○	The manuscript is currently under review for publication Please provide the name of the journal:		
◉	It is intended that the manuscript will be published, but it has not yet been submitted to a journal		
Student's signature:		Main supervisor's signature:	
This form should be placed at the beginning of each relevant thesis chapter.			

[6] Refer to the Massey University Publishing and Authorship guidelines (OneMassey for staff, Stream for students) and/ or Contributor Roles Taxonomy (CRediT) guidelines for guidance.

References (Appendices)

Aksoy, M., Pootakham, W., & Grossman, A. R. (2014). Critical function of a *Chlamydomonas reinhardtii* putative polyphosphate polymerase subunit during nutrient deprivation. *Plant Cell*, *26*, 4214-4229. https://doi.org/10.1105/tpc.114.129270

Tammana, D., & Tammana, T. V. S. (2017). *Chlamydomonas* FAP265 is a tubulin polymerization promoting protein, essential for flagellar reassembly and hatching of daughter cells from the sporangium. *PLOS ONE*, *12*, e0185108. https://doi.org/10.1371/journal.pone.0185108

Yasumoto, K., Nishigami, A., Yasumoto-Hirose, M., Kasai, F., Okada, Y., Kusumi, T., & Ooi, T. (2005). Aliphatic sulfates released from *Daphnia* induce morphological defense of phytoplankton: Isolation and synthesis of kairomones. *Tetrahedron Letters*, *46*, 4765-4767. https://doi.org/10.1016/j.tetlet.2005.05.027